RP TU Rheinland-Pfälzische Technische Universität Kaiserslautern Landau

Tracing the evolution of bilin biosynthesis: from emergence to primary endosymbionts

vom Fachbereich Biologie

der Rheinland-Pfälzischen Technischen Universität Kaiserslautern-Landau

zur Verleihung des akademischen Grades Dr. rer. nat. genehmigte

Dissertation

von

Federica Frascogna, M.Sc., geb. in Mugnano di Napoli

Mündliche Prüfung: 23/07/2024
Dekan: Prof. Dr. Stefan Kins
Promotionskommissionsvorsitzender: Prof. Dr. Stefanie Müller-Schüssele
Berichterstattende: Prof. Dr. Nicole Frankenberg-Dinkel
Prof. Dr. Michael Schroda
Prof. Dr. Wolfgang Gärtner

D 386

A Nonna Checca e Nonna Maria…

“e ancora proteggi la grazia del mio cuore
adesso e per quando tornerà l'incanto
di te vicino a me”

Table of contents

Abbreviations

Abbreviations of the International System of Units (SI) are not listed. The single letter or three letter code is used for designation of amino acids.

ε	molar absorption coefficient
λ	wavelength
AHT	anhydrotetracycline
Amp	ampicillin
AP	alkaline phosphatase
APC	allophycocyanin
APS	ammonium persulfate
BBAG	bilin biosynthesis-associated globins
BCIP	5-bromo-4-chloro-3-indolyl phosphate
Bph	bacterial phytochrome
BSA	bovine serum albumin
BV	biliverdin IXα
Chl	chlorophyll
Cph	cyanobacterial phytochrome
CV	column volume
DAD	diode-array detector
DHBV	dihydrobiliverdin
DMF	dimethylformamide
DMSO	dimethyl sulfoxide
DNA	deoxyribonucleic acid
dNTP	deoxynucleoside triphosphate
DR	dark reversion
DTT	dithiothreitol
EDTA	ethylenediaminetetraacetic acid
em	emission
EtOH	ethanol
exc	excitation
Fd	ferredoxin
FDBR	ferredoxin-dependent bilin reductase
FNR	ferredoxin-$NADP^+$ reductase
Fph	fungal phytochrome
FPLC	fast protein liquid chromatography
FRL	far-red light
fwd	forward
GAF	cGMP-specific phosphodiesterase/adenylyl cyclase/FhlA
G-6-P	glucose-6-phosphate
G-6-P DH	glucose-6-phosphate dehydrogenase
HF	high fidelity
HK	histidine kinase
HKRD	histidine kinase-related domain
HPLC	high performance liquid chromatography
HY2	phytochromobilin synthase

IPTG	isopropyl β-D-1-thiogalactopyranoside
Kan	kanamycin
kb	kilobase
kDa	kilodalton
LB	lysogeny broth
MAG	metagenome-assembled genome
MBV	mesobiliverdin (18^1,18^2-dihydrobiliverdin)
MeOH	methanol
MSA	MSA
MW	molecular weight
MWCO	molecular weight cut-off
NADP	nicotinamide-adenine-dinucleotide phosphate
NBT	nitro blue tetrazolium chloride
NRS	NADPH regenerating system
OD_{600}	optical density at 600 nm
PΦB	phytochromobilin
PAS	Per-ARNT-Sim
PBS	phycobilisome
PBP	phycobiliprotein
PC	phycocyanin
Pcb	prochlorophyte chlorophyll-binding protein
PCB	phycocyanobilin
PCR	polymerase chain reaction
PcyA	phycocyanobilin:ferredoxin oxidoreductase
PDB	protein data bank
PE	phycoerythrin
PEB	phycoerythrobilin
PebA	15,16-dihydrobiliverdin (DHBV):ferredoxin oxidoreductase
PebB	phycoerythrobilin:ferredoxin oxidoreductase
PebS	phycoerythrobilin synthase
PEC	phycoerythrocyanin
PEG 8000	polyethylene glycol 8000
Pfr	phytochrome far-red light-absorbing form
pH	potential hydrogen
Phy	plant phytochrome
PHY	phytochrome domain
pLDDT	predicted local distance difference test
PUB	phycourobilin
PUBS	phycourobilin synthase
PVB	phycoviolobilin
PVDF	polyvinylidene fluoride
Pr	phytochrome red light-absorbing form
PS	photosystem
PTFE	polytetrafluoroethylene
QC	QuikChange
REC	receiver
rev	reverse
RL	red light

rpm	rounds per minute
ROS	reactive oxygen species
SEC	size exclusion chromatography
SDS	sodium dodecyl sulfate
SDS-PAGE	sodium dodecyl sulfate-polyacrylamide gel electrophoresis
TBE	transfer bootstrap expectation
TEMED	tetramethylethylenediamine
TES	N-[Tris(hydroxymethyl)methyl]-2-aminoethanesulfonic acid
TFA	trifluoroacetic acid
Tris	tris(hydroxymethyl)aminomethane
UV/Vis	ultraviolet/visible
v/v	volume per volume
w/v	weight per volume
WT	wild type
Z/*E*	*zusammen*/*entgegen*

1 Introduction

1.1 Bilins, an essential class of the pigments of life

Bilins are a class of open chain tetrapyrrole molecules, widely distributed in nature and often referred to as “pigments of life”, alongside all other tetrapyrroles (Battersby, 1985). The discovery of bilins stemmed from the isolation of pigments from animal bile in the 19th century. Later on, these pigments were found to share structural similarities with chlorophyll breakdown products (Fischer & Röse, 1914; Fischer & Reindel, 1923; Siedel & Fischer, 1933; Fischer, 1937; Fischer & Plieninger, 1942). This resemblance led to the recognition of a broader group of molecules, which encompass those found in both bile and chlorophyll degradation pathways, ultimately termed “bilins”. Excluding hydroxymethylbilane, the precursor of porphyrins, naturally occurring linear tetrapyrroles are all derived from metalloporphyrins, heme and chlorophyll (Frankenberg & Lagarias, 2003a). Structurally, bilins consist of four substituted pyrrole rings connected by methine bridges. The linear arrangement of the four pyrroles creates an extended conjugated configuration with π electrons delocalized over the entire ring system, which imparts distinctive spectroscopic features, such as absorption of light in the visible region (Falk, 1989; Taniguchi & Lindsey, 2023) (Figure 1.1). Given their diverse photochemical and photophysical properties, these tetrapyrroles find numerous applications in green, red and white biotechnology (Chernov *et al.*, 2017; Li *et al.*, 2019; Pagels *et al.*, 2019; Sekar & Chandramohan, 2008; Sun *et al.*, 2023).

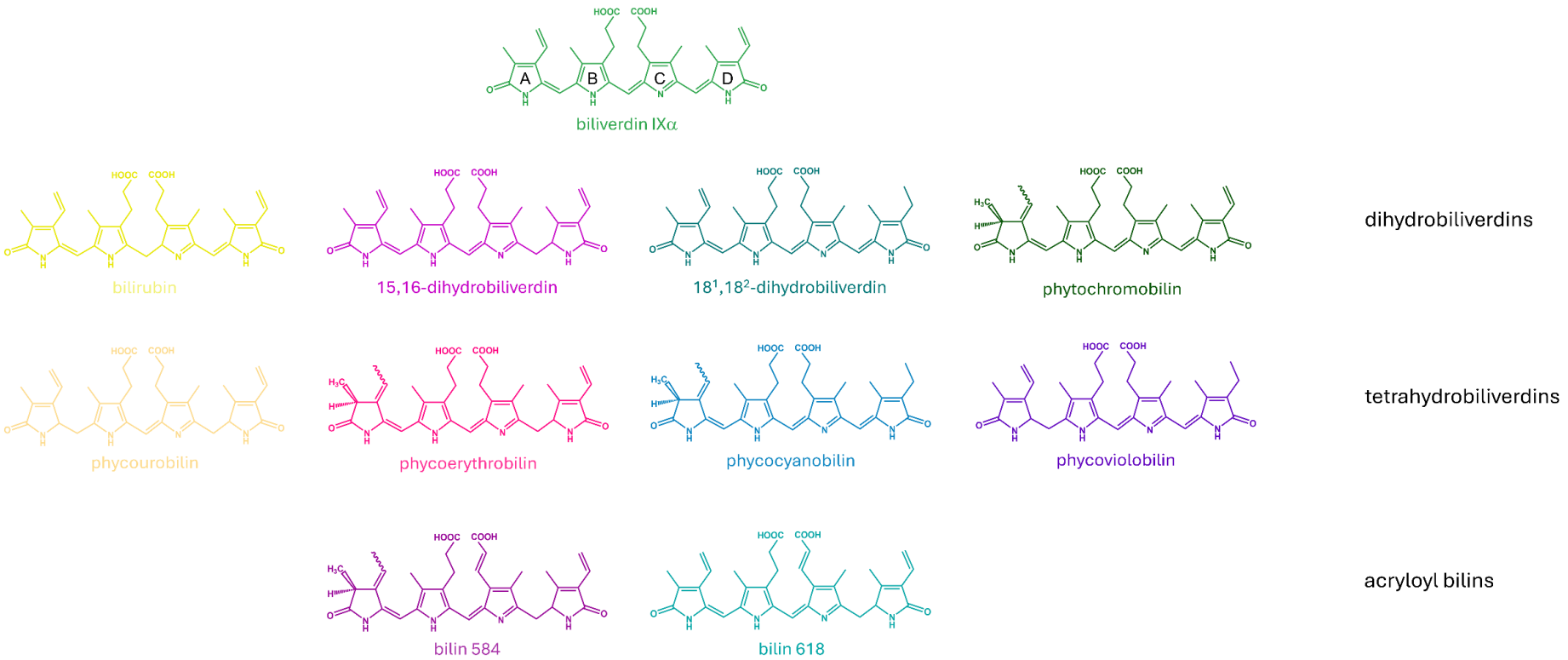

Figure 1.1 Overview of bilin structures.
Bilins are open chain tetrapyrroles widely distributed in nature and endowed with an extended plethora of functions. Structures are colored according to the pigmentation conferred by the conjugation system. Pyrrole rings nomenclature is highlighted in the structure of biliverdin IXα. Wavy bonds at the A-ring indicate the possible occurrence of two $C3^1$ stereoisomers.

Bilins exhibit a broad spectrum of functions, encompassing involvement in regulatory mechanisms, determination of pigmentation, mediation of light harvesting and light sensing. First, bilins function as key players in the detoxification of reactive oxygen species and iron acquisition (Duanmu *et al.*, 2013). More recently, bilins were found to bind the GENOMES UNCOUPLED 4 (GUN4) protein and partake in the regulation chlorophyll biosynthesis by enhancing the turnover of magnesium chelatase (Hu *et al.*, 2021; Rockwell & Lagarias, 2023; Zhang *et al.*, 2021). The most striking example of bilin contribution in pigmentation is the coloration of eggshells, fishes and insects (Oxford & Gillespie, 1998; Hamchand *et al.*, 2020; Stavenga, 2023). Additionally, their involvement in specialized protein complexes enables light harvesting in bacteria and algae, as well as various light-regulated mechanisms in plants, certain bacteria, algae and fungi (Glazer, 1977; Sharrock, 2008; Sanfilippo *et al.*, 2019a).

1.2 Light harvesting is strictly dependent on bilins

Photosynthesis, the conversion of light energy into carbohydrates-stored chemical energy, is arguably one of the most important biological processes on earth. In the majority of photosynthetic organisms, light harvesting is performed by chlorophyll-containing antenna complexes and carotenoids. Chlorophyll (Chl) absorbs mostly blue and red-light (400 - 480 nm and 650 - 720 nm), whereas carotenoids absorb light wavelengths around 450 - 500 nm, leaving the green region of the light spectrum unused and generating the so-called “Green Gap” (Green & Parson, 2003; Blankenship, 2008; Polívka & Frank, 2010; Chen & Blankenship, 2011). Cyanobacteria, Glaucophytes, Rhodophytes and Cryptophytes are capable of enhancing their light harvesting machinery by employing phycobiliproteins (PBPs). PBPs, made of an apo-protein moiety binding bilin chromophores, absorb light in the 480 - 650 nm region, thus “filling the green gap” (Croce & Van Amerongen, 2014; Glazer, 1994b; MacColl & Guard-Friar, 2018). Four main types of PBPs exist: allophycocyanin (APC), phycocyanin (PC), phycoerythrocyanin (PEC) and phycoerythrin (PE). All PBPs are made of an α and a β subunit, which form a stable αβ heterodimer. The heterodimers subsequently assemble in $(\alpha\beta)_3$ trimers, generating a minimal functional unit (Apt *et al.*, 1995; Sidler, 1994). The complete biological unit of PBPs is ultimately obtained by associating two $(\alpha\beta)_3$ face-to-face into $(\alpha\beta)_6$ hexamers, in a process mediated by the interaction between residues of the α-subunits of each trimer and additional linkers (Adir *et al.*, 2001; Schirmer *et al.*, 1986) (Figure 1.2).

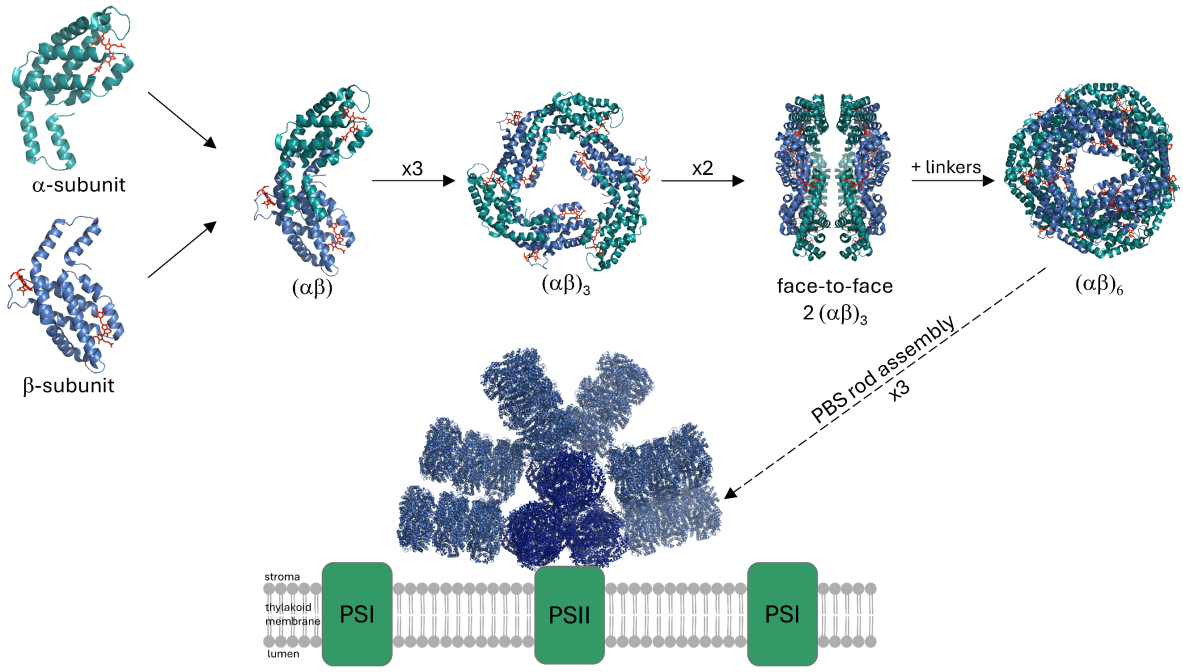

Figure 1.2 Phycobiliprotein oligomerization process and assembly in the phycobilisome.
The crystal structure of *Synechocystis* sp. PCC 6803 phycocyanin in different oligomerization states (PDB accession code: 7SC8, phycocyanin extracted from the rod) is displayed in cartoon representation (top). The α-subunit are colored in deepteal, whereas the β-subunit in marine. Phycocyanobilins bound to each subunit are shown as sticks and colored in red for reasons of display clarity. The top panel shows the overall process of phycocyanin hexamer formation. Three hexamers are ultimately assembled into each phycobilisome rod and shown as marine cartoons (bottom). The rods depart from a core of three allophycocyanins shown as blue cartoons. The holo-PBS structure in the up-up conformation was modified from the structure in Supplement Data of Domínguez-Martín *et al.*, 2022. The phycobilisome is schematically represented in its potential location on top of the thylakoid membrane.

In the case of APC, the trimeric minimal functional unit corresponds to the biological unit (Brejc *et al.*, 1995; Murray *et al.*, 2007; Sonani *et al.*, 2015). Although sharing the overall globin-like fold and complex quaternary structure, PBPs differ in the associated chromophores (Glazer, 1994b; MacColl, 1998; Schirmer *et al.*, 1986). The process of chromophore attachment is a post-translational modification conducted by phycobiliprotein lyases and is directed towards specific conserved cysteine (Cys) residues on both PBP subunits (Biswas *et al.*, 2010; Scheer & Zhao, 2008; Schluchter *et al.*, 2010). APC is turquoise (in the simplest $(\alpha\beta)_3$ trimeric form, $\lambda_{absorbance}$ = 650 nm; $\lambda_{emission}$ = 660 nm) and only possesses two chromophores, both phycocyanobilin (PCB), bound to α-Cys82 and β-Cys82 (DeLange *et al.*, 1981; Sidler *et al.*, 1981; Offner & Troxler, 1983; Minami *et al.*, 1985; Arciero *et al.*, 1988; Zhou *et al.*, 2024). The most common PC type, C-PC, is blue ($\lambda_{absorbance}$ = 620 nm; $\lambda_{emission}$ = 640 nm) and possesses PCB at α-Cys84, β-Cys84 and β-Cys155 (Frank *et al.*, 1978; Schirmer *et al.*, 1985; Fairchild *et al.*, 1992; Stec *et al.*, 1999; Padyana *et al.*, 2001; Zhao *et al.*, 2006; Zhao *et al.*, 2007; Ferraro *et al.*, 2020). Other PC with different absorption/emission properties arise as a result of the attachment of at least one phycoerythrobilin/phycourobilin (PEB/PUB) on either one of the subunits (Alvey *et al.*, 2011a, 2011b). PEC is solely found in

cyanobacteria, exhibits purple-blue color ($\lambda_{absorbance}$ = 570 nm; $\lambda_{emission}$ = 625 nm) and has a phycoviolobilin (PVB) attached at α-Cys84 and PCB at both β-Cys84 and β-Cys155 (Bryant, 1982; Hirose *et al.*, 2019). Finally, the pink PE shows the greatest chromophore heterogeneity of all PBPs, classifying in five types. All have five PEB/PUB chromophorylation sites (α-Cys84, α-Cys143, β-Cys50,61 for double linkage, β-Cys84, β-Cys155), whereas PE-II shows one addition at α-Cys75 (MacColl, 1991; Ong & Glazer, 1991; Six *et al.*, 2007; Dagnino-Leone *et al.*, 2022). Due to the extremely high heterogeneity of chromophores, spectroscopical properties also vary immensely ($\lambda_{absorbance}$ = 495-545/545/566 nm; $\lambda_{emission}$ = 575 nm) (Bryant, 1982; Xie *et al.*, 2021).

In cyanobacteria, glaucophytes and red algae, PBPs assemble into a tridimensional structure named phycobilisome (PBS) (Figure 1.2). The PBS is usually attached to the external surface of the thylakoid membrane and is responsible for the transfer of light energy to the reaction centers of both photosystem I and photosystem II, therefore acting as the major light harvesting complex in these organisms (Gantt & Conti, 1966; Glazer, 1977; Grossman *et al.*, 1993; Watanabe & Ikeuchi, 2013). This massive antenna system (~ 5 - 20 MDa) typically consists of an APC central core and PC-PE fan-distributed peripheral rods, built with the help of non-chromophorylated linker proteins, but it can ultimately assemble in many different conformations (Bryant *et al.*, 1979; Bryant & Canniffe, 2018; Stadnichuk & Kusnetsov, 2023). Most cyanobacterial PBSs are hemidiscoidal, composed of a core made of two to five APC trimers from which six to eight cylindrical rods depart (Zheng *et al.*, 2021; Kawakami *et al.*, 2022; Domínguez-Martín *et al.*, 2022; Perevedentseva *et al.*, 2024). Three main exceptions are worthy of mention: the cases of *Gloeobacter,* Prochlorophytes and *Acaryochloris*. The genus *Gloeobacter* lacks thylakoids, therefore PBSs are located on the cytoplasmatic membrane and, due to space constraints, adapt a “bundle-shape” with only vertical cylinders (Guglielmi *et al.*, 1981; Jiang *et al.*, 2023; Krogmann *et al.*, 2007; Mendoza-Hernández *et al.*, 2010; Rippka *et al.*, 1974; Yokono *et al.*, 2008). Prochlorophytes completely lack PBSs and employ prochlorophyte Chl (*a/b*) binding proteins (Pcb) as the antennae, forming supercomplexes with both photosystems (Hiller & Larkum, 1985; Tomitani *et al.*, 1999; Bibby *et al.*, 2003a, 2003b; Chen & Bibby, 2005; Boichenko *et al.*, 2007; Barrera-Rojas *et al.*, 2018). Nevertheless, *Prochlorococcus*, oceans second biggest primary producer, was also shown to attach PE, besides Pcb, on the lumen side of the thylakoid membrane (Hess *et al.*, 1996, 1999; Lokstein *et al.*, 1999; Penno *et al.*, 2000; Ting *et al.*, 2001; Steglich *et al.*, 2003, 2005; Wiethaus *et al.*, 2010). However, PE is only present in extremely low amounts, hindering any further investigation on its specific role and additionally posing the hypothesis that it could rather be used as blue/green receptor for phytochrome-like signal transduction (Beale, 2008; Steglich *et al.*, 2003). The case of *Acaryochloris* is somewhat similar to *Prochlorococcus*. These cyanobacteria employ Pcb, although located on the cytoplasmic side of the thylakoid

membrane and associated with Chl-*d* and Chl-*a,* and only two species were shown to possess PBPs*, A. marina* MBIC11017 and *A. thomasi* (Chen *et al.*, 2002; Itoh *et al.*, 2007; Ohashi *et al.*, 2008; Theiss *et al.*, 2011; Badshah *et al.*, 2017; Partensky *et al.*, 2018; Bar-Zvi *et al.*, 2018; Niedzwiedzki *et al.*, 2019; Xu *et al.*, 2021; Shen *et al.*, 2024). Moreover, the PBPs genes are not encoded in the chromosome but in a large plasmid, suggesting their acquirement via horizontal gene transfer (HGT) (Miyake, 2022; Miyake *et al.*, 2020, 2022).

The emergence of the earliest oxygenic photosynthetic eukaryotes is traceable to a primary endosymbiosis event, wherein a heterotrophic eukaryotic host cell engulfed a cyanobacterium, leading to its integration as the plastid (Archibald, 2009; Keeling, 2004, 2010; Sibbald & Archibald, 2020). This pivotal event led to the formation of the Archaeplastida supergroup, which further diverged into the Glaucophytes, Rhodophytes and Viridiplantae lineages (Adl *et al.*, 2005; Rodríguez-Ezpeleta *et al.*, 2005). The emergence of the Archaeplastida also introduced new PBS features. The PBS of the Glaucophyta *Cyanophora paradoxa* only bears APC and PC and is believed to morphologically resemble a typical cyanobacterial hemidiscoidal type, with the main difference related to the linker proteins. In *C. paradoxa*, CpcC, typical PC rod linker, is absent, but its function is thought to be fulfilled by two Glaucophyte-specific linker proteins, CpcK1 and CpcK2 (Jackson *et al.*, 2015; Price *et al.*, 2012, 2017; Steiner & Löffelhardt, 2011; Watanabe *et al.*, 2012). Members of the Cyanidiophyceae, the earliest diverging red algae, are also believed possess the simplest hemidiscoidal PBS type with a tricylindrical APC core and only PC containing rods, reinforcing the theory of chloroplast endosymbiosis (Eisele *et al.*, 2000; Offner & Troxler, 1983; Parys *et al.*, 2021; Samsonoff & MacColl, 2001; Stec *et al.*, 1999; Ueno *et al.*, 2015; Wollman, 1979). The PBS of Rhodophytina, on the other hand, results to be much more sophisticated because of the presence of both PE (which constitutes > 80% of the attached PBPs), with bound PEB and PUB, and γ-subunits, representing chromophorylated linker proteins (Camara-Artigas *et al.*, 2012; Contreras-Martel *et al.*, 2001; Dagnino-Leone *et al.*, 2017; Liberti *et al.*, 2023; Miyabe *et al.*, 2017; Rathbone *et al.*, 2021; Ritter *et al.*, 1999; Vásquez-Suárez *et al.*, 2018; Xie *et al.*, 2021). Moreover, recent findings proved red algal PBSs can either be hemi-ellipsoidal or block-shaped. *Porphyridium purpureum* contains hemi-ellipsoidal PBSs with a mass of 14.8 MDa and with 1600 attached phycobilins, whereas *Griffithsia pacifica* possesses block-type PBSs, with an 18 MDa mass and more than 2000 attached phycobilins (Dodson *et al.*, 2023; Ma *et al.*, 2020; Zhang *et al.*, 2017).

The engulfment of a red alga by a heterotrophic eukaryote in a secondary endosymbiosis event gave birth to the Cryptophytes (Archibald, 2009; Archibald & Keeling, 2002; Bhattacharya *et al.*, 2004; Sibbald & Archibald, 2020). The light-harvesting system of these organisms exploits Chl *a/c* and unique PBPs (Neilson & Durnford, 2010; Hoffman *et al.*, 2011; Overkamp *et al.*, 2014a, 2014b; Cunningham *et al.*, 2019; Rathbone *et al.*, 2023). Cryptophyte

PBPs (Cr-PBPs) encompass nine types of Cr-PCs and Cr-PEs, designated by the wavelength of the major absorbance peak (Glazer & Wedemayer, 1995; Greenwold *et al.*, 2019; Hill & Rowan, 1989; Hoef-Emden & Archibald, 2017; Merritt & Richardson, 2024; Michie *et al.*, 2023; Richardson & Campbell, 2022). These PBP exist as heterodimers (αβ)(α'β). While one β-subunit is encoded in the plastid genome, several α-subunits (up to 20) are encoded in the nucleus to be transported to the chloroplast (Apt *et al.*, 1995; Curtis *et al.*, 2012; Douglas, 1992; Rathbone *et al.*, 2021, 2023). The β-subunit directly descends from red algae PBPs subunit, justifying its plastid location, whereas the α-subunits are thought to have evolved from red algal PBS scaffolding proteins (Apt *et al.*, 1995; Rathbone *et al.*, 2021). Unlike Cyanobacteria, Glaucophytes and Rhodophytes PBPs, Cr-PBPs do not assemble in PBSs, but rather occupy the chloroplast lumen (Michie *et al.*, 2023; Mirkovic *et al.*, 2009; Spear-Bernstein & Miller, 1989; Wehrmeyer, 1983). Moreover, in addition to PCB and PEB, Cr-PBPs bind four unique bilins. Besides 15,16-dihydrobiliverdin (15,16-DHBV) and 18^1,18^2-dihydrobiliverdin (18^1,18^2-DHBV or MBV), also present in other bilin-containing organisms as intermediates in, respectively, PEB and PCB biosynthesis, Cr-PBPs bind bilin 584 and bilin 618. These unique chromophores are C12 acryloyl-derivates of PEB and 15,16-DHBV, respectively (Glazer & Wedemayer, 1995; Overkamp *et al.*, 2014b; Wedemayer *et al.*, 1992, 1996). Cryptophytes are additionally endowed with a unique type of photoacclimation. In many organisms, PBPs play a key role in modulating the light harvesting machinery in response to changes in light conditions, in a process named chromatic acclimation (CA) (Hirose *et al.*, 2019; Kehoe & Gutu, 2006; Sanfilippo *et al.*, 2019a; Wang & Chen, 2022). To date, seven types of CA have been described, all sharing the selective use of different bilins and resulting solely in alteration of relative PBPs concentration. Recently, a new photoacclimation response causing shifts in PBPs absorbance peaks was discovered in *Hemiselmis pacifica* and *Proteomonas sulcata* and associated to chromophore changes on the β-subunit (Heidenreich & Richardson, 2020; Spangler *et al.*, 2022).

1.3 Bilins mediate light sensing

The ability of various organism, photosynthetic and non-, to sense light quality and intensity can also be a bilin-dependent process. Indeed, bilins serve as chromophores of the photoreceptor class of proteins, among them the most widespread and studied are arguably phytochromes (Anders & Essen, 2015; Briggs & Spudich, 2005; Hegemann, 2008; Möglich *et al.*, 2010; Montgomery & Lagarias, 2002; Sharrock, 2008; Tu & Lagarias, 2005). The ultimate discovery of phytochromes is traceable to 1959, when, after years of previous speculation and studies on red/far-red light induced responses in plant germination and flowering (Borthwick *et al.*, 1952, 1954; Borthwick & Parker, 1938a, 1938b, 1939; Downs *et al.*, 1957; Downs & Borthwick, 1956; Garner & Allard, 1920; Hendricks *et al.*, 1956; Parker *et*

al., 1952; Sage, 1992), Butler and colleagues, finally observed the responsible pigment *in vivo* (Butler *et al.*, 1959). Plant phytochromes (Phys) have been extensively studied since then and their influence on several developmental processes like chloroplast migration, shade avoidance, seed germination and photomorphogenesis has been elucidated (Casal & Sánchez, 1998; Chen & Chory, 2011; DeBlasio *et al.*, 2003; Franklin, 2008; Haupt, 1982; Jiao *et al.*, 2007; Kadota *et al.*, 2000; Nagy & Schäfer, 2002; Pierik & De Wit, 2014; Shinomura *et al.*, 1996; Smith & Whitelam, 1997; Whitelam & Devlin, 1997). Only decades later, phytochromes were additionally discovered in bacteria, algae and fungi. In bacteria and algae, phytochromes play roles related to regulation of pigmentation, photosynthesis, respiration and phototaxis (Auldridge & Forest, 2011; Duanmu *et al.*, 2017; Hughes & Lamparter, 1999; Kaneko *et al.*, 1996; Karniol *et al.*, 2005; Moon *et al.*, 2011; Rockwell & Lagarias, 2017b; Wilde *et al.*, 2002; Wiltbank & Kehoe, 2019), whereas in fungi these photoreceptors are involved in temperature sensing, sexual development and mycotoxins production (Blumenstein *et al.*, 2005; Froehlich *et al.*, 2005; Idnurm & Heitman, 2005; Purschwitz *et al.*, 2008; Yu *et al.*, 2019).

Regardless of their origin, these photoreceptors share a dimeric conformation and an overall similar architecture, made of a N-terminal photosensory domain and a C-terminal regulatory domain (Nagatani, 2010; Quail, 2010; Rockwell *et al.*, 2006; Rockwell & Lagarias, 2006) (Figure 1.3).

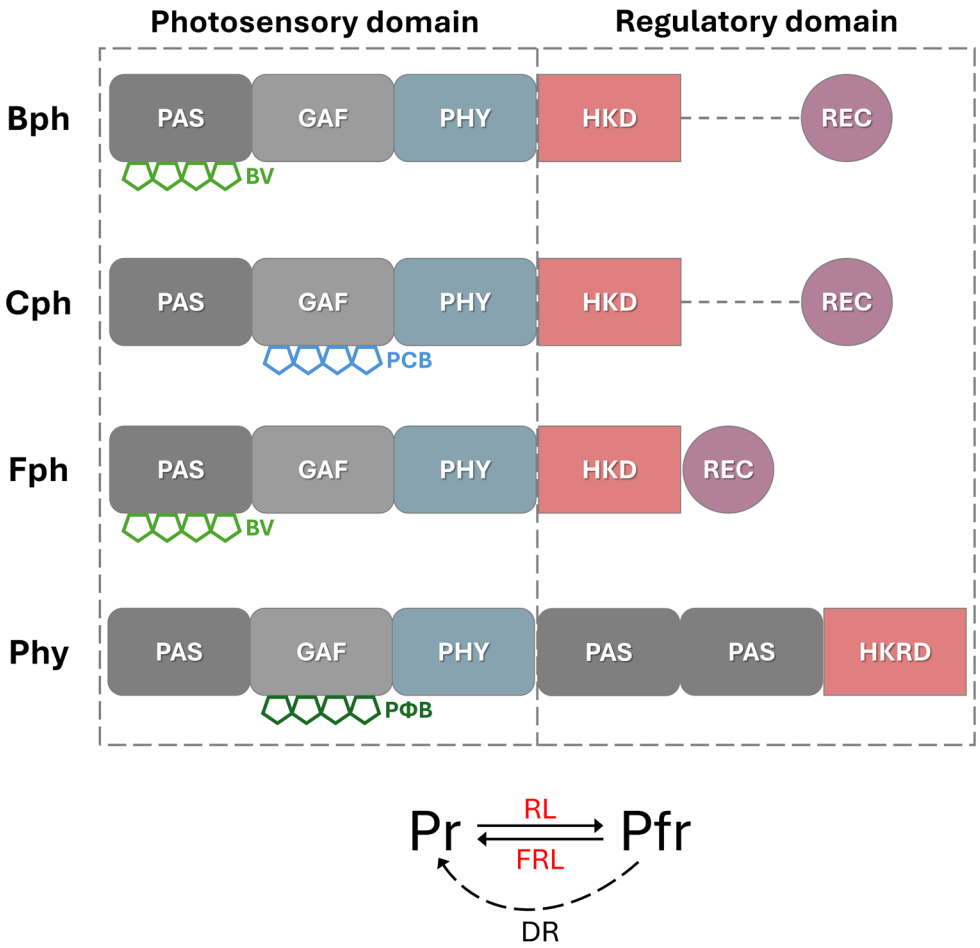

Figure 1.3 Domain organization of phytochromes from different organisms and scheme of prototypical phytochrome activity.
Phytochromes consist of a photosensory and a regulatory domain (top). The photosensory domain comprises three subdomains: PAS (Per-Arnt-Sim, dark grey box), GAF (cGMP-specific phosphodiesterases/adenylyl cyclase/FhlA, light grey box), and PHY (phytochrome-specific, light blue box). The N-terminal domain carries the chromophore. In bacterial phytochromes (Bphs) and fungal phytochromes (Fphs), the chromophore biliverdin IXα (BV, depicted as green pentagons) is bound to the PAS domain, although located in the GAF domain. In cyanobacterial phytochromes (Cphs), the chromophore phycocyanobilin (PCB, depicted as cyan pentagons) is bound within the GAF domain. Plant phytochromes (Phys) chromophore-binding site is also the GAF domain, albeit phytochromobilin (PΦB, depicted as dark green pentagons) is attached instead of PCB. The composition of the C-terminal regulatory domain is more variable. In Bphs, Cphs and Fphs, it consists of a bacterial-type histidine kinase (HKD, red box) and a response regulator (REC, purple circle). The REC domain is fused to the HKD in Fphs, whereas in Bphs and Cphs is located farther away. The C-terminal of Phys consists of 2 PAS domains (dark grey boxes) and a serine/threonine kinase domain (HKRD, red box).
The mechanism of prototypical phytochrome activity involves a photoisomerization (bottom). Absorption of red light (RL) by the phytochrome ground state red-absorbing form (Pr) induces photoisomerization to the far-red light-absorbing form (Pfr). Pfr reverts to Pr upon far-red light illumination (FRL) or dark reversion (DR). A photoisomerization in the opposite direction is representative of bathy phytochromes.

The photosensory part is particularly conserved among bacteria, fungi, algae and plants and is composed of contiguous PAS-GAF-PHY domains (Burgie *et al.*, 2014; Rockwell & Lagarias, 2020). The PAS (Per-Arnt-Sim) domain is generally responsible for signaling. The GAF (cGMP-specific phosphodiesterases/adenylyl cyclases/FhlA) is not associated with any known enzymatic activity and represents the site of bilin attachment in Phys and cyanobacterial phytochromes (Cphs). Finally, PHY consists of a phytochrome-specific

domain distantly related to PAS and occasionally involved in photoisomerization (Fischer *et al.*, 2020). A loop specifically intertwines the PAS and GAF domains, whereas the PHY is separated from the first two via the so-called tongue, a hairpin-like structure (Anders *et al.*, 2014; Essen *et al.*, 2008; Hughes, 2010; Yang *et al.*, 2008). The C-terminal is the most variable region. In Phys, two PAS are followed by a histidine kinase-related domain (HKRD). However, this HKRD does not exhibit a typical mechanism since it lacks the conserved phosphoryl group-accepting histidine residue and ultimately acts as a serine/threonine kinase (Cashmore, 1998; Elich & Chory, 1997; Yeh *et al.*, 1997; Yeh & Lagarias, 1998). The opposite is true for bacterial (Bphs), cyanobacterial and fungal phytochromes (Fphs), where the regulatory function is, indeed, carried out by a typical two-component histidine kinase mechanism (TC-HKs) (Bhoo *et al.*, 2001; Brandt *et al.*, 2008; Hérivaux *et al.*, 2016; Psakis *et al.*, 2011; Wahlgren *et al.*, 2022). In particular, the TC-HK motif of Fphs is fused to the response regulator receiver (REC) domain, case that is only found in rare examples of Bphs and Cphs (Brandt *et al.*, 2008; Brych *et al.*, 2021; Heintzen, 2012; Sharrock, 2008).

As aforementioned, the ability of phytochromes to perceive light dwells on the binding of a bilin chromophore and light-stimulated responses are elicited by its conformational changes (Bongards & Gärtner, 2010; Grombein *et al.*, 1975; Lagarias & Rapoport, 1980; Rockwell & Lagarias, 2006; Rüdiger & Thümmler, 1994; Siegelman *et al.*, 1966). Generally, in the absence of light, prototypical phytochromes are assembled in the cytoplasm and adapt a red light-absorbing conformation (Pr). The absorption of red light converts the Pr-isoform into the far-red light-absorbing conformation (Pfr) and triggers the translocation to the nucleus, where several signaling mechanisms take place (Huq *et al.*, 2003; Kevei *et al.*, 2007; Kircher *et al.*, 2002; Klose *et al.*, 2015; Li *et al.*, 2011; Matsushita *et al.*, 2003). The phytochrome can revert to the ground Pr state in case of absorption of far-red light or incubation in the dark, by means of a process named dark/thermal reversion (DR) (Braslavsky *et al.*, 1997; Furuya & Schäfer, 1996; Klose *et al.*, 2020; Medzihradszky *et al.*, 2013; Schäfer & Nagy, 2006; Taylor, 1968) (Figure 1.3). Contrastingly, in a second type of bacterial phytochromes, named bathy phytochromes, the ground state is the Pfr and, therefore, the direction of the DR is inverted (Huber *et al.*, 2024; Rottwinkel *et al.*, 2010; Tasler *et al.*, 2005). The Pr ↔ Pfr transition is elicited by a C15 isomerization of the bilin chromophore: in Pr, the bilin adopts a C15-*Z*,anti conformation, and the isomerization to C15-*E*,anti leads to the formation of Pfr (Chen *et al.*, 2004; Fodor *et al.*, 1988; Kneip *et al.*, 1999; Matysik *et al.*, 1995). Differences between canonical plant phytochromes and bacterial/fungal phytochromes are mostly related to the chromophore and the attachment region. Phys use phytochromobilin (PΦB), which is autocatalytically attached to a conserved Cys in the N-terminal GAF (Cornejo, 1992; Fischer *et al.*, 2005; Lagarias & Lagarias, 1989; Lagarias & Rapoport, 1980; Terry *et al.*, 1995). Interestingly, streptophyte algae, the clade within which land plants evolved, were shown to

employ a PCB chromophore (Rockwell *et al.*, 2017; Wu *et al.*, 1997). PCB is also the chromophore of Cphs and is attached to the conserved GAF-Cys, as in Phy (Fischer *et al.*, 2005; Montgomery & Lagarias, 2002; Nagano, 2016). Bphs and Fphs use BV instead and, in contrast to Phys and Cphs, attach it to a Cys in a region preceding the PAS domain (Lamparter *et al.*, 2002, 2004; Wagner *et al.*, 2005; Yang *et al.*, 2008). Ultimately, the presence of different chromophores leads to an enormous spectral diversity, with a covered light spectrum between 610 and 760 nm.

Some exceptions are worthy of mention. Among Bphs, the photosynthetic plant symbiont *Bradyrhizobium* sp. ORS278 bears three phytochromes and one of them, *Br*BphP3, binds PCB and not BV (Jaubert *et al.*, 2007). This BphP exhibits an unusual ground state orange-absorbing form (Po) with maximum absorption at 610 nm and an active Pr absorbing at 670 nm, being, thus far, the phytochrome absorbing the shortest wavelength reported. Moreover, its C-terminal does not find homology with any other Bph. These, together with several other uncommon properties, led to the conclusion that this phytochrome was acquired via lateral gene transfer and serves for measuring light intensity rather than quality (Jaubert *et al.*, 2007).

Moving to cyanobacteria, CphB of *Fremyella diplosiphon*, which lacks the typical GAF-Cys, naturally binds BV. However, the attachment of BV is not covalent and substitution with PCB was shown to be possible *in vitro* (Quest *et al.*, 2007).

While the bilin D-ring is important for photoisomerization, its A-ring is the moiety effectively being recognized by the phytochrome. Phytochromes are endemically promiscuous since they can additionally accommodate bilins other than the natural one, as long as the A-ring configuration is conserved (Lagarias & Rapoport, 1980; Li & Lagarias, 1992; Xu *et al.*, 2019). Indeed, Phys and Cphs covalently attach bilins with A-ring C3 ethylidene moiety (PCB, PEB, PΦB, PUB), whereas Bphs and Fphs only recognize an endo-vinyl group (BV, 15,16-DHBV, 18^1,18^2-DHBV). Nonetheless, the attachment of a bilin lacking the C15=C16 double bond prevents photoisomerization. This event leads to an insufficient de-excitation of the chromophore and the formation of a fluorescent product named phytofluor (Murphy & Lagarias, 1997).

1.4 The biosynthesis of bilins is prerogative of ferredoxin-dependent bilin reductases

The precursor to most open chain tetrapyrroles, bilins included, is the cyclic tetrapyrrole heme. The first step in bilin biosynthesis is the cleavage of the heme macrocycle by electron- and oxygen-dependent heme oxygenases (Ortiz De Montellano, 2000; Wilks, 2002; Yoshida & Migita, 2000) (Figure 1.4). The electron source is organism-dependent: heme oxygenases from bacteria and photosynthetic eukaryotes use [2Fe-2S]-ferredoxins (Fd), whereas the ones from mammals are NADPH-cytochrome P450 reductase dependent (Beale & Cornejo,

1984a; Frankenberg-Dinkel, 2004; Muramoto *et al.*, 1999; Rhie & Beale, 1992; Schacter *et al.*, 1972; Wang *et al.*, 2007; Wang & Ortiz de Montellano, 2003; Wilks & Schmitt, 1998). This reaction can result in four different isomer products (biliverdin IXα, IXβ, IXγ and IXδ), depending on the oxidized carbon bridge (Benedikt *et al.*, 1988; Cunningham *et al.*, 2000; Gisk *et al.*, 2012; Paiva-Silva *et al.*, 2006; Ratliff *et al.*, 2001). Although all four isomers are found in nature, the most abundant is biliverdin IXα (BV) (Bonnett & McDonagh, 1973; Frankenberg & Lagarias, 2003a; Koglin & Behrends, 2002; Montorzi *et al.*, 2002; Muramoto *et al.*, 2002; Ó Carra & Colleran, 1969; Pendrak *et al.*, 2004; Pereira *et al.*, 2007). The production of BV, through the oxidation of the heme α-meso bridge, concomitantly liberates CO and Fe^{2+} (Kikuchi *et al.*, 2005; Tenhunen *et al.*, 1968, 1969).

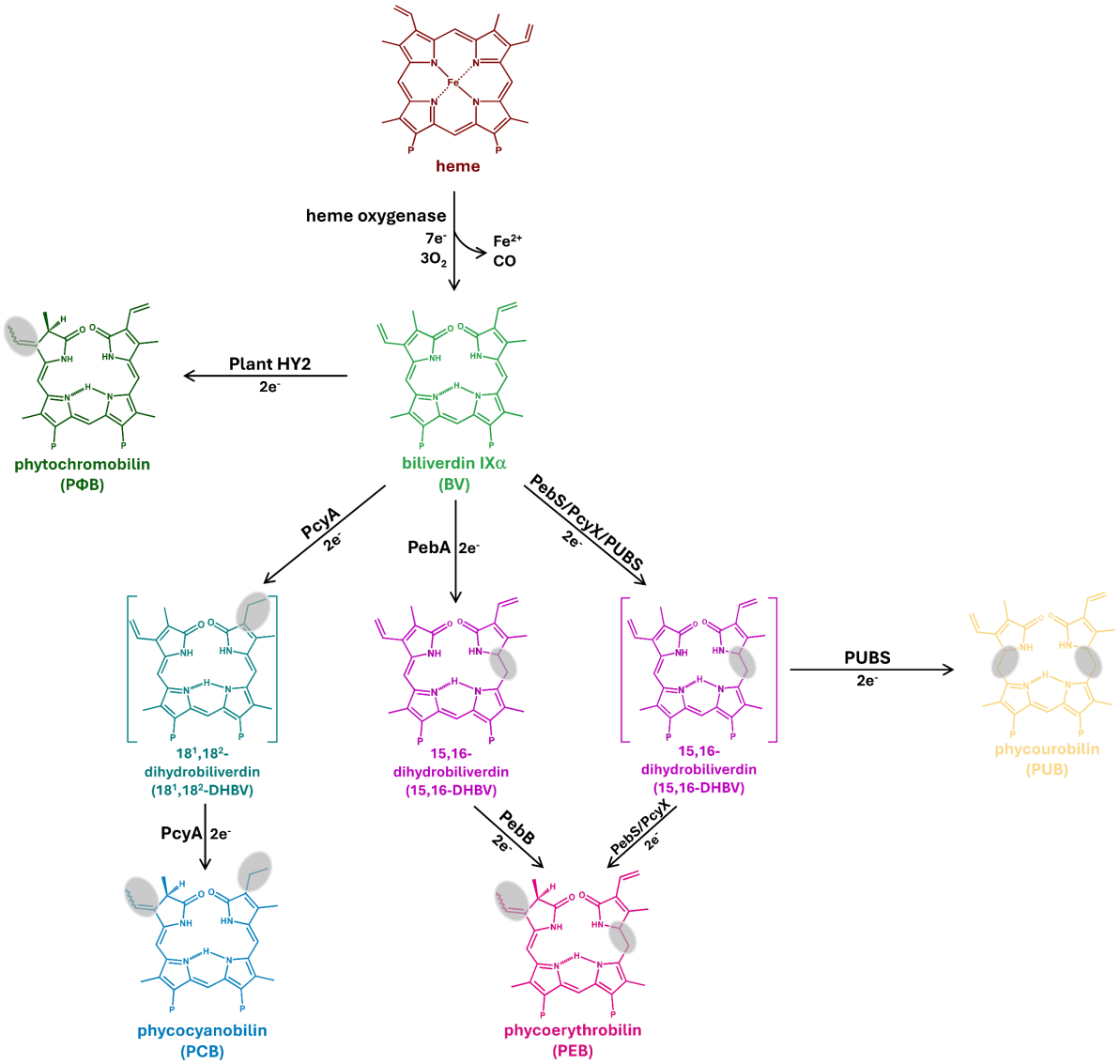

Figure 1.4 Overview of the reactions catalyzed by characterized FDBRs.
Biliverdin IXα (BV), the universal precursor of bilins, is the product of the oxidation of heme α-meso bridge by heme oxygenase. BV is the substrate for all FDBRs except for PebB. "P" indicates the propionate side chains. Wavy bonds at the A-ring indicate the possible occurrence of two $C3^1$ stereoisomers. Bilins represented in brackets are intermediates not being released from the active site during the reaction.
The enzyme phytochromobilin synthase (HY2) catalyzes the $2e^-$ reduction of BV to phytochromobilin in plants. In Cyanobacteria, Glaucophytes and Chlorophytes, PcyA mediates the $4e^-$ reduction of BV to phycocyanobilin, via

$18^1,18^2$-dihydrobiliverdin. In Cyanobacteria, Rhodophytes and Cryptophytes, PebA catalyzes the reduction of BV to 15,16-dihydrobiliverdin (15,16-DHBV). 15,16-DHBV acts as the substrate for PebB. The $2e^-$ reduction of 15,16-DHBV mediated by PebB yields phycoerythrobilin. In phages, PebS and PcyX couple PebA and PebB in a single $4e^-$-dependent reaction. PUBS, solely discovered in Viridiplantae, catalyzes the $4e^-$ reduction of BV to phycourobilin via 15,16-DHBV.

Following this universal reaction, BV can be further reduced by a class of regio-specific enzymes named ferredoxin-dependent bilin reductases (FDBRs) in a phylogenetic-related manner (Dammeyer & Frankenberg-Dinkel, 2008; Rockwell & Lagarias, 2017a). Chronologically speaking, the first FDBR to ever be characterized was phytochromobilin synthase (HY2) from *Avena sativa* L. cv Garry. HY2 catalyzes the $2e^-$ reduction of BV A-ring $2,3,3^1,3^2$-diene system to PΦB, the phytochrome chromophore (McDowell & Lagarias, 2001). Cyanobacteria and algae, where bilins are employed as chromophores in PBPs and phytochromes, encode several other FDBRs. The biosynthesis of PCB, attached to PC and APC and employed in photoreceptors of cyanobacteria and streptophyte algae, requires a $4e^-$ reduction of BV catalyzed by phycocyanobilin:ferredoxin oxidoreductase (PcyA). The reaction starts with the reduction of the $C18^1$-$C18^2$ exo-vinyl group to yield the transient intermediate $18^1,18^2$-DHBV and proceeds with the reduction of the A-ring $2,3,3^1,3^2$-diene system (Frankenberg & Lagarias, 2003b; Hagiwara *et al.*, 2010; Tu *et al.*, 2004, 2007). Interestingly, *pcyA* was also found in cyanophage genomes and its protein product proven to be involved in the same reaction as cyanobacterial and algal sequences (Dammeyer *et al.*, 2008a). Additionally, *pcyA* homologs are present in genomes of organisms lacking PBSs and phytochromes as *Chlamydomonas reinhardtii* and *Prochlorococcus*. In *C. reinhardtii*, *PCYA* was demonstrated to be an essential gene and to be involved in bilin-based retrograde signaling, specifically related to the detoxification of reactive oxygen species and iron acquisition (Duanmu *et al.*, 2013). On the other hand, the function of *pcyA* in *Prochlorococcus* is still enigmatic (Dammeyer *et al.*, 2007; Wiethaus *et al.*, 2010).

Although being a tetrahydrobiliverdin like PCB, the biosynthesis of PEB is achieved by two subsequent FDBR reactions. In the first step, BV is reduced at the C15=C16 methine bridge to 15,16-DHBV by 15,16-dihydrobiliverdin:ferredoxin oxidoreductase (PebA) (Busch *et al.*, 2011b). 15,16-DHBV is then directly delivered via metabolic channeling to phycoerythrobilin:ferredoxin oxidoreductase (PebB) which subsequently reduces its A-ring, similarly to HY2 and PcyA although with a different substrate specificity (Aras *et al.*, 2020; Dammeyer *et al.*, 2008a; Sommerkamp *et al.*, 2019). Cyanophages, on the other hand, combine PebA and PebB activity in only one enzyme, phycoerythrobilin synthase (PebS) (Dammeyer *et al.*, 2008a; Busch *et al.*, 2011a). Additionally, PcyX, discovered in marine phage metagenomes, works similarly to PebS although showing highest sequence homology to PcyA (Ledermann *et al.*, 2016, 2018).

The yellow chromophore phycourobilin (PUB) can be found in cyanobacteria and red algae as PBP chromophore (Bryant *et al.*, 1981; Glazer, 1994a; Hess *et al.*, 1996; Ma *et al.*, 2020; Ritter *et al.*, 1999; Sepúlveda-Ugarte *et al.*, 2011; Swanson *et al.*, 1991; Vásquez-Suárez *et al.*, 2018; Wilbanks & Glazer, 1993; Yu *et al.*, 1981). In these organisms, PUB is synthesized from PEB via isomerization (Blot *et al.*, 2009; Carrigee *et al.*, 2021, 2022; Shukla *et al.*, 2012). However, a little bit over ten years ago, a new FDBR responsible for the $4e^-$ reduction of BV to PUB was discovered in the Bryophyta *Physcomitrium patens*. This FDBR, named phycourobilin synthase (PUBS), was shown to catalyze the subsequent reductions of the C15=C16 and C4=C5 methine bridges of BV, yielding 15,16-DHBV as intermediate (Chen *et al.*, 2012). Therefore, alongside PebA, PUBS is the only other FDBR not being able to reduce BV A-ring 2,3,3^1,3^2-diene system.

1.4.1 FDBRs share a common structural pattern and reaction mechanism

Despite their relatively low sequence identity, FDBRs share a common structural pattern (Ledermann *et al.*, 2017; Sommerkamp *et al.*, 2019; Sugishima *et al.*, 2020) (Figure 1.5A - F).

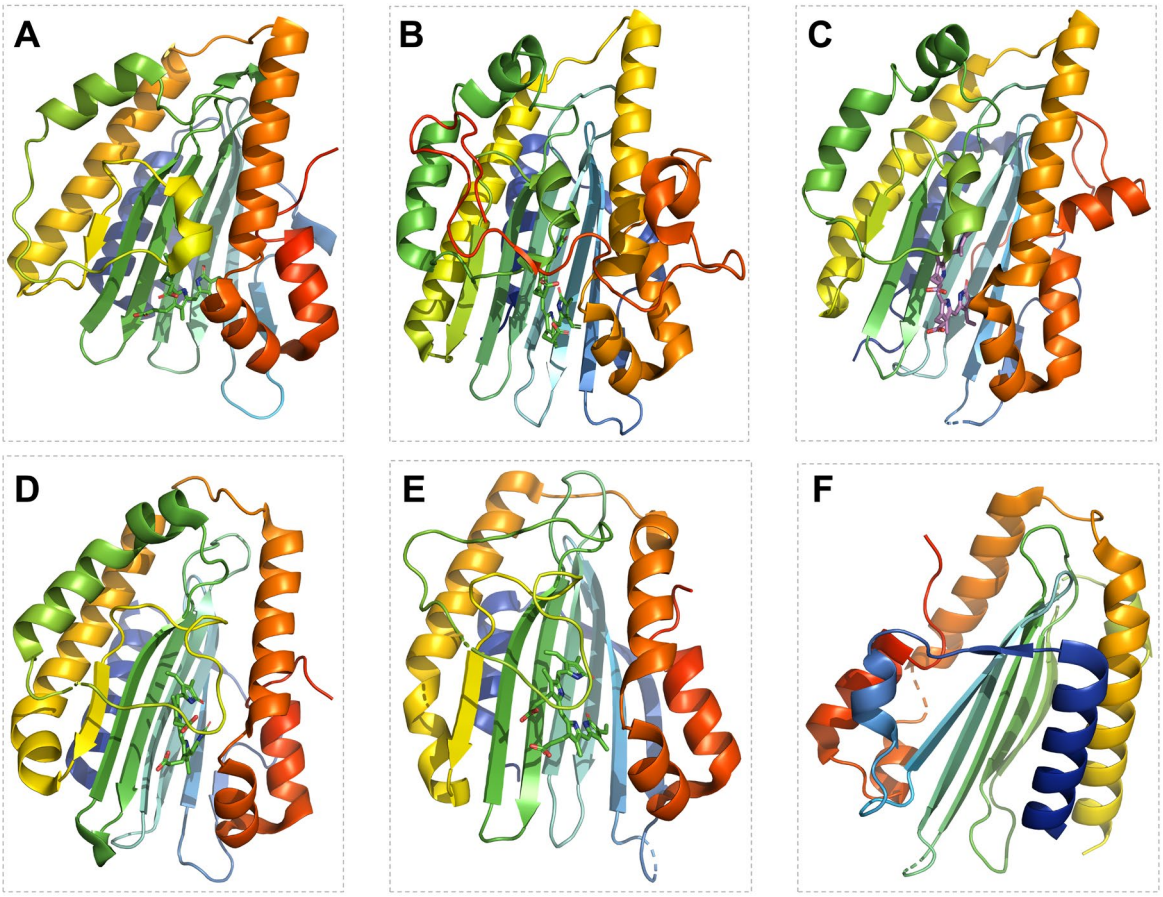

Figure 1.5 Experimentally determined FDBR structures.
FDBR structures are displayed in cartoon representation and colored from the N-terminal (blue) to the C-terminal (red) using the PyMOL rainbow pre-set (DeLano, 2020). Co-crystallized BV substrate is shown as green sticks representation in the active site of A, B, D, E. Co-crystallized 15,16-dihydrobiliverdin substrate is shown as violet sticks representation in the active site of C.

(A) Crystal structure of PcyA from *Synechocystis* sp. PCC 6803 (PDB accession code: 2D1E).
(B) Crystal structure of HY2 from *Solanum lycopersicum* (PDB accession code: 6KME).
(C) Crystal structure of PEBB from *Guillardia theta* (PDB accession code: 6QX6).
(D) Crystal structure of PebA from *Synechococcus* sp. WH 8020 (PDB accession code: 2X9O).
(E) Crystal structure of PebS from P-SSM2 (PDB accession code: 2VCK).
(F) Crystal structure of PcyX from phage marine metagenome (PDB accession code: 5OWG).

All FDBRs exhibit a monomeric globular structure with a central a six- or seven-stranded antiparallel β-sheet flanked by 5-10 α-helices, generating an α/β/α-sandwich fold. The active site is located between the β-sheet and the C-terminal α-helices and, in most cases, accommodates BV (except PebB) in a cyclic porphyrin-like conformation, with the A- and D-ring buried in the cavity and the two propionate side chains exposed to the solvent (Hagiwara *et al.*, 2006a; Dammeyer *et al.*, 2008b). Ferredoxin, bound to the basic patch of the substrate binding site, directly transfers electrons to BV through the propionate groups (Hagiwara *et al.*, 2006a). As Fd is only able to transfer one electron at a time, the reactions proceed via the formation of radical intermediates (Frankenberg & Lagarias, 2003b; Busch *et al.*, 2011a; Busch *et al.*, 2011b; Ledermann *et al.*, 2018; Tu *et al.*, 2004; Tu *et al.*, 2007; Tu *et al.*, 2008). In particular, the reaction starts with the binding of Fd and the substrate to the active site, facilitated by interactions with cationic residues. Fd donates an electron to the substrate, leading to the formation of a radical species. The radical intermediate is then substrate for protonation by water molecules or acidic residues of the catalytic site. The reaction mechanism terminates with the transfer of additional electrons from Fd to yield the final phycobilin product (Busch *et al.*, 2011a; Unno *et al.*, 2015).

1.4.2 The activity of FDBRs is contingent on acidic residues and substrate binding mode

The first FDBR structure to be solved was the one of PcyA from *Synechocystis* sp. PCC 6803 (*Syn*PcyA) (Hagiwara *et al.*, 2006a) (Figure 1.6A). X-ray crystallization revealed the importance of three catalytic residues in light of the radical reaction mechanism: Glu^{76}, His^{88}, Asp^{105}. Reaction is initiated by the protonation of BV mediated by the carboxyl group of Asp^{105}, while Glu^{76} is responsible for the second protonation at the D-ring exo-vinyl. The involvement of His^{88} was evident but its role has been enigmatic until the structure of *Nostoc* sp. PCC 7120 PcyA (*Nos*PcyA) was solved. This residue participates first in D-ring reduction, helping the transfer of the second proton, and gets re-protonated for the successive steps by a proton relay system starting from the bulk solvent (Tu *et al.*, 2007). The proton relay system was subsequently found to be guaranteed by Ile^{86}, which plays a key role in stabilizing BVH^+ (Hagiwara *et al.*, 2016; Joutsuka *et al.*, 2023). Site-directed variants of *Nos*PcyA reinforced the proposed involvement of these three residues in BV reduction. *Nos*PcyA_D102N (where Asp^{102} corresponds to *Syn*PcyA Asp^{105}) and *Nos*PcyA_H85Q (where His^{85} corresponds to

*Syn*PcyA His[88]) almost completely lost catalytic activity, in accordance with their supposed involvement in the initial D-ring exo-vinyl reduction (Kabasakal *et al.*, 2013; Tu *et al.*, 2007). The substitution of Glu[73] (Glu[76] in *Syn*PcyA) to a Gln led to a variant retaining the ability to reduce BV A-ring endo-vinyl to PΦB, therefore changing reduction regiospecificity and mimicking HY2 activity (Tu *et al.*, 2007). The ineffectiveness in producing 18^1,18^2-DHBV ultimately confirmed the essential role of this residue for D-ring reduction. Another residue essential for correct *Syn*PcyA functioning is Val[225]. The exchange of this residue elicits serious effects the surface potential in the active site, resulting in an alteration of BV binding (Wada *et al.*, 2010).

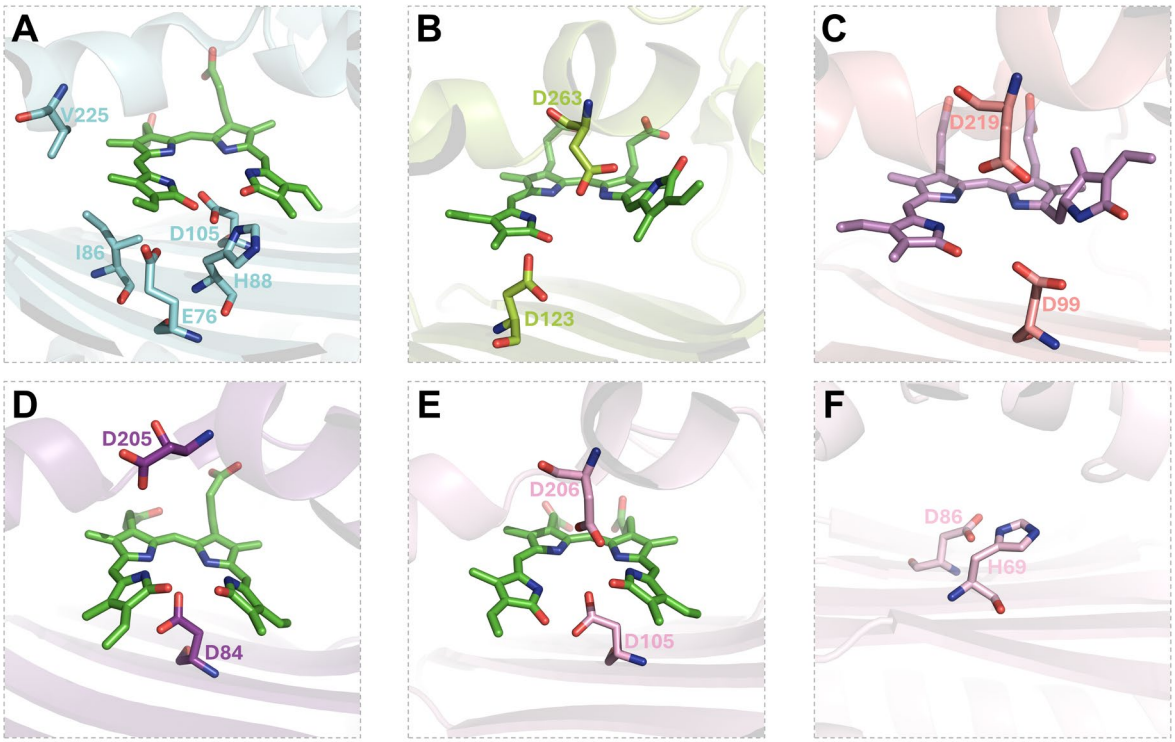

Figure 1.6 Overview of the active sites of crystallized FDBRs and the residues directly involved in catalysis.
(A) Active site of PcyA from *Synechocystis* sp. PCC 6803 (PDB accession code: 2D1E) displayed as transparent aquamarine cartoon. Amino acid residues essential for catalysis are labeled and shown as aquamarine sticks. BV is represented as green sticks.
(B) Active site of HY2 from *Solanum lycopersicum* (PDB accession code: 6KME) displayed as transparent limon cartoon. Amino acid residues essential for catalysis are labeled and shown as limon sticks. BV is represented as green sticks.
(C) Active site of PEBB from *Guillardia theta* (PDB accession code: 6QX6) displayed as transparent salmon cartoon. Amino acid residues essential for catalysis are labeled and shown as salmon sticks. 15,16-dihydrobiliverdin is represented as violet sticks.
(D) Active site of PebA from *Synechococcus* sp. WH 8020 (PDB accession code: 2X9O) displayed as transparent violetpurple cartoon. Amino acid residues essential for catalysis are labeled and shown as violetpurple sticks. BV is represented as green sticks.
(E) Active site of PebS from P-SSM2 (PDB accession code: 2VCK) displayed as transparent pink cartoon. Amino acid residues essential for catalysis are labeled and shown as pink sticks. BV is represented as green sticks.
(F) Active site of PcyX from phage marine metagenome (PDB accession code: 5OWG) displayed as lightpink transparent cartoon. Amino acid residues essential for catalysis are labeled and shown as lightpink sticks. The structure was crystallized in the absence of substrate.

The reaction mechanism of HY2, after initial indication gained for the *Arabidopsis thaliana* enzyme (*At*HY2), was further clarified following the crystallization of the ortholog from *Solanum lycopersicum* (*Sl*HY2) (Sugishima *et al.*, 2020; Tu *et al.*, 2008) (Figure 1.6B). The most striking feature is the binding of BV: in contrast to PcyA, HY2 binds BV in a flipped binding mode, with reversed A- and D-ring positioning and with the D-ring tilted out of the gross planar conformation (Hagiwara *et al.*, 2006a, 2006b; Sugishima *et al.*, 2020). This *ZZZssa* conformation is stabilized by Arg^{259} and might also be a consequence of the substitution of the typical PcyA Asp residue (*Syn*PcyA Asp^{105}) with an Asn (*Sl*HY2 Asn^{140}), which may destabilize the *syn* conformation of the C15=C16 double bond. The reduction of BV A-ring to PΦB is carried out by the two acid catalysts Asp^{123} and Asp^{263}. The substitution of these with Asn in single variants resulted in loss of catalytic activity with slight reducing ability retained only by *Sl*HY2_D123N, similarly to what shown for *At*HY2 (Sugishima *et al.*, 2020; Tu *et al.*, 2008).

Although accommodating a different substrate, PebB partially shares the binding mode with HY2 (Sommerkamp *et al.*, 2019). The structure of *Guillardia theta* PEBB (*Gt*PEBB) revealed 15,16-DHBV is bound in a *ZZZssa* configuration (Figure 1.6C). However, the enzyme retains the Asp residue forming the hydrogen bond with the lactam oxygen of A-ring and therefore the substrate is closer toward the entrance of the binding pocket than in *Sl*HY2 (Sommerkamp *et al.*, 2019). In this case too, responsible for the reduction of 15,16-DHBV to PEB is an Asp pair with the additional assistance of an Arg: Asp^{99} transfers a proton to the A-ring forming a protonated 15,16-DHBV$^+$ and, after the acceptance of an e^- from Fd, Asp^{219} and Arg^{215} enable tautomerization. The determinant for the second protonation step remains unclear (Busch *et al.*, 2011b; Sommerkamp *et al.*, 2019).

The only other $2e^-$ reducing FDBR is PebA. The structure of PebA from *Synechococcus* sp. WH 8020 reveals a *ZZZ*-all-*syn* substrate binding mode, albeit BV adopts an unusual roof-like conformation with both A- and D-ring tilted 40° out of the plane (Busch *et al.*, 2011b) (Figure 1.6D). Moreover, the conserved Asp (here Asp^{205}) is facing outside of the active site, proving its systematic involvement only in A-ring reduction. Here, Asp^{84} is responsible for the C15=C16 double bond reduction.

PebS shows a high substrate-binding pocket flexibility with two possible BV binding modes: besides the usual porphyrin-like, BV can also be accommodated in a helical conformation (Dammeyer *et al.*, 2008b). Moreover, by combining PebA and PebB activities, its function relies on an Asp pair: Asp^{206} and Asp^{105}. PebS_D206N is able to reduce BV to 15,16-DHBV, proving the involvement of Asp^{206} only in A-ring reduction (in accordance with PcyA, HY2 and PebB). On the other hand, PebS_D105N is at all inactive and therefore Asp^{105} is essential for the first step, i.e. the reduction of BV C15=C16, which precedes A-ring reduction (Busch *et al.*, 2011a) (Figure 1.6E).

Although sharing high homology with PcyA, PcyX catalyzes the reduction of BV to PEB. The reaction proceeds similarly to the one catalyzed by PebS but with a much slower substrate turnover rate (Ledermann *et al.*, 2016). As true for PcyA, the His (*Syn*PcyA His^{88} - PcyX His^{69}) and Asp (*Syn*PcyA Asp^{105} - PcyX Asp^{86}) residues are indeed critical for PcyX-catalyzed reduction of BV, specifically in the frame of D-ring reduction (Figure 1.6F). The main divergence relates to the residue corresponding to *Syn*PcyA Glu^{76}: in PcyX, the corresponding residue, Asp^{55}, was shown, via site-directed mutagenesis studies, not to play the critical exo-vinyl reduction role. Moreover, as PcyX lacks PebS Asp^{206}, the A-ring reduction might work in a similar proton-relay context as in PcyA (Ledermann *et al.*, 2018). Hitherto, PUBS is the only FDBR member whose structure has still not been determined. Ultimately, although showing a similar overall fold, the combination of specific catalytic residues and binding mode of the substrate dictates the reaction specificity of FDBRs.

1.5 Phylogeny and evolution of ferredoxin-dependent bilin reductases: the disruptive divergence caused by primary endosymbiosis

Several studies provide strong indication that bilin biosynthesis is ubiquitous and essential among oxygenic photosynthetic organism, however the origin of FDBRs still remains enigmatic. FDBRs clade in three lineages: PcyA, PebA/PebS/PUBS and PebB/HY2. The PcyA lineage comprises cyanobacterial and algal sequences. PebA/PebS/PUBS is present in cyanophages, cyanobacteria, red algae, streptophytes and cryptophytes. PebB/HY2 is present in cyanobacteria, red algae, streptophytes and cryptophytes (Rockwell & Lagarias, 2017a). In accordance with the phylogenetic tree of life, given that the first bilin biosynthesis reported occurs in cyanobacteria, one could argue that either PcyA or PebA/PebB would be the first appearing FDBR. More hints point toward PcyA being the precursor of all FDBRs since *pcyA* is a ubiquitous and essential gene for photosynthetic cyanobacteria, in contrast to *pebA* and *pebB*, which are also exclusively found in PEB-containing cyanobacteria (Alvey *et al.*, 2011b). However, speculating that the first occurring FDBR was already characterized by a $4e^-$ reduction ability poses a risk. Indeed, it would seem far more plausible to consider a $2e^-$ reducing ability as the initial evolutionary step. Several new genomes have been sequenced in the past years and helped in trying to put the pieces together to underline a path for FDBRs evolution. Firstly, around half a decade ago *pcyA* genes were also found in α-proteobacteria and phylogenetic analysis revealed these sequences did not descend from cyanobacterial ones (Ledermann *et al.*, 2018). In particular, these genes clade, together with PcyX, in a newly described FDBR lineage, named AX clade (Ledermann *et al.*, 2018; Rockwell *et al.*, 2023). Only last year, FDBR-related genes were also found in heterotrophic bacteria. These so-called pre-PcyAs (or pre-FDBRs) form three distinct clades: pre-1, pre-2

and pre-3 (Rockwell *et al.*, 2023). Pre-1 and Pre-2 sequences are found in both metagenome-assembled genomes (MAGs) and cultured organism, whereas Pre-3 is exclusively found in MAGs. Additionally, while Pre-1 is present in several phyla (β- and γ-proteobacteria, Acidobacteria, Planctomycetes, Verrucomicrobia and others), Pre-2 and Pre-3 are almost exclusively limited to δ-proteobacteria. Pre-2 and Pre-3 are typically encoded in a cluster with heme oxygenase and bilin-biosynthesis associated globins (BBAGs). Pre-1 clusters exhibit a higher degree of heterogeneity, with instances where bilin-related genes are located farther away from it. These pre-PcyAs exhibit significant divergence from the canonical cyanobacterial PcyAs, particularly concerning the active site. As previously mentioned, PcyA activity is strictly dependent on a Glu-His-Asp triad. However, these pre-PcyA lineages display systematic variations in these residues. Notably, both Glu and His are consistently absent across all of them. Pre-1 lacks the entire triad (except for one member containing the Asp), while Pre-2 and Pre-3 possess the Asp. The indirect investigation of the activity of one member from each clade hinted at the inability to catalyze PCB production (Rockwell *et al.*, 2023). These findings imply that canonical PcyA potentially evolved from these pre-PcyA sequences.

Archaeplastidal FDBRs were discovered not to have evolved from cyanobacterial sequences, suggesting a substantial divergence since primary endosymbiosis (Rockwell & Lagarias, 2017a). *PCYA* genes can be found in Glaucophytes, two clades of Cyanidiophyceae and Chlorophytes. The presence of only PCYA in Glaucophytes is in accordance with their PBS and phytochrome composition (Watanabe *et al.*, 2012). Of particular interest is the case of the Cyanidiophyceae, the earliest diverging Rhodophytes. This class comprises four clades: Cyanidioschyzonales, Cyanidiales, Cavernulicolales and Galdieriales (Park *et al.*, 2023). Despite their classification as red algae, all Cyanidiophyceae members actually exhibit a dark green coloration due to their pigment composition. Specifically, the PBS of these organism is solely made of the APC core and PC rods, with PE lacking completely (Lin *et al.*, 1990; Ohta *et al.*, 2003; Seckbach, 1995, 2010; Van Etten, 2020). *PCYA* genes can be found in the Cyanidioschyzonales and Cyanidiales, whereas no nuclear genome is hitherto available for the Cavernulicolales. In stark contrast to their PBS composition, the Galdieriales exclusively possess *PEBA* and *PEBB*. The presence of *PEBA* and *PEBB*, instead of *PCYA*, raises a significant question on PCB biosynthesis. Over 30 years ago, PCB was postulated to be produced via PEB isomerization in *Galdieria sulphuraria* (back then misclassified as *Cyanidium caldarium*) (Beale & Cornejo, 1991a, 1991b, 1991c). However, to date, the enzyme responsible for this reaction is still unknown. A similar scenario is also theoretically envisioned to occur in Rhodophytina. The PBS of these organisms exhibits a more elaborate structure, including PE rods, yet no *PCYA* homolog is found in their genomes.

The rise of the Viridiplantae, including Streptophyta and Chlorophyta, was accompanied by the loss of the phycobilisome (Green, 2019; Koziol *et al.*, 2007; Kunugi *et al.*, 2016). In these organisms, light harvesting primarily relies on the photosystems and their associated chlorophyll-binding proteins (Ago *et al.*, 2016; Alboresi *et al.*, 2008; Caffarri *et al.*, 2009; Caspy *et al.*, 2021; Iwai *et al.*, 2024; Neilson & Durnford, 2010). Nevertheless, both lineages are still endowed with FDBRs and bilins (Rockwell *et al.*, 2017; Rockwell & Lagarias, 2017b). Although some green algae also lack phytochromes, they still possess PCYA, and its function might be related to the retrograde signaling pathway already demonstrated in *C. reinhardtii* (Duanmu *et al.*, 2013). Streptophytes encompass streptophyte algae and, their descendent, land plants (Becker & Marin, 2009; Bierenbroodspot *et al.*, 2024; Donoghue & Clark, 2024; Harris *et al.*, 2022; Wodniok *et al.*, 2011). Streptophyte algae are able to perform light sensing through phytochromes, similarly to land plants. However, while land plants employ PΦB as the phytochrome chromophore, streptophyte algae were shown to use PCB (Rockwell *et al.*, 2017; Wu *et al.*, 1997). The first evidence of a PCB-phytochrome was obtained in *Mesotaenium caldariorum*, where PCB biosynthesis was also revealed to proceed through the formation of PΦB as the intermediate (Wu *et al.*, 1997). Phylogenetic analysis revealed that, as land plants, streptophyte algae do not harbor PCYA but only HY2, raising questions on PCB biosynthesis. Two decades later, indirect studies pointed toward a HY2-synthesized PCB in the alga *Klesbormidium nitens* (back then misclassified as *Klebsormidium flaccidum*) (Rockwell *et al.*, 2017). In addition to HY2, some streptophytes were also shown to bare a Viridiplantae-specific FDBR named PUBS. PUBS was firstly discovered in the Bryophyta *Physcomitrium patens*, where it was proven to catalyze the reduction of BV to PUB (Chen *et al.*, 2012). The emergence of new sequenced genomes has uncovered candidate PUBS sequences in several streptophyte algae. Nevertheless, besides speculations drawn from the behavior of phenotypic *P. patens* mutants, the physiological function of this chromophore, and therefore of the corresponding FDBR, is still unknown (Chen *et al.*, 2012).

1.6 Objectives of this work

The present study is mainly focused on tracing the evolution of PCB biosynthesis from its origin to the great divergence stemmed from primary endosymbiosis. The increasing availability of sequenced genomes has allowed for the identification of FDBR sequences in heterotrophic, non-photosynthetic bacteria, paving the way for a better understanding of the emergence of this enzyme family. In this work, an initial characterization of these newly discovered enzymes was performed, shedding light on the development of a functional PCB-biosynthetic PcyA. The primary endosymbiosis event giving rise to Archaeplastida resulted in an increased intricacy of PCB-biosynthesis. In Rhodophytes, PCYA, required for PCB biosynthesis within PBS employment, was lost and theoretically substituted by a PEB to PCB

isomerase. The inability to record previously confirmed isomerase activity in *Galdieria sulphuraria*, prompted a heterologous characterization of the harbored FDBRs, *Gs*PEBA and *Gs*PEBB, and a bioinformatic study to confirm the need of this new, unidentified enzyme with chromophore isomerase activity. Finally, streptophyte algae, the clade within which land plants evolved, are endowed with PCB-containing phytochromes but lack a *PCYA* homolog. The HY2 of the streptophyte alga *Klebsormidium nitens* has been indirectly indicated to be responsible for PCB biosynthesis, in contrast to its phylogenetic classification. This study provides a comprehensive biochemical characterization of this unusual HY2, offering insights into the reaction mechanism. The characterization of two other members of the HY2 lineage ultimately led to underlining the evolution of this FDBR lineage among Streptophytes. Lastly, a brief section of this thesis focuses on the initial characterization of PUBS activity in streptophyte algae. This enzyme, involved in PUB biosynthesis in Viridiplantae, was discovered around a decade ago but its characterization has since received limited attention.

2 Materials and methods

2.1 Material and chemicals

2.1.1 Equipment

Table 2.1 Devices.

Instrument	Name	Manufacturer
Agarose gel electrophoresis chamber	MAXI VARIGEL 700-7213	VWR
Autoclave	VX 150	Systec
Centrifuges & Rotors	Sorvall LYNX 6000; rotors F9 and T29 5810 R; rotor A-4-62 5415 D; rotor F45-24-11 Spectrafuge™ 24D	Thermo Fisher Scientific Eppendorf Eppendorf Labnet
FPLC & column	Äkta Explorer Superdex™ 75 10/300 GL	GE Healthcare GE Healthcare
Gel imaging system	Gel iX20 Imager	Intas Science Imaging Instruments GmbH
Glass filtration unit	FilterSys™	Phenomenex
High pressure homogenizer	LM 10 Microfluidizer	Microfluidics™
HPLC & column	1100 series Luna 5 µm C18	Agilent Phenomenex
Incubator & Shaker	B6200 New Brunswick™ INNOVA® 44 New Brunswick™ innova® 2300	Heraeus Eppendorf Eppendorf
Lyophilizer	Alpha 2-4 LSC plus	Martin Christ GmbH
Magnetic stirrer	MR 3001	Heidolph
pH meter	pH 50+ DHS	XS Instruments
Photometer	8453 UV-visible Spectroscopy System FP-8300 Spectrofluorometer	Agilent Jasco
Pipettes	PIPETMAN Classic™ Research® Plus	Gilson Eppendorf

Power supply	KONSTANTER SLP 240-40 PowerPac™ HC Power Source 300V	G. METRAWATT Bio-Rad VWR
Scales	4000/AR Acculab Atilon ATL-6201 R200D	Europe Sartorius AG Sartorius AG
SDS-PAGE apparatus	Mini-PROTEAN® II	Bio-Rad
Thermoblock	ThermoStat plus Thermocell Cooling & Heating Block	Eppendorf BIOER
Thermocycler	peqSTAR 2 Tpersonal FG-TC01	PEQLAB Biometra NIPPON Genetics
Ultrasonic homogenizer	Sonopuls HD 2200; tip KE76	Bandelin
Ultra-pure water system	MilliQ® Integral Water Purification System	Merck Millipore
Vacuum pump	LABOPORT® N820	KNF Neuberger GmbH
Vortexer	Vortex-Mixer	VWR

2.1.2 Special chemicals, materials, enzymes, antibodies and kits

All chemicals and reagents used in this study were ACS grade or better and were purchased from AppliChem GmbH (Darmstadt, Germany), Bio-Rad (Feldkirchen, Germany), Carl Roth GmbH + Co. KG (Karlsruhe, Germany), Frontier Scientific Inc. (Newark, Dekaware, USA), IBA Lifesciences GmbH (Göttingen, Germany), Merck KGaA (Darmstadt, Germany), New England Biolabs GmbH (Frankfurt am Main,Germany), SERVA Electrophoresis GmbH (Heidelberg, Germany), Sigma-Aldrich (Taufkirchen, Germany), Thermo Fisher Scientific GmbH (Dreieich, Germany) and VWR Chemicals (Darmstadt, Germany), unless stated otherwise.

Table 2.2 Special chemicals, materials, enzymes, antibodies and kits.

Type of product	Name of product	Manufacturer
Chemicals and materials		
Affinity Chromatography Resins	Strep-Tactin® Sepharose® TALON® Superflow™	IBA Lifesciences GmbH Cytiva
Blotting Membrane	Transfer membrane ROTI® PVDF 0.45 µm	Carl Roth GmbH + Co. KG

Centrifugal filter units	Amicon® Ultra-4, 10 kDa NMWCO Amicon® Ultra-4, 10 kDa NMWCO	Merck Millipore
Cuvettes	CUVETTES semi-micro Ultra-Micro cell QS 10 mm Sealable cell QS 10 mm Ultra-Micro cell QS 3 x 3mm	Ratiolab GmbH Hellma GmbH & Co. KG Hellma GmbH & Co. KG Hellma GmbH & Co. KG
Dialysis tubing	SERVAPOR® dialysis tubing, MWCO 12000-14000	SERVA
DNA loading dye	Gel Loading Dye, Purple (6x)	New England Biolabs GmbH
DNA ladder	GeneRuler™ 1 kb Plus DNA Ladder	Thermo Fisher Scientific
Filtering units	0.22 µm Syringe Filter, PVDF (sterile), 33 mm 0.2 µm Syringe Filter, Phenex™-PTFE (non-sterile), 4 mm 0.45 µm Filter Membranes, Phenex™-PTFE, 47 mm	Starlab GmbH Phenomenex Phenomenex
Optical filters	636FS10-50, 636.2 nm Filter 730FS10-50, 730 nm Filter 750FS10-50, 750 nm Filter	Andover Corporation Andover Corporation Andover Corporation
Protein marker	Unstained Protein Standard, Broad Range Color Prestained Protein Standard, Broad Range	New England Biolabs GmbH New England Biolabs GmbH
Solid phase extraction columns	Sep-Pak C18 Plus Light Cartridges	Waters Corporation
Enzymes		
*Bam*HI	*Bam*HI-HF®	New England Biolabs GmbH
Catalase	Catalase from bovine liver	Sigma-Aldrich
DNaseI	DNaseI	Applichem GmbH
DNA ligase	Taq DNA ligase	New England Biolabs GmbH
DNA polymerase	Phusion DNA polymerase	Lab collection
dNTPs	dNTP-Mix (dATP, dCTP, dGTP, DTTP)	Axon Labortechnik GmbH
*Dpn*I	*Dpn*I	New England Biolabs GmbH

Glucose Oxidase	Glucose Oxidase Type II from *Aspergillus niger*	Sigma-Aldrich
Glucose-6-phosphate dehydrogenase	Glucose-6-phosphate dehydrogenase from baker's yeast	Sigma-Aldrich
Lysozyme	Lysozyme, lyophilized	Carl Roth GmbH + Co. KG
*Nde*I	*Nde*I	New England Biolabs GmbH
Antibody		
Strep-tag II antigen	Strep-Tactin® AP conjugate (1:4000)	IBA Lifesciences GmbH
Kits		
PCR Clean-up	NucleoSpin® Gel and PCR Clean-up kit	Macherey-Nagel GmbH & Co. KG
Plasmid preparation	NucleoSpin® Plasmid EasyPure kit	Macherey-Nagel GmbH & Co. KG
	E.Z.N.A.® Plasmid DNA Mini Kit I	Omega Bio-Tek Inc

2.2 Bacterial strains, plasmids and oligonucleotides

2.2.1 Bacterial strains

Table 2.3 Bacterial strains.

Bacterial strain	Genotype	Reference
E. coli DH5α	F^- *endA1 glnV44 thi-1 recA1 relA1 gyrA96 deoR nupG purB20 φ80dlacZ*ΔM15 Δ*(lacZYA-argF)*U169, *hsd*R17($r_K^-m_K^+$), λ^-	Hanahan, 1983
E. coli BL21(DE3)	F^- *ompT gal dcm lon hsdS*$_B$($r_B^-m_B^-$) λ(DE3 [*lacI lacUV5-T7p07 ind1 sam7 nin5*]) [*malB*$^+$]$_{K-12}$(λ^S)	Studier & Moffatt, 1986
E. coli BL21(DE3) pASK75B-Cph1 5' modi	*E. coli* BL21(DE3) + pASK75B-Cph1 5' modi; Amp^R	This study

2.2.2 Plasmids

Table 2.4 Plasmids.

Plasmid	Features	Accession number	Reference
pET28a_*KflaHY2*	pET-28a(+) derivate carrying the codon-optimized *HY2* gene from *Klebsormidium nitens* (catalytic core region lacking the predicted chloroplast transit peptide); N-terminal His_6-tag	A0A1Y1I5X3 (UniProt)	Donation of J. Clark Lagarias, UC Davis
pET28a_*KflaHY2*_N105D	pET28a_*KflaHY2* derivate obtained by site-directed mutagenesis		Frascogna *et al.*, 2023
pET28a_*KflaHY2*_N105H	pET28a_*KflaHY2* derivate obtained by site-directed mutagenesis		This study
pET28a_*KflaHY2*_D122N	pET28a_*KflaHY2* derivate obtained by site-directed mutagenesis		Frascogna *et al.*, 2023
pET28a_*KflaHY2*_D242N	pET28a_*KflaHY2* derivate obtained by site-directed mutagenesis		Frascogna *et al.*, 2023
pET28a_*KflaHY2*_N105D_ D122N	pET28a_*KflaHY2* derivate obtained by site-directed mutagenesis		Frascogna *et al.*, 2023
pET28a_*KflaHY2*_N105D_ D242N	pET28a_*KflaHY2* derivate obtained by site-directed mutagenesis		Frascogna *et al.*, 2023
pET28a_*KflaHY2*_T247I	pET28a_*KflaHY2* derivate obtained by site-directed mutagenesis		This study
pGEX_*pcyA*	pGEX-6P-1 derivate carrying the *pcyA* gene from *Synechocystis* sp. PCC 6803; N-terminal GST-tag	Q93TN0 (UniProt)	Frankenberg *et al.*, 2001
pGEX_*AtHY2*	pGEX-6P-1 derivate carrying the mature *HY2* gene from *Arabidopsis thaliana*; N-terminal GST-tag	Q9SR43 (UniProt)	Kohchi *et al.*, 2001
pGEX_*petF*_P-SSM2	pGEX-6P-3 derivate carrying the *petF* gene from the cyanophage P-SSM2; N-terminal GST-tag	Q58M74 (UniProt)	Dammeyer *et al.*, 2008a
pGEX_*petH*	pGEX-6P-1 derivate carrying the *petH* gene from *Synechococcus* sp. PCC 7002; N-terminal GST-tag	P31973 (UniProt)	Unpublished, lab collection

pET_*cph1*	pET derivate carrying the *cph1* gene from *Synechocystis* sp. PCC 6803; C-terminal His_6-tag	Q55168 (UniProt)	Donation of J. Clark Lagarias, UC Davis
pASK75B-Cph1 5'modi	pASK75B derivate carrying the N-terminal of *cph1* gene from *Synechocystis* sp. PCC 6803; C-terminal Strep-tag I	Q55168 (UniProt)	Donation of J. Clark Lagarias, UC Davis
pASK_*bphP*	pASK-IBA3 derivate carrying the *bphP* gene from *Pseudomonas aeruginosa*; C-terminal Strep-tag II	Q9HWR3 (UniProt)	Tasler *et al.*, 2005
pGEX-4T-1_*CepuHY2*	pGEX-4T-1 derivate carrying the *HY2* gene from *Ceratodon purpureus*; N-terminal GST-tag	FFPD-2057880 (OneKP)	Frascogna *et al.*, 2023
pGEX-4T-1_*NediHY2*	pGEX-4T-1 derivate carrying the *HY2* gene from *Netrium digitus*; N-terminal GST-tag	FFGR-2000050 (OneKP)	Frascogna *et al.*, 2023
pET28a_*KflaPUBS*	pET-28a(+) derivate carrying the reverse-translated gene sequence of putative *PUBS* from *Klebsormidium nitens* (catalytic core lacking the predicted chloroplast transit peptide); N-terminal His_6-tag	A0A1Y1IM74 (UniProt)	This study
pET28a_MCC5789364	pET-28a(+) derivate carrying the reverse-translated gene sequence of putative FDBR MCC5789364 from *Opitutales* bacterium metagenome; N-terminal His_6-tag	MCC5789364.1 (GenBank)	This study
pET28a_CAP_1520	pET-28a(+) derivate carrying the reverse-translated gene sequence of putative FDBR CAP_1520 from *Chondromyces apiculatus* DSM 436; N-terminal His_6-tag	EYF06823 (GenBank)	This study
pET28a_MBL9008304	pET-28a(+) derivate carrying the reverse-translated gene sequence of putative FDBR MBL9008304 from *Myxococcales* bacterium metagenome; N-terminal His_6-tag	MBL9008304 (GenBank)	This study
pET28a_*GsPEBA*_harmo	pET-28a(+) derivate carrying the codon-harmonized *PEBA* gene sequence from *Galdieria sulphuraria*; N-terminal His_6-tag	M2XA99 (UniProt)	This study

pASK-IBA45(+)_*GsPEBB*	pASK-IBA45(+) derivate carrying the codon-optimized *PEBB* gene sequence from *Galdieria sulphuraria*; N-terminal Strep-tag II	M2X9Q0 (UniProt)	Andrea Busch, Ruhr University Bochum, 2011
pASK-IBA45(+)_*SycpebA*	pASK-IBA45(+) derivate carrying the *pebA* gene from *Synechococcus* sp. WH 8020; N-terminal Strep-tag II	Q02189 (UniProt)	Marco Aras, Technical University of Kaiserslautern, 2018
pACYC_*GsPEBA*revtrans	pACYCDuet-1 derivate carrying the reverse-translated *PEBA* gene sequence from *Galdieria sulphuraria* in MCS-1; N-terminal His_6-tag	M2XA99 (UniProt)	This study
pACYC_*GsPEBB*	pACYCDuet-1 derivate carrying the codon optimized *PEBB* gene sequence from *Galdieria sulphuraria* in MCS-2	M2X9Q0 (UniProt)	This study
pACYC_*GsPEBA*revtrans_ *GsPEBB*	pACYCDuet-1 derivate carrying the *PEBA* gene sequence from *Galdieria sulphuraria* (reverse translated sequence, N-terminal His_6-tag) in MCS-1 and the *PEBB* gene (codon optimized) from *Galdieria sulphuraria* in MCS-2	M2XA99 (UniProt); M2X9Q0 (UniProt)	This study
pCOLA_*Syn*ho1	pCOLADuet-1 derivate carrying the *ho1* gene sequence from *Synechocystis* sp. PCC 6803; N-terminal His_6-tag	P72849 (UniProt)	This study

2.2.3 Oligonucleotides

Table 2.5 Oligonucleotides.

Oligonucleotide	Sequence (5'→3')
pET28a_*KflaHY2*_N105D_ fwd	CAATCTGCAAGTTCTGGATCTGATCGCGTTTCCG
pET28a_*KflaHY2*_N105D_ rev	CGGAAACGCGATCAGATCCAGAACTTGCAGATTG
pET28a_*KflaHY2*_N105H_ fwd	CAATCTGCAAGTTCTGCATCTGATCGCGTTTCC
pET28a_*KflaHY2*_N105H_ rev	GGAAACGCGATCAGATGCAGAACTTGCAGATTG
pET28a_*KflaHY2*_D122N_ fwd	CGTACTTCTGTGCAAACCTGGTCACCCTG

pET28a_*KflaHY2*_D122N_rev	CAGGGTGACCAGGTTTGCACAGAAGTACG
pET28a_*KflaHY2*_D242N_fwd	GGCGTGCAGAAAAAAATCCGGGTCGTCCG
pET28a_*KflaHY2*_D242N_rev	CGGACGACCCGGATTTTTTTCTGCACGCC
pET28a_*KflaHY2*_T247I_fwd	CCGGGTCGTCCGATTATTACGCGCCTGTATGGC
pET28a_*KflaHY2*_T247I_rev	GCCATACAGGCGCGTAATAATCGGACGACCCGG
pET28a_*KflaPUBS*_fwd	CTGGTGCCGCGCGGCAGCCACGACAGGTTTCCCGATGATAG
pET28a_*KflaPUBS*_rev	GTCGACGGAGCTCGAATTCGTTAGCTCACGTCGAAGTG
pET28a_ MCC5789364_fwd	CTGGTGCCGCGCGGCAGCCACAAGACATCAATAGAAAAACC
pET28a_ MCC5789364_rev	GTCGACGGAGCTCGAATTCGTTATTGCAGCAACACCTTATG
pET28a_CAP_1520_fwd	CTGGTGCCGCGCGGCAGCCACATTGACGCTTCCTCGCTTAAG
pET28a_CAP_1520_rev	GTCGACGGAGCTCGAATTCGTTACGGGCTGCCCAGGAG
pET28a_MBL9008304_fwd	CTGGTGCCGCGCGGCAGCCAAACCAACCCGGATTGTGCAACCTATC
pET28a_MBL9008304_rev	GTCGACGGAGCTCGAATTCGTTACGGACCGCCGCCGCT
pET28a_*GsPEBA*_harmo_fwd	CTGGTGCCGCGCGGCAGCCAGGATTCGAACAGCTTAGTTAG
pET28a_*GsPEBA*_harmo_rev	GTCGACGGAGCTCGAATTCGTTAGGTCTTGTTATCAAGACT
pACYC_*GsPEBA*_revtrans_fwd	ACCATCATCACCACAGCCAGGATTCTAACTCACTAGTAAGC
pACYC_*GsPEBA*_revtrans_rev	GCGCGCCGAGCTCGAATTCGTTAGGTTTTGTTGTCCAG
pACYC_*GsPEBB*_fwd	GTATAAGAAGGAGATATACAATGAATTCGTTGTATTCCCC
pACYC_*GsPEBB*_rev	TATCCAATTGAGATCTGCCATTAGGTGCTCAGTTTGCG
pCOLA_*Synho1*_fwd	ACCATCATCACCACAGCCAGATGAGTGTCAACTTAGCTTCCC
pCOLA_*Synho1*_rev	GCGCGCCGAGCTCGAATTCGTTAGCCTTCGGAGGTGGC

2.3 Microbiology methods

2.3.1 Sterilization

All media and supplements employed in cell culture cultivation underwent sterilization prior to use. Heat-resistant solutions and plasticware were autoclaved at 120°C and 1 bar for 20 min. Heat-sensitive solutions were filter-sterilized using 0.2 µm filters. Glassware was sterilized by dry heat at 180°C for 3 hours.

2.3.2 Culture media & supplements

Escherichia coli liquid cultures were grown in lysogeny broth (LB) with appropriate antibiotics and supplements (Table 2.6). Solid medium was prepared by adding 1.5%$_{w/v}$ agar-agar to LB (LB-agar), prior to sterilization.

Table 2.6 Culture media, antibiotics and supplements.

LB medium		**LB-agar**	
Tryptone	10 g/L	LB medium	1x
Yeast Extract	5 g/L	Agar-Agar	1.5%$_{w/v}$
NaCl	5 g/L		
Antibiotics			
Ampicillin (in H_2O)	100 µg/mL		
Kanamycin (in H_2O)	50 µg/mL		
Chloramphenicol (in 70%$_{v/v}$ EtOH)	34 µg/mL		
Supplements			
IPTG	0.5 – 1 mM		
Anhydrotetracycline (in DMF)	200 ng/mL		

2.3.3 Storage of *E. coli* cells

Fort short-term storage, *E. coli* cells were streaked on LB-agar, with appropriate antibiotics if required, and stored at 4°C. For long-term storage, 2 mL of an *E. coli* overnight culture (chapter 2.3.4) were harvested by centrifugation (Eppendorf 5415 D, 4000 rpm, 3 min, room temperature). The cell pellet was diluted in fresh LB medium, with appropriate antibiotics if required, transferred to a cryovial and sterile glycerol was added to a final concentration of 40%$_{v/v}$. The resulting glycerol stocks were flash-frozen in liquid nitrogen and stored at -80°C.

2.3.4 Cultivation of *E. coli* cells

E. coli glycerol stocks (chapter 2.3.3) or transformation plates (chapter 2.3.7) served as starting material for cultivation. Using a sterile inoculation loop, bacteria were scraped off the glycerol stock and streaked onto an LB-agar plate, supplemented with appropriate antibiotics if required (selective LB-agar). Plates were incubated overnight at 37°C (Heraeus B6200). Subsequently, a single colony was picked from the plate and used to inoculate LB medium, supplemented with appropriate antibiotics if required, in a test tube or Erlenmeyer flask to prepare overnight cultures. The resulting cultures were incubated overnight at 37°C under constant shaking (New Brunswick™ innova® 2300, 160 rpm).

2.3.5 Determination of *E. coli* cells density

Cell density of liquid cultures (1 mL) was determined photometrically as optical density (OD) at 600 nm (OD_{600}). LB medium was used as reference for the measurement.

2.3.6 Preparation of chemically competent *E. coli* cells

E. coli cells lack the inherent capability to uptake foreign DNA from their surroundings. Nevertheless, this capability, named competence, can be induced through several treatments. Among these methods, in this study, *E. coli* cells were made competent via a chemical approach. For this purpose, 100 mL LB medium, supplemented with appropriate antibiotics if required, was inoculated with an overnight culture of the chosen *E. coli* strain in a 1:100 ratio. This main culture was incubated at 37°C under constant shaking (New Brunswick™ innova® 2300, 160 rpm) until the OD_{600} reached 0.4 - 0.6. Subsequently, the culture was harvested by centrifugation (Eppendorf 5810 R, 4000 rpm, 10 min, 4°C). The cell pellet was resuspended in 50 mL ice-cold 50 mM $CaCl_2$ and stored on ice for 1 h. The resuspension was centrifuged as aforementioned, and the pellet resuspended in 5 mL ice-cold 50 mM $CaCl_2$ supplemented with 15%$_{v/v}$ glycerol. The resulting chemically competent *E. coli* cells were distributed in 200 µL aliquots, flash-frozen in liquid nitrogen and stored at -80°C.

2.3.7 Transformation of chemically competent *E. coli* cells

The term transformation designates the process in which competent cells uptake foreign DNA. For this purpose, chemically competent *E. coli* cells (chapter 2.3.6), previously thawed on ice, were gently mixed with 50-100 ng of plasmid DNA or 10 µL of PCR product (chapters 2.4.7 and 2.4.9) and incubated on ice for 15 min. Subsequently, a heat-shock step was performed wherein the mix was incubated at 42°C for 2 min. After 2 min recovery on ice, 700 µL of fresh LB medium were added and the mix incubated at 37°C for 1 - 1.5 h under constant shaking (New Brunswick™ innova® 2300, 160 rpm). Cells were harvested by

centrifugation (Eppendorf 5415 D, 4000 rpm, 3 min, room temperature) and most of the supernatant discarded. The cell pellet was resuspended in the remaining supernatant (100 - 200 µL) and streaked on selective LB-agar. The LB-agar plate was incubated overnight at 37°C. The following day, the transformation plates were stored at 4°C or used directly in subsequent experiments.

2.4 Molecular Biology methods

2.4.1 Preparation of plasmid DNA

To isolate plasmid DNA, a single colony of *E. coli* DH5α was picked from the transformation plate (chapter 2.3.7) and inoculated in 5 mL selective LB medium. The culture was incubated overnight at 37°C under constant shaking (New Brunswick™ innova® 2300, 160 rpm). The following day, 4 mL of the culture were centrifuged (Eppendorf 5415 D, 4000 rpm, 3 min, room temperature) and the plasmid isolated using either the NucleoSpin® Plasmid EasyPure Kit (Macherey-Nagel GmbH & Co. KG, Düren, Germany) or the E.Z.N.A.® Plasmid DNA Mini Kit I (Omega Bio-Tek Inc, Norcross, Georgia, USA) according to the manufacturer's instructions.

2.4.2 Estimation of DNA concentration in solution

The concentration of DNA in solution was determined photometrically at 260 nm using the NanoDrop™ Lite (Thermo Fisher Scientific GmbH). 1 µL of DNA was used for the measurement and the elution buffer (either provided from the plasmid isolation or PCR product purification kit, Table 2.2) served as the reference. The ratio of absorption at 260 nm and 280 nm was used for purity assessment. An absorption ratio 260nm/280nm of ~ 1.8 was accepted as adequately pure for double-stranded DNA. The concentration estimated using this method was seldomly ascertained with an agarose gel (chapter 2.4.6).

2.4.3 Restriction digestion

Restriction digestion of plasmids was performed using restriction endonucleases or high-fidelity (HF®) restriction endonucleases (Table 2.2) according to the manufacturer's instructions. The DNA was incubated for 1 h (restriction endonucleases) or 15 min (HF® restriction endonucleases) at 37°C. In the case of digestion with two restriction endonucleases, both enzymes were mixed together in a double digestion approach. If possible, the incubation was followed by heat-inactivation according to the manufacturer's instructions. Successful digestion was verified by agarose gel electrophoresis (chapter 2.4.6).

2.4.4 Amplification of DNA via Polymerase chain reaction (PCR)

Polymerase chain reaction (PCR) was used to amplify specific DNA fragments (Mullis *et al.*, 1986). The laboratory's own stock of purified Phusion HF-DNA polymerase was used for the PCR reactions. Reactions were performed in 5x NEB HF buffer (New England Biolabs GmbH, B0518S). The PCR mixes, including the polymerase, the buffer, the oligonucleotides, the template DNA and dNTPS, had a final volume of 50 µL (Table 2.7). The PCR program was outlined considering the amplification speed of the polymerase, characteristics of the oligonucleotides and the size of the DNA fragment (Table 2.8). Specifically, the annealing temperature was determined using the NEB Tm Calculator (https://tmcalculator.neb.com/). Following the reaction, PCR products were analyzed via agarose gel electrophoresis (chapter 2.4.6).

Table 2.7 PCR components.

Component	Final concentration/volume
Template DNA	10 - 100 ng
Primer fwd	250 nM
Primer rev	250 nM
dNTPs (mix)	200 nM (each)
Phusion HF-polymerase	1 µL
5x Phusion HF-buffer	1x
H_2O	to 50 µL

Table 2.8 PCR program.

Reaction step	Temperature	Time	
Initial denaturation	98°C	30 s	
Denaturation	98°C	30 s	30 cycles
Annealing	primer-specific	30 s	
Extension	72°C	15 s/kb	
Final extension	72°C	5 min	
Cooling	4°C	∞	

2.4.5 Purification of PCR products

Following amplification, PCR products were purified using the NucleoSpin™ Gel and PCR Clean-up Kit (Macherey-Nagel GmbH & Co. KG, Düren, Germany) according to the manufacturer's instructions.

2.4.6 Agarose gel electrophoresis

Agarose gel electrophoresis was used to separate DNA fragments in an electric field according to their size (Aaij & Borst, 1972). 0.8%$_{w/v}$ agarose was added to TAE buffer and dissolved by heating. The crystal-clear solution was poured in a horizontal gel chamber, a well comb was placed, and polymerization occurred at room temperature. DNA samples were mixed with DNA loading dye (Table 2.2) and applied in the gel wells. Additionally, a DNA ladder (Table 2.2) was used as reference for fragments size and amount. Electrophoresis was performed at a constant voltage of 120 V in TAE buffer for 45 - 60 min. Subsequently, the gel was incubated in an ethidium bromide solution for 10 min to, following rinsing, record the fluorescence of the DNA:ethidium bromide complex at λ_{exc}=312 nm using the Gel imaging system (Table 2.1).

TAE buffer	
Tris-Acetate pH 8	40 mM
EDTA	1 mM

2.4.7 Construction of expression vectors

All expression vectors presented in this study were constructed using Gibson Assembly®. This method allows the cloning of multiple fragments at a time without the need of compatible restriction sites, in contrast to traditional restriction-digest cloning. It consists of a PCR reaction in which one or more DNA fragments are inserted into a destination vector by the means of user-defined homologous overlapping ends. The reaction is carried out under isothermal conditions (50°C) and involves 3 enzymatic activities in a single tube: a 5' exonuclease to generate overhangs, a DNA polymerase to fill in the gaps of the annealed single-strand regions, and a DNA ligase to seal the resulting nicks. Thus, only adding the digested destination plasmid and the amplified target DNA fragment to the Gibson Assembly® Master Mix results in a seamless expression vector (Gibson *et al.*, 2009). The genes of interest were ordered as synthetic DNA fragments from Twist Bioscience (South San Francisco, California, USA) (sequences of employed genes in Appendix). The genes were amplified via PCR (chapter 2.4.4) using specific overhang primers (Table 2.5). In the meantime, the destination plasmid was digested with the appropriate restriction endonuclease(s) (chapter 2.4.3) (Table 2.2). After validation of both the PCR and restriction digestion products via agarose gel electrophoresis (chapter 2.4.6), their concentration was estimated (chapter 2.4.2). NeBioCalculator® (https://nebiocalculator.neb.com/#!/ligation) was used to calculate the mass of insert to use for the ligation. As a rule of thumb, a ratio of 3:1 insert:vector was chosen. The calculated amounts of insert and vector were mixed with 15 µL

of Gibson Assembly® Master Mix (Table 2.9) and incubated at 50°C for 1 h. 10 µL of the isothermal reaction were subsequently used for transforming competent *E. coli* DH5α.

Table 2.9 Gibson Assembly® Master Mix components.

Component	Final concentration/volume
Phusion HF-polymerase	80 U/mL
Taq DNA ligase	6 U/µL
T5 Exonuclease	12 U/mL
Isothermal reaction buffer (5x)*	1x
H_2O	to final desired volume

*500 mM Tris-HCl pH 7.5, 50 mM $MgCl_2$, 50 mM DTT, 5 mM NAD^+, 1 mM (each) dNTPs, 25%$_{w/v}$ PEG 8000

2.4.8 Colony PCR

Successful cloning was validated via colony PCR. Single colonies of *E. coli* DH5α transformed with the Gibson Assembly® isothermal reaction product were picked, streaked onto a selective LB-agar plate, and resuspended in 10 µL H_2O. 1 µL of this suspension was used as template in PCR amplification (chapter 2.4.4). Oligonucleotides annealing to the vector backbone, up- and downstream of the insertion site, were used in the colony PCR reaction (Table 2.10, Table 2.11). PCR products were verified via agarose gel electrophoresis (chapter 2.4.6)

Table 2.10 Colony PCR mix.

Component	Final concentration/volume
Colony DNA	1 µL
Primer fwd	200 nM
Primer rev	200 nM
dNTPs (mix)	200 nM (each)
DMSO	2%$_{v/v}$
Phusion HF-polymerase	0.5 µL
5x Phusion HF-buffer	1x
H_2O	to 25 µL

Table 2.11 Colony PCR program.

Reaction step	Temperature	Time	
Initial denaturation	95°C	10 min	
Denaturation	95°C	30 s	30 cycles
Annealing	primer-specific	30 s	
Extension	72°C	15 s/kb	
Final extension	72°C	5 min	
Cooling	4°C	∞	

2.4.9 Site-directed mutagenesis

Site-directed mutagenesis is used for the targeted introduction of specific mutations in a DNA sequence, allowing the investigation of the resulting impact on the structure and function of the encoded protein. Tailored oligonucleotides (Table 2.5) were designed to induce nucleobase substitutions within the *KflaHY2* gene. The concentration of components and the employed PCR programs in two subsequent reactions are listed in Table 2.12 and Table 2.13. Following the PCR reactions, the methylated parental plasmid was removed via restriction digestion (chapter 2.4.3) with *Dpn*I (Table 2.2). 20 µL of the digested sample were subsequently transformed in *E. coli* DH5α (chapter 2.3.7). The plasmid was isolated from single colonies (chapter 2.4.1) and the insertion of the desired mutation(s) was validated by Sanger sequencing (chapter 2.4.10).

Table 2.12 QC-PCR first reaction components and thermocycler program.

First reaction			
fwd reaction		**rev reaction**	
Template	30 ng	Template	30 ng
Primer fwd	500 nM	Primer rev	500 nM
dNTPs (mix)	200 mM (each)	dNTPs (mix)	200 nM (each)
Phusion HF-polymerase	0.5 µL	Phusion HF-polymerase	0.5 µL
5x Phusion HF-buffer	1x	5x Phusion HF-buffer	1x
H_2O	to 50 µL	H_2O	to 50 µL
QC-PCR program			
Initial denaturation	98°C	30 s	
Denaturation	98°C	15 s	8 cycles
Annealing	55°C	30 s	
Extension	72°C	3 min 30 s	

Cooling	4°C	∞

Table 2.13 QC-PCR second reaction components and thermocycler program.

Second reaction			
fwd reaction	25 µL		
rev reaction	25 µL		
Phusion HF-polymerase	0.5 µL		
QC-PCR program			
Initial denaturation	98°C	30 s	
Denaturation	98°C	15 s	18 cycles
Annealing	55°C	30 s	
Extension	72°C	3 min 30 s	
Final Extension	72°C	10 min	
Cooling	4°C	∞	

2.4.10 Analysis of DNA sequences

All constructed plasmids were validated using Sanger sequencing (Sanger *et al.*, 1977) performed by Eurofins Genomics Germany GmbH (Ebersberg, Germany). The mix of DNA, oligonucleotide and H_2O was prepared according to the company's instructions. The sequencing result was analyzed using SnapGene (https://snapgene.com/) or Nucleotide BLAST (blastn, https://blast.ncbi.nlm.nih.gov/Blast.cgi).

2.5 Biochemical and biophysical methods

2.5.1 Heterologous production of recombinant proteins in *E. coli*

For the production of recombinant His-tagged proteins, LB medium (2 L for *Kfla*HY2 and *Kfla*HY2 variants; 3 L for pre-PcyAs, *Gs*PEBA and *Kfla*PUBS) supplemented with 50 µg/mL kanamycin was inoculated 1:100 with an overnight culture of *E. coli* BL21(DE3) carrying the desired plasmid. Cells were grown at 37°C and 100 rpm (New Brunswick™ INNOVA® 44) to an OD_{600} of 0.4 - 0.6. The temperature was decreased to 17°C and gene expression was induced by the addition of IPTG (final concentration of 1 mM for pET28a_MCC5789364, pET28a_CAP_1520, pET28a_MBL9008304, pET28a_*GsPEBA*, pET28a_*KflaHY2*, pET28a_*KflaPUBS*; 0.5 mM for all the pET28a_*KflaHY2* variants). The cultures were incubated under shaking for 19 additional hours and harvested by centrifugation for 10 min at 17000 × g and 4°C (Sorvall LYNX 6000, Rotor F9).

For the production of recombinant Strep-tagged *Gs*PEBB, 3 L LB medium supplemented with 100 µg/mL ampicillin was inoculated 1:100 with an overnight culture of *E. coli* BL21(DE3) carrying pASK-IBA45(+)_*GsPEBB*. Cells were grown at 37°C and 100 rpm (New Brunswick™ INNOVA® 44) to an OD_{600} of 0.4 - 0.6. The temperature was decreased to 17°C and gene expression was induced by the addition of 200 ng/mL AHT. The cultures were incubated under shaking for 19 additional hours and harvested by centrifugation for 10 min at 17000 × g and 4°C (Sorvall LYNX 6000, Rotor F9).

2.5.2 Cell disruption

The pellets containing His-tagged proteins were resuspended in His-Binding buffer in a ratio of 3 mL buffer/g wet cell weight. After the addition of a spatula tip of DNaseI (AppliChem) and lysozyme (Sigma-Aldrich), the suspension was kept on ice for 30 min. The cells containing His-*Kfla*HY2 and His-*Kfla*HY2_variants were disrupted by sonication (Bandelin Sonopuls HD 2200, tip KE76; 5 min, 5 s pulses, 10 s pauses; cycle 6/10; ~ 40% power output) and centrifuged for 45 min at 50000 × g and 4°C (Sorvall LYNX 6000, rotor T29). The cells containing His-pre-PcyAs, His-*Gs*PEBA and His-*Kfla*PUBS were disrupted using a microfluidizer (LM 10 Microfluidizer, Microfluidics™; 3 cycles; 15000 psi) and centrifuged for 45 min at 50000 × g and 4°C (Sorvall LYNX 6000, Rotor T29).
The pellet containing Strep-*Gs*PEBB was resuspended in Strep-Binding buffer in a ratio of 3 mL buffer/g wet cell weight. After the addition of a spatula tip of DNaseI (AppliChem) and lysozyme (Sigma-Aldrich), the suspension was kept on ice for 30 min. The cells were disrupted using a microfluidizer (LM 10 Microfluidizer, Microfluidics™; 3 cycles; 15000 psi) and centrifuged for 45 min at 50000 × g and 4°C (Sorvall LYNX 6000, Rotor T29).

His-Binding buffer	
Sodium-phosphate pH 7.4	20 mM
NaCl	500 mM

Strep-Binding buffer	
Tris-HCl pH 8	100 mM
NaCl	300 mM
EDTA	1 mM

2.5.3 Purification of recombinant proteins

The crude extracts containing His-tagged proteins were loaded onto a gravity flow column containing 3 mL of TALON® Superflow™ resin (Cytiva, Freiburg im Breisgau, Germany). The column was washed with 10 column volumes (CV) of His-Binding buffer and the elution was performed using 4 CV of His-Elution buffer.
The crude extract containing Strep-*Gs*PEBB was loaded onto a gravity flow column containing 3 mL of Strep-Tactin® Sepharose® (IBA Lifesciences GmbH). The column was

washed with 10 CV of Strep-Binding buffer and the elution was performed using 4 CV of Strep-Elution buffer.

Strep-tagged *Syc*PebA, GST-tagged *Syn*PcyA, GST-tagged *At*HY2, GST-tagged *Cepu*HY2 and GST-tagged *Nedi*HY2 were produced and purified as described elsewhere (Aras *et al.*, 2020; Frankenberg *et al.*, 2001; Frankenberg & Lagarias, 2003b; Frascogna *et al.*, 2023). Apo-*Syn*Cph1 and apo-*Pa*BphP lysates were obtained as described elsewhere (Fiege & Frankenberg-Dinkel, 2020; Tasler *et al.*, 2005).

His-Elution buffer	
Sodium-phosphate pH 7.4	20 mM
NaCl	500 mM
Imidazole	500 mM

Strep-Elution buffer	
Tris-HCl pH 8	100 mM
NaCl	300 mM
EDTA	1 mM
Desthiobiotin	2.5 mM

2.5.4 Reconstitution of *G. sulphuraria* FDBRs pathway in *E. coli*

The reconstitution of *G. sulphuraria* bilin biosynthesis in *E. coli* required simultaneous expression of three plasmids. Firstly, transformant cells harboring pASK75B-Cph1 5'modi were made chemically competent (chapter 2.3.6). These competent cells were co-transformed with the desired combinations presented in Table 2.14. 2 L LB medium supplemented with half of the amount of the appropriate antibiotics (25 µg/mL kanamycin, 50 µg/mL ampicillin and 17 µg/mL chloramphenicol, depending on the combinations) were inoculated 1:100 with an overnight culture carrying the desired plasmids. Cells were grown at 37°C and 100 rpm (New Brunswick™ INNOVA® 44) to an OD_{600} of 0.4 - 0.6. The temperature was decreased to 30°C and expression of bilin biosynthesis-related genes was induced first by the addition of 0.5 mM IPTG. After 1 h, 200 ng/mL AHT was added to induce apo-phytochrome expression, cells were incubated under shaking at 30°C for 3 additional hours and ultimately harvested by centrifugation for 10 min at 17000 × g and 4°C (Sorvall LYNX 6000, Rotor F9). The cell pellets were washed with 50 mL Cph1-Wash buffer and a second centrifugation step was performed (Sorvall LYNX 6000, Rotor T29; 5000 × g, 5 min, 4°C). The pellets were resuspended in Cph1-Lysis buffer in a ratio of 3 mL buffer/g wet cell weight and disruption was conducted using a microfluidizer (LM 10 Microfluidizer, Microfluidics™; 3 cycles; 15000 psi). The lysates were cleared by centrifugation for 45 min at 50000 × g and 4°C (Sorvall LYNX 6000, Rotor T29). 0.23 g $(NH_4)_2SO_4$ were slowly added per mL of lysates and the samples were incubated at 4°C under constant stirring overnight. After centrifugation (Sorvall LYNX 6000, Rotor T29; 17000 × g, 20 min, 4°C), the pellets were resuspended in Cph1-Lysis buffer, in a volume corresponding to ¼ of the starting lysate volume, and cleared

again by centrifugation (Sorvall LYNX 6000, Rotor T29; 30000 × g, 15 min, 4°C). The samples were incubated with 40 µg/mL avidin on ice for 10 min and subsequently loaded onto a gravity flow column containing 1 mL of Strep-Tactin® Sepharose® (IBA Lifesciences GmbH). The columns were washed with 10 CV of Cph1-Lysis buffer and the elution was performed using 4 CV of Cph1-Elution buffer.

Cph1-Wash buffer	
Tris-HCl pH 8	20 mM
NaCl	20 mM
EDTA	1 mM

Cph1-Lysis buffer	
Tris-HCl pH 8	50 mM
NaCl	100 mM
NP40	0.05%$_{v/v}$
PMSF	2 mM
DTT	1 mM

Cph1-Elution buffer	
Tris-HCl pH 8	50 mM
NaCl	100 mM
NP40	0.05%$_{v/v}$
PMSF	2 mM
DTT	1 mM
Desthiobiotin	2.5 mM

Table 2.14 Overview of constructs used in coexpressions.

Short name	Coexpression
ABHC	pASK75B-Cph1 5’ + pCOLA_*Synho1* + pACYC_*GsPEBA*revtrans_*GsPEBB*
AHC	pASK75B-Cph1 5’ + pCOLA_*Synho1* + pACYC_*GsPEBA*revtrans
BHC	pASK75B-Cph1 5’ + pCOLA_*Synho1* + pACYC_*GsPEBB*
HC	pASK75B-Cph1 5’ + pCOLA_*Synho1*

2.5.5 SDS-PAGE

Proteins were separated and analyzed according to their molecular weight by SDS-polyacrylamide gel electrophoresis (SDS-PAGE) (Laemmli, 1970). In SDS-PAGE, proteins are denatured and coated with SDS, a detergent. By imparting a negative charge, the SDS neutralizes any intrinsic charge on the proteins, so that the successive migration through the gel is primarily based on their size. The denatured proteins are loaded onto a polyacrylamide gel, typically in the presence of a reducing agent, like β-mercaptoethanol or dithiothreitol (DTT), which breaks disulfide bonds and further unfolds the proteins. When an electric current

is applied, the negatively charged proteins migrate through the gel towards the positively charged electrode according to their size: larger proteins migrate slower than smaller ones. The separation of the proteins was conducted in a discontinuous system which consisted of a stacking gel (pH 6.8) with an acrylamide concentration of 6%$_{v/v}$ and a separation gel (pH 8.8) with an acrylamide concentration of 12%$_{v/v}$. Prior to gel application, samples were mixed with 4x sample buffer, incubated for 5 - 10 min at 95°C and centrifuged (Eppendorf 5415 D; 10000 rpm, 3 min, room temperature). Each gel pocket was loaded with 16 µL of sample. Additionally, a protein marker (either 4 µL Unstained Protein Standard, Broad Range or 6 µL Color Prestained Protein Standard, Broad Range, New England Biolabs GmbH, Table 2.2) was used as reference for protein size estimation. Electrophoresis was performed applying a constant voltage of 180 V for ~ 60 min in SDS running buffer.

Stacking gel 6% (10 mL)	
Tris-HCl 0.5 M pH 6.8	2.5 mL
H_2O	5.4 mL
Acrylamide*	2 mL
SDS 20%$_{w/v}$	50 µL
APS 10%$_{w/v}$	100 µL
TEMED	10 µL

*ROTIPHORESE® Gel 30 (37,5:1), 30% Acrylamide/Bisacrylamide solution

Resolving Gel 12% (10 mL)	
Tris-HCl 1.5 M pH 8.8	2.5 mL
H_2O	2.3 mL
Acrylamide*	5 mL
SDS 20%$_{w/v}$	50 µL
APS 10%$_{w/v}$	100 µL
TEMED	10 µL

*ROTIPHORESE® Gel 30 (37,5:1), 30% Acrylamide/Bisacrylamide solution

4x Sample buffer	
Tris-HCl pH 6.5	0.5 M
Bromophenol Blue	0.08%$_{v/v}$
Glycerol	40%$_{v/v}$
SDS	8%$_{w/v}$
β-Mercaptoethanol	16%$_{v/v}$

SDS running buffer	
Tris-HCl pH 8.8	25 mM
Glycine	192 mM
SDS	0.1%$_{w/v}$

2.5.6 Coomassie staining

After electrophoresis, the proteins were visualized by staining the gel with Staining solution containing Coomassie and subsequent discoloration in Destaining solution.

Staining solution	
Acetic Acid	10%$_{v/v}$
Ethanol	30%$_{v/v}$
Coomassie Brilliant Blue G-250	0.25%$_{v/v}$

Destaining solution	
Acetic Acid	10%$_{v/v}$
Ethanol	30%$_{v/v}$

2.5.7 Western Blot

Western Blotting was used to detect a specific protein in a sample. Proteins were first separated by SDS-PAGE (chapter 2.5.5) and subsequently transferred from the polyacrylamide gel onto a PVDF membrane. This transfer allows the proteins to be immobilized on the membrane while preserving their spatial arrangement. Prior to the immobilization, the PVDF membrane was activated in methanol for 15 min, rapidly washed with H_2O and equilibrated, together with 2x blotting paper (Whatman® 3 mm, Cytiva) and the polyacrylamide gel, in Towbin buffer for 15 min. Immobilization was performed for 18 min at a constant voltage of 15 V using the semidry technique. Following the transfer, the PVDF membrane was incubated with 10 mL BSA blocking solution for 1 h at room temperature to saturate non-specific binding sites. For the detection of Strep-*Gs*PEBB, the membrane was washed with PBS-T three times for 5 min and subsequently incubated with 2 µg/mL avidin in PBS-T for 10 min, to prevent *E. coli* endogenous biotinylated proteins from generating spurious signals. The membrane was washed again three times with PBS-T for 5 min each, before it was incubated with the Strep-Tactin® AP conjugate (IBA Lifesciences GmbH) for 1 h. After three rounds of 1 min washing with PBS-T and two with PBS, the membrane was equilibrated in AP Buffer for 5 min. The detection, enabled by the alkaline phosphatase (AP), was mediated by nitro blue tetrazolium chloride (NBT) and 5-bromo-4-chloro-3-indolyl phosphate (BCIP). The reaction, resulting in the formation of a purple coloration, was stopped by washing the membrane with H_2O.

Towbin buffer	
Tris-HCl pH 8.3	25 mM
Glycine	192 mM

PBS	
Na_2HPO_4	10 mM
NaH_2PO_4	1.8 mM
NaCl	140 mM
KCl	2.7 mM
NaOH	to pH 7.3

PBS-T	
PBS	1x
TWEEN® 20	$0.1\%_{v/v}$

BSA blocking solution	
PBS	1x
BSA	$3\%_{w/v}$

AP Buffer	
Tris-HCl pH 9.5	100 mM
NaCl	100 mM
$MgCl_2$	5 mM

NBT	
NBT	100 mg/mL
DMF	70%$_{v/v}$

BCIP	
BCIP	50 mg/mL
DMF	100%$_{v/v}$

2.5.8 Dialysis

Protein-containing fractions were pooled and dialyzed overnight at 4°C against TES-KCl buffer using a 12 - 14 kDa MW cutoff dialysis tube (SERVAPOR® dialysis tubing, MWCO 12000-14000).

TES-KCl buffer	
TES-KOH pH 7.5	25 mM
KCl	100 mM
Glycerol	10%$_{v/v}$

2.5.9 Estimation of protein and bilin concentration

The concentration of the purified proteins was determined photometrically, on the basis of absorbance at 280 nm, and calculated in accordance with Lambert-Beer's law:

$$C = \frac{A_{280nm}}{\varepsilon_{280nm} \times l}$$

C = concentration

A_{280nm} = absorbance at 280 nm

ε_{280nm} = molar absorption coefficient (in $M^{-1}cm^{-1}$)

l = optical path length (in cm)

The molar absorption coefficient of each protein was calculated using ProtParam (https://web.expasy.org/protparam/) (Gasteiger *et al.*, 2005) (Table 2.15).

Table 2.15 Molar absorption coefficients (or extinction coefficients) calculated for proteins used in this study.

Protein	Extinction coefficient [$M^{-1}cm^{-1}$]
His-MCC5789364	40575
His-CAP_1520	25815
His-MBL9008304	30980
His-*Gs*PEBA	54570
StrepII-*Gs*PEBB	49850
His-*Kfla*HY2	48610
His-*Kfla*PUBS	37485

The concentration of bilins used in anaerobic bilin reductase activity assays (chapter 2.5.11) and HPLC analyses (chapter 2.5.13) was calculated photometrically using the following molar absorption coefficients:

BV: ε_{698nm} = 36.2 $mM^{-1}cm^{-1}$ in 2.5% HCl in MeOH (Heirwegh *et al.*, 1991)

15,16-DHBV: ε_{564nm} = 46.9 $mM^{-1}cm^{-1}$ in 5% HCl in MeOH (Gossauer & Klahr, 1979)

18^1,18^2-DHBV: ε_{372nm} = 35.8 $mM^{-1}cm^{-1}$ in DMSO (Boiadjiev & Lightner, 2001)

PEB: ε_{594nm} = 46.9 $mM^{-1}cm^{-1}$ in 5% HCl in MeOH (Gossauer & Klahr, 1979)

PCB: ε_{685nm} = 37.15 $mM^{-1}cm^{-1}$ in 2% HCl in MeOH (Weller & Gossauer, 1980)

PΦB: ε_{386nm} = 64.6 $mM^{-1}cm^{-1}$ in 2% HCl in MeOH (Terry *et al.*, 1995)

2.5.10 Size exclusion chromatography

The determination of proteins oligomerization state was performed via size exclusion chromatography (SEC). The separation of analytes in SEC is based on their hydrodynamic radius. In the case of globular proteins, the hydrodynamic radius directly correlates to their size (Moore, 1964). The determination of size and oligomerization state is then determined by comparison of the elution volume of the target protein with that of standard proteins. Since all of the proteins analyzed in this study are putative FDBRs and, therefore, monomeric with a size ~ 30 kDa, a Superdex™ 75 10/300 GL column (GE Healthcare, Solingen, Germany), which enables the separation of proteins with MW between 3 and 70 kDa, was chosen. The column, equipped onto an Äkta Explorer FPLC system (GE Healthcare), was equilibrated with TES-KCl buffer prior to use. After equilibration, the previously-filtered samples were injected to the column using a 0.5 mL sample loop. The elution, monitored measuring the absorbance at 280 nm, was conducted at the flow rate of 0.2 mL/min for 1 CV (~ 24 mL). The calibration

curve for size determination was generated by plotting the log of the MW of standard proteins against the K_{AV}, i.e. the fraction of accessible volume available to the target protein:

$$K_{AV} = \frac{V_e - V_0}{V_c - V_0}$$

V_e = protein elution volume

V_0 = column void volume

V_c = measured column volume

The column volume (V_c) was measured using acetone and the void volume (V_0) with Blue Dextran (2000 kDa). The calibration was performed using the following protein standards: bovine serum albumin (BSA, 66.4 kDa), ovoalbumin (44 kDa), carbonic anhydrase (29 kDa) and RNase A (13.7 kDa). The fitting of the calibration curve was estimated using a linear regression function in Origin (OriginLab Corporation, Northampton, Massachusetts, USA).

2.5.11 Anaerobic bilin reductase activity assay

The activity of purified FDBRs was tested in a UV-Vis spectroscopy assay performed under anaerobic conditions, to prevent bilins oxidation and stabilize radical intermediates. The anaerobic condition was ensured by a continuous nitrogen gas flow. The assays, performed using an Agilent 8453 spectrophotometer, were conducted employing equimolar amounts of the FDBR and the substrate. The *ratio* of the assay is based on the dependency of this class of enzyme on ferredoxin (PetF). PetF, either from *Synechococcus* sp. PCC 7002 or from the cyanophage P-SSM2, was therefore included in the reaction mix. Specifically, in order for the FDBR to reduce the substrate to the phycobilin product, reduced PetF ($PetF^{RED}$) is used as the electron source. However, a constant supply of $PetF^{RED}$ is required to yield a constant electron flow and ultimately ensure FDBR-mediated reactions. Hence, to constantly replenish $PetF^{RED}$, the ferredoxin-$NADP^+$ reductase (FNR or PetH) from *Synechococcus* sp. PCC 7002 was added to the mix. In turn, this enzyme requires a constant supply of NADPH, which is ensured by a NADPH-regenerating system (NrS). This NrS consists of glucose-6-phosphate (G-6-P) and glucose-6-phosphate dehydrogenase (G-6-P DH) and has the additional function of removing residual oxygen from the mix (Figure 2.1). The components of the reaction and their concentrations are listed in Table 2.16.

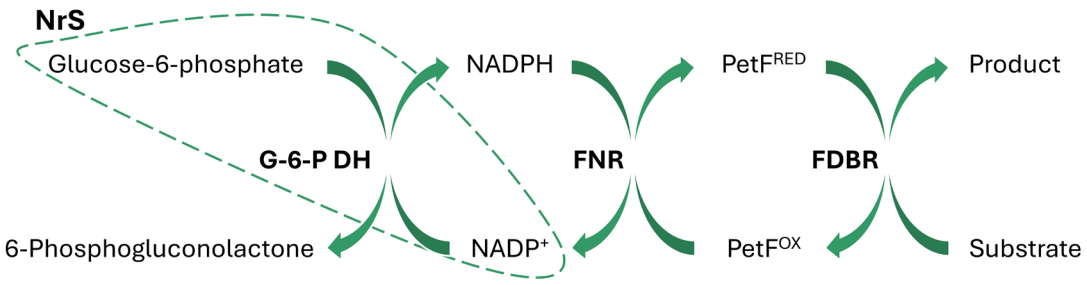

Figure 2.1 Scheme of anaerobic bilin reductase activity assay.
Overview of the activity assay *ratio*. The ferredoxin-dependent bilin reductase (FDBR) activity relies on constant supply of reduced ferredoxin ($PetF^{RED}$). $PetF^{RED}$ is replenished by a ferredoxin-$NADP^+$ reductase (FNR), requiring NADPH. Coupling a glucose-6-phosphate dehydrogenase (G-6-P DH) continuously provides NADPH. The G-6-P DH reaction and the supplied $NADP^+$ compose the NADPH-regenerating system (NrS).

Table 2.16 FDBR assay components

Component	Concentration
Glucose	100 mM
Glucose-Oxidase	50 U/mL
Catalase	5 µM
PetH	0.01 µM
PetF	1 µM
BSA	10 µM
FDBR(s)	10 µM
Substrate	10 µM
TES-KCl buffer	to 1.9 mL*

*2.9 mL for time course assay

NrS	Concentration
G-6-P	65 mM
G-6-P DH	11 U/mL
$NADP^+$	8.2 mM

In particular, all of the components of the reaction mix, except for the FDBR:substrate complex and the NrS, were transferred into a gas-tight cuvette and the temperature of the system was set to 20°C. The mix was incubated for 20 min under a continuous nitrogen gas flow and constant stirring to deplete oxygen. Subsequently, the FDBR:substrate complex was added to the cuvette and the first spectrum was recorded. The reaction was promptly started by the addition of the NrS. Spectra were recorded every 30 s for a total reaction time varying between 10 and 60 min. Finally, the reaction was stopped by 1:10 dilution of the mix in ice-cold 0.1%$_{v/v}$ TFA.

2.5.12 Bilin isolation from activity assay mix

Following the activity assay, a solid phase extraction (Sep-Pak C18 Plus Light cartridges, Waters Corporation, Milford, Massachusetts, USA) was performed to separate the products from the non-polar components of the reaction mixture. The cartridges were conditioned prior to sample application as follows:

Acetonitrile	3 mL
H_20	3 mL
$0.1\%_{v/v}$ TFA	3 mL
$10\%_{v/v}$ MeOH in $0.1\%_{v/v}$ TFA	3 mL
Acetonitrile	3 mL
H_20	3 mL
$0.1\%_{v/v}$ TFA	3 mL
$10\%_{v/v}$ MeOH in $0.1\%_{v/v}$ TFA	3 mL

Following the application of the sample, the cartridges were washed with 5 mL $0.1\%_{v/v}$ TFA before eluting the bilins with 1 mL acetonitrile. The eluted bilins were frozen at -80°C and freeze-dried (0.04 mbar, -40°C, 24 - 48 h) using an Alpha 2-4 LSC plus lyophilizer (Martin Christ GmbH, Osterode, Germany).

2.5.13 HPLC Analyses

The products of the anaerobic bilin reductase assays were analyzed using an Agilent 1100 series chromatograph equipped with a Luna 5 µm reversed-phase C18 column (Phenomenex, Torrance, CA, USA) and a diode-array detector (DAD). The mobile phase consisted of $50\%_{v/v}$ acetone and $50\%_{v/v}$ 20 mM formic acid and the elution was isocratic at a constant flow rate of 0.6 mL/min. The lyophilized samples were dissolved in DMSO and mixed with the mobile phase. After filtration using a 0.2 µm PTFE filter, the samples were injected using a 200 µL sample loop. The analytes were monitored using a DAD set at 380, 480, 560 and 650 nm, in accordance with characteristic absorbances of bilins. Absorbance spectra were recorded between 350 nm and 800 nm. Reaction products were identified by comparison of the retention time with known standards as well as whole spectrum analysis of the elution peaks. Analytes to be further examined were collected directly after the outlet of the DAD, frozen at -80°C and lyophilized as described in the previous chapter.

HPLC Mobile phase	
Acetone	$50\%_{v/v}$
20 mM Formic Acid	$50\%_{v/v}$

2.5.14 Coupled phytochrome assembly assay

In vitro chromophore assembly of the apo-phytochromes *Syn*Cph1 and *Pa*BphP with different bilins was carried out using the lysate of a pET_*cph1* or a pASK_*bphP* overexpression after centrifugation and filtration. The assembly was tested employing 50 µL lysate incubated either with 40 µM standard bilin or with 4 µL of bilin solutions of unknown concentration for 30 min

at room temperature, in the dark. Afterwards, the volume was adjusted to 500 µL with PBS. Absorbance spectra were recorded after incubation for 3 min with red light (636 nm – Pfr spectrum) and after incubation for 3 min with far-red light (730 nm for *Syn*Cph1; 750 nm for *Pa*BphP – Pr spectrum) using an Agilent 8453 spectrophotometer. Difference spectra were calculated by the subtraction of the Pfr from the Pr spectrum.

2.5.15 Phytofluor Analysis

Phytofluor formation was evaluated via fluorescence measurements (Murphy & Lagarias, 1997). Briefly, 50 µL lysate of a pET_*cph1* or a pASK_*bphP* overexpression, after centrifugation and filtration, was incubated with 4 µL of the FDBR reaction product, for 30 min, at room temperature, in the dark. Afterwards, the volume was adjusted to 500 µL with PBS and fluorescence spectra were recorded (FP-8300 spectrofluorometer, JASCO, Tokyo, Japan).

2.5.16 Phylogenetic Analysis

A multiple sequence alignment (MSA) of FDBRs was constructed using ClustalW (https://www.ebi.ac.uk/jdispatcher/msa/clustalo/). The obtained MSA was processed employing PhyML 3.0 (http://www.atgc-montpellier.fr/phyml/) (Guindon *et al.*, 2010) with the following command line: -D aa -B 100 -M WAG -V e -C 4 -F m -A e -O tlr. Statistical support was assessed using the transfer bootstrap expectation (TBE) in BOOSTER (https://booster.pasteur.fr/) (Lemoine *et al.*, 2018). The tree was displayed and modified using iTOL (https://itol.embl.de/) (Letunic & Bork, 2021).

2.5.17 Protein structure prediction and analyses

FDBRs structure prediction was performed using AlphaFold2 via ColabFold (Jumper *et al.*, 2021; Mirdita *et al.*, 2022). Parameters set for the AlphaFold2 algorithm were the following: msa_mode: MMseqs2 (UniRef + Environmental), pair_mode: unpaired + paired, model_type: auto, num_recycles: 3. The models (all characterized by a pLDDT > 80) were compared to other crystalized FDBRs using the molecular visualization software PyMOL (DeLano, 2020).

3 Results

The origin and evolution of PCB biosynthesis remain unanswered questions. This study aims to outline this process, starting from the characterization of newly identified bilin biosynthesis-related enzymes from non-photosynthetic bacteria. Following primary endosymbiosis, PCB biosynthesis pathways underwent significant divergence. Specifically, in Rhodophytes, PCB biosynthesis was hinted not to rely on FDBRs but rather on a hypothesized chromophore isomerase. The necessity of this novel enzyme was assessed in this study. Additionally, in streptophyte algae, PCB production for phytochrome-mediated responses was found not to be dependent on a PCYA but rather on a HY2-homolog. A comprehensive characterization of this class of HY2s occupies a significant portion of this work.
The concluding section of this chapter briefly delves into the characterization of an algal PUBS, an enzyme discovered solely in Viridiplantae, which catalyzes PUB production.

3.1 Pre-1 is a functional FDBR catalyzing the reduction of BV to PΦB

The putative FDBR sequence discovered in *Opitutales* bacterium grown in a bioreactor metagenome was reverse-translated using the GenScript codon optimization tool (https://www.genscript.com/tools/gensmart-codon-optimization) to match *E. coli* codon usage. The resulting gene was cloned in a pET28a(+) vector downstream the His-tag coding sequence (Figure S1A) and overexpressed to produce a His-fusion protein, named MCC5789364 (also Pre-1 or MCC), based on its accession ID. Protein purification was conducted via affinity chromatography and its outcome was subsequently analyzed by SDS-PAGE. SDS-PAGE followed by Coomassie staining revealed the presence in the elution fractions of a mostly pure protein with a predicted MW of ~ 28 kDa, alongside two larger contaminants (Figure 3.1).

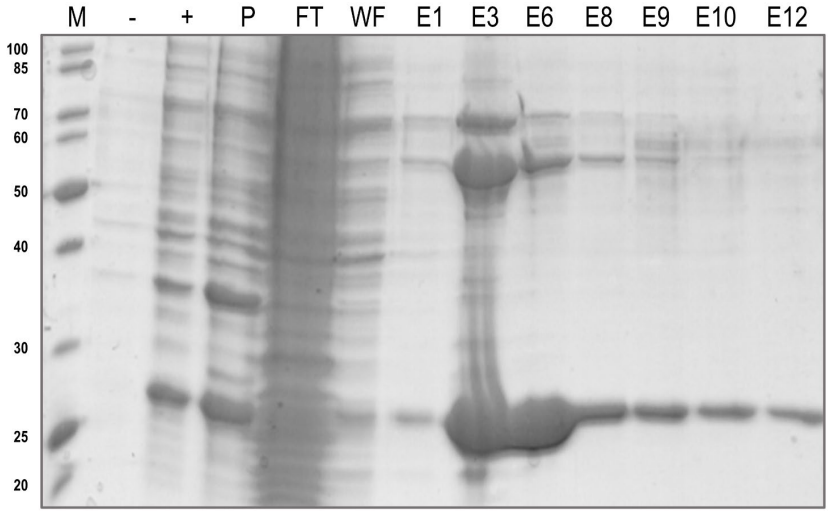

Figure 3.1 Heterologous production and purification of MCC5789364.
Coomassie-stained SDS-PAGE gel following production and affinity chromatography purification of MCC5789364 with TALON® Superflow™. (M) Molecular size marker – NEB, Unstained Protein Standard, Broad Range (MW on the left side of the figure reported in kDa); (-) Cells before induction of gene expression; (+) Cells after induction of gene expression; (P) Pellet after cell lysis; (FT) Purification flow-through fraction; (WF) Purification wash fraction; (En) Elution fractions. MCC5789364 has a predicted molecular weight of ~ 28 kDa.

The activity of MCC5789364 was investigated in an anaerobic bilin-reductase assay, employing equimolar amounts of enzyme and BV, as the potential substrate (Figure 3.2A).

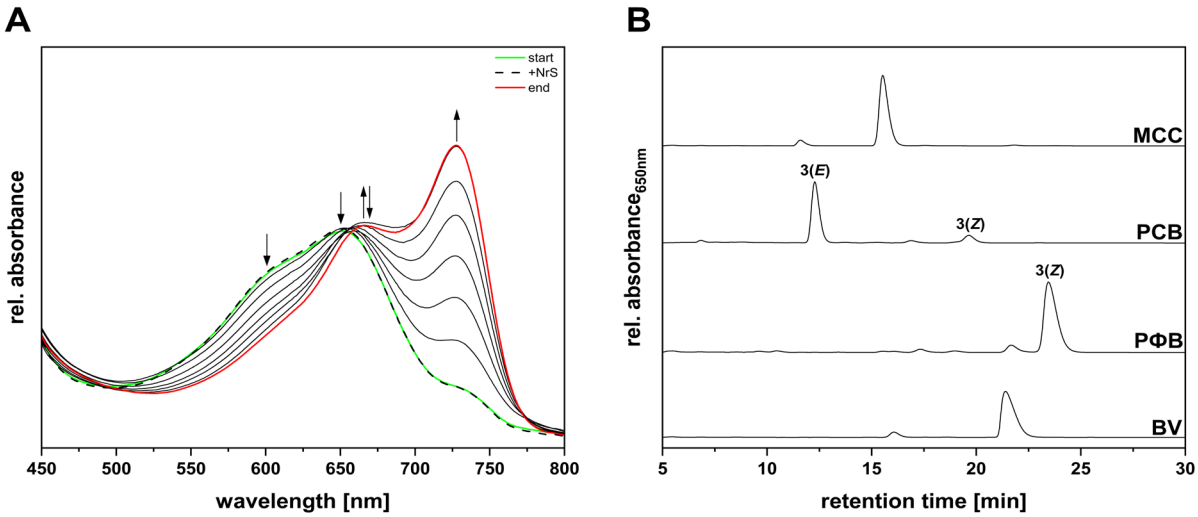

Figure 3.2 Activity assay of recombinant MCC5789364 employing BV as the substrate and characterization of reaction products.
(A) Time-resolved UV-Vis spectra of an anaerobic bilin reductase activity assay of recombinant MCC5789364 employing BV as the substrate. The total reaction time was 20 min and spectra were recorded every 30 s. The course of the absorbance during the reaction is marked by arrows. For reasons of clarity, only relevant spectra are shown. The green spectrum was recorded upon incubation of BV and MCC5789364, without starting the reaction. The dashed spectrum represents the first recorded after starting the reaction. Spectra recorded during the reaction are shown as solid black lines. The red curve represents the end spectrum. Curves were smoothed applying a 50 pt. Savitzky-Golay filter.
(B) HPLC analysis of the reaction products of MCC5789364 with BV as substrate (MCC). The products were analyzed using a reversed-phase 5 µm C18 Luna column (Phenomenex) as stationary phase. The mobile phase consisted of 50%$_{v/v}$ acetone and 50%$_{v/v}$ 20 mM formic acid flowing at 0.6 mL/min. Absorbance was continuously recorded at 650 nm. PCB, phycocyanobilin standard; PΦB, phytochromobilin standard; BV, biliverdin IXα standard.

Interestingly, the putative reductase and substrate formed a vivid teal-colored complex with an absorbance maximum at ~ 650 nm and a small shoulder at ~ 600 nm, suggesting the ability of the protein to bind the substrate. The presence of an additional shoulder at ~ 730 nm indicated the presence of BV in its protonated form (BVH^+) (Tu *et al.*, 2004, 2007, 2008; Busch *et al.*, 2011a) (Figure 3.2A – start). Upon start of the reaction (Figure 3.2A – +NrS), no obvious effect could be observed. Nonetheless, as the reaction progressed, the absorbance of the main peak shifted over time towards ~ 670 nm, while a simultaneous rise in absorbance at ~ 730 nm suggested the presence of substrate radical intermediates (Figure 3.2A – end). The product was isolated from the reaction mix and identified through HPLC analysis (Figure 3.2B). HPLC analysis revealed the formation of a main product with a retention time of 15.5

min (Figure 3.2B – MCC), not overlapping with any bilin standard (Figure 3.2B – PCB, PΦB, BV). To elucidate its identity, the product was further investigated in coupled phytochrome assembly assays, employing apo-Cph1 from *Synechocystis* sp. PCC 6803 (apo-*Syn*Cph1) and apo-BphP from *Pseudomonas aeruginosa* (apo-*Pa*BphP). *Syn*Cph1 binds PCB as its natural chromophore, while *Pa*BphP uses BV. However, as previously mentioned (chapter 1.3), phytochromes are also able to accommodate different bilins as long as they possess the same A-ring configuration as the natural chromophore. Thus, *Syn*Cph1 is able to covalently bind bilins possessing an ethylidene group at the A-ring, whereas *Pa*BphP only covalently binds bilins with an A-ring endo-vinyl group. The incubation of the unidentified product with apo-*Pa*BphP failed in yielding a photoactive adduct, as no characteristic difference spectrum was obtained (data not shown), ultimately indicating the lack of the A-ring endo-vinyl group. Consistent with this observation, incubating the product with apo-*Syn*Cph1 resulted in a difference spectrum nearly identical to the one obtained with PΦB (Kohchi *et al.*, 2001; Lu *et al.*, 2017; Mukougawa *et al.*, 2006; Muramoto *et al.*, 2005; Sawers *et al.*, 2004; Zhao *et al.*, 2007) (Figure 3.3). This suggests that the produced bilin might be 3(*E*)-PΦB. The PΦB used as standard for the HPLC analysis, originated from an anaerobic bilin-reductase activity assay performed using the HY2 from *Arabidopsis thaliana*. It is common knowledge that FDBRs tend to favor the production of the 3(*Z*) bilin isomer, as also observed for *At*HY2 (Frankenberg *et al.*, 2001). The discovery that MCC5789364 exclusively generates 3(*E*)-PΦB is, hitherto, the first reported instance of a FDBR exhibiting, *in vitro,* a shift towards 3(*E*)-isomer production.

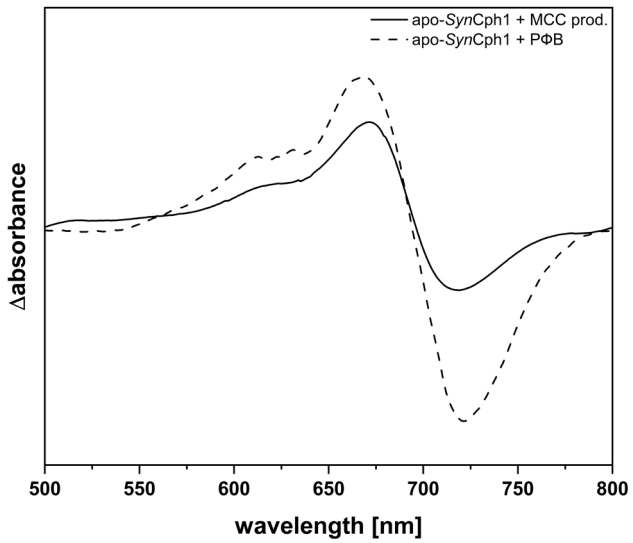

Figure 3.3 Red/far-red light induced difference spectra of coupled phytochrome assembly assays employing PΦB and the product of the MCC5789364 reaction (MCC prod.).
Absorbance spectra were recorded after incubation for 3 min with red light (636 nm – Pfr spectrum) and after incubation for 3 min with far-red light (730 nm – Pr spectrum). Difference spectra were calculated by the subtraction of the Pfr from the Pr spectrum. The apo-*Syn*Cph1 + PΦB difference spectrum (dashed line) was smoothed

applying a 10 pt. Savitzy-Golay filter. The apo-*Syn*Cph1 + MCC prod. difference spectrum (solid line) was smoothed applying a 40 pt. Savitzky-Golay filter and the signal was 3x enhanced.

3.2 Pre-2 is a functional FDBR catalyzing the reduction of BV to PΦB

The gene encoding for the putative FDBR sequence discovered in *Chondromyces apiculatus* DSM 436 (donation of Nathan Rockwell, UC Davis, USA) was cloned in a pET28a(+) vector downstream the His-tag coding sequence (similarly to Figure S1A) and overexpressed to produce a His-fusion protein, named CAP_1520 (or Pre-2), based on its locus tag. Protein purification was conducted via affinity chromatography and its outcome was subsequently analyzed by SDS-PAGE. SDS-PAGE followed by Coomassie staining revealed the presence in the elution fractions of a protein with predicted MW of ~ 32 kDa and several other contaminants (Figure 3.4). In order to remove the contaminants before monitoring the activity, the elution fractions were pooled and further purified via ultrafiltration using 50 kDa and 10 kDa centrifugal concentrators.

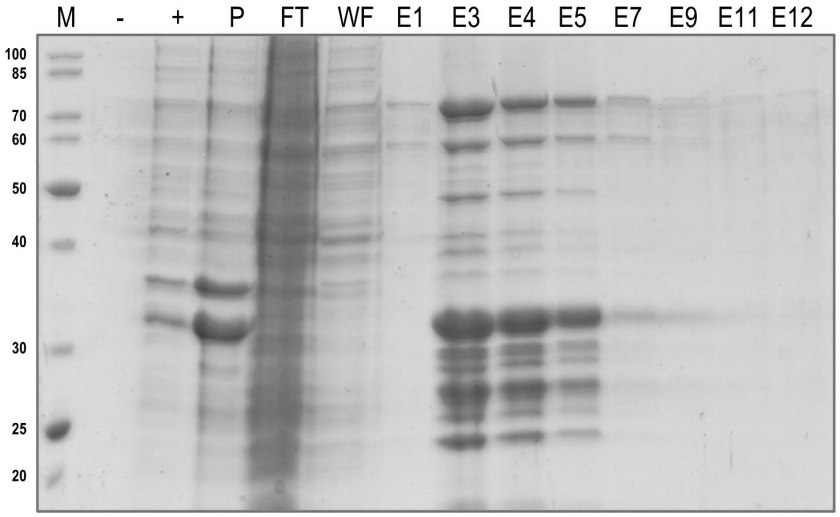

Figure 3.4 Heterologous production and purification of CAP_1520.
Coomassie-stained SDS-PAGE gel following production and affinity chromatography purification of CAP_1520 with TALON® Superflow™. (M) Molecular size marker – NEB, Unstained Protein Standard, Broad Range (MW on the left side of the figure reported in kDa); (-) Cells before induction of gene expression; (+) Cells after induction of gene expression; (P) Pellet after cell lysis; (FT) Purification flow-through fraction; (WF) Purification wash fraction; (En) Elution fractions. CAP_1520 has a predicted molecular weight of ~ 32 kDa.

The activity of CAP_1520 was investigated in an anaerobic bilin-reductase assay, employing equimolar amounts of enzyme and BV (Figure 3.5A). Given that the gene cluster containing CAP_1520 also includes a heme oxygenase, BV was already presumed to be the specific substrate (Rockwell *et al.*, 2023).

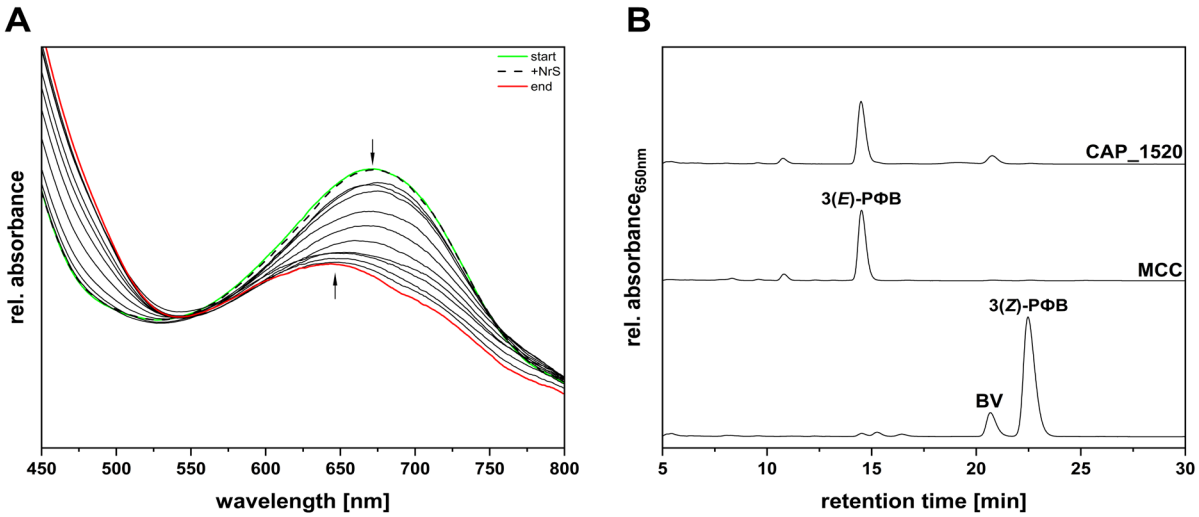

Figure 3.5 Activity assay of recombinant CAP_1520 employing BV as the substrate and characterization of reaction products.
(A) Time-resolved UV-Vis spectra of an anaerobic bilin reductase activity assay of recombinant CAP_1520 employing BV as the substrate. The total reaction time was 30 min and spectra were recorded every 30 s. The course of the absorbance during the reaction is marked by arrows. For reasons of clarity, only relevant spectra are shown. The green spectrum was recorded upon incubation of BV and CAP_1520, without starting the reaction. The dashed spectrum represents the first recorded after starting the reaction. Spectra recorded during the reaction are shown as solid black lines. The red curve represents the end spectrum. Curves were smoothed applying an 80 pt. Savitzky-Golay filter.
(B) HPLC analysis of the reaction products of CAP_1520 with BV as substrate (CAP_1520). The products were analyzed using a reversed-phase 5 µm C18 Luna column (Phenomenex) as stationary phase. The mobile phase consisted of 50%$_{v/v}$ acetone and 50%$_{v/v}$ 20 mM formic acid flowing at 0.6 mL/min. Absorbance was continuously recorded at 650 nm. 3(*Z*)-PΦB, 3(*Z*)-phytochromobilin; 3(*E*)-PΦB, 3(*E*)-phytochromobilin; MCC, product of MCC5789364 with BV as substrate.

The incubation of Pre-2 with the substrate led to the formation of a complex with an absorbance maximum at ~ 670 nm (Figure 3.5A – start). The start of the reaction nearly did not affect the initial absorbance peak (Figure 3.5A – +NrS). The reaction seemed to proceed at a slow pace, culminating in a final product absorbing at 645 nm (Figure 3.5A – end). The HPLC analysis of the isolated product revealed the reaction was incomplete, as evidenced by the presence of residual BV at ~ 21 min elution time, with the main product eluting at 14.5 min (Figure 3.5B – CAP_1520). Similarly to the previously characterized protein, this product also lacked a direct match among bilin standards, but it completely overlayed with the product of the Pre-1 reaction (MCC), suggesting the reduction of BV to 3(*E*)-PΦB. The discrepancy in retention time compared to the previously identified Pre-1 product is ascribable to the change of the mobile phase. The putative production of 3(*E*)-PΦB was confirmed performing phytochrome assembly assays with apo-*Syn*Cph1 and apo-*Pa*BphP. Once again, only the incubation of the product with apo-*Syn*Cph1 led to the formation of a photoactive adduct, displaying typical PΦB-Cph1 photocycle (Figure 3.6). Based on these findings, it can be concluded that Pre-2, like Pre-1, catalyzes the conversion of BV to 3(*E*)-PΦB, albeit at a considerably slower turnover rate.

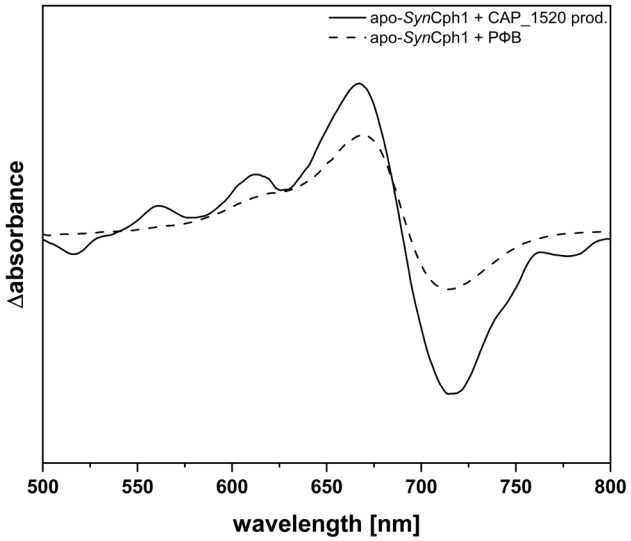

Figure 3.6 Red/far-red light induced difference spectra of coupled phytochrome assembly assays employing PΦB and the product of the CAP_1520 reaction (CAP_1520 prod.).
Absorbance spectra were recorded after incubation for 3 min with red light (636 nm – Pfr spectrum) and after incubation for 3 min with far-red light (730 nm – Pr spectrum). Difference spectra were calculated by the subtraction of the Pfr from the Pr spectrum. The apo-*Syn*Cph1 + PΦB difference spectrum (dashed line) was smoothed applying a 10 pt. Savitzy-Golay filter. The apo-*Syn*Cph1 + CAP_1520 prod. difference spectrum (solid line) was smoothed applying a 20 pt. Savitzky-Golay filter and the signal 3x enhanced.

3.3 Pre-3 is the first reported FDBR catalyzing the reduction of BV to PEB via PΦB

The gene encoding for the putative FDBR sequence discovered in *Myxococcales* bacterium from a bioreactor metagenome (donation of Nathan Rockwell, UC Davis, USA) was cloned in a pET28a(+) vector downstream of the His-tag coding sequence (similarly to Figure S1A) and overexpressed to produce a His-fusion protein, named MBL9008304 (also Pre-3 or MBL), based on the accession ID. Protein purification was conducted via affinity chromatography and its outcome was subsequently analyzed by SDS-PAGE. SDS-PAGE followed by Coomassie staining revealed the presence in the elution fractions of a protein with predicted MW of ~ 31 kDa and two contaminants of much bigger size, as in the case of Pre-1 (Figure 3.7).

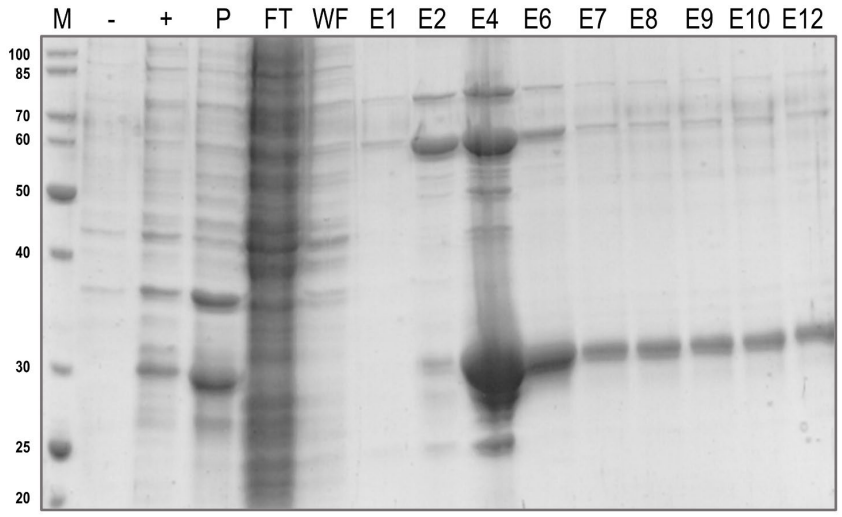

Figure 3.7 Heterologous production and purification of MBL9008304.
Coomassie-stained SDS-PAGE gel following production and affinity chromatography purification of MBL9008304 with TALON® Superflow™. (M) Molecular size marker – NEB, Unstained Protein Standard, Broad Range (MW on the left side of the figure reported in kDa); (-) Cells before induction of gene expression; (+) Cells after induction of gene expression; (P) Pellet after cell lysis; (FT) Purification flow-through fraction; (WF) Purification wash fraction; (En) Elution fractions. MCC5789364 has a predicted molecular weight of ~ 31 kDa.

Similarly to CAP_1520, MBL9008304 is encoded in a gene cluster alongside a heme oxygenase, thus BV was used as the substrate in an anaerobic bilin-reductase activity assay (Rockwell *et al.*, 2023). The initially performed 20 min assay revealed a color shift of the reaction mix from teal to antique pink, potentially indicating the conversion of BV to PEB, as hinted by Rockwell and colleagues (data not shown). Nevertheless, an unusual amount of shifts in absorbance peaks were observed, prompting a subsequent time course assay. In the time course assay, samples were isolated from the reaction mix after 5, 9 and 20 minutes from the start to potentially gain more insights on the reaction course (Figure 3.8A).

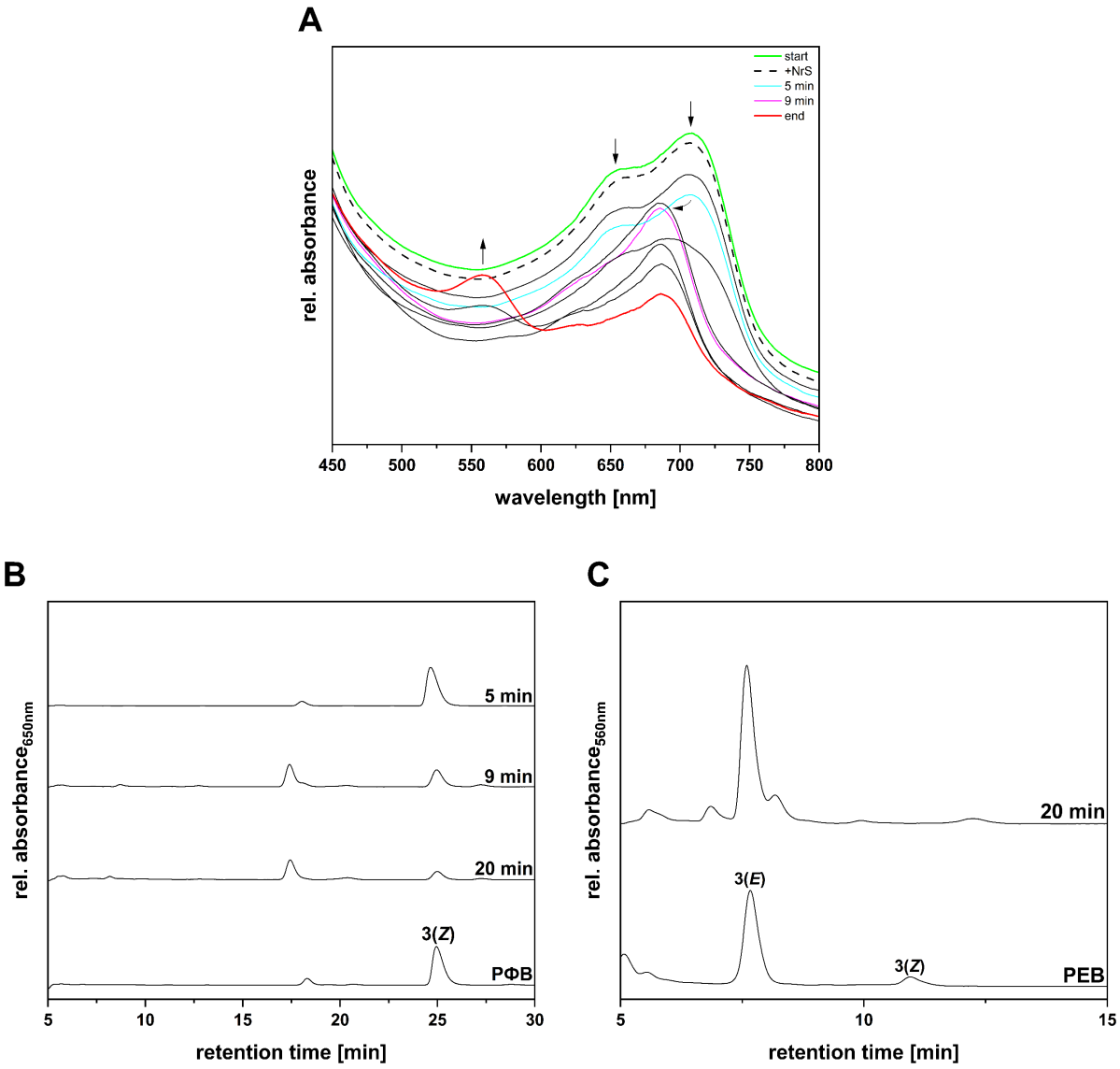

Figure 3.8 Activity assay of recombinant MBL9008304 employing BV as the substrate and characterization of reaction products.
(A) Time-resolved UV-Vis spectra of an anaerobic bilin reductase activity assay of recombinant MBL9008304 employing BV as the substrate. The total reaction time was 20 min and spectra were recorded every 30 s. The course of the absorbance during the reaction is marked by arrows. For reasons of clarity, only relevant spectra are shown. The green spectrum was recorded upon incubation of BV and MBL9008304, without starting the reaction. The dashed spectrum represents the first recorded after starting the reaction. Spectra recorded during the reaction are shown as solid black lines. The cyan spectrum represents the product formed after 5 min. The violet spectrum represents the product formed after 9 min. The red curve represents the end spectrum. Curves were smoothed applying a 40 pt. Savitzky-Golay filter.
(B) HPLC analysis of the reaction products of MBL9008304 with BV as substrate. The products were analyzed using a reversed-phase 5 µm C18 Luna column (Phenomenex) as stationary phase. The mobile phase consisted of 50%$_{v/v}$ acetone and 50%$_{v/v}$ 20 mM formic acid flowing at 0.6 mL/min. Absorbance was continuously recorded at 650 nm. PΦB, phytochromobilin standard.
(C) HPLC analysis of the 20 min reaction product of MBL9008304 with BV as substrate. The products were analyzed using a reversed-phase 5 µm C18 Luna column (Phenomenex) as stationary phase. The mobile phase consisted of 50%$_{v/v}$ acetone and 50%$_{v/v}$ 20 mM formic acid flowing at 0.6 mL/min. Absorbance was continuously recorded at 560 nm. PEB, phycoerythrobilin standard.

The incubation of Pre-3 with BV led to the formation of a complex with dual absorbance at ~ 660 nm and ~ 710 nm, with the latter likely indicating the presence of BVH^+ (Figure 3.8A –

start). Following the start of the reaction (Figure 3.8A – +NrS), no discernible effects were observed, and absorbance peaks remained consistent until 5 min from the reaction start (Figure 3.8A – 5 min). By 9 min, the double peak transitioned into a single peak with absorbance at ~ 690 nm (Figure 3.8A – 9 min), whereas the final 20 min product retained this absorbance and exhibited an additional peak at ~ 560 nm (Figure 3.8A – end). Subsequent HPLC analysis of these three products revealed an initial conversion of BV to predominantly 3(*Z*)-PΦB (Figure 3.8B). The intensity of this DAD signal decreased over time, as 3(*Z*)-PΦB seemingly appeared to undergo a reduction to 3(*E*)-PEB (Figure 3.8C). This reduction involved an isomerization shift from a 3(*Z*) to 3(*E*) bilin. As reduction from 3(*Z*)-PΦB to 3(*E*)-PEB would need a transition to a 3(*E*) conformer, the 17 min retention time DAD signal rising over time possibly indicated the isomerization from 3(*Z*) to 3(*E*)-PΦB (Figure 3.8B).
Pre-3 was ultimately shown to catalyze the first reported instance of a $4e^-$ reduction of BV to PEB, with the formation of PΦB as the intermediate.

3.4 Pre-PcyAs are functioning in a monomeric state

As previously mentioned, all the members of the FDBR family are known to function as monomers (chapter 1.4.1). To ascertain whether this holds true for these newly characterized pre-FDBRs, their oligomerization state was determined via size exclusion chromatography using a Superdex® 75 10/300 GL column (GE Healthcare) (Figure 3.9).

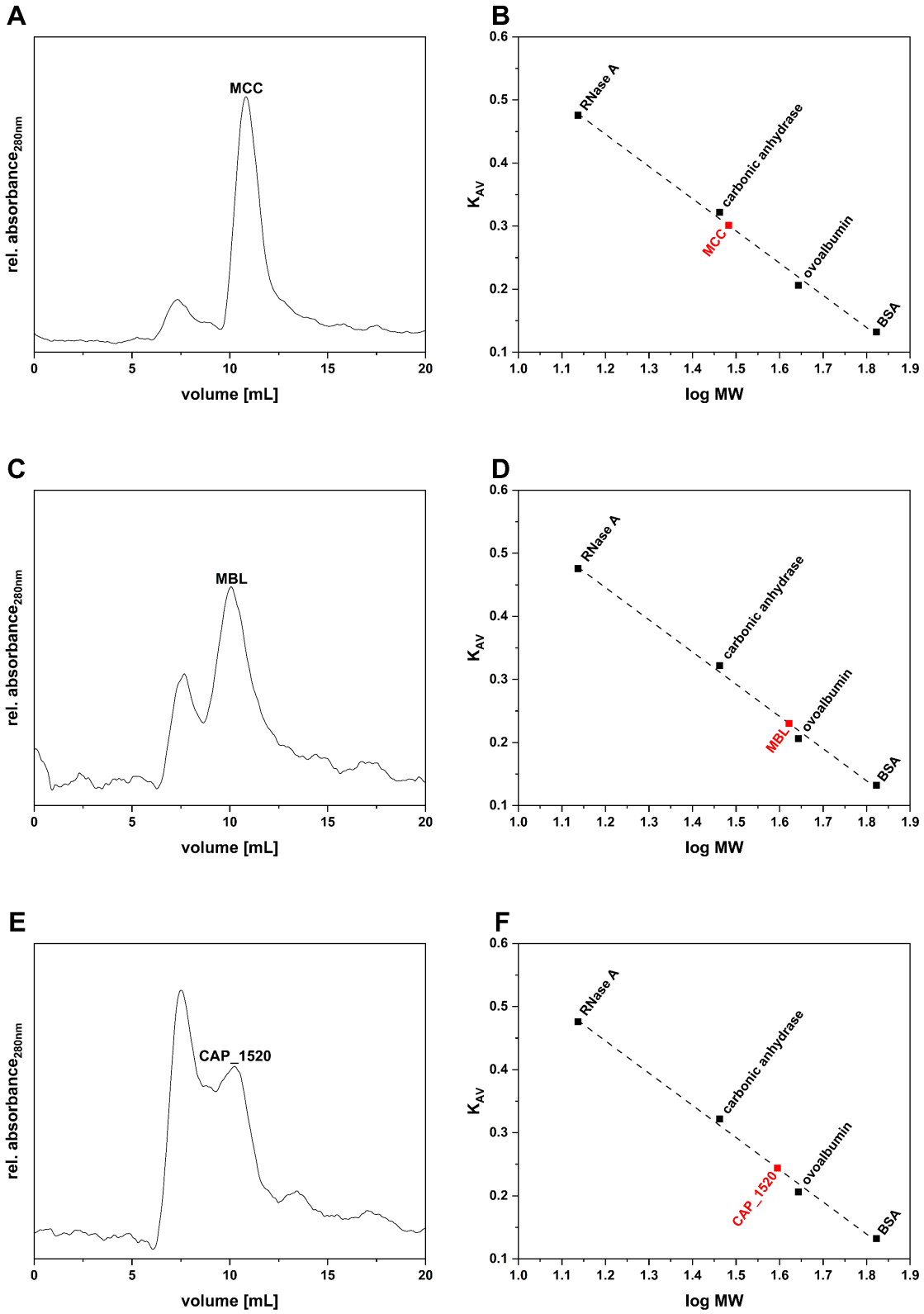

Figure 3.9 Determination of the oligomerization state of pre-FDBRs.
(A) Size exclusion chromatography of His-MCC5789364 (MCC) using a Superdex® 75 10/300 GL equilibrated with TES-KCl buffer. Absorbance was continuously measured at 280 nm. The chromatogram was smoothed applying a 60 pt. Savitzky-Golay filter due to detection issues of the Äkta Explorer UV module.
(B) Calibration curve of the Superdex® 75 10/300 GL column. RNAse A (MW = 13.7 kDa), carbonic anhydrase (MW = 29 kDa), ovoalbumin (MW = 44 kDa) and BSA (MW = 66.4 kDa) were used for calibration. The calibration curve was obtained by plotting the K_{AV} of the standards against the logarithm of the molecular weight (log MW) (black squares) and fitted (dashed line) using a linear regression function in Origin. The red square indicates MCC on the calibration curve.

(C) Size exclusion chromatography of His-MBL9008304 (MBL) using a Superdex® 75 10/300 GL equilibrated with TES-KCl buffer. Absorbance was continuously measured at 280 nm. The chromatogram was smoothed applying a 70 pt. Savitzky-Golay filter due to detection issues of the Äkta Explorer UV module.
(D) Calibration curve of the Superdex® 75 10/300 GL column. RNAse A (MW = 13.7 kDa), carbonic anhydrase (MW = 29 kDa), ovoalbumin (MW = 44 kDa) and BSA (MW = 66.4 kDa) were used for calibration. The calibration curve was obtained by plotting the K_{AV} of the standards against the logarithm of the molecular weight (log MW) (black squares) and fitted (dashed line) using a linear regression function in Origin. The red square indicates MBL on the calibration curve.
(E) Size exclusion chromatography of His-CAP_1520 (CAP_1520) using a Superdex® 75 10/300 GL equilibrated with TES-KCl buffer. Absorbance was continuously measured at 280 nm. The chromatogram was smoothed applying a 50 pt. Savitzky-Golay filter due to detection issues of the Äkta Explorer UV module.
(F) Calibration curve of the Superdex® 75 10/300 GL column. RNAse A (MW = 13.7 kDa), carbonic anhydrase (MW = 29 kDa), ovoalbumin (MW = 44 kDa) and BSA (MW = 66.4 kDa) were used for calibration. The calibration curve was obtained by plotting the K_{AV} of the standards against the logarithm of the molecular weight (log MW) (black squares) and fitted (dashed line) using a linear regression function in Origin. The red square indicates CAP_1520 on the calibration curve.

His-MCC eluted at 10.95 mL (Figure 3.9A) corresponding to a monomer with MW ~ 30 kDa, according to the calibration curve (Figure 3.9B), thus resulting slightly larger than the bioinformatically predicted size. The void volume of the column was determined to be 7.6 min; hence, the smaller peak eluting earlier likely represents protein aggregates (Figure 3.9A). A similar situation was found to be true for His-MBL. Besides the presence of aggregates, the main protein peak eluted at ~ 10.3 min (Figure 3.9C), corresponding to a monomeric protein with a MW ~ 40 kDa (Figure 3.9D), also larger than the predicted 31 kDa and in contrast to the SDS-PAGE analysis (Figure 3.7). This discrepancy between the predicted and analytically-determined MW could be attributed either to be the presence of contaminants in the samples or the shape of the protein. SEC specifically measures the hydrodynamic radius of molecules, which is related to their size and shape in solution (Moore, 1964). The size estimation of not-fully globular proteins is therefore not extremely precise.
Finally, His-CAP_1520 showed mainly the presence of protein aggregates, with only partially soluble protein eluting at ~ 10.4 min as a monomeric protein with MW ~ 38 kDa, once more highlighting a disparity between the predicted and analytically-determined MW (Figure 3.9E, F). The prevalence of aggregates might also account for the anaerobic bilin-reductase assay result, wherein no evident change in absorbance between the start and the end of the reaction could be observed (Figure 3.5A).
Based on these data, the precursors to FDBRs were also shown to be functioning as monomers.

3.5 *Gs*PEBA catalyzes the reduction of BV to 15,16-DHBV

Around three decades ago, the biosynthesis of PCB in the Cyanidiophycea *Galdieria sulphuraria* was suggested not to be mediated by FDBRs but rather by an unknown chromophore isomerase (Beale & Cornejo, 1991a, 1991b, 1991c). In the search for the isomerase, it is nevertheless fundamental to exclude any unpredicted side reaction of the bilin reductases. Over the past few years, our research group made several attempts to explore

the activity of PEBA from *G. sulphuraria* (*Gs*PEBA) (Eichler, 2016; Hartmann, 2018). Unfortunately, the protein was prone to aggregation in several expression constructs and conditions. Ultimately, only a slight hint of activity was observed when using the original *GsPEBA* sequence cloned downstream of the Strep-tag II coding sequence in a pASK-IBA45(+) construct, proceeding with an overexpression in *E. coli* BL21-CodonPlus-RIL (Agilent Technologies Inc., Santa Clara, California, USA) and cultivation in minimal medium (Hartmann, 2018). Producing a eukaryotic protein in a prokaryotic host presents numerous challenges, primarily stemming from differences in codon usage (Kane, 1995; Kurland & Gallant, 1996; Sahdev *et al.*, 2008). The arrangement of codons in mRNA can significantly influence protein translation efficiency, affecting various aspects such as protein yield, solubility, folding and, therefore, functionality. Most often, the strategy adopted to avoid these issues is to fully optimize the gene sequence to the host codon usage. However, when all the codons in a mRNA sequence are commonly used, the ribosomes tend to move consistently faster along the mRNA during translation, potentially impacting protein folding kinetics and quality control mechanisms (Cortazzo *et al.*, 2002; Komar *et al.*, 1999; Orešič & Shalloway, 1998; Walsh *et al.*, 2020). In recent years, several algorithms have been developed in the attempt to find a balance between codon usage, mRNA stability and protein folding. Among these, codon harmonization, unlike codon optimization, aims to synchronize the codon usage of the gene of interest and the host translation machinery. The algorithm starts by assessing the codon usage patterns of both the origin organism and the heterologous expression host. Leveraging on this information, the codon usage pattern of the gene of interest in the heterologous host is adjusted to match that of the origin organism (Rodriguez *et al.*, 2018; Wright *et al.*, 2022).

In light of these considerations, a new attempt was conducted employing a *GsPEBA* sequence harmonized using the CHARMING algorithm (http://www.codons.org/codons.html). The encoded protein (named *Gs*PEBA_harmo) was recombinantly produced in *E. coli* BL21(DE3) in standard LB medium and purified via affinity chromatography. Despite predominantly yielding inclusion bodies (predicted MW ~ 31 kDa, Figure 3.10 – P), small quantities of soluble protein were obtained after purification, notably in highest abundance in elution fractions 3 to 5 (Figure 3.10 – E3, E5).

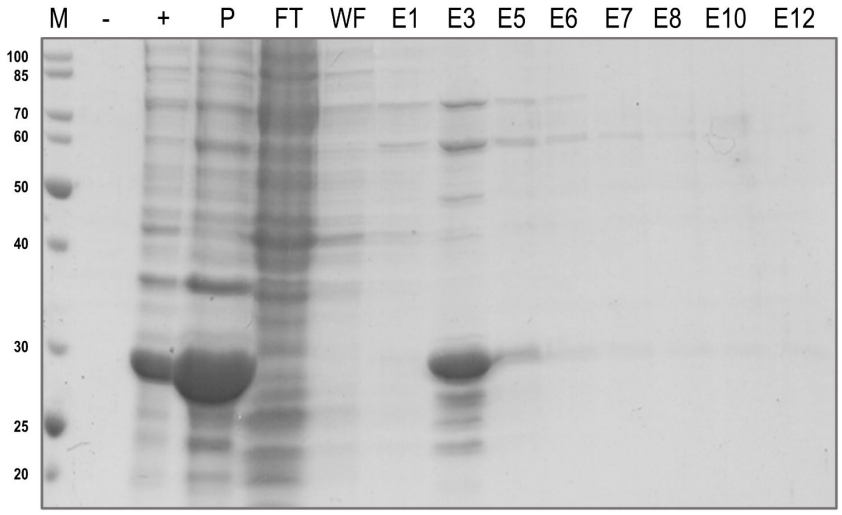

Figure 3.10 Heterologous production and purification of *Gs*PEBA_harmo.
Coomassie-stained SDS-PAGE gel following production and affinity chromatography purification of *Gs*PEBA_harmo with TALON® Superflow™. (M) Molecular size marker – NEB, Unstained Protein Standard, Broad Range (MW on the left side of the figure reported in kDa); (-) Cells before induction of gene expression; (+) Cells after induction of gene expression; (P) Pellet after cell lysis; (FT) Purification flow-through fraction; (WF) Purification wash fraction; (En) Elution fractions. MCC5789364 has a predicted molecular weight of ~ 31 kDa.

His-*Gs*PEBA_harmo-containing fractions were pooled, dialyzed against TES-KCl buffer and concentrated with a 10 kDa MW cutoff Centricon®. The activity assay was performed using His-*Gs*PEBA_harmo and BV, its designated substrate, in equimolar amounts (Figure 3.11A).

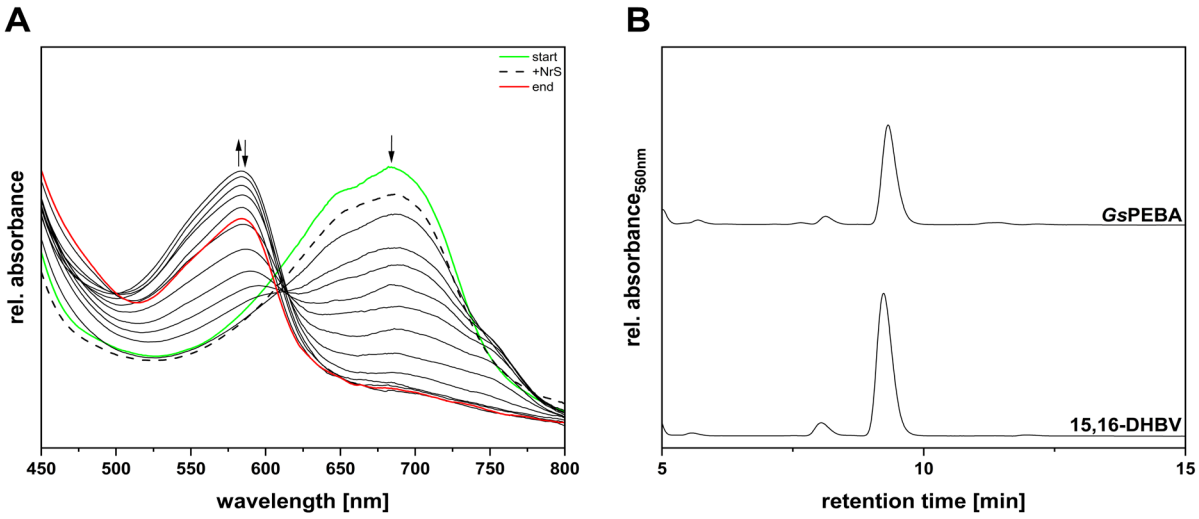

Figure 3.11 Activity assay of recombinant *Gs*PEBA employing BV as the substrate and characterization of reaction products.
(A) Time-resolved UV-Vis spectra of an anaerobic bilin reductase activity assay of recombinant *Gs*PEBA employing BV as the substrate. The total reaction time was 20 min and spectra were recorded every 30 s. The course of the absorbance during the reaction is marked by arrows. For reasons of clarity, only relevant spectra are shown. The green spectrum was recorded upon incubation of BV and *Gs*PEBA, without starting the reaction. The dashed spectrum represents the first recorded after starting the reaction. Spectra recorded during the reaction are shown as solid black lines. The red curve represents the end spectrum. Curves were smoothed applying a 40 pt. Savitzky-Golay filter.
(B) HPLC analysis of the reaction products of *Gs*PEBA with BV as substrate (*Gs*PEBA). The products were analyzed using a reversed-phase 5 µm C18 Luna column (Phenomenex) as stationary phase. The mobile phase

consisted of 50%$_{v/v}$ acetone and 50%$_{v/v}$ 20 mM formic acid flowing at 0.6 mL/min. Absorbance was continuously recorded at 560 nm. 15,16-DHBV, 15,16-dihydrobiliverdin standard.

The reductase and the substrate formed a complex with an absorbance maximum at ~ 685 nm (Figure 3.11A – start). Following the addition of the NrS, a modest decrease in absorbance of the complex peak could be observed (Figure 3.11A – +NrS). Ultimately, *Gs*PEBA_harmo revealed activity, with the ~ 585 nm absorbing product being accumulated mainly within 12 minutes and subsequently undergoing non-specific degradation over time (Figure 3.11A – end). HPLC analysis confirmed *Gs*PEBA is indeed catalyzing the reduction of BV to 15,16-DHBV, akin to a canonical PebA (Figure 3.11B – *Gs*PEBA).

3.6 *Gs*PEBB catalyzes the reduction of 15,16-DHBV to PEB

In a previous study, an *E. coli* codon-optimized *GsPEBB* sequence was cloned in pASK-IBA45(+) expression vector, downstream of the Strep-tag II coding sequence (Busch, 2011). *Gs*PEBB has already been demonstrated to reduce 15,16-DHBV to PEB within a 20 min activity assay (Eichler, 2016). However, to exclude the possibility of additional isomerization to PCB conducted by the same enzyme (scenario that will be depicted for *Kfla*HY2_N105D and *Kfla*HY2_N105D_D242N in chapter 3.11), it was necessary to extend the duration of the activity assay. The construct mentioned earlier in this chapter was thus used to investigate this hypothesis. The outcome of protein purification was verified using SDS-PAGE followed by Coomassie staining and Western Blot analysis (Figure 3.12A, B).

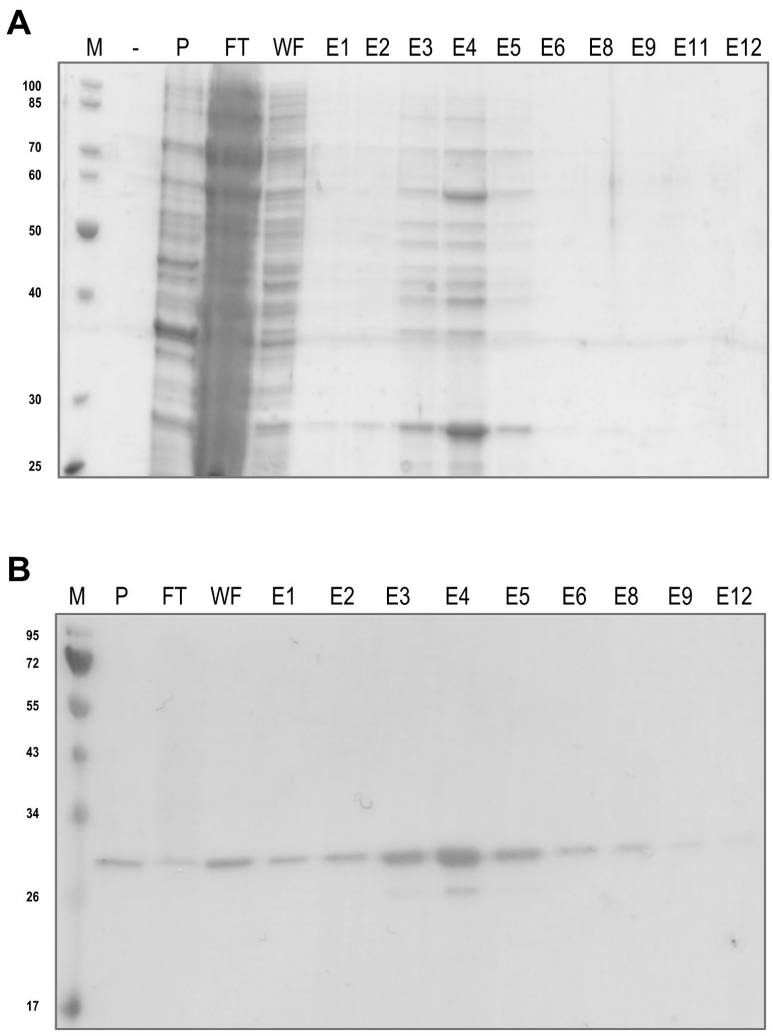

Figure 3.12 Heterologous production and purification of *Gs*PEBB and immunological detection via Western Blot.
(A) Coomassie-stained SDS-PAGE gel following production and affinity chromatography purification of *Gs*PEBB with Strep-Tactin® Sepharose®. (M) Molecular size marker – NEB, Unstained Protein Standard, Broad Range (MW on the left side of the figure reported in kDa); (-) Cells before induction of gene expression; (P) Pellet after cell lysis; (FT) Purification flow-through fraction; (WF) Purification wash fraction; (En) Elution fractions. *Gs*PEBB has a predicted molecular weight of ~ 28 kDa.
(B) Immunological detection via Western Blot of StrepII-*Gs*PEBB using Strep-Tactin® AP conjugate. (M) Molecular size marker – NEB, Color Prestained Protein Standard, Broad Range (MW on the left side of the figure reported in kDa); (P) Pellet after cell lysis; (FT) Purification flow-through fraction; (WF) Purification wash fraction; (En) Elution fractions.

Consistent with previous findings (Eichler, 2016), the Coomassie-stained gel indicated an overall poor purification, yet a protein signal with a size between 25 and 30 kDa, compatible with the calculation, was detected (Figure 3.12A). The identification of this signal as Strep-*Gs*PEBB was achieved via Western Blot, using a Strep-Tactin AP conjugate (Figure 3.12B). The elution fractions containing Strep-*Gs*PEBB were pooled, dialyzed against TES-KCl buffer and concentrated with a 10 kDa MW cutoff Centricon®. An activity assay was performed using Strep-*Gs*PEBB and 15,16-DHBV, in equimolar amounts (Figure 3.13A).

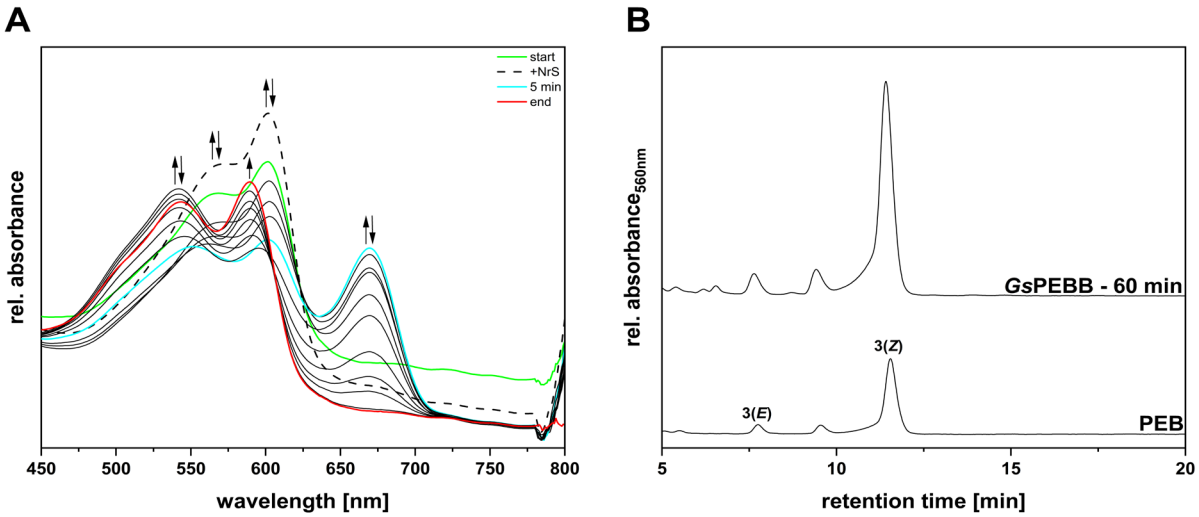

Figure 3.13 Activity assay of recombinant *Gs*PEBB employing 15,16-DHBV as the substrate and characterization of reaction products.
(A) Time-resolved UV-Vis spectra of an anaerobic bilin reductase activity assay of recombinant *Gs*PEBB employing 15,16-DHBV as the substrate. The total reaction time was 60 min and spectra were recorded every 30 s. The course of the absorbance during the reaction is marked by arrows. For reasons of clarity, only relevant spectra are shown. The green spectrum was recorded upon incubation of BV and *Gs*PEBB, without starting the reaction. The dashed spectrum represents the first recorded after starting the reaction. Spectra recorded during the reaction are shown as solid black lines. The cyan spectrum represents the product formed after 5 min. The red curve represents the end spectrum. Curves were smoothed applying a 40 pt. Savitzky-Golay filter.
(B) HPLC analyses of the reaction products of *Gs*PEBB with 15,16-DHBV as substrate (*Gs*PEBB – 60 min). The products were analyzed using a reversed-phase 5 µm C18 Luna column (Phenomenex) as stationary phase. The mobile phase consisted of 50%$_{v/v}$ acetone and 50%$_{v/v}$ 20 mM formic acid flowing at 0.6 mL/min. Absorbance was continuously recorded at 560 nm. PEB, phycoerythrobilin standard.

The ability of Strep-*Gs*PEBB to bind 15,16-DHBV was evidenced by a double absorbance peak at ~ 565 nm and ~ 600 nm (Figure 3.13A – start). Upon initiating the reaction, a slight increase in the absorbance of both peaks was noted, attributed to residual Strep-*Gs*PEBB:15,16-DHBV in the NrS-injection syringe (Figure 3.13A – +NrS). Within 5 min from the start, in addition to a decrease in the absorbance of the initial complex, a new peak at ~ 670 nm emerged (Figure 3.13A – 5 min). Over time, the absorbance of these peaks decreased, ultimately resulting in a product absorbing at ~ 545 nm and ~ 590 nm (Figure 3.13A – end). HPLC analysis of the final product confirmed the presence of predominantly 3(*Z*)-PEB, alongside minor traces of 3(*E*)-PEB and residual 15,16-DHBV (9.4 min product), therefore excluding any isomerizing ability of *Gs*PEBB (Figure 3.13B – *Gs*PEBB - 60 min). Unfortunately, the 5 min product could not be characterized via HPLC due to limitations related to the reaction mix volume and detection with the photometer. Furthermore, conducting an additional assay was not feasible due to insufficient amounts of 15,16-DHBV. An alternative approach to provide *Gs*PEBB with its substrate involves coupling its reaction with that of PebA, which could directly supply 15,16-DHBV. Since these results were obtained before achieving a functional *Gs*PEBA, *Gs*PEBB was initially coupled to the PebA of *Synechococcus* sp. WH 8020 (*Syc*PebA) (Figure 3.14A).

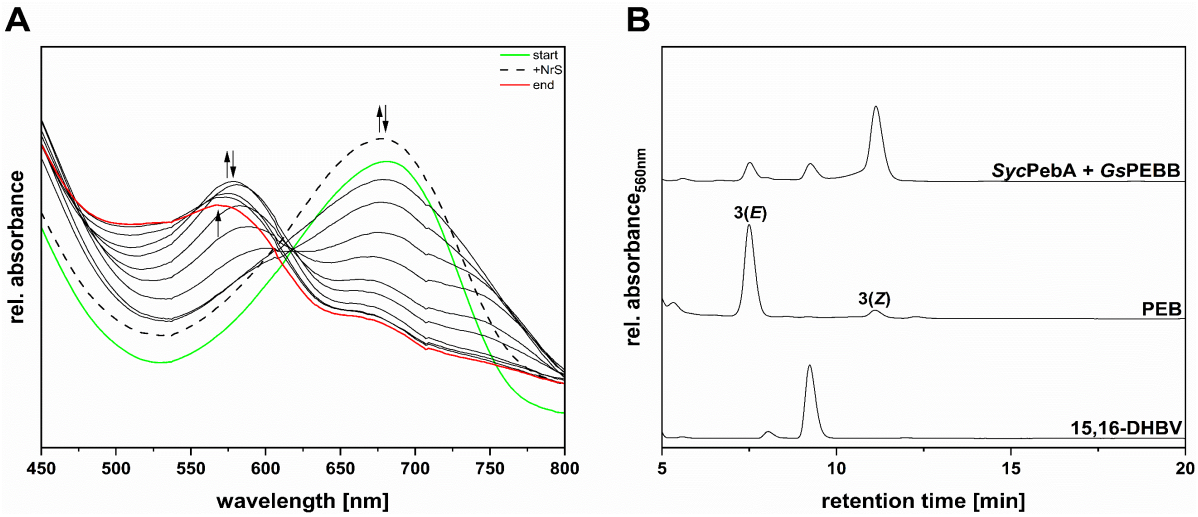

Figure 3.14 Coupled activity assay of recombinant *Syc*PebA and *Gs*PEBB employing BV as the substrate and characterization of reaction products.
(A) Time-resolved UV-Vis spectra of an anaerobic bilin reductase activity assay of coupled recombinant *Syc*PebA and *Gs*PEBB employing BV as the substrate. The total reaction time was 30 min and spectra were recorded every 30 s. The course of the absorbance during the reaction is marked by arrows. For reasons of clarity, only relevant spectra are shown. The green spectrum was recorded upon incubation of BV, *Syc*PebA and *Gs*PEBB, without starting the reaction. The dashed spectrum represents the first recorded after starting the reaction. Spectra recorded during the reaction are shown as solid black lines. The red curve represents the end spectrum. Curves were smoothed applying a 100 pt. Savitzky-Golay filter.
(B) HPLC analysis of the reaction products of coupled *Syc*PebA and *Gs*PEBB with BV as substrate (*Syc*PebA + *Gs*PEBB). The products were analyzed using a reversed-phase 5 µm C18 Luna column (Phenomenex) as stationary phase. The mobile phase consisted of 50%$_{v/v}$ acetone and 50%$_{v/v}$ 20 mM formic acid flowing at 0.6 mL/min. Absorbance was continuously recorded at 560 nm. PEB, phycoerythrobilin standard; 15,16-DHBV, 15,16-dihydrobiliverdin standard.

Both enzymes were added to reaction mix from the start, in equimolar amounts, and BV was used as substrate. The spectrum acquired following the addition of the enzymes and substrate displayed a peak at ~ 680 nm (Figure 3.14A – start), which slightly increased in absorbance upon initiating the reaction, attributable to residual *Gs*PEBB:*Syc*PebA:BV in the syringe (Figure 3.14A – +NrS). Unfortunately, no formation of the ~ 670 nm peak observed for the *Gs*PEBB:15,16-DHBV reaction could be recorded this time, preventing the characterization of this product once again. The absence of this peak in these assay conditions might suggest it is representative of substrate radicals, albeit the short absorbance wavelength. Regardless, following the initial production of an intermediate absorbing at ~ 580 nm, a final ~ 570 nm absorbing product was detected (Figure 3.14A – end). The final product was analyzed via HPLC, revealing the presence of both PEB isomers (with majority of 3(*Z*)) and residual traces of the intermediate 15,16-DHBV (Figure 3.14B – *Syc*PebA+*Gs*PEBB), similarly to the single *Gs*PEBB:15,16-DHBV reaction (Figure 3.13B – *Gs*PEBB - 60 min).
To finally exclude any other non-specific reaction, an additional *Gs*PEBB single activity assay was carried out using BV as the substrate. This assay confirmed that this reductase, like all other PebBs, exclusively accommodates 15,16-DHBV and does not exhibit broad substrate specificity (data not shown).

3.7 A *Gs*PEBA-*Gs*PEBB synergy is excluded: the FDBRs in *G. sulphuraria* are not responsible for PCB biosynthesis

PEB → PCB isomerase activity was only shown in a *G. sulphuraria* enriched protein fraction with a MW > 60 kDa. An alternative hypothesis, besides a new enzyme, would prompt a synergy between the two reductases, resulting in a complex of approximately this size. To disprove a potential synergism, a coupled activity assay was conducted (Figure 3.15A).

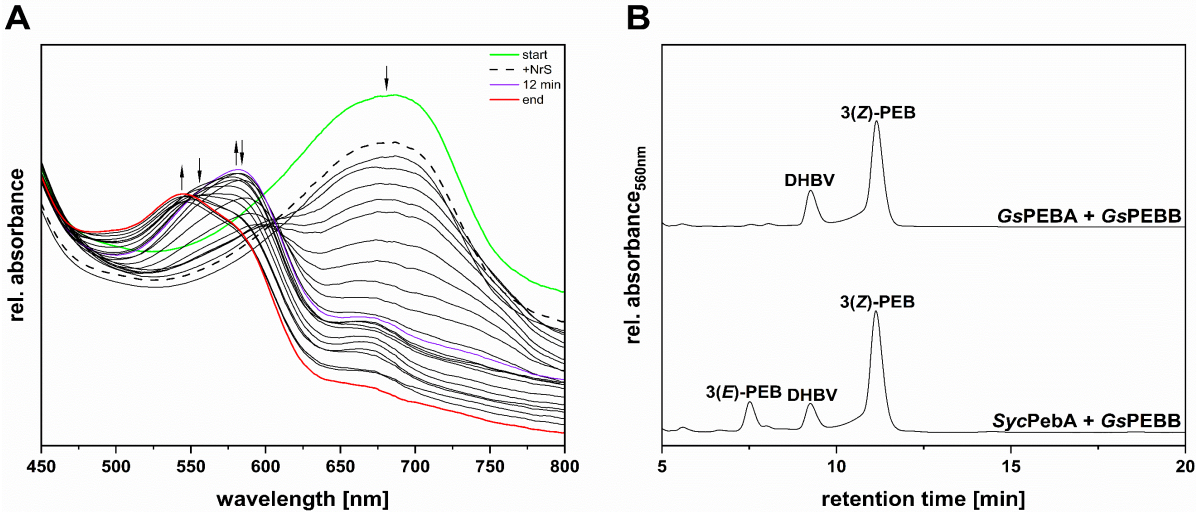

Figure 3.15 Coupled activity assay of recombinant *Gs*PEBA and *Gs*PEBB employing BV as the substrate and characterization of reaction products.
(A) Time-resolved UV-Vis spectra of an anaerobic bilin reductase activity assay of coupled recombinant *Gs*PEBA and *Gs*PEBB employing BV as the substrate. The total reaction time was 40 min and spectra were recorded every 30 s. The course of the absorbance during the reaction is marked by arrows. For reasons of clarity, only relevant spectra are shown. The green spectrum was recorded upon incubation of BV, *Gs*PEBA and *Gs*PEBB, without starting the reaction. The dashed spectrum represents the first recorded after starting the reaction. Spectra recorded during the reaction are shown as solid black lines. The violet spectrum represents the product formed after 12 min. The red curve represents the end spectrum. Curves were smoothed applying a 60 pt. Savitzky-Golay filter.
(B) HPLC analyses of the reaction products of coupled *Gs*PEBA and *Gs*PEBB with BV as substrate (*Gs*PEBA + *Gs*PEBB). The products were analyzed using a reversed-phase 5 µm C18 Luna column (Phenomenex) as stationary phase. The mobile phase consisted of 50%$_{v/v}$ acetone and 50%$_{v/v}$ 20 mM formic acid flowing at 0.6 mL/min. Absorbance was continuously recorded at 560 nm. *Syc*PebA + *Gs*PEBB, reaction products of coupled *Syc*PebA and *Gs*PEBB with BV as substrate.

Both enzymes were added to the reaction mix simultaneously, in equimolar amounts, with BV serving as substrate. The spectrum acquired upon enzymes and substrate injection displayed a peak at ~ 680 nm (Figure 3.15A – start), which decreased in absorbance after the NrS was added (Figure 3.15A – +NrS). After the initial formation of a product with an absorbance at ~ 580 nm (Figure 3.15A – 12 min), the enzymes ultimately converted the substrate to a ~ 545 nm absorbing product (Figure 3.15A – end). HPLC analysis of the final product unveiled the presence of 15,16-DHBV and PEB (Figure 3.15B – *Gs*PEBA + *Gs*PEBB), mirroring the outcome of the *Syc*PebA+*Gs*PEBB reaction (Figure 3.15B – *Syc*PebA + *Gs*PEBB). This fully disproves any synergistic effect of the reductases in driving the additional isomerization of PEB to PCB.

3.8 Cyanobacterial phytochrome coexpression with reconstituted *G. sulphuraria* bilin biosynthesis resulted in porphyrins accumulation

Parallel to the *in vitro* assessment of the single reductases, another approach was developed to investigate the potential synergistic effects of *G. sulphuraria* FDBRs. In this approach, the whole FDBRs pathway was reconstituted in *E. coli* and coupled to a detection system. Specifically, the genes encoding the two reductases were cloned in a pACYCDuet-1 expression vector and coexpressed with a heme oxygenase 1 (*Synho1* in pCOLADuet-1) and the N-terminal photosensory domain of the apo-phytochrome Cph1 (*Syncph1* 5' modi in pASK75B*)* from *Synechocystis* sp. PCC 6803. The coexpression with *Synho1* ensures the production of BV, to be turned over by *Gs*PEBA_*Gs*PEBB¸ while the presence of apo-Cph1 provides an easy detection method of the produced bilin, either with the coupled phytochrome assembly assay or the phytofluor assessment. Out of several pACYCDuet-1 vectors designed, the only one providing visible evidence of BV turnover was the one bearing a reverse translated *GsPEBA* sequence and *GsPEBB* adapted sequence (*GsPEBArevtrans_GsPEBB*, construct in Figure S1B). The coexpression of *GsPEBArevtrans_GsPEBB* with *Synho1* and *Syncph1* (or simply ABHC) resulted in the buildup of a pink bacterial pellet, hinting at PEB production (Figure 3.16).

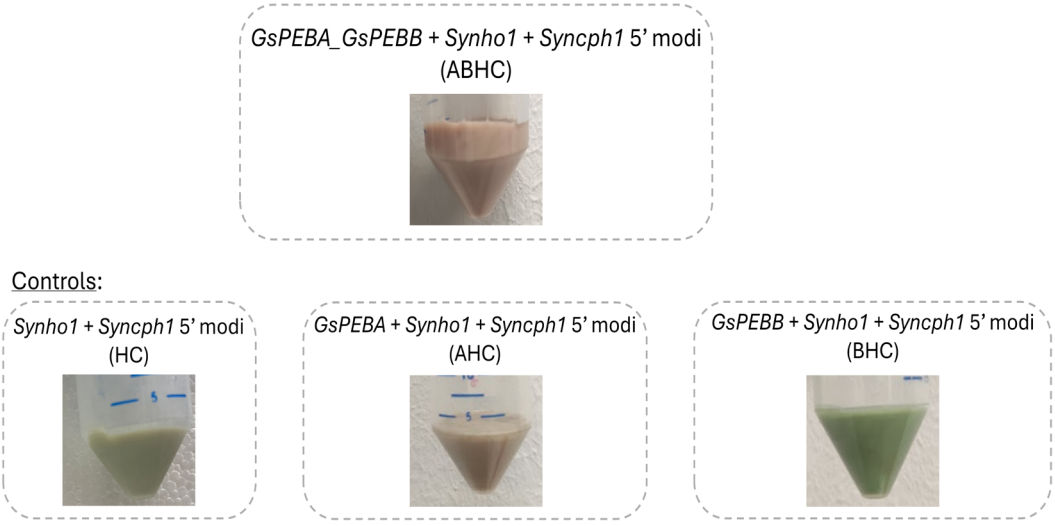

Figure 3.16 Coexpression studies for the heterologous reconstitution of *Galdieria sulphuraria* known bilin biosynthesis pathway.
Coexpression of BV biosynthesis pathway, *G. sulphuraria* bilin biosynthesis pathway and apo-phytochrome was conducted in *E. coli* BL21(DE3). Shown are the cell pellets after culture harvesting.

To validate this hypothesis, additional controls were performed. Coexpression of *Synho1* and *Syncph1* (or simply HC) resulted in a green pellet, indicating, as expected, only formation of BV by the heme oxygenase. Similarly, when *GsPEBB* was added to the latter coexpression

system (BHC), only a green pellet was formed, suggesting that BV cannot be processed by *Gs*PEBB, consistent to what mentioned at the end of chapter 3.6. Unexpected was, on the other hand, the outcome of the *Synho1* + *Syncph1* + *GsPEBArevtrans* coexpression (or simply AHC). Knowing *Gs*PEBA catalyzes the reduction of BV to 15,16-DHBV, a pink-violet cell pellet was expected. Surprisingly, the cell pellet obtained was beige-pink colored. Subsequent lysis of the cell pellets (chapter 2.5.4) presented evident issues. The investigation of potential ABHC and AHC lysate phytofluors resulted in a pattern clearly compatible with porphyrins (Fischer *et al.*, 2005) (Figure 3.17).

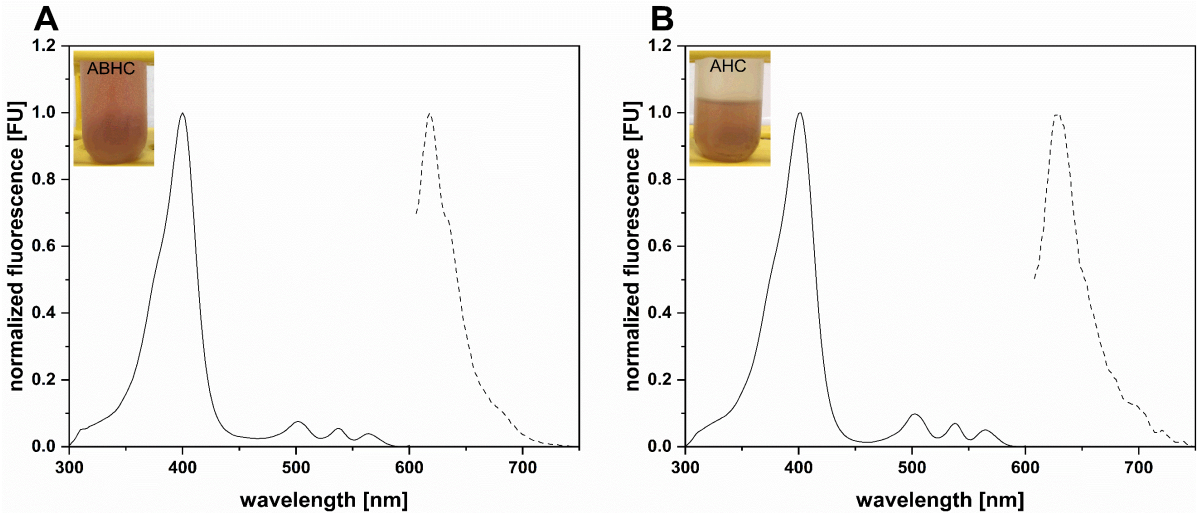

Figure 3.17 Phytofluor investigation of ABHC and AHC lysates.
(A) ABHC pellet was disrupted via sonication and centrifuged. The inset shows the lysate after centrifugation. Excitation spectrum (solid line) was recorded after emission at 620 nm. Fluorescence emission (dashed line) was recorded after excitation at 570 nm. Fluorescence intensity was normalized between 0 and 1.
(B) AHC pellet was disrupted via sonication and centrifuged. The inset shows the lysate after centrifugation. Excitation spectrum (solid line) was recorded after emission at 620 nm. Fluorescence emission (dashed line) was recorded after excitation at 570 nm. Fluorescence intensity was normalized between 0 and 1.

Ideally, ABHC should yield PEB production and therefore a phytofluor emitting at ~ 580 - 590 nm (Murphy & Lagarias, 1997). If AHC, on the other hand, would have yielded 15,16-DHBV, a pink-violet pellet should have been observed. Furthermore, no covalent binding to the phytochrome would have occurred due to the absence of the bilin A-ring ethylidene group (similarly to what would happen for HC). However, the conspicuous porphyrins fluorescence observed for both ABHC (Figure 3.17A) and AHC (Figure 3.17B) suggested bottlenecks in bilin biosynthesis, specifically indicating porphyrins accumulation as the main issue leading to failure of the experiment. Unfortunately, proceeding with additional lysate clarification steps (chapter 2.5.4) did not enhance specific bilin fluorescence (data not shown), hence a successful reconstitution can only be achieved through an efficient prevention of porphyrins accumulation by precisely adjusting coexpression conditions.

3.9 In contrast to phylogenetic classification, *Kfla*HY2 catalyzes the reduction of BV to PCB

It has been known for quite some time that the phytochromes of streptophyte algae use PCB as their chromophore, instead of the PΦB found in land plant phytochromes (Rockwell *et al.*, 2017; Wu *et al.*, 1997). Nonetheless, streptophyte algae do not possess a *PCYA* homolog, rather a *HY2* and a *PUBS*. Interestingly, the HY2 of the streptophyte alga *Klebsormidium nitens* was indirectly suggested to be producing the phytochrome chromophore PCB (Rockwell *et al.*, 2017). To biochemically investigate this, the reductase was recombinantly overproduced in *E. coli* with a N-terminal His-tag and purified via affinity chromatography. SDS-PAGE followed by Coomassie staining revealed the presence in the elution fractions of a protein with predicted MW of ~ 36 kDa, purified almost to homogeneity (Figure 3.18).

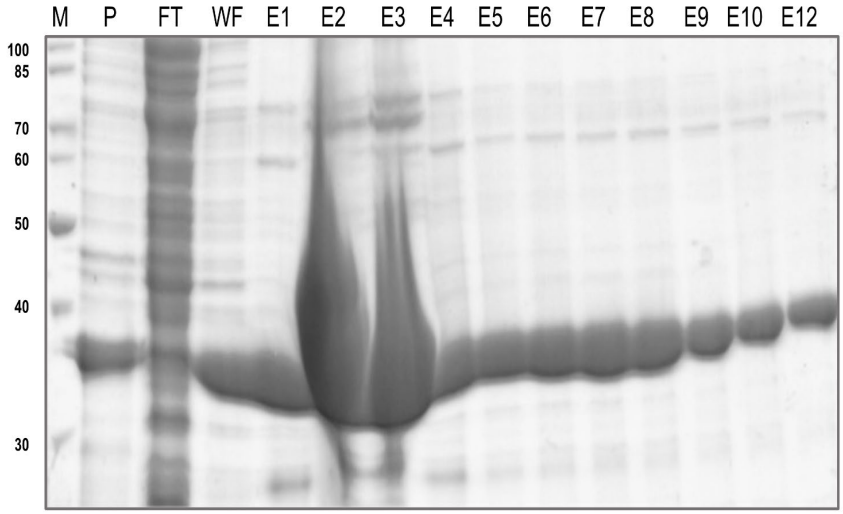

Figure 3.18 Heterologous production and purification of *Kfla*HY2.
Coomassie-stained SDS-PAGE gel following production and affinity chromatography purification of *Kfla*HY2 with TALON® Superflow™. (M) Molecular size marker – NEB, Unstained Protein Standard, Broad Range (MW on the left side of the figure reported in kDa); (P) Pellet after cell lysis; (FT) Purification flow-through fraction; (WF) Purification wash fraction; (En) Elution fractions. *Kfla*HY2 has a predicted molecular weight of ~ 36 kDa.

The oligomerization state of the protein was assessed as previously described for the pre-FDBRs (chapter 3.4) (Figure 3.19).

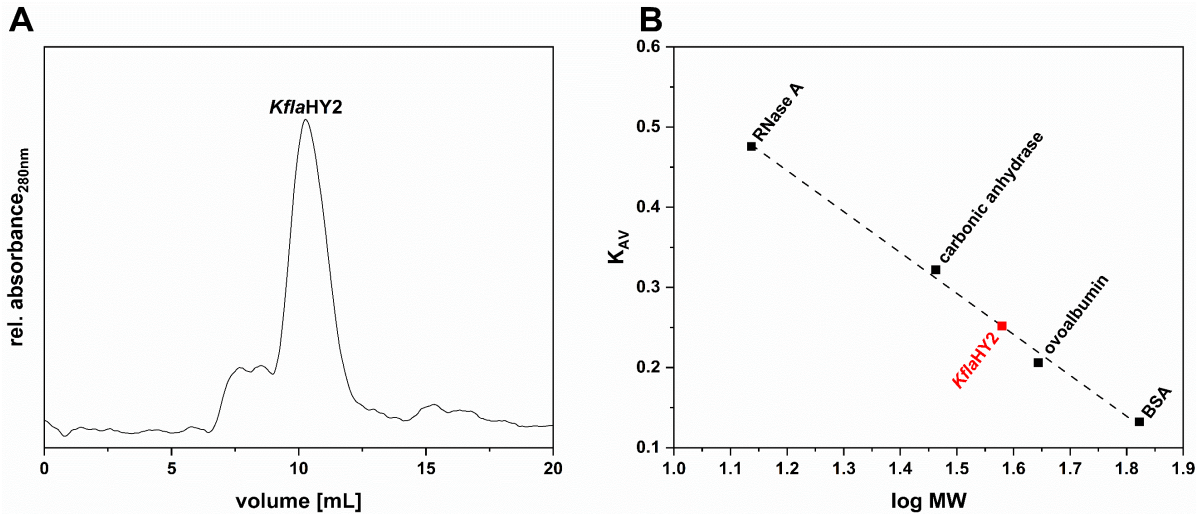

Figure 3.19 Determination of the oligomerization state of His-*Kfla*HY2.
(A) Size exclusion chromatography of His-*Kfla*HY2 (*Kfla*HY2) using a Superdex® 75 10/300 GL equilibrated with TES-KCl buffer. Absorbance was continuously measured at 280 nm. The chromatogram was smoothed applying a 60 pt. Savitzky-Golay filter due to detection issues of the Äkta Explorer UV module.
(B) Calibration curve of the Superdex® 75 10/300 GL column. RNAse A (MW = 13.7 kDa), carbonic anhydrase (MW = 29 kDa), ovoalbumin (MW = 44 kDa) and BSA (MW = 66.4 kDa) were used for calibration. The calibration curve was obtained by plotting the K_{AV} of the standards against the logarithm of the molecular weight (log MW) (black squares) and fitted (dashed line) using a linear regression function in Origin. The red square indicates *Kfla*HY2 on the calibration curve.

His-*Kfla*HY2 eluted at a volume of ~ 10.4 ml (Figure 3.19A). Based on the calibration curve, this corresponds to a monomer with MW ~ 38 kDa (Figure 3.19B), with a slight deviation from the predicted MW most likely imputable to the protein shape.
FDBR activity was subsequently monitored employing *Kfla*HY2 and BV in equimolar amounts (Figure 3.20A).

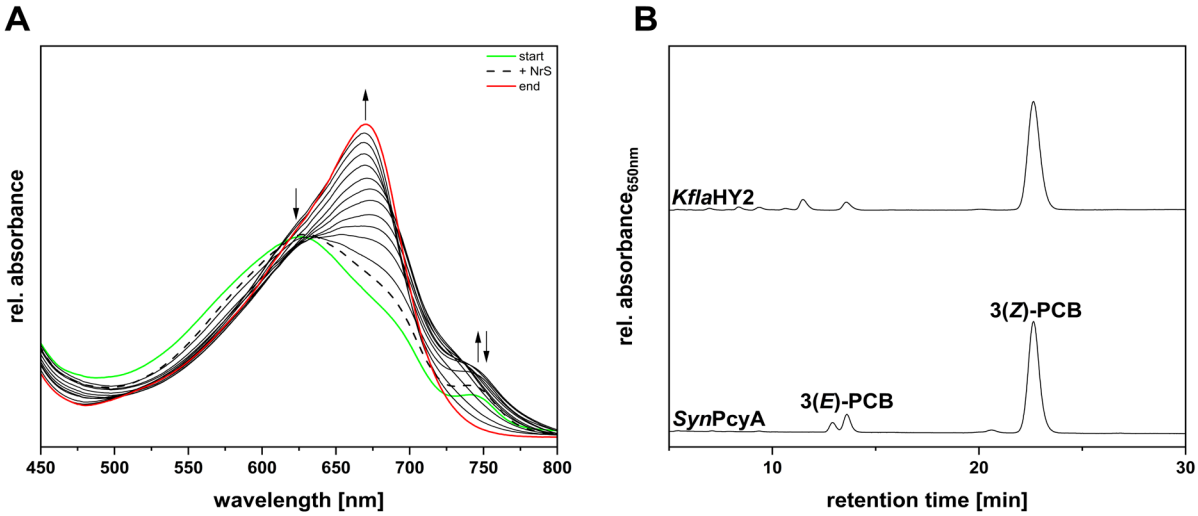

Figure 3.20 Activity assay of recombinant *Kfla*HY2 employing BV as the substrate and characterization of reaction products.
(A) Time-resolved UV-Vis spectra of an anaerobic bilin reductase activity assay of recombinant *Kfla*HY2 employing BV as the substrate. The total reaction time was 10 min and spectra were recorded every 30 s. The course of the absorbance during the reaction is marked by arrows. For reasons of clarity, only relevant spectra are shown. The green spectrum was recorded upon incubation of BV and *Kfla*HY2, without starting the reaction. The dashed

spectrum represents the first recorded after starting the reaction. Spectra recorded during the reaction are shown as solid black lines. The red curve represents the end spectrum. Curves were smoothed applying a 20 pt. Savitzky-Golay filter.
(B) HPLC analyses of the reaction products of *Kfla*HY2 with BV as substrate. The products were analyzed using a reversed-phase 5 µm C18 Luna column (Phenomenex) as stationary phase. The mobile phase consisted of 50%$_{v/v}$ acetone and 50%$_{v/v}$ 20 mM formic acid flowing at 0.6 mL/min. Products of an anaerobic turnover of BV to PCB mediated by *Syn*PcyA served as standards. Absorbance was continuously recorded at 650 nm.

The reductase and the substrate formed an intense turquoise-colored complex with an absorbance maximum at 625 nm, suggesting the ability of the protein to bind BV (Figure 3.20A – start). The presence of a shoulder at ~ 750 nm indicated the presence of BV in its protonated form (Frankenberg & Lagarias, 2003b; Tu *et al.*, 2004; Busch *et al.*, 2011a). After the reaction was started, the absorbance shifted instantly (Figure 3.20A – +NrS). Moreover, the rapid formation of a product with an absorbance maximum at 670 nm was observed (Figure 3.20A – end). Subsequent HPLC analysis revealed that *Kfla*HY2 forms 3(*Z*)-PCB as the main reaction product (Figure 3.20B).

3.10 *Kfla*HY2 reaction can proceed via two intermediates

As the reaction product PCB is a tetrahydrobiliverdin, the reaction should proceed via a two-electron reduced intermediate: either the A-ring reduced PΦB or the D-ring reduced 18^1,18^2-DHBV. Intermediates of the reaction were isolated using the products of an activity assay conducted with 1e$^-$ equivalent of NADPH. HPLC analyses of the products revealed the reaction proceeds via two intermediates (Figure 3.21 – *Kfla*HY2 1e$^-$, “Inter 1” and “Inter 2”). The intermediates possessed the same retention times of 3(*E*)-PΦB (~ 19 min) and 3(*Z*)-PΦB (~ 27 min) (Figure 3.21 – *At*HY2). However, 18^1,18^2-DHBV, the intermediate of the cyanobacterial PcyA reaction, and 3(*E*)-PΦB are roughly characterized by the same retention time. Therefore, “Inter 1” was not definitively identified.

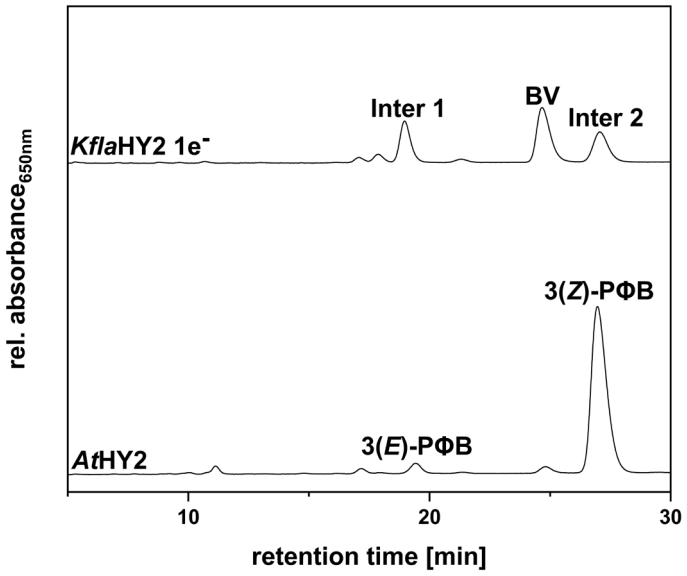

Figure 3.21 HPLC analyses of the reaction products of an anaerobic activity assay employing equimolar amounts of *Kfla*HY2 and BV with 1 electron equivalent of NADPH.
Products were resolved using a reversed-phase 5 µm C18 Luna column (Phenomenex) as stationary phase and a mixture of 50%$_{v/v}$ acetone and 50%$_{v/v}$ 20 mM formic acid as mobile phase flowing at 0.6 mL/min. The products of an anaerobic turnover of BV to PΦB mediated by HY2 derived from *A. thaliana* (*At*HY2) were used as standards. Absorbance was continuously recorded at 650 nm. Inter 1, Intermediate 1; Inter 2, Intermediate 2.
Figure modified from Frascogna *et al.*, 2023.

To verify the nature of the intermediates, coupled phytochrome assembly assays of the isolated intermediates with apo-*Syn*Cph1 and apo-*Pa*BphP were conducted (Figure 3.22). The incubation of “Inter 1” with apo-*Syn*Cph1 did not produce a photoactive adduct since no characteristic difference spectrum was obtained, indicating the lack of the ethylidene group at the A-ring C3 side chain (Hahn *et al.*, 2006; Lamparter *et al.*, 2001; Li *et al.*, 1995; Xu *et al.*, 2019) (Figure 3.22A – dashed line). This led to the conclusion that “Inter 1” could not have been 3(*E*)-PΦB. On the other hand, the incubation “Inter 2” with apo-*Syn*Cph1 (Figure 3.22A – dotted line) led to a difference spectrum like that obtained for the incubation of apo-*Syn*Cph1 with 3(*Z*)-PΦB (Figure 3.22A – solid line). In accordance with this finding, “Inter 2” failed to form a photoactive adduct with apo-*Pa*BphP (Figure 3.22B – dotted line), whereas “Inter 1” incubated with apo-*Pa*BphP resulted in a photoactive adduct with a difference spectrum (Figure 3.22B – dashed line) similar to the one obtained when apo-*Pa*BphP was incubated with 18^1,18^2-DHBV (Figure 3.22B – solid line). These results, together with the HPLC analyses, led to the identification of “Inter 1” as 18^1,18^2-DHBV and “Inter 2” as 3(*Z*)-PΦB.

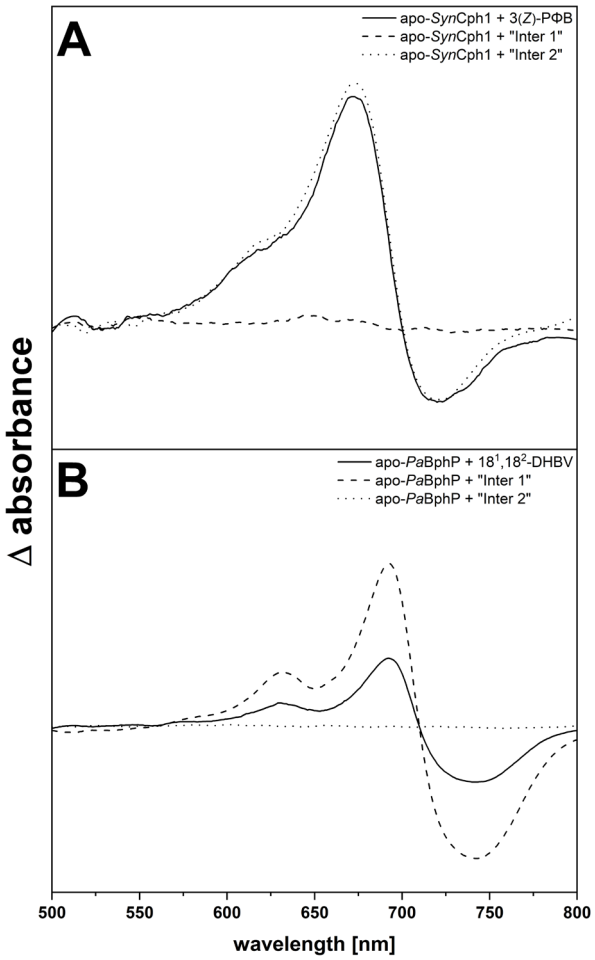

Figure 3.22 Red/far-red light induced difference spectra of coupled phytochrome assembly assays employing the intermediates of the *Kfla*HY2 reaction.
Absorbance spectra were recorded after incubation for 3 min with red light (636 nm – Pfr spectrum) and after incubation for 3 min with far-red light (730 nm for *Syn*Cph1; 750 nm for *Pa*BphP – Pr spectrum). Difference spectra were calculated by the subtraction of the Pfr from the Pr spectrum. All calculated difference spectra were smoothed applying a 20 pt. Savitzky-Golay filter.
(A) Coupled phytochrome assembly assays employing apo-*Syn*Cph1 and “Inter 1” (dashed line); apo-*Syn*Cph1 and “Inter 2” (dotted line); apo-*Syn*Cph1 and 3(*Z*)-PΦB (solid line).
(B) Coupled phytochrome assembly assay employing apo-*Pa*BphP and “Inter 1” (dashed line); apo-*Pa*BphP and “Inter 2” (dotted line); apo-*Pa*BphP and 18^1,18^2-DHBV (solid line).
Figure modified from Frascogna ***et al.***, 2023.

In order to ascertain whether the intermediates are solely artifacts resulting from the *in vitro* assay or if they indeed serve as suitable substrates for *Kfla*HY2-catalyzed BV reduction, both compounds were employed as substrates for *Kfla*HY2 in activity assays (data not shown). Subsequent HPLC analyses indicated that both bilins are predominately converted to 3(*Z*)-PCB, therefore proving *Kfla*HY2 can fulfill its function in two possible routes (Figure 3.23).

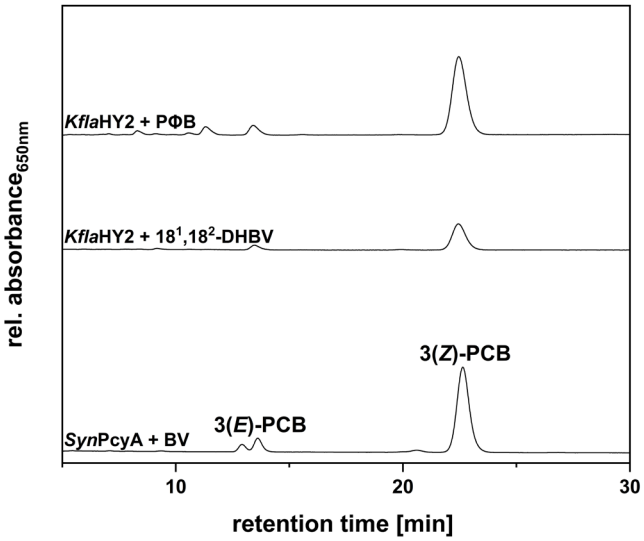

Figure 3.23 HPLC analyses of the reaction products of activity tests employing 3(*Z*)-PΦB and 18[1],18[2]-DHBV as substrates for *Kfla*HY2.
Products were analyzed using a 5 µm reversed-phase C18 Luna column (Phenomenex) as stationary phase. The mobile phase consisted of 50%$_{v/v}$ acetone and 50%$_{v/v}$ 20 mM formic acid flowing at 0.6 mL/min. Reaction products of a *Syn*PcyA-mediated reduction of BV to PCB were used as standards. Absorbance was continuously measured at 650 nm.
Figure modified from Frascogna *et al.*, 2023.

3.11 *Kfla*HY2 variants provide insights into the reaction mechanism

In order to gain further insight on the unexpected behavior of *Kfla*HY2, an amino acid sequence alignment employing different FDBRs was constructed (Figure 3.24).

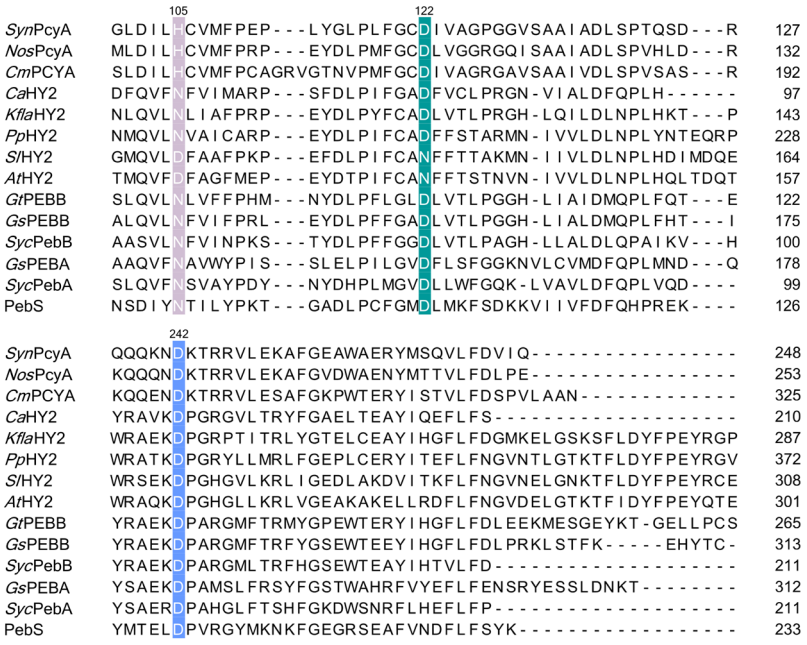

Figure 3.24 FDBR sequences alignment.
The alignment was constructed using Clustal Omega (Madeira *et al.*, 2022) (https://www.ebi.ac.uk/jdispatcher/msa/clustalo) and modified using Jalview (Waterhouse *et al.*, 2009). The amino acid residues mentioned in the text are highlighted in different colors and labeled according to *Kfla*HY2 sequence

numbering. Accession codes of the employed sequences are listed in Table S1. *Syn*PcyA: PcyA from *Synechocystis* sp. PCC 6803; *Nos*PcyA: PcyA from *Nostoc* sp. PCC 7120; *Cm*PCYA: PCYA from *Cyanidioschyzon merolae* 10D; *Ca*HY2: HY2 from *Chlorokybus atmophyticus*; *Kfla*HY2: HY2 from *Klebsormidium nitens*; *Pp*HY2: HY2 from *Physcomitrium patens*; *Sl*HY2: HY2 from *Solanum lycopersicum*; *At*HY2: HY2 from *Arabidopsis thaliana*; *Gt*PEBB: PEBB from *Guillardia theta*; *Gs*PEBB: PEBB from *Galdieria sulphuraria*; *Syc*PebB: PebB from *Synechococcus* sp. WH 8020; *Gs*PEBA: PEBA from *Galdieria sulphuraria*; *Syc*PebA: PebA from *Synechococcus* sp. WH 8020; PebS: PebS from P-SSM2.

The immediate focus was placed on Asn^{105}, Asp^{122}, and Asp^{242}. *Kfla*HY2 Asn^{105} represents the homolog to the conserved His found in cyanobacterial PcyAs, which has been demonstrated to be involved in protonation and substrate positioning in the active site (Hagiwara *et al.*, 2006a, 2006b, 2010; Tu *et al.*, 2007; Unno *et al.*, 2015). The substitution of this His to an Asn is not uncommon, as it is also found in other FDBRs like PebA, PebB and PebS. Contrastingly, in land plant HY2s, an Asp is typically found in this position, which has been shown to be essential for substrate positioning in *At*HY2 and involved in catalysis in *Sl*HY2 (Sugishima *et al.*, 2020; Tu *et al.*, 2008) (Figure 3.24 – highlighted in lilac). *Kfla*HY2 Asp^{122} has a homolog in all the FDBRs except for those from land plants. In PcyA and PebS, it is located in the central β-sheet of the binding pocket and has been identified as the initial proton donor (Hagiwara *et al.*, 2006a; Tu *et al.*, 2007; Busch *et al.*, 2011a) (Figure 3.24 – highlighted in teal). Lastly, *Kfla*HY2 Asp^{242} has a homolog in *At*HY2 Asp^{256}, *Sl*HY2 Asp^{263}, PebS Asp^{206}, and *Gt*PEBB Asp^{219} (Figure 3.24 – highlighted in cyan). All of these Asp residues have been proven to be involved in the reduction of the A-ring 2,3,3^1,3^2-diene system (Busch *et al.*, 2011a; Sommerkamp *et al.*, 2019; Sugishima *et al.*, 2020; Tu *et al.*, 2008).

Based on these considerations, protein variants were generated to examine potential involvement of the aforementioned residues in the *Kfla*HY2 catalyzed reaction. In order to investigate the impact of ionization on catalysis, Asp^{122} and Asp^{242} were replaced by Asn residues whereas Asn^{105} was replaced by an Asp. Asn^{105} was additionally substituted with a His, to more closely resemble a canonical PcyA active site. Furthermore, two double variants were generated. Specifically, one was designed for *Kfla*HY2 to mimic a plant HY2, and the other to prove the presence of two Asp residues in the active is sufficient for reducing BV to PCB. The activity of the purified variant enzymes was investigated *in vitro* via FDBR assays and subsequent HPLC analyses (Figure 3.25).

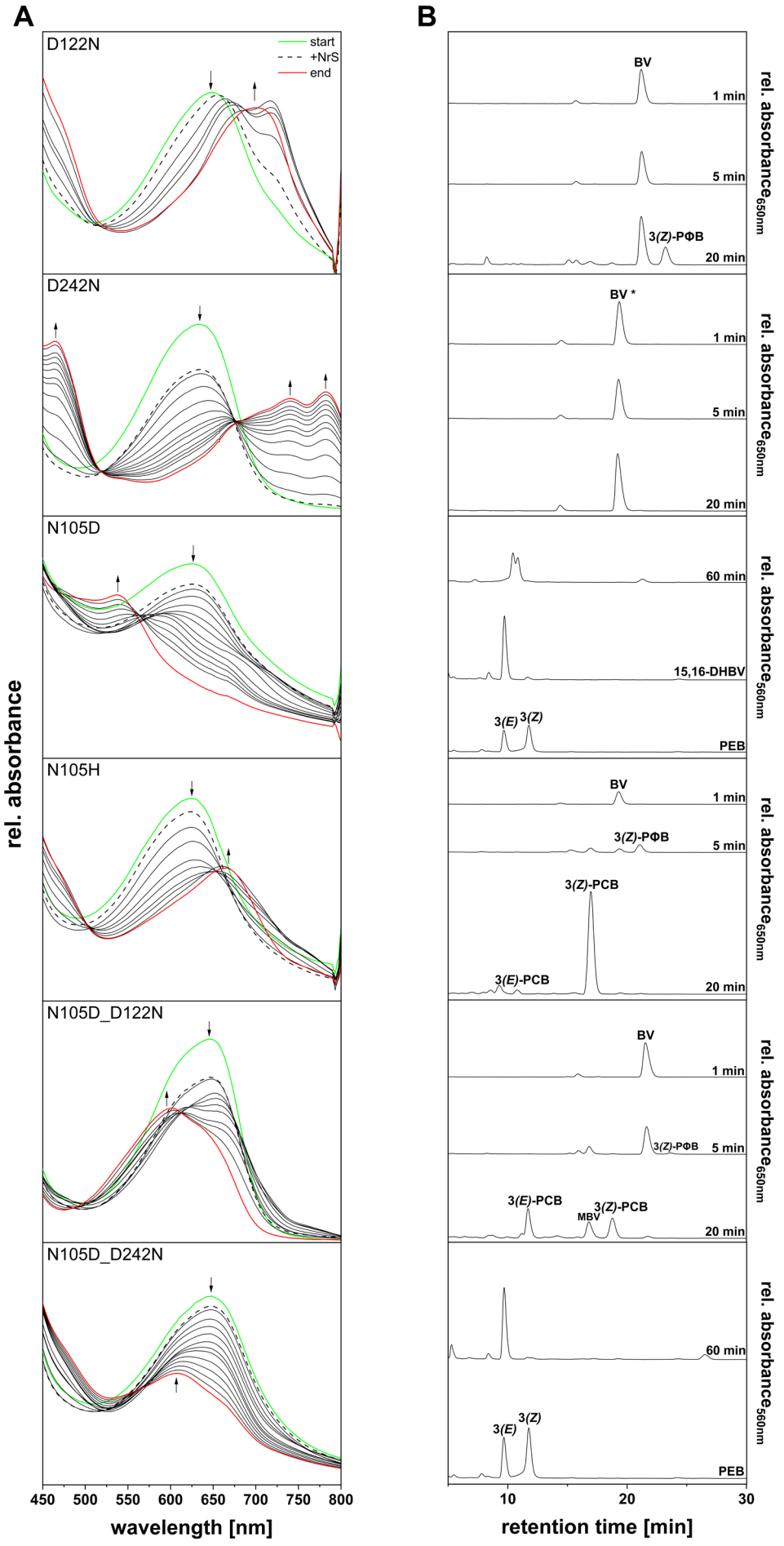
A
B
D122N
start
+NrS
end
D242N
N105D
N105H
N105D_D122N
N105D_D242N
rel. absorbance
450 500 550 600 650 700 750 800
wavelength [nm]
BV
1 min
5 min
3(Z)-PΦB
20 min
BV *
60 min
15,16-DHBV
3(E) 3(Z)
PEB
3(Z)-PCB
3(E)-PCB
MBV
rel. absorbance650nm
rel. absorbance560nm
10 20 30
retention time [min]

Figure 3.25 Activity assay and characterization of reaction products of recombinant *Kfla*HY2 variants.
(A) UV-Vis spectra of the anaerobic FDBR assays performed using *Kfla*HY2 variants and BV as the substrate. The total reaction time was 20 min for *Kfla*HY2_D122N, *Kfla*HY2_D242N, *Kfla*HY2_N105H and *Kfla*HY2_N105D_D122N and 60 min for *Kfla*HY2_N105D and *Kfla*HY2_N105D_D242N. Spectra were recorded every 30 s. For reasons of clarity, only relevant spectra are shown. The arrow indicates the course of absorbance during the reaction. Curves were smoothed applying a 20 pt. Savitzky-Golay filter with the only exception of non-smoothed *Kfla*HY2_D242N.
(B) HPLC elution profiles of the reaction products of *Kfla*HY2 variants. The stationary phase consisted in a Luna 5 µm reversed-phase C18 column (Phenomenex). The mobile phase consisted of a mixture of 50%$_{v/v}$ acetone and 50%$_{v/v}$ 20 mM formic acid flowing at 0.6 mL/min. Absorbance was continuously recorded at 560 or 650 nm. (*) BV shows change in the retention time due to substitution of the mobile phase between the different HPLC measurements. 3(*Z*)-PΦB, 3(*Z*)-phytochromobilin; 3(*E*)-PCB, 3(*E*)-phycocyanobilin; 3(*Z*)-PCB, 3(*Z*)-phycocyanobilin; DHBV, 15,16-dihydrobiliverdin; PEB, phycoerythrobilin; MBV, 18^1,18^2-dihydrobiliverdin.

*Kfla*HY2_D122N was able to bind BV and use it as substrate, as indicated by the formation of a peak at ~ 720 nm, signifying substrate protonation (Figure 3.25A – D122N). Intermediates were isolated from the reaction mix at specific time points and analyzed via HPLC. Time-course HPLC analyses revealed the formation of small amounts of 3(*Z*)-PΦB after 20 min from the start of the reaction (Figure 3.25B – D122N). Hence, this variant partially retains the capability to reduce BV A-ring but is completely unable to reduce the D-ring, proving the importance of Asp^{122} for D-ring reduction (Hagiwara *et al.*, 2006a; Tu *et al.*, 2007; Busch *et al.*, 2011a).
*Kfla*HY2_D242N retained the ability to bind BV but failed in its reduction. The observed increases in absorbance at ~ 460, ~ 740, and ~ 790 nm merely suggested the formation of substrate radical intermediate species (Tu *et al.*, 2004, 2007; Busch *et al.*, 2011a; Ledermann *et al.*, 2018) (Figure 3.25A – D242N). HPLC elution profiles were compatible with BV at all time points, thereby confirming the inactivity (Figure 3.25B – D242N). This outcome is consistent with what was found for *At*HY2_D256N and *Sl*HY2_D263N, indicating the critical role of this residue in BV protonation (Sugishima *et al.*, 2020; Tu *et al.*, 2008).
*Kfla*HY2_N105D exhibited an unexpected behavior. The assay was initially performed for 20 min, revealing the formation of a violet-colored product with a peak ~ 570 nm (data not shown). In order to potentially accumulate more of this violet compound, a second reaction was performed for 60 min. This second assay showed the formation of a final product with an absorbance peak at ~ 540 nm (Figure 3.25A – N105D). Time-based HPLC analyses unveiled that the bilin produced after 5 min from the start of the reaction was indeed PCB, while a pattern consistent with an unidentified compound and mostly 3(*Z*)-PCB was obtained for the 20 min product (Figure S2). Concerning the final 60 min product, a double peak with retention time of 10.5 and 10.8 min, not entirely matching with either 15,16-DHBV or PEB, was recorded (Figure 3.25B – N105D, 60 min). To identify the unknown bilin, its integration in apo-*Syn*Cph1 and apo-*Pa*BphP was evaluated. Both PEB and 15,16-DHBV lack the C15=C16 double bond required for the photoconversion of the phytochrome between the two isoforms. As mentioned in chapter 1.3, a phytochrome binding this kind of bilin would be locked in the red-light absorbing form. Under these circumstances, the bilin is not completely de-excited,

leading to the formation of a fluorescent product named phytofluor (Murphy & Lagarias, 1997). This unidentified bilin was incubated in parallel with the two apo-phytochromes and fluorescence was measured. The formation of a characteristic phytofluor was only recorded upon incubation with apo-*Syn*Cph1, thus indicating the product is PEB (Figure 3.26).

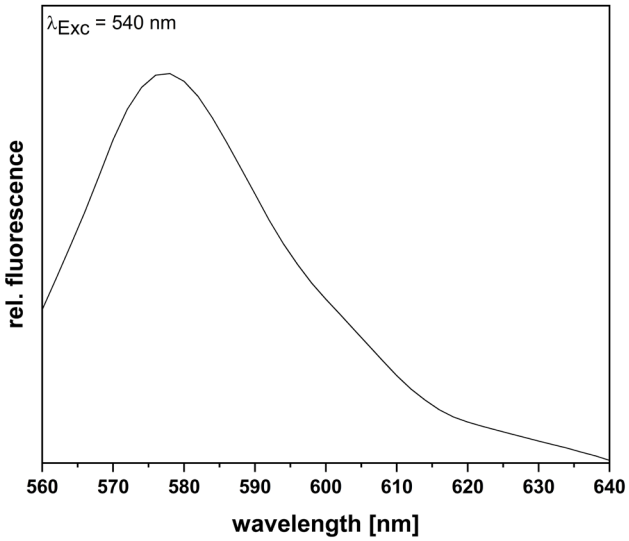

Figure 3.26 Fluorescence emission spectrum of the apo-*Syn*Cph1 + *Kfla*HY2_N105D reaction product adduct.
The isolated bilin produced by *Kfla*HY2_N105D was incubated for 30 min in the dark with the lysate of a pET_*cph1* overexpression. Fluorescence emission was recorded after excitation at 540 nm.

*Kfla*HY2_N105H was generated to investigate the effect of partially reconstituting the active site of PcyA in *Kfla*HY2. *Kfla*HY2_N105H was investigated for reductase activity (Figure 3.25A – N105H) and revealed the production of a mix of PCB isomers, with mostly 3(*Z*), along with remaining traces of the intermediate 18^1,18^2-DHBV (Figure 3.25B – N105H). Thus, *Kfla*HY2_N105H catalyzes BV → PCB reduction in a manner similar to that of the native enzyme, albeit at a considerably slower rate.

The double variant *Kfla*HY2_N105D_D122N, constructed to mimic a plant HY2, surprisingly retained the native activity. Contrary to the expected $2e^-$ reduction to PΦB, this variant generated PCB (Figure 3.25B – N105D_D122N), albeit with a considerably slower turnover rate and a different absorbance pattern for the final product (Figure 3.25A – N105D_D122N) compared to the native enzyme (Figure 3.20), suggesting a rearrangement of the pocket around the substrate. This outcome prompted the hypothesis that the presence of two Asp in the active site, even if positioned differently than in the native enzyme, is sufficient for the reduction of BV to PCB. To further investigate it, the double variant *Kfla*HY2_N105D_D242N was generated. A scenario comparable to *Kfla*HY2_N105D was observed: performing the assay for 60 min resulted in the formation of a ~ 600 nm absorbing pink product (Figure 3.25A

– N105D_D242N). This product was unequivocally identified as PEB via HPLC (Figure 3.27B – N105D_D242N), thus disproving the initial hypothesis.

3.12 The drivers of intermediate accumulation are still unknown

Recently, two residues were proven to be essential for PcyA intermediate accumulation. This discovery stemmed from the identification of two functionally diversified PcyA sequences in the cyanobacterium *Acaryochloris marina* MBIC 11017: *Am*PcyAc, encoded in the chromosome, which supplies 18^1,18^2-DHBV to the cyanobacteriochrome photoreceptor; *Am*PcyAp, encoded on a plasmid, which synthesizes PCB for the PBS (Miyake *et al.*, 2020). A multiple sequence alignment uncovered two key drivers of this functional diversification. Firstly, a substitution of a Leu conserved among all PcyAs (*Syn*PcyA Leu^{151}) with an Ile is found in *Am*PcyAc. Secondly, both *Am*PcyAs exhibit a substitution of a conserved Val (*Syn*PcyA Val^{225}, important for substrate positioning) also with an Ile (Miyake *et al.*, 2022). In light of the unsuccessful attempt to force *Kfla*HY2 to solely produce PΦB (*Kfla*HY2_N105D_D122N), its sequence was analyzed at the corresponding positions to determine whether intermediate formation might, also in this instance, be influenced by these residues. The residue corresponding to *Am*PcyAc Ile^{146} (or *Syn*PcyA Leu^{151}) is a Leu in *Kfla*HY2, yet this residue is facing outside of the active site. In contrast, *Kfla*HY2 has a superimposing homolog to *Am*PcyAc Ile^{220} (or *Syn*PcyA Val^{225}) in Thr^{247}. Since Miyake and colleagues additionally showed an accumulation of 18^1,18^2-DHBV for the single variant where only the latter residue was exchanged, a *Kfla*HY2_T247I variant was generated to investigate the potential role of this residue in intermediate accumulation (Figure 3.27).

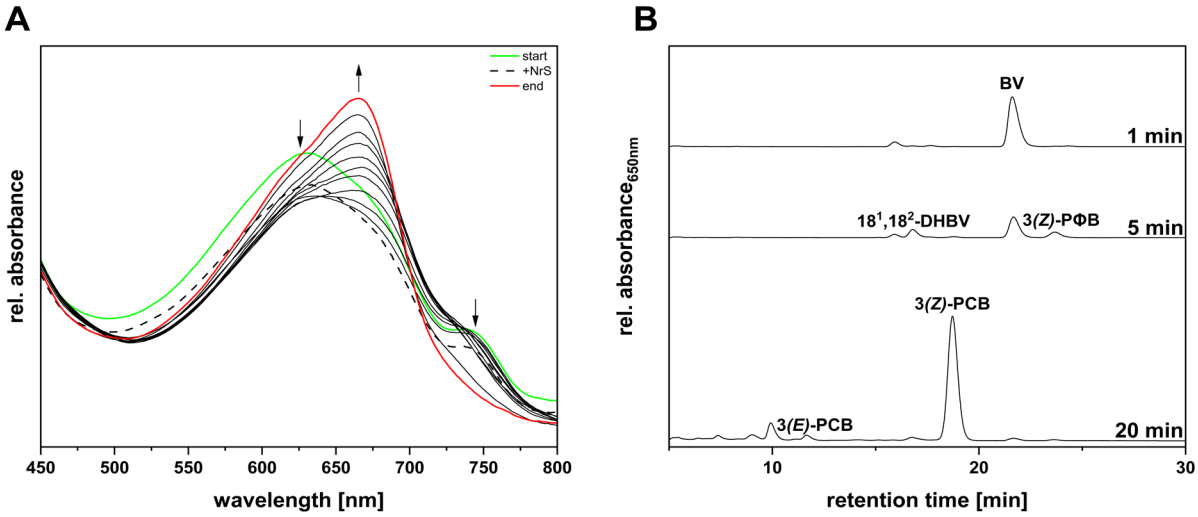

Figure 3.27 Activity assay of recombinant *Kfla*HY2_T247I employing BV as the substrate and characterization of reaction products.
(A) Time-resolved UV-Vis spectra of an anaerobic bilin reductase activity assay of recombinant *Kfla*HY2_T247I employing BV as the substrate. The total reaction time was 20 min and spectra were recorded every 30 s. The course of the absorbance during the reaction is marked by arrows. For reasons of clarity, only relevant spectra

are shown. The green spectrum was recorded upon incubation of BV and *Kfla*HY2_T247I, without starting the reaction. The dashed spectrum represents the first recorded after starting the reaction. Spectra recorded during the reaction are shown as solid black lines. The red curve represents the end spectrum. Curves were smoothed applying a 50 pt. Savitzky-Golay filter.
(B) HPLC analyses of the reaction products of *Kfla*HY2_T247I with BV as substrate. The products were analyzed using a reversed-phase 5 µm C18 Luna column (Phenomenex) as stationary phase. The mobile phase consisted of 50%$_{v/v}$ acetone and 50%$_{v/v}$ 20 mM formic acid flowing at 0.6 mL/min. Absorbance was continuously recorded at 650 nm. 18^1,18^2-DHBV, 18^1,18^2-dihydrobiliverdin; 3(*Z*)-PΦB, 3(*Z*)-phytochromobilin; 3(*E*)-PCB, 3(*E*)-phycocyanobilin; 3(*Z*)-PCB, 3(*Z*)-phycocyanobilin.

Nevertheless, the activity assay of *Kfla*HY2_T247I (Figure 3.27A) showed a pattern consistent with the native enzyme (Figure 3.20), proving intermediate accumulation is not influenced by this residue. In support of this consideration, HPLC analysis proved the variant primarily produces 3(*Z*)-PCB, via the same intermediates of the native enzyme (Figure 3.27B). Intermediate production in *Kfla*HY2 must be influenced by other hitherto unidentified residues.

3.13 HY2 lost the ability to produce PCB with the emergence of Bryophyta

Since the attempt to convert *Kfla*HY2 into a plant type HY2 with PΦB biosynthetic activity by only exchanging the active site residues failed, a phylogenetic tree of the HY2 lineage was constructed (Figure 3.28) to select sequences for biochemical assays and identify where the change of activity happened.

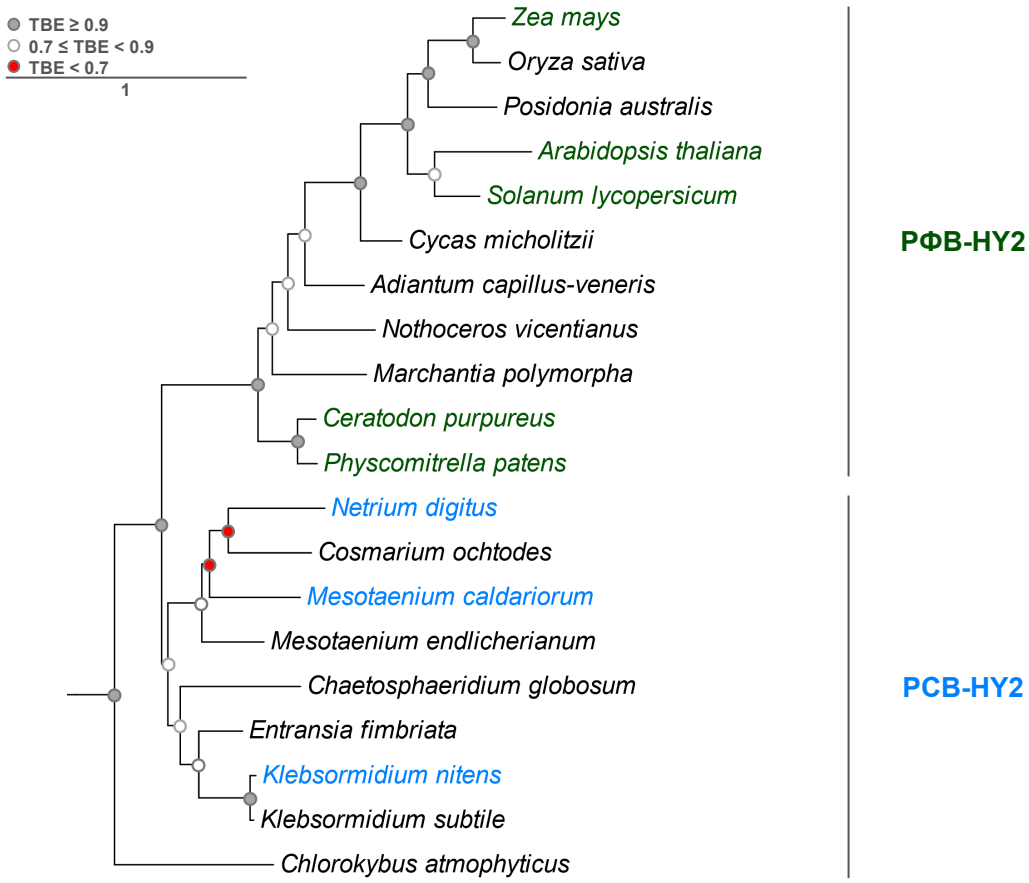

Figure 3.28 Phylogenetic analysis of HY2 lineage.
The maximum-likelihood tree was inferred using PhyML (Guindon *et al.*, 2010). TBE was used for support. Circles at nodes indicate TBE (gray, TBE ≥ 0.9; white, 0.7 ≤ TBE < 0.9; red, TBE < 0.7). The scale bar is provided under TBE values. The represented tree is an excerpt of a full tree including members of all the FDBRs lineages. Accession numbers of the employed sequences shown in this figure are available in Table S1. Labels indicate HY2-belonging organism. The color of the label represents the produced bilin (cyan for PCB, dark green for PΦB). Only HY2s with experimentally proven activity are colored.

Besides extensive research in Embryophytes, the HY2 of streptophyte algae have been largely overlooked (Chiu *et al.*, 2010; Hu *et al.*, 2021; Kohchi *et al.*, 2001; McDowell & Lagarias, 2001; Muramoto *et al.*, 2005; Perez-Santangelo *et al.*, 2022; Rockwell *et al.*, 2017; Sawers *et al.*, 2004). Specifically, while there is considerable understanding of HY2 function in Angiosperms, less attention has been given to the clade from which they originated. Concerning Bryophytes, the only HY2 partially studied around a decade ago was the one of *Physcomitrium patens*, shown to convert BV to PΦB (Chen *et al.*, 2012; Shih-Long Tu, Academia Sinica, Taiwan, personal communication). As for streptophyte algae, besides the HY2 of *K. nitens*, the only other HY2 investigated pathway, albeit with an indirect *in vivo* approach, was the one of *Mesotaenium caldariorum*, which was shown to synthesizes its PCB phytochrome chromophore via PΦB (Wu *et al.*, 1997). The most straightforward way to trace an evolution of HY2 catalytic activity would have been to select sequences that lie between those of *P. patens* and *M. caldariorum* in the phylogenetic tree. Thus, starting from

the HY2 lineage phylogenetic tree, the HY2s from *Ceratodon purpureus* (*Cepu*HY2) and *Netrium digitus* (*Nedi*HY2) were chosen and their activity was investigated similarly to *Kfla*HY2. Both proteins were produced and purified by a collaborator (Fjoralba Zeqiri, Ruhr University Bochum). Unfortunately, both were prone to aggregation (data not shown), but just sufficient catalytic activity for product identification was attained. While the *Cepu*HY2 confirmed previous indirect evidence and synthesized PΦB from BV (Lamparter *et al.*, 1995) (Figure 3.29A, B), *Nedi*HY2 was shown to produce PCB in a coupled phytochrome assembly assay using apo-*Syn*Cph1 (Figure 3.29C, D).

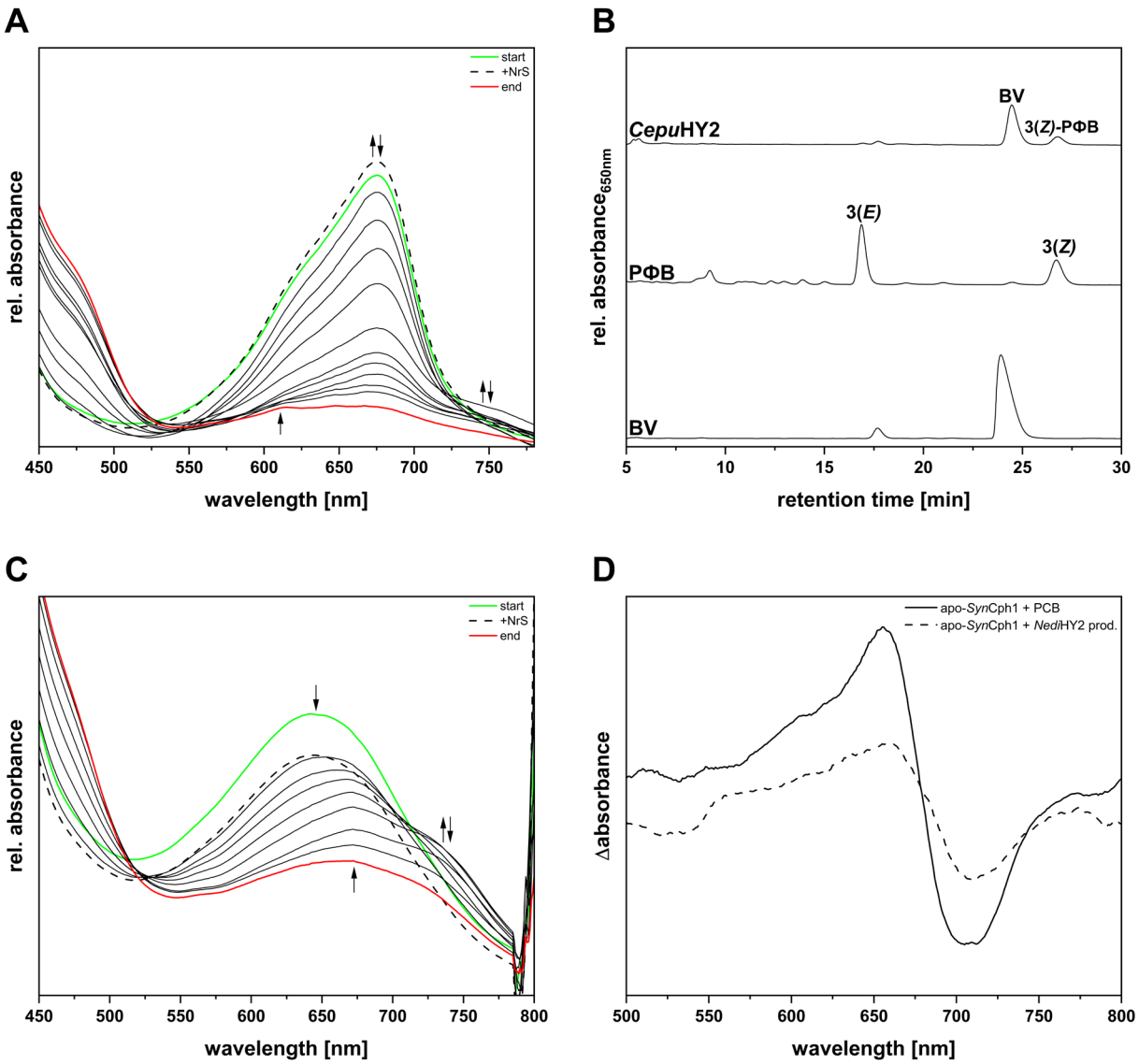

Figure 3.29 Activity assay of recombinant *Cepu*HY2 and *Nedi*HY2 employing BV as the substrate and characterization of reaction products.
(A) Time-resolved UV-Vis spectra of an anaerobic bilin reductase activity assay of recombinant *Cepu*HY2 employing BV as the substrate. The total reaction time was 35 min and spectra were recorded every 30 s. The course of the absorbance during the reaction is marked by arrows. For reasons of clarity, only relevant spectra are shown. The green spectrum was recorded upon incubation of BV and *Cepu*HY2, without starting the reaction. The dashed spectrum represents the first recorded after starting the reaction. Spectra recorded during the reaction are shown as solid black lines. The red curve represents the end spectrum. Curves were smoothed applying a 20 pt. Savitzky-Golay filter.

(B) HPLC analyses of the reaction products of *Cepu*HY2 with BV as substrate. The products were analyzed using a reversed-phase 5 µm C18 Luna column (Phenomenex) as stationary phase. The mobile phase consisted of 50%$_{v/v}$ acetone and 50%$_{v/v}$ 20 mM formic acid flowing at 0.6 mL/min. Absorbance was continuously recorded at 650 nm. PΦB, phytochromobilin standard; BV, biliverdin IXα standard.
(C) Time-resolved UV-Vis spectra of an anaerobic bilin reductase activity assay of recombinant *Nedi*HY2 employing BV as the substrate. The total reaction time was 20 min and spectra were recorded every 30 s. The course of the absorbance during the reaction is marked by arrows. For reasons of clarity, only relevant spectra are shown. The green spectrum was recorded upon incubation of BV and *Nedi*HY2, without starting the reaction. The dashed spectrum represents the first recorded after starting the reaction. Spectra recorded during the reaction are shown as solid black lines. The red curve represents the end spectrum. Curves were smoothed applying a 30 pt. Savitzky-Golay filter.
(D) Red/far-red light induced difference spectra of coupled phytochrome assembly assays employing PCB and the product of the *Nedi*HY2 reaction (*Nedi*HY2 prod.). Absorbance spectra were recorded after incubation for 3 min with red light (636 nm – Pfr spectrum) and after incubation for 3 min with far-red light (730 nm – Pr spectrum). Difference spectra were calculated by the subtraction of the Pfr from the Pr spectrum. The apo-*Syn*Cph1 + PCB difference spectrum (solid line) was smoothed applying a 20 pt. Savitzy-Golay filter. The apo-*Syn*Cph1 + *Nedi*HY2 prod. difference spectrum (dashed line) was smoothed applying an 80 pt. Savitzky-Golay filter and the signal was 4x enhanced.

Based on these findings, it could be concluded that the switch of activity from a PCB-producing to a PΦB-producing HY2 enzyme likely happened between *N. digitus* and *P. patens* within the streptophyta HY2 lineage.

3.14 *Kfla*PUBS catalyzes the reduction of BV to PUB via 15,16-DHBV

In addition to HY2, *K. nitens* stands out as one of the streptophyte algae harboring a putative PUBS (Rockwell & Lagarias, 2017a). The protein sequence was deprived of the N-terminal signal peptide (UniProt: A0A1Y1IM74, residues 1 - 100) and fed to the GenScript codon optimization tool (https://www.genscript.com/tools/gensmart-codon-optimization) to yield a reverse-translated DNA sequence matching *E. coli* codon usage. The putative reductase was recombinantly overproduced in *E. coli* with a N-terminal His-tag (construct similar to Figure S1A) and purified via affinity chromatography. SDS-PAGE followed by Coomassie staining revealed the presence in the elution fractions of a protein with predicted MW of ~ 33 KDa, alongside two larger contaminants (Figure 3.30).

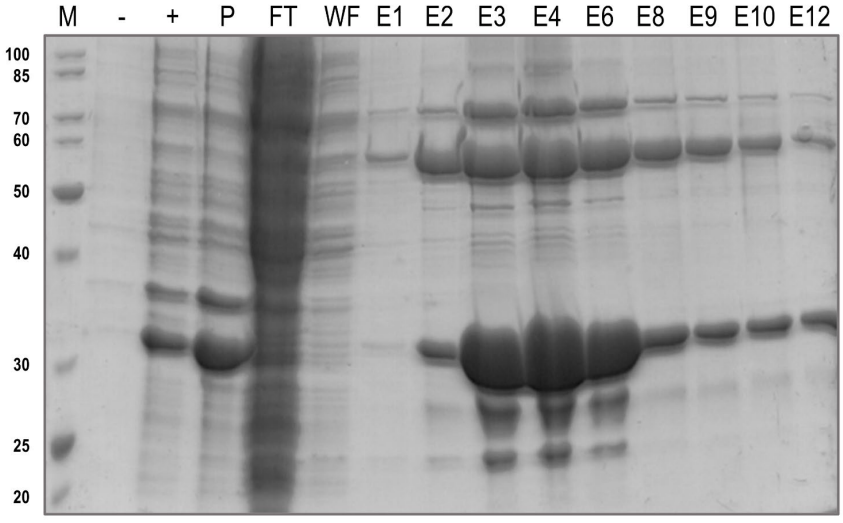

Figure 3.30 Heterologous production and purification of *Kfla*PUBS.
Coomassie-stained SDS-PAGE gel following production and affinity chromatography purification of *Kfla*PUBS with TALON® Superflow™. (M) Molecular size marker – NEB, Unstained Protein Standard, Broad Range (MW on the left side of the figure reported in kDa); (-) Cells before induction of gene expression; (+) Cells after induction of gene expression; (P) Pellet after cell lysis; (FT) Purification flow-through fraction; (WF) Purification wash fraction; (En) Elution fractions. *Kfla*PUBS has a predicted molecular weight of ~ 33 kDa.

The oligomerization state of the protein was assessed as previously described for the pre-FDBRs and *Kfla*HY2 (chapters 3.4 and 3.9). His-*Kfla*PUBS eluted at ~ 10.6 ml (Figure 3.31A). Based on the calibration curve, this corresponds to a monomer with MW ~ 35 kDa (Figure 3.31B), with a slight deviation from the predicted MW most likely imputable to the protein shape.

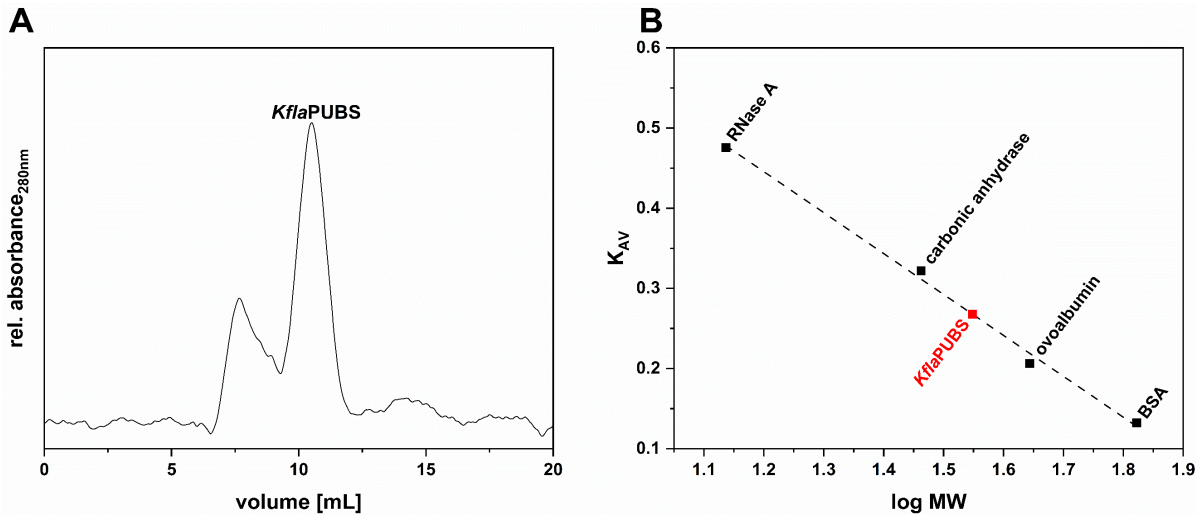

Figure 3.31 Determination of the oligomerization state of His-*Kfla*PUBS.
(A) Size exclusion chromatography of His-*Kfla*PUBS (*Kfla*PUBS) using a Superdex® 75 10/300 GL equilibrated with TES-KCl buffer. Absorbance was continuously measured at 280 nm. The chromatogram was smoothed applying a 60 pt. Savitzky-Golay filter due to detection issues of the Äkta Explorer UV module.
(B) Calibration curve of the Superdex® 75 10/300 GL column. RNAse A (MW = 13.7 kDa), carbonic anhydrase (MW = 29 kDa), ovoalbumin (MW = 44 kDa) and BSA (MW = 66.4 kDa) were used for calibration. The calibration curve was obtained by plotting the K_{AV} of the standards against the logarithm of the molecular weight (log MW) (black squares) and fitted (dashed line) using a linear regression in Origin. The red square indicates *Kfla*PUBS on the calibration curve.

FDBR-activity was monitored using His-*Kfla*PUBS and BV in equimolar amounts (Figure 3.32A).

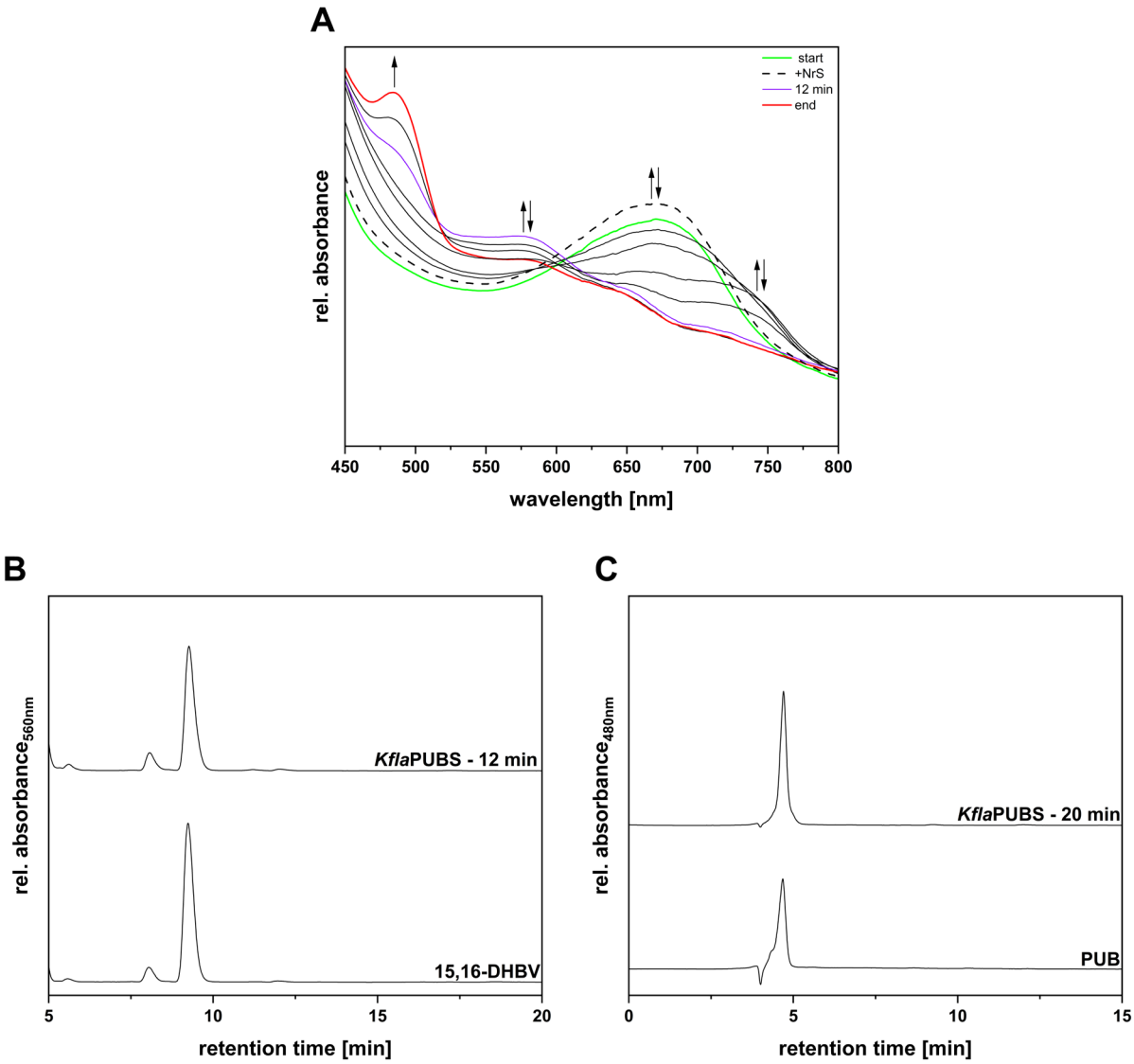

Figure 3.32 Activity assay of recombinant *Kfla*PUBS employing BV as the substrate and characterization of reaction products.
(A) Time-resolved UV-Vis spectra of an anaerobic bilin reductase activity assay of recombinant *Kfla*PUBS employing BV as the substrate. The total reaction time was 20 min and spectra were recorded every 30 s. The course of the absorbance during the reaction is marked by arrows. For reasons of clarity, only relevant spectra are shown. The green spectrum was recorded upon incubation of BV and *Kfla*PUBS, without starting the reaction. The dashed spectrum represents the first recorded after starting the reaction. Spectra recorded during the reaction are shown as solid black lines. The violet spectrum represents the product formed after 12 min. The red curve represents the end spectrum. Curves were smoothed applying a 50 pt. Savitzky-Golay filter.
(B) HPLC analysis of the 12 min reaction products of *Kfla*PUBS with BV as substrate (*Kfla*PUBS – 12 min). The products were analyzed using a reversed-phase 5 µm C18 Luna column (Phenomenex) as stationary phase. The mobile phase consisted of 50%$_{v/v}$ acetone and 50%$_{v/v}$ 20 mM formic acid flowing at 0.6 mL/min. Absorbance was continuously recorded at 560 nm. 15,16-DHBV, 15,16-dihydrobiliverdin standard.
(C) HPLC analysis of the 20 min reaction product of *Kfla*PUBS with BV as substrate (*Kfla*PUBS – 20 min). The products were analyzed using a reversed-phase 5 µm C18 Luna column (Phenomenex) as stationary phase. The mobile phase consisted of 50%$_{v/v}$ acetone and 50%$_{v/v}$ 20 mM formic acid flowing at 0.6 mL/min. Absorbance was continuously recorded at 480 nm. PUB, phycourobilin standard.

The reductase and the substrate formed a complex with an absorbance maximum at ~ 670 nm, suggesting the ability of the protein to bind BV (Figure 3.32A – start). After the reaction was started, a slight increase in the absorbance could be detected due to remaining

*Kfla*PUBS:BV in the NrS-injection syringe (Figure 3.32A – +NrS). Following the buildup of an absorbance shoulder ~ 745 nm, indicating BVH^+, the substrate was initially converted to a product absorbing at ~ 570 nm (Figure 3.32A – 12 min) which eventually transitioned to a final ~ 485 nm absorbing compound (Figure 3.32A – end). Both the 12 min and 20 min products were analyzed via HPLC (Figure 3.32B, C). The 12 min product exhibited a retention time consistent with 15,16-DHBV (Figure 3.32B – *Kfla*PUBS - 12 min), whereas the final 20 min product eluted solely at ~ 4.8 min, overlaying with PUB obtained from a *Pp*PUBS reaction (Figure 3.32C – *Kfla*PUBS - 20 min).

These findings confirm the presence of a PUBS in *K. nitens* and demonstrate that the reaction proceeds similarly to the only other characterized PUBS reaction to date, that of *Pp*HY2 (Chen *et al.*, 2012).

4 Discussion

4.1 Bilin biosynthesis originated in non-photosynthetic bacteria

The discovery of FDBR sequences in heterotrophic, non-photosynthetic bacteria presents an opportunity to explore the evolutionary history of both this enzyme family and bilin-based light harvesting systems, whose origins are poorly understood. These newly discovered sequences are basal to the AX lineage and form two clades, with the second split in two branches: pre-1, pre-2 and pre-3 (Rockwell *et al.*, 2023). Focusing on relevant internal nodes, one sequence from each clade was selected from the phylogenetic tree present in Rockwell *et al.*, 2023 (Figure S3 in Rockwell *et al.*, 2023). These proteins were heterologously produced and purified from *E. coli*, and their activity tested in anaerobic bilin reductase assays. Pre-1 (MCC5789364) and Pre-2 (CAP_1520) exhibited robust reduction of BV to 3(*E*)-PΦB. This peculiar result is noteworthy as FDBRs tend to typically favor the production of bilin 3(*Z*) isomers (Frankenberg & Lagarias, 2003b; Ledermann *et al.*, 2016; Sugishima *et al.*, 2020; Tu *et al.*, 2008). Older studies have indeed identified 3(*Z*) as precursor to 3(*E*) for both PCB and PΦB (Beale & Cornejo, 1984b; Terry *et al.*, 1995; Weller *et al.*, 1996). Since bilin-binding proteins were thought to be solely specific for 3(*E*) chromophore stereochemistry, 3(*Z*) → 3(*E*) isomerization was formerly hypothesized to require the mediation of specific bilin isomerases (Beale, 1993; Frankenberg *et al.*, 2001; Terry *et al.*, 1995). However, PBPs and phytochromes were shown to attach both stereoisomers and the isomerization is now acknowledged to be spontaneous (Bishop *et al.*, 1991; Duerring *et al.*, 1991; C. Li *et al.*, 2022; J. Li *et al.*, 2011; Schirmer *et al.*, 1987; Schmidt *et al.*, 1987; Weller *et al.*, 1996). Thermodynamically, the *E* isomer is more stable than the *Z* (Weller & Gossauer, 1980). In fact, both ethylidene isomers of PCB can be isolated from PC but the 3(*Z*) spontaneously isomerizes to 3(*E*) during methanolysis or ethanolysis at high temperature (Cornejo, 1992; Fu *et al.*, 1979; Kamo *et al.*, 2021; Roda-Serrat *et al.*, 2018; Terry *et al.*, 1993; Wilkinson *et al.*, 2023). This heat-induced side reaction was also thought to be responsible for the partial isomerization of the 3(*Z*) to the 3(*E*) bilin products recorded in the first FDBR studies. In this case, heat reactions were thought to occur during SpeedVac concentration of the bilin preparations (Frankenberg *et al.*, 2001). However, in this investigation, bilin concentration was achieved via sublimation using a lyophilizer. Therefore, by maintaining a constant temperature throughout the process, the risk of heat-induced isomerization was prevented. Given that the formation of 3(*E*)-PΦB does not result from a heat-induced side reaction, immediate formation of 3(*Z*)- before 3(*E*)-PΦB in the reactions catalyzed by Pre-1 and Pre-2 could be eventually tracked in a time course assay.

Regarding the reaction catalyzed by Pre-1, further investigation is necessary to elucidate the mechanism behind the pronounced and steadily increasing radical formation (Figure 3.2A, λ_{abs} ~ 730 nm).

In contrast to Pre-1 and Pre-2, Pre-3 (MBL9008304) was found to perform a 4e$^-$ reduction. Following the reduction of BV A-ring diene system to PΦB, an additional reduction of the latter at C15=C16 to PEB was observed. A similar scenario was previously only documented for PebA, shown to be able to successfully convert a mix of 3(Z)/3(*E*)-PΦB to 3(Z)/3(*E*)-PEB (Dammeyer & Frankenberg-Dinkel, 2006). However, since the *in vivo* substrate for PebA is certainly BV, this reaction is an *in vitro* artifact solely demonstrating the promiscuity of this reductase. In the case of Pre-3, BV is its *bona fide* substrate, as the reductase is encoded in a gene cluster alongside a heme oxygenase (Rockwell *et al.*, 2023).

Overall, the production of a dihydrobiliverdin rather than a tetrahydrobiliverdin in Pre-1 and Pre-2 is coherent with a stepwise evolutionary process, wherein a 2e$^-$ reduction sets the stage for the acquirement of successive 4e$^-$ reductions capabilities, first in Pre-3 and subsequently in the AX lineage (Figure 4.1).

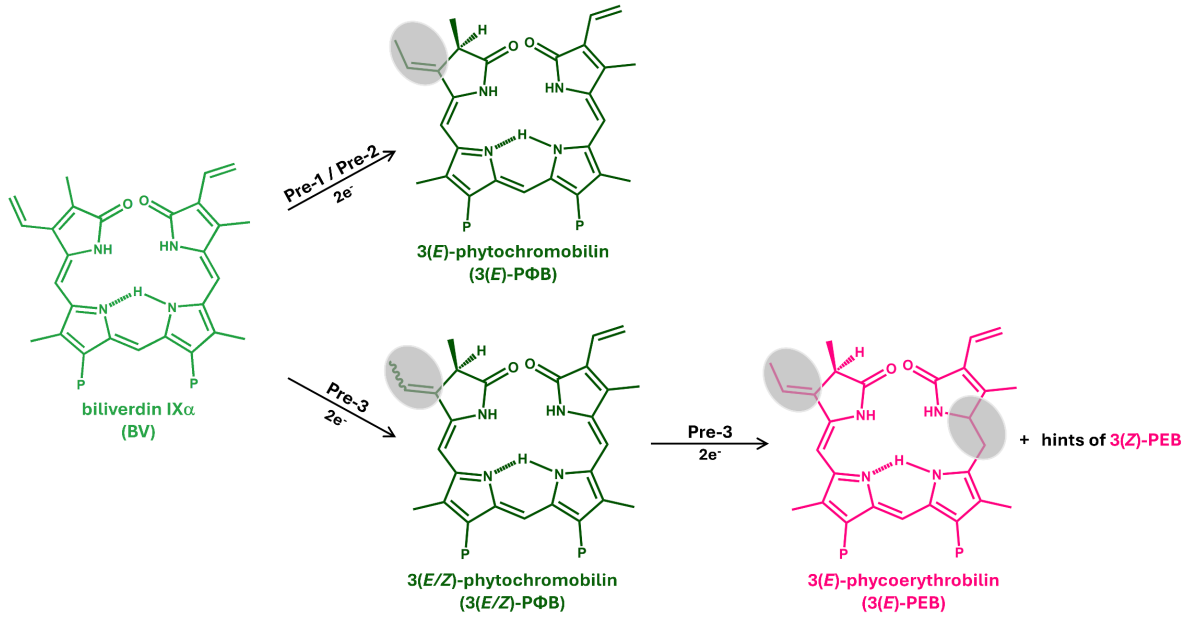

Figure 4.1 Overview of the reactions catalyzed by the investigated pre-FDBRs.
BV is the substrate of the 3 FDBRs. "P" indicates the propionate side chains. Pre-1 and Pre-2 catalyze the 2e$^-$ reduction of BV to 3(*E*)-PΦB. Pre-3 catalyzes the 4e$^-$ reduction of BV to PEB via the intermediate PΦB. BV reduction sites are highlighted in gray.

4.2 A look into the past: the first draft of a FDBR active site and the evolution of PcyA-catalyzed PCB-biosynthesis

Analysis of the pre-PcyA sequences reveals significant variation in the typical PcyA active site residues (Figure 4.2). As mentioned in chapter 1.4, PcyA activity is strictly dependent on three residues: Glu^{76}, His^{88}, Asp^{105} (*Syn*PcyA numbering). Glu^{76}, crucial for the initial 2e$^-$ reduction of BV D-ring exo-vinyl to 18^1,18^2-DHBV, is absent in all three pre-PcyAs. The substitution of this residue with a non-polar one in *Nos*PcyA_E73Q resulted in a protein variant only able to catalyze BV A-ring reduction to PΦB, in a scenario strongly resembling the native activity of Pre-1 and Pre-2, also in terms of stereospecificity (Tu *et al.*, 2007). Glu^{76} is additionally absent in PcyX, where the corresponding position is occupied by an Asp residue. However, this residue has been proven not to fulfill the same role as the catalytic Glu in PcyA, explaining PcyX inability, like the pre-PcyAs, to reduce BV D-ring exo-vinyl (Ledermann *et al.*, 2016, 2018). Similarly to Glu^{76}, His^{88} is also absent in the three analyzed pre-FDBRs, in accordance with its role of adjuvant in D-ring reduction. Asp^{105}, responsible for initial BV protonation in PcyA, is only conserved in Pre-2 and Pre-3. However, Pre-1 features a Glu in that position, which side chain has similar properties to the one of Asp. Based on homology, these acidic residues (Pre-1 Glu^{91}, Pre-2 Asp^{91}, Pre-3 Asp^{96}) could likely serve the same function as *Syn*PcyA Asp^{105}. Lastly, the residue responsible for the additional reduction of PΦB D-ring to PEB in Pre-3 is not identifiable from the sequence alignment.

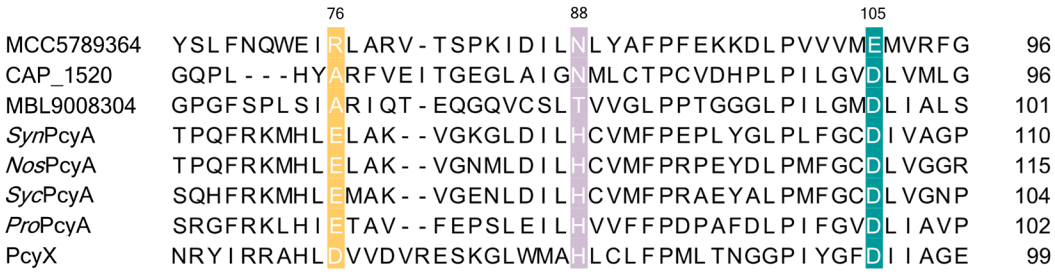

Figure 4.2 Sequence alignment of pre-PcyAs, PcyAs and PcyX.
The alignment was constructed using Clustal Omega (Madeira *et al.*, 2022) (https://www.ebi.ac.uk/jdispatcher/msa/clustalo) and modified using Jalview (Waterhouse *et al.*, 2009). The amino acid residues mentioned in the text are highlighted in different colors and labeled according to *Syn*PcyA sequence numbering. Accession codes of most of the employed sequences are listed in Table S1. MCC5789364: Pre-1 (GenBank accession code: MCC5789364); CAP_1520: Pre-2 (GenBank accession code: EYF06823); MBL9008304: Pre-3 (GenBank accession code: MBL9008304); *Syn*PcyA: PcyA from *Synechocystis* sp. PCC 6803; *Nos*PcyA: PcyA from *Nostoc* sp. PCC 7120; *Syc*PcyA: PcyA from *Synechococcus* sp. WH 7002; *Pro*PcyA: PcyA from *Prochlorococcus marinus* CCMP 1375; PcyX: PcyX from marine metagenome (PDB accession code: 5OWG).

Additional support to these considerations was gained by generating pre-PcyAs AlphaFold model structures (Jumper *et al.*, 2021; Mirdita *et al.*, 2022) (Figure 4.3). The structural alignments of the pre-PcyAs with *Syn*PcyA reveal the conserved Asp/Glu residues are positioned similarly, reinforcing the hypotheses drawn from the sequence alignment (Figure

4.3A, B, C). Despite the additional reduction of PΦB to PEB, the comparison of the active sites of Pre-3 and *Syn*PcyA reveals a striking similarity (Figure 4.3B). One might initially speculate that the mechanism for the second reduction step involves tilting the residue corresponding to *Syn*PcyA Asp^{220} toward the inside of the active site, similarly to HY2, PebS, and PcyX. However, Pre-3 features an Arg in the corresponding position (not shown in Figure 4.3B), which, even if tilted, could not serve as the catalyst. As discussed in chapter 3.10, only *Kfla*HY2 is able to genuinely metabolize PΦB. In the case of Pre-3, the reduction of PΦB does not occur at D-ring C18^1-C18^2 exo-vinyl, but rather at C15=C16. Analysis of the model structure of Pre-3 suggests that Glu^{217} might play a role in this context. This residue, which does not find homologs in any other FDBR (and corresponds to Thr^{222} in *Syn*PcyA), appears to be positioned in a manner that could facilitate interaction with BV D-ring, supposing a *ZZZ*-all-syn BV binding mode. Eventually, biochemical data on a function-disruptive variant might offer insights into solving this mystery.

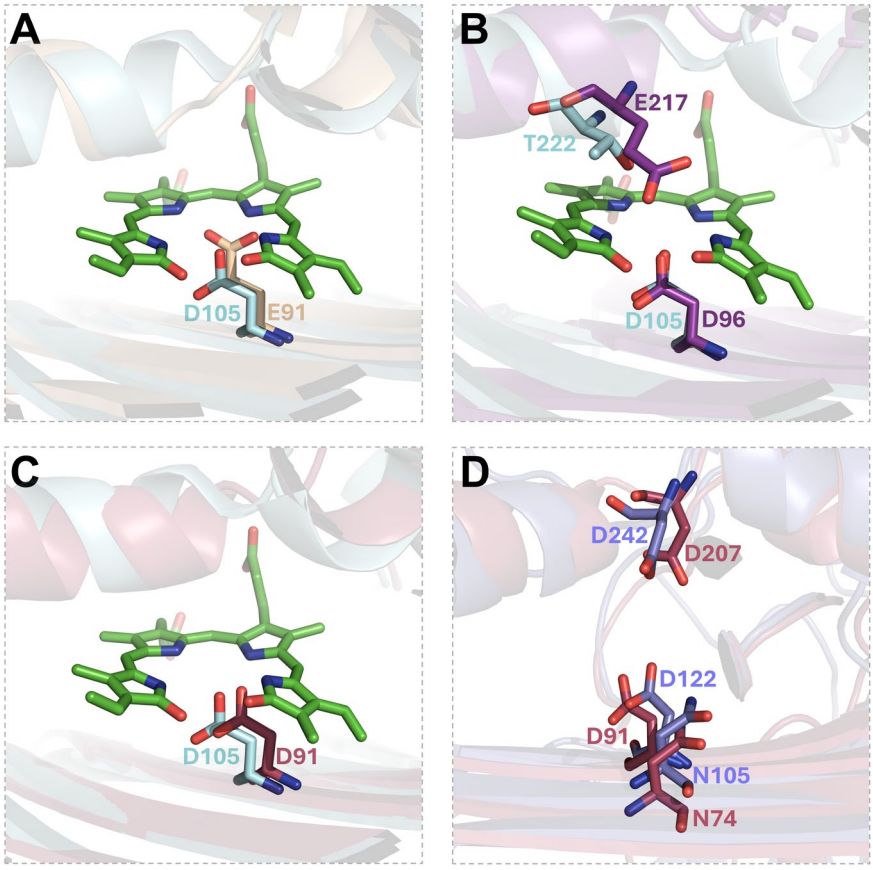

Figure 4.3 Structure alignments of pre-PcyAs with other FDBRs.
The model structures of all three pre-PcyAs were obtained using AlphaFold2 (https://colab.research.google.com/github/sokrypton/ColabFold/blob/main/AlphaFold2.ipynb) (Jumper *et al.*, 2021; Mirdita *et al.*, 2022). The alignments were generated using PyMOL (DeLano, 2020).
(A) Overlay of the active sites of Pre-1 and *Syn*PcyA. The model structure of Pre-1 is displayed as transparent wheat cartoon. The crystal structure of *Syn*PcyA (PDB accession code: 2D1E) is displayed as transparent aquamarine cartoon. BV, in the conformation bound in the active site of *Syn*PcyA, is shown as green sticks. Amino acid residues of interest are shown as labeled sticks and colored as the belonging structure.
(B) Overlay of the active sites of Pre-3 and *Syn*PcyA. The model structure of Pre-3 is displayed as transparent violetpurple cartoon. The crystal structure of *Syn*PcyA (PDB accession code: 2D1E) is displayed as transparent

aquamarine cartoon. BV, in the conformation bound in the active site of *Syn*PcyA, is shown as green sticks. Amino acid residues of interest are shown as labeled sticks and colored as the belonging structure.
(C) Overlay of the active sites of Pre-2 and *Syn*PcyA. The model structure of Pre-2 is displayed as transparent raspberry cartoon. The crystal structure of *Syn*PcyA (PDB accession code: 2D1E) is displayed as transparent aquamarine cartoon. BV, in the conformation bound in the active site of *Syn*PcyA, is shown as green sticks. Amino acid residues of interest are shown as labeled sticks and colored as the belonging structure.
(D) Overlay of the active sites of Pre-2 and *Kfla*HY2. The model structure of Pre-2 is displayed as transparent raspberry cartoon. The model structure of *Kfla*HY2 is displayed as transparent slate cartoon. Amino acid residues of interest are shown as labeled sticks and colored as the belonging structure.

Noteworthy is the similarity between the active sites of CAP_1520 and *Kfla*HY2 (Figure 4.3D). As discussed in chapter 3.11, the reduction of BV to PCB catalyzed by *Kfla*HY2 relies on an Asp pair, Asp^{122} and Asp^{242}, which is conserved in CAP_1520. Furthermore, these residues are fully overlapping in the model structures alignment. However, despite this striking similarity of the active sites, the two enzymes catalyze two different reactions and potentially rely on a different substrate binding mode. This finding agrees with a common feature of FDBRs, i.e. the impossibility to predict catalytic activity solely based on an amino acid sequence alignment or the conservation of specific residues in the active site (Dammeyer *et al.*, 2008b; Ledermann *et al.*, 2016, 2018; Rockwell & Lagarias, 2017a). One of the main reasons behind this phenomenon lies in the substrate binding mode. Indeed, while the crystal structure of *Syn*PcyA and *Nos*PcyA exhibit a BV *ZZZsss* binding mode, both *Gt*PEBB and *Sl*HY2 reveal a *ZZZssa* flipped binding mode of the linear tetrapyrrole substrate, resulting in inverted positioning of the A- and D-ring (Dammeyer *et al.*, 2008b; Hagiwara *et al.*, 2006a, 2006b; Sommerkamp *et al.*, 2019; Sugishima *et al.*, 2020; Tu *et al.*, 2007). A flipped binding mode has also been proposed for *Kfla*HY2 based on its reaction mechanism and the conservation of critical residues for BV *ZZZssa* stabilization in the active site (Sugishima *et al.*, 2020; chapter 4.8). Evolutionarily, one would suggest that, being hitherto the earliest emerging FDBRs, Pre-PcyAs would bind BV in a *ZZZ*-all-syn conformation, as PcyA. Nevertheless, due to the high similarity to *Kfla*HY2, it would be intriguing to investigate the potential metabolization of PΦB by CAP_1520.
Ultimately, the most striking divergence between pre-PcyAs and cyanobacterial PcyAs lies in the active site Glu. Biochemical and phylogenetic evidence suggest that the evolution of PcyA occurred via the acquisition of this residue, and therefore C18-exo-vinyl reduction specificity. Based on these considerations, it is plausible that cyanobacteria obtained PcyA via HGT from a proteobacterium.

4.3 Why did heterotrophic bacteria evolve bilin biosynthesis?

The presence of active FDBRs in non-photosynthetic bacteria raises the question on their significance. BV serves as the precursor to all linear tetrapyrroles and its biosynthesis relies on oxygen-dependent heme cleavage (Ortiz De Montellano, 2000; Wilks, 2002; Yoshida & Migita, 2000). Thus, the function of FDBRs, including pre-PcyAs, is strictly associated with the presence of O_2. The hypothesis that FDBRs evolved from non-photosynthetic bacteria seems to contrast with the strict dependency on O_2, which would suggest an emergence in photosynthetic bacteria. The latest diverging pre-FDBRs, Pre-2 and Pre-3, are almost-exclusively found in heterotrophs within δ-proteobacteria (Muñoz-Dorado & Arias, 1995; Rockwell *et al.*, 2023; Shimkets, 1990). It is plausible that early cyanobacteria may have coexisted alongside these organisms in a microbial consortium. As cyanobacteria started performing photosynthesis, the associated microbes might have evolved a heme oxygenase to deplete both oxygen and free heme simultaneously. Therefore, these bilin-related pathways might have emerged as detoxification strategies in bacteria and were subsequently acquired by cyanobacteria to serve different purposes. The pre-PcyA sequences are additionally associated to distant PBP homologs named BBAGs. These BBAGs form two distinct clades. BBAG-1 and BBAG-3, associated with pre-1 and pre-3, form a single lineage from which cyanobacterial BBAGs descended, whereas BBAG-2, associated with pre-2, form a clade with linear tetrapyrrole-binding photoglobins (Rockwell *et al.*, 2023; Schneider *et al.*, 2022). BBAG-2, the ancestral lineage, has been found to be specific for BV. Contrastingly, BBAG-1 and BBAG-3 bind several bilins to specific Cys residues, in the absence of lyase-like proteins. Despite the overall conformation of the bilins in BBAGs is similar to that of PBPs, BBAGs are not highly fluorescent and are not efficient in light-harvesting. The function of BBAGs is therefore still unknown and might not be essential, since a broad range of cyanobacteria, including the earliest diverging ones, do not possess them (Rockwell *et al.*, 2023). Phylogenetic analysis indicates that cyanobacteria did not acquire PBPs with PcyA and BBAGs, leaving the origin of PBPs still an open subject. Nonetheless, the emergence of PBPs-mediated light harvesting unquestionably required several evolutionary steps, from the loss of autocatalytic binding of chromophores, and emergence of bilin lyases, to the gain of the characteristic fluorescence.

4.4 The loss of PCYA complicates PCB biosynthesis in Rhodophytes

FDBRs greatly diverged following primary endosymbiosis. Despite being the basal clade of Rhodophyta, the Cyanidiophyceae exhibit a dark green coloration, due to the absence of PE

in their PBSs. Based on pigments composition, Cyanidiophyceae should only encode for a *PCYA*, responsible for synthesizing PCB to be subsequently bound to APC and PC. While this holds true for the earliest diverging Cyanidiophyceae, i.e. the Cyanidioschyzonales and the Cyanidiales, the situation gets significantly trickier moving down the evolutionary line, starting from the Galdieriales (Park *et al.*, 2023; Rockwell & Lagarias, 2017a). Phylogenetic analysis has highlighted that these organisms possess *PEBA* and *PEBB*, but not a *PCYA*. In accordance with this finding, several decades ago, prior to the identification of FDBRs, the PCB chromophore of *Galdieria sulphuraria*, formerly mistaken for *Cyanidium caldarium*, was discovered to be synthesized from BV via PEB (Beale & Cornejo, 1991a, 1991b, 1991c). Beale and Cornejo envisaged the existence of an isomerase responsible for the conversion of PEB, after its biosynthesis, to PCB (Figure 4.4). This scenario is likely applicable to more complex Rhodophytes (Rhodophytina), where PE is additionally present in the PBS. The presence of PE justifies the existence of *PEBA* and *PEBB* in these organisms, yet no *PCYA* is encoded for direct PCB biosynthesis starting from BV.

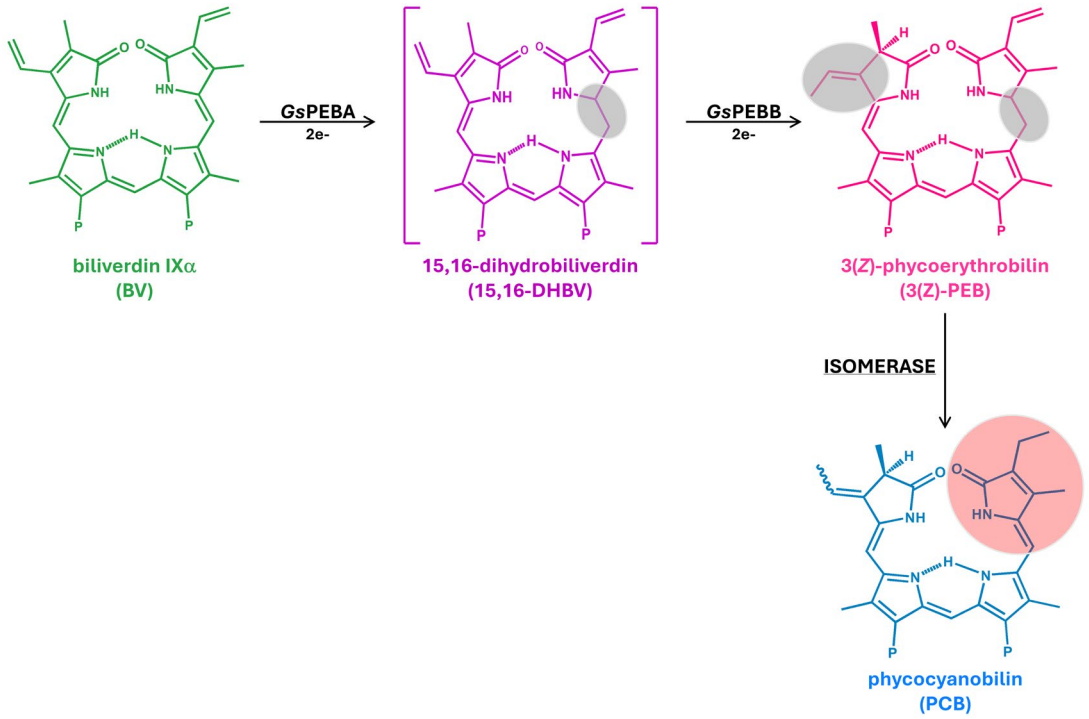

Figure 4.4 Overview of the proposed PCB biosynthesis pathway in *Galdieria sulphuraria*.
"P" indicates the propionate side chains. *Gs*PEBA catalyzes the $2e^-$ reduction of BV to 15,16-DHBV. *Gs*PEBB subsequently reduces 15,16-DHBV to mostly 3(*Z*)-PEB. BV reduction sites are highlighted in gray. 3(*Z*)-PEB is the substrate for an isomerase relocating the $C18^1$=$C18^2$ double bond to C15-C16 to yield PCB. Isomerization site is highlighted in red.

Via *in vivo* experiments, the isomerase activity proposed in 1991 was also confirmed by our research group. In particular, a *G. sulphuraria* protein-enriched fraction with a MW > 60 kDa was found to convert exogenous PEB to PCB (Hartmann, 2018; Mudler, 2020). However, the attempt to identify the putative isomerase in this fraction via mass spectrometry was

unsuccessful. ~ 390 proteins were identified in the sample, of which 36 uncharacterized and around 10 annotated isomerases. In this context, the aim would have been to further enrich this fraction, reducing the number of potential candidates, and proceed with a recombinant approach for the characterization of the putative isomerase. Unfortunately, despite obtaining enrichment outcomes similar to previous successful experiments, the initial attempts consistently resulted in an inactive protein fraction. Since the enrichment involves several purification steps, a concomitant loss of protein function during this process is plausible. Proteins or cofactors that might be essential for the proper function of the isomerase could have been inadvertently lost during the enrichment procedure. The first approach to investigate this possibility involved performing activity assays during different stages of purification. However, technical issues related to cell lysis came into play. Since the cell wall of *Galdieria* is greatly proteinaceous (~ 55% protein content), particularly rigid and thick (~ 50 nm), its breakage can only be achieved using heavy mechanical lysis methods like homogenization (Bailey & Staehelin, 1968; Mercer *et al.*, 1962; Oesterhelt *et al.*, 2008). The unforeseen impossibility to keep using a high-pressure homogenizer, hindered any subsequent enrichment procedure. In this context, the recent discovery of a cell wall-less haploid mutant of *Galdieria partita* could greatly simplify the breakage procedure and facilitate the recovery of isomerase activity (Hirooka *et al.*, 2022). The only drawback associated with using this strain is the requirement for heterotrophic growth, during which the transcription of photosynthesis and pigment biosynthesis-related genes has been shown to be strongly downregulated (Perez Saura *et al.*, 2022).

4.5 A computational approach to facilitate the search for the isomerase

An *in silico* analysis using bioinformatics was additionally conducted as another potential approach to facilitate the identification of the isomerase. As previously mentioned, the Cyanidioschyzonales and the Cyanidiales, sister lineages to the Galdieriales, harbor *PCYA*. The PCYA of *Cyanidioschyzon merolae* was previously investigated and confirmed to be a genuine PCYA, catalyzing the typical reduction of BV to PCB (Mudler, 2020). Leveraging on this significant bilin-biosynthesis pathway distinction, a proteome subtraction was conducted between *G. sulphuraria* and *C. merolae*. *C. merolae* is somewhat of a simple eukaryote, possessing a reduced genome (16 Mb) resulting in 4775 protein-coding genes (Nozaki *et al.*, 2007). *G. sulphuraria* is slightly more complex, with still a relatively small genome for a eukaryote (13.7 Mb), resulting in 6622 protein-coding genes (Schönknecht *et al.*, 2013). However, the subtraction of the two proteomes was not particularly successful, as ~ 4100 proteins unique to *G. sulphuraria* were identified, consistent with findings from Schönkneckt

and colleagues, and ~ 300 of these proteins remain uncharacterized. The additional comparison of these unique proteins with the ~ 390 identified via mass spectrometry in the enriched fraction led to a ~ 90% reduction of potential candidates to 41, all resulting from nucleus-encoded genes (Table 4.1). Nonetheless, the amount remains excessive to proceed with characterization of each in a recombinant approach.

Table 4.1 Proteins identified in the *Galdieria sulphuraria* isomerase-active enriched fraction, absent in *Cyanidioschyzon merolae*.

Accession (UniProt)	Annotation	Size (kDa)	Signal peptide?
M2X4W0	Uncharacterized protein	13	No
M2XTV5	BAR domain-containing protein	34	No
M2XZL8; M2Y956; M2XGZ7	Formamidase	43; 51; 31	No; No; No
M2VXK0	Glutathione S-transferase	25	No
M2X7L6	Uncharacterized protein	53	No
M2WZJ6	BAR domain-containing protein	34	No
M2W312	Uncharacterized protein	27	Yes
M2Y7Y6	Ribonuclease	69	No
M2XBW2	Uncharacterized protein	25	No
M2VY74	Uncharacterized protein	35	No
M2Y9J5	Glycerol dehydrogenase	42	No
M2W040	Uncharacterized protein	55	No
M2W7C7	Acylaminoacyl-peptidase-related protein	109	No
M2W3V0	Histone H1	26	No
M2WZU6	Formamidase	41	No
M2VX96	Ferric-chelate reductase	98	Yes
M2XGU0	Carboxymethylenebutenolidase	31	No
M2WPS8	Uncharacterized protein	21	No
M2W3T8	Oxidoreductase family protein	40	No
M2X4X4	Uncharacterized protein	21	No
M2Y389; M2Y3M5	LAO/AO transport system kinase isoform 2	39; 44	No; No
M2XT78	Methyltransferase type 12 domain-containing protein	30	No
M2XYW3	Uncharacterized protein	153	No
M2X690	MARVEL domain-containing protein	22	No

M2VUV4	Replication factor A1	14	No
M2XZV1	2-dehydropantoate 2-reductase	38	No
M2WRJ7; M2XSP8	Proteasome family protein isoform 1	41; 42	No; No
M2XXE2	Alpha-mannosidase	113	No
M2WYU9	Uncharacterized protein	14	Yes
M2XTZ5	Polysaccharide deacetylase	36	No
M2XQJ6	Uncharacterized protein	29	No
M2Y6I1	CUE domain-containing protein	25	No
M2W7H1	DNA-binding protein, putative	54	No
M2XUP9; M2XVD8	Uncharacterized protein	33; 35	Yes; Yes
M2XWI1	Uncharacterized protein	23	No
M2XVH6	Uncharacterized protein	36	No

4.6 Is the isomerase really required?

As emphasized in this study, the catalytic activity of FDBRs cannot be easily predicted in the absence of biochemical data. Since the search for the isomerase became intricate, two alternative possibilities needed to be ruled out to further confirm the necessity of a new enzyme: the activity of extant PEBA and PEBB and the plethora of PBP lyases in Rhodophytes. The ability of *Gs*PEBB to catalyze the reduction of 15,16-DHBV to PEB was previously confirmed, alongside its inability to metabolize BV, a feature shared with all other PebBs (Busch *et al.*, 2011b; Eichler, 2016). On the other hand, the biochemical investigation of *Gs*PEBA proved to be consistently challenging. This protein exhibited a high tendency to aggregation across multiple recombinant production strategies. Eventually, the decision to harmonize the gene sequence proved beneficial. Despite remaining largely insoluble, the small soluble fraction obtained was shown to be active in catalyzing the reduction of BV to 15,16-DHBV. Therefore, individually, *Gs*PEBA and *Gs*PEBB do indeed mediate the reactions expected by *in silico* analysis. Since the isomerase activity was only detected in a protein fraction with a MW > 60 kDa, another avenue of investigation was the possibility of a *Gs*PEBA-*Gs*PEBB synergy, resulting in a different product than the single reactions. However, a coupled activity assay disproved this hypothesis, further confirming that PCB production in *G. sulphuraria*, and most likely in all Rhodophytes besides the Cyanidioschyzonales and the Cyanidiales, is not FDBR-related.

The possibility of the involvement of a bilin lyase-isomerase was solely investigated through bioinformatics. In theory, one could envision the existence of a PEB-specific lyase-isomerase responsible for isomerizing the PEB produced by the FDBRs to PCB and for the simultaneous

attachment to PC subunits. Such mechanisms are typical of cyanobacteria, where the synthesis of PUB and PVB and attachment to PE and PEC, respectively, relies on lyases-isomerases (Blot *et al.*, 2009; Carrigee *et al.*, 2021, 2022; Mahmoud *et al.*, 2017; Sanfilippo, *et al.*, 2019b; Shukla *et al.*, 2012; C. Zhao *et al.*, 2017; K. H. Zhao *et al.*, 2005). While bilin lyases and lyase-isomerases remain poorly characterized in Rhodophytes, a BLAST search led to the identification of only PC-related enzymes, namely CpcE/F, CpcS/U and CpcT, in both *C. merolae* and *G. sulphuraria*, suggesting the isomerization should occur prior to the attachment to the PBP and not concomitantly.

Ultimately, the identification of the isomerase is contingent on new methodological approaches. Recently, the development of a click chemistry PCB probe, specifically a PCB adduct bearing a biotinylated C12-alkyne, allowed for the identification of molecular targets responsible for its bioactivity (Wilkinson *et al.*, 2023). The probe was added to mammalian cells and enriched through biotin-avidin affinity, enabling the identification of PCB-interacting partners in a chemical proteomics approach. In the search for the isomerase, a similar strategy could be envisaged starting from a PEB clickable probe. Introducing this probe to cell-free extracts or chloroplast isolates could potentially facilitate screening for the isomerase among the pool of interacting partners. The success of this approach heavily relies on efficient cell breakage. Ideally, utilizing the easily breakable cell wall-less *G. partita*, wherein PEB is not detectable as in all other Cyanidiophyceae, would provide a lysis advantage and additionally mitigate the risk of PEB cross-reactions. Furthermore, since the absence of *PCYA* is also a common trait of Rhodophytina, the search for the isomerases could be moved to another organism. However, in this scenario, the presence of PEB, a greater complexity in terms of PBS, PBP lyases and the overall more disperse genomes, may only partially offset the challenges associated with easier cell lysis.

4.7 The HY2 of an early diverging Streptophyta has a PcyA-like activity

The employment of PCB as phytochrome chromophore in Streptophyte algae is in contrast with the presence of only *HY2*-related sequences in their genomes (Rockwell & Lagarias, 2017a; Rockwell *et al.*, 2017). Indirect phytochrome reconstitution studies have hinted that the HY2 of one of the earliest diverging streptophytes, *Klebsormidium nitens* (formerly *Klebsormidium flaccidum*), might be responsible for PCB formation (Rockwell *et al.*, 2017). To biochemically investigate this unexpected behavior, in this study, *Kfla*HY2 was heterologously produced and purified from *E. coli* to assess its bilin reductase activity. The HY2 of *K. nitens* was confirmed to be a functional FDBR, which, in contrast to the phylogenetic classification as a HY2, possesses a PcyA-like activity, catalyzing the reduction of BV to PCB.

As the product is a tetrahydrobiliverdin, requiring 4e$^-$ reduction of BV, the reaction must proceed via a dihydrobiliverdin intermediate. PcyA-mediated PCB formation typically starts with BV reduction at the D-ring exo-vinyl, resulting in 18^1,18^2-DHBV as the 2e$^-$ reduced intermediate (Frankenberg & Lagarias, 2003b; Hagiwara *et al.*, 2010; Tu *et al.*, 2004). However, theoretically, the formation of PCB could also occur through the initial reduction of BV A-ring, followed by D-ring reduction, yielding PΦB as the initial intermediate. To determine whether *Kfla*HY2 exhibits a similar mechanism to PcyA or favors the latter pathway, an activity assay with a limited e$^-$ supply was performed. The assay enabled the identification of both 18^1,18^2-DHBV and 3(*Z*)-PΦB as intermediates. This finding was somewhat surprising, as its implies that *Kfla*HY2 can mediate the reduction of BV to PCB employing both reaction routes (Figure 4.5).

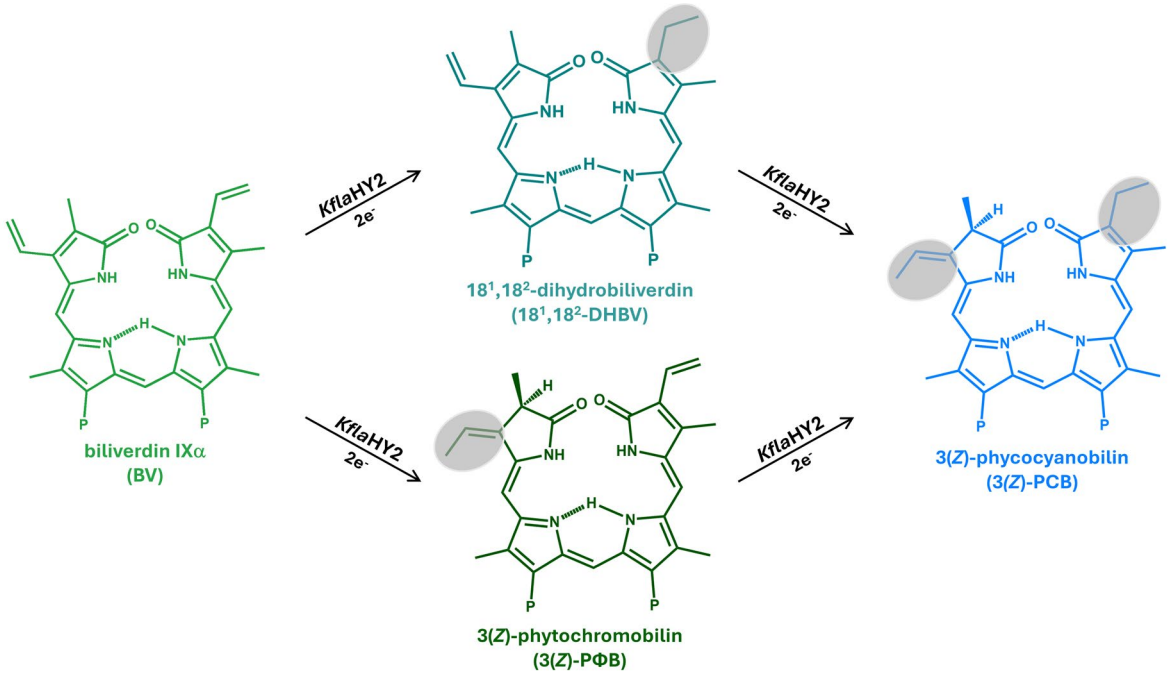

Figure 4.5 Overview of *Kfla*HY2 reaction routes recorded *in vitro*.
BV is the substrate of *Kfla*HY2. "P" indicates the propionate side chains. *Kfla*HY2-catalyzed PCB biosynthesis can proceed either starting with the 2e$^-$ reduction of BV D-ring (top), yielding 18^1,18^2-DHBV, or BV A-ring (bottom), yielding 3(*Z*)-PΦB. The reaction proceeds, respectively, with the reduction of 18^1,18^2-DHBV A-ring endo-vinyl (top) or 3(*Z*)-PΦB D-ring exo-vinyl (bottom) to ultimately yield 3(*Z*)-PCB. BV reduction sites are highlighted in gray.

The identification of 3(*Z*)-PΦB as an intermediate in PCB biosynthesis aligns with previous research on the phytochrome of the Zygnematophycea *Mesotaenium caldariorum*, which also harbors a HY2 (Wu *et al.*, 1997). Taking this into consideration, one might propose PΦB serves as the genuine intermediate in the *Kfla*HY2-catalyzed conversion of BV to PCB, while the formation of the 18^1,18^2-DHBV intermediate could rather be an artifact of the experimental setup. Here, it is plausible that, during *in vitro* enzyme assays, BV is forced in 2 orientations within the active site, leading to the formation of the two observed dihydrobiliverdins. *In vivo*,

the substrate might be directly channeled from the preceding enzyme, heme oxygenase. A similar scenario has been documented for certain heme oxygenases from pathogenic bacteria, where the orientation of the substrate dictates the product formed (Caignan *et al.*, 2002). Ultimately, in the absence of a crystal structure, the *in vitro* identification of the *de facto* intermediate could be facilitated by coupling *Kfla*HY2 with *Kfla*HY1 (the heme oxygenase of *K. nitens*), so that BV would be directly channeled to the FDBR in the correct conformation. Nevertheless, *Kfla*HY2 was shown to accept both 18^1,18^2-DHBV and PΦB as potential substrates and convert them to PCB. This scenario is not unusual since all BV-converting FDBRs are somewhat promiscuous. For instance, *Nos*PcyA was shown to catalyze PCB production starting from its native intermediate 18^1,18^2-DHBV but also from 3(*Z*)-PΦB, similarly to *Kfla*HY2 (Frankenberg & Lagarias, 2003b). PebS is also able to metabolize 15,16-DHBV, its transient intermediate, to PEB (Dammeyer *et al.*, 2008a). Moreover, rather strangely, the $2e^-$ reduction mediated by PebA can also occur, instead of the original BV to 15,16-DHBV conversion, starting from PΦB and resulting in the formation of PEB (Dammeyer & Frankenberg-Dinkel, 2006). The only FDBR showing high specificity for its substrate is PebB (Dammeyer & Frankenberg-Dinkel, 2006). According to these findings, it appears that FDBR substrate recognition is more a function of the ring conjugation rather than the configuration of the single A-ring.

4.8 *Kfla*HY2 active site: conserved residues, different purposes

The ability of FDBRs to catalyze bilin formation is not dependent on cofactors but rather on specific residues in the active site, which serve as acid catalysts for substrate reduction. Therefore, a $4e^-$ dependent reduction theoretically requires the presence of an additional acidic residue in *Kfla*HY2 active site driving the reduction of the D-ring, absent in land plant HY2s. A sequence alignment of *Kfla*HY2 with PcyAs and land plant HY2s was generated to get an initial peek into the main differences (Figure S3). Previous investigations revealed the HY2-mediated reduction of BV A-ring 2,3,3^1,3^2-diene system is dependent on an Asp pair (*Sl*HY2 Asp^{123} / *Sl*HY2 Asp^{263}; *At*HY2 Asp^{116} / *At*HY2 Asp^{256}) (Sugishima *et al.*, 2020; Tu *et al.*, 2008). *Kfla*HY2 only possesses a homolog to one of these two aspartates (*Kfla*HY2 Asp^{242}; *Sl*HY2 Asp^{263}; *At*HY2 Asp^{256}), whereas the second Asp is substituted with an Asn (*Kfla*HY2 Asn^{105}; *Sl*HY2 Asp^{123}; *At*HY2 Asp^{116}). The presence of only one of the two residues responsible for the A-ring reduction already hints at substantial reaction mechanism variations in *Kfla*HY2. However, the most striking difference between *Kfla*HY2 and other HY2s is the presence of a homolog to the Asp residue responsible for initial BV protonation in PcyAs (*Syn*PcyA Asp^{105}; *Nos*PcyA Asp^{110} in Figure S3), suggesting it might serve the same purpose in *Kfla*HY2 (Hagiwara *et al.*, 2006a, 2010; Tu *et al.*, 2007; Unno *et al.*, 2015). Consistent with

all other HY2s, *Kfla*HY2 lacks the Glu residue (*Syn*PcyA Glu[76]; *Nos*PcyA Glu[81] in Figure S3) responsible for BV D-ring reduction in PcyA, and thus essential for 18[1],18[2]-DHBV formation (Tu *et al.*, 2007). The absence of a Glu homolog indicates *Kfla*HY2 relies on another acidic residue or a water molecule to perform the said reduction. To corroborate these initial considerations, a *Kfla*HY2 model structure was obtained using AlphaFold2 (Jumper *et al.*, 2021; Mirdita *et al.*, 2022) and structural alignments were generated using PyMOL (DeLano, 2020) (Figure 4.6).

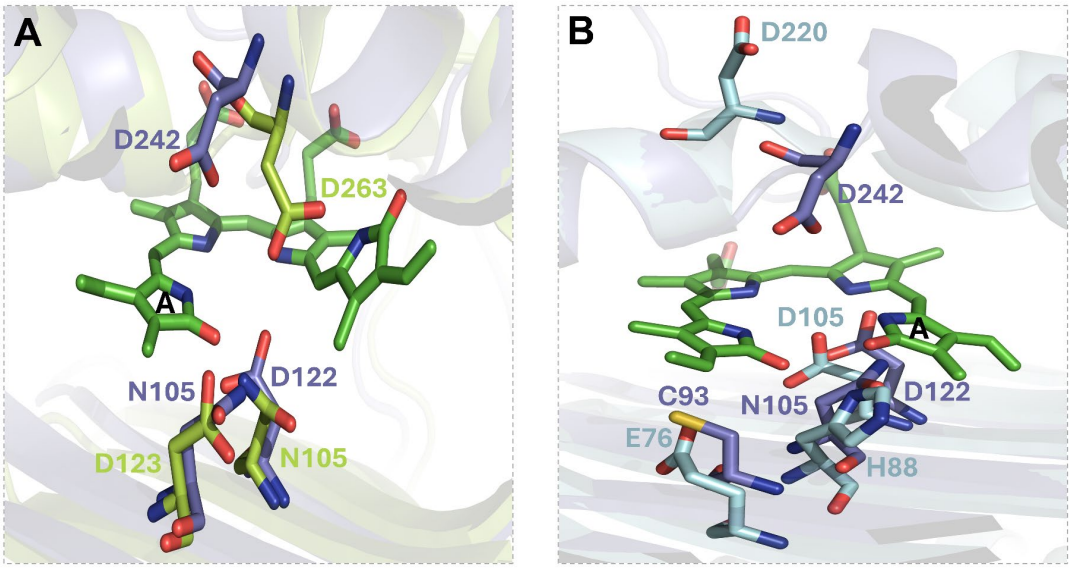

Figure 4.6 Structure alignments of *Kfla*HY2 with *Sl*HY2 and *Syn*PcyA.
The model structure of *Kfla*HY2 (displayed in transparent slate cartoon) was obtained using AlphaFold2 (https://colab.research.google.com/github/sokrypton/ColabFold/blob/main/AlphaFold2.ipynb) (Jumper *et al.*, 2021; Mirdita *et al.*, 2022). The alignments were generated using PyMOL (DeLano, 2020).
(A) Overlay of the active sites of *Kfla*HY2 and *Sl*HY2. The crystal structure of *Sl*HY2 (PDB accession code: 6KME) is displayed as transparent limon cartoon. BV, in the conformation bound in the active site of *Sl*HY2, is shown as green sticks, with A-ring being labeled. Amino acid residues of interest are shown as labeled sticks and colored as the belonging structure.
(B) Overlay of the active sites of *Kfla*HY2 and *Syn*PcyA. The crystal structure of *Syn*PcyA (PDB accession code: 2D1E) is displayed as transparent aquamarine cartoon. BV, in the conformation bound in the active site of *Syn*PcyA, is shown as green sticks, with A-ring being labeled. Amino acid residues of interest are shown as labeled sticks and colored as the belonging structure.

The first alignment was made with the crystal structure of *Sl*HY2, which shares 40% sequence identity with *Kfla*HY2 (Sugishima *et al.*, 2020) (Figure 4.6A) The second alignment was with the crystal structure of *Syn*PcyA, catalyzing BV to PCB reduction as *Kfla*HY2 (Hagiwara *et al.*, 2006a) (Figure 4.6B). These alignments revealed a higher similarity of the *Kfla*HY2 active site to the one of *Sl*HY2. Critical residues of the bottom β-sheet superimpose, and the distal Asp residue (*Sl*HY2 Asp[263] – *Kfla*HY2 Asp[242]), crucial for A-ring reduction, exhibits a similar positioning (Sugishima *et al.*, 2020; Tu *et al.*, 2008). In contrast, the corresponding residue in *Syn*PcyA (Asp[220]) faces outside of the active site and has been demonstrated not to participate in catalysis (Hagiwara *et al.*, 2006a). *Kfla*HY2 Asp[242] involvement in the reaction

found proof in the complete inability of the variant *Kfla*HY2_D242N to sustain any kind of BV reduction, at both the A- and D-ring. Conversely, the reduction of the D-ring exo-vinyl group in *Syn*PcyA has been shown to be catalyzed by the residue Glu^{76}, which does not have a homolog in *Kfla*HY2 (Hagiwara *et al.*, 2006a). In *Kfla*HY2, this function could potentially be fulfilled by Asp^{122}, since the exchange of this residue with an Asn resulted in a protein variant only able to perform slight A-ring 2,3,3^1,3^2-diene system reduction. Moreover, the complete inactivity of *Kfla*HY2_D242N could indicate that the reduction of the A-ring occurs prior to that of the D-ring, as the latter does not take place in the absence of the former. Contrastingly, the reduction of the A-ring still occurs in the absence of D-ring reduction. These considerations, combined with the phylogenetic classification as a HY2, further support the hypothesis that the authentic reaction intermediate is PΦB (Figure 4.7).

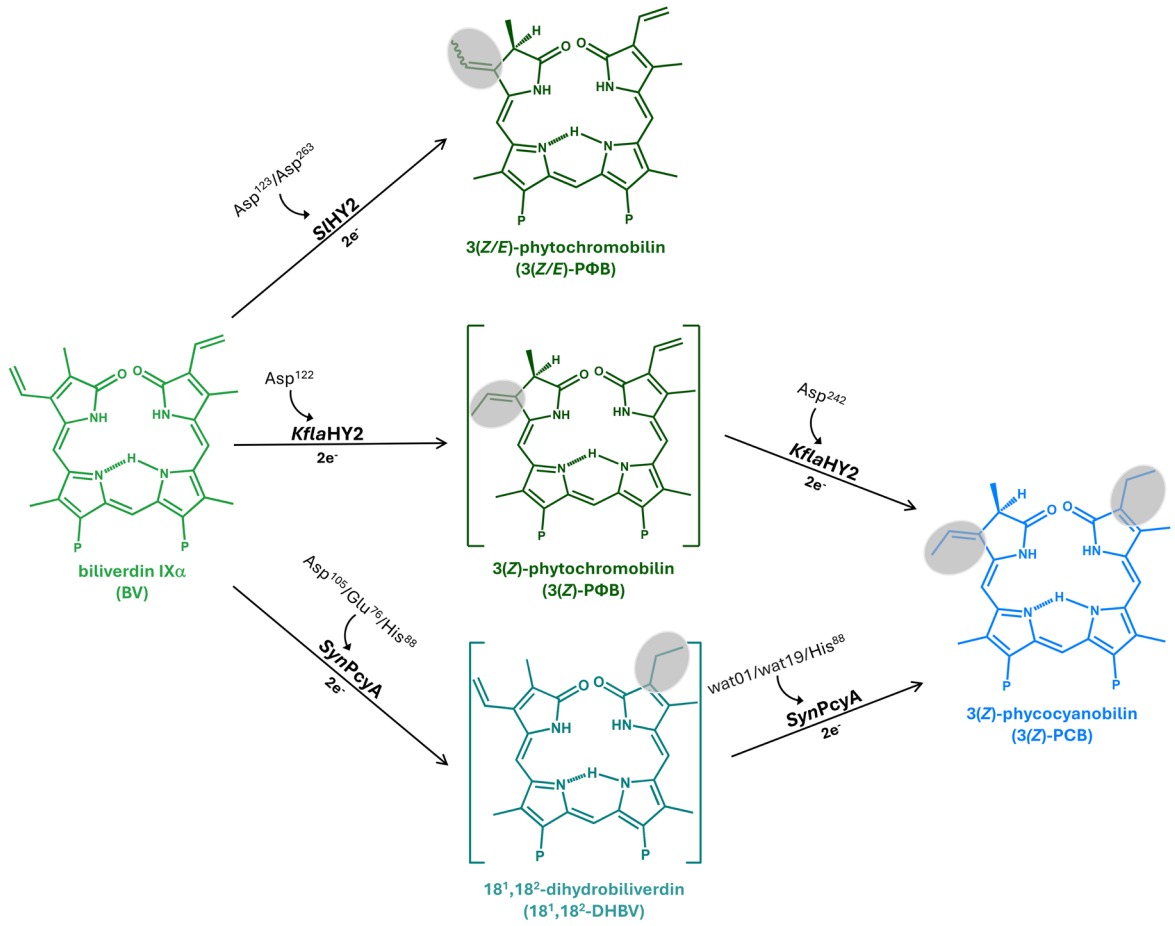

Figure 4.7 Overview of the reactions catalyzed by *Sl*HY2, *Kfla*HY2 and *Syn*PcyA.
BV is the substrate of the three FDBRs. "P" indicates the propionate side chains. *Sl*HY2, as all other land plant HY2s, catalyzes the 2e- reduction of BV to PΦB (top). *Kfla*HY2 catalyzes the 4e- reduction of BV to PCB (middle). Based on homology with *Mesotaenium caldariorum* HY2 and *Kfla*HY2 variants investigation, the genuine intermediate is presumed to be 3(*Z*)-PΦB. *Syn*PcyA, as all other cyanobacterial PcyAs, catalyzes the 4e- reduction of BV to PCB via the intermediate 18^1,18^2-DHBV (bottom). BV reduction sites are highlighted in gray. Essential residues in each reaction step are highlighted on top of the reaction arrows.

The specificity of reduction is additionally influenced by the substrate binding mode, which has been demonstrated to be flipped in the PebB/HY2 lineage of FDBRs (Sommerkamp *et al.*, 2019; Sugishima *et al.*, 2020). This likely also applies to *Kfla*HY2, as two critical amino acid residues responsible for the stabilization of BV in the *ZZZssa* flipped binding mode are conserved (*Kfla*HY2 Ser^{174} – *Sl*HY2 Ser^{195}; *Kfla*HY2 Arg^{238} – *Sl*HY2 Arg^{259}). Overall, these data suggest that the ability of *Kfla*HY2 to synthesize PCB has evolved independently from the biosynthesis catalyzed by PcyA.

4.9 A bilin reductase-isomerase?

In addition to the identification of the acid catalysts, the generation of protein variants led to the discovery that an additional proton-donating residue on the bottom β-sheet of the active site induces the isomerization of the product to PEB, thus eliciting a reductase-isomerase function (Figure S4). In particular, the variant *Kfla*HY2_N105D was the first one proven to catalyze the additional isomerization of PCB to PEB. This reaction happened spontaneously even when simply mixing the enzyme with PCB. However, any attempt to isolate PEB from the mix was unsuccessful due to the different chemical stabilities of the two isomers. The conversion of PEB to PCB in acidic environments, typical of bilin isolation, is greatly favored, resulting in the re-isomerization of PEB to PCB (Chapman *et al.*, 1967). The discovery of a reductase-isomerase function of these protein variants initially suggested a similar scenario might take place in *G. sulphuraria*, where the isomerization of PEB to PCB might be elicited by similar amino acids exchanges in *Gs*PEBB. However, both a sequence alignment (Figure 3.24) and a biochemical investigation of this FDBR (chapter 3.6) debunked the hypothesis.

4.10 The lies of phylogeny on FDBR activity and the evolution of the plant phytochrome chromophore

Surprisingly, the attempt to convert *Kfla*HY2 into a land plant HY2 by swapping the bottom β-sheet pair was unsuccessful in yielding PΦB. Hence, product specificity in the HY2 lineage may be dependent more on the architecture of the active site and other residues in the surroundings of the binding pocket. In this regard, a recent study identified two residues responsible for intermediate accumulation in *A. marina* PcyAc (Miyake *et al.*, 2020, 2022). However, *Kfla*HY2 only possesses a homolog to one of the two and its substitution (*Kfla*HY2_T247I) did not lead to alteration of the native catalysis, hence the driving forces of intermediate accumulation are yet to be identified. Nevertheless, the hypothesis that the architecture of the active site plays a key role in product specificity became even more evident when studying the FDBRs from *Netrium digitus* and *Ceratodon purpureus*. Both FDBRs share

approximately 48% sequence identity with *Kfla*HY2 and the same catalytic pair. However, while the HY2s of *N. digitus* and *K. nitens* are PCB-producing and group well with the other indirectly-characterized HY2 from a steptophyte alga (*M. caldariorum* HY2) in the phylogenetic tree, the enzyme from *C. purpureus* is PΦB-producing and forms a monophyletic group with the HY2 from *P. patens* and land plant HY2s. Based on these data and earlier phylogenetic studies by Rockwell and colleagues, it appears that, within the HY2 lineage, 2 monophyletic groups diverged from a common HY2 ancestor: the PCB-HY2 clade and the PΦB-HY2 clade (Rockwell *et al.*, 2017; Rockwell & Lagarias, 2017a) (Figure 3.28). Putting these data into perspective, one might therefore suggest that phytochromes containing a PΦB chromophore originated in Bryophytes, or the common ancestor of land plants, while, in contrast, streptophyte algae continued to use a PCB-containing phytochrome. In this regard, the complementation of a *hy2* mutant of *A. thaliana* with PcyA resulted in a fully photosensitive PCB-incorporating phytochrome A. However, if photosensitivity was not affected by the chromophore change, an altered sensitivity to far-red high irradiance response was recorded in these mutant plants (FR-HIR) (Hanzawa *et al.*, 2002; Kami *et al.*, 2004). FR-HIR was recently discovered to have evolved relatively early in plant evolution, as this signaling mechanism was found in *Marchantia polymorpha* and indicated to be closely related to that of *Arabidopsis* (Inoue *et al.*, 2019). Apart from a possible adaptive advantage conferred by PΦB, the change of the chromophore may also be related to the available light wavelength to these organisms. Streptophyte algae include both aquatic and terrestrial organisms (Bierenbroodspot *et al.*, 2024; de Vries & Archibald, 2018; Hori *et al.*, 2014; Rindi *et al.*, 2008; Timme *et al.*, 2012; Wang *et al.*, 2020; Wodniok *et al.*, 2011). Since members of the Chlorokybophyceae and Klebsormidiophyceae are already capable to inhabit land, the current prevailing hypothesis posits for a terrestrial origin of streptophyte algae, with an aquatic lifestyle adaptation occurring solely after the colonization of land by plants (Harholt *et al.*, 2016). The enhanced ability of the latter to thrive in terrestrial habitats and perceive red/far-red light would eventually explain why, not only in aquatic habitats but also in the said environment, streptophyte algae are restricted to sensing shorter light wavelengths, and consequently utilize PCB-phytochromes (Han *et al.*, 2019).

4.11 PCB biosynthesis evolution: 1000 ways to the same outcome

Leveraging on all the findings presented in the previous chapters, a putative scenario for PCB biosynthesis evolution from cyanobacteria to primary endosymbionts can be drafted (Figure 4.8).

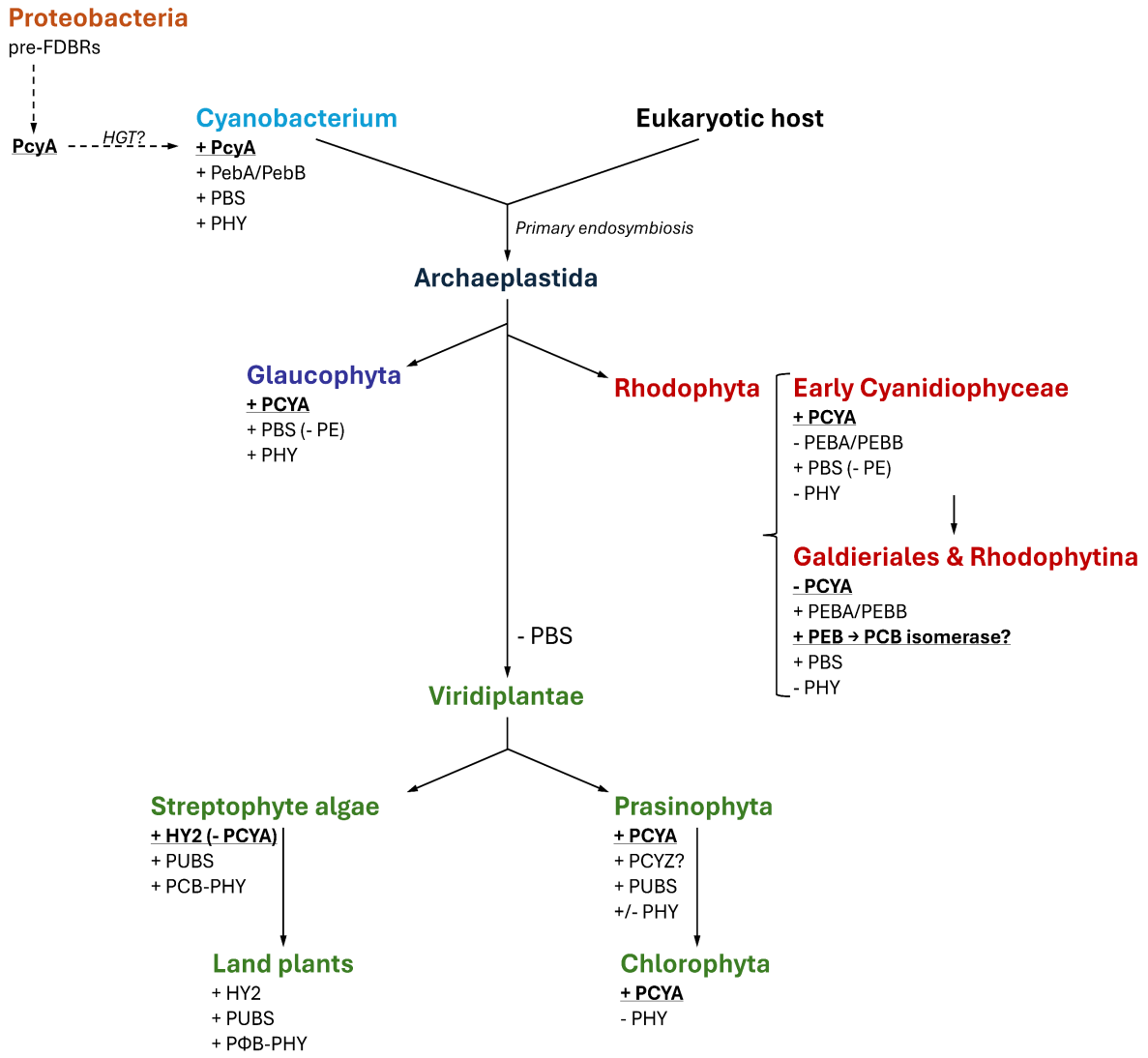

Figure 4.8 Proposed evolution of PCB biosynthesis.
Simplified scheme of Archaeplastida emergence and evolution. Every lineage is associated with the harbored FDBR sequences and biliproteins (PBPs and phytochromes). PCB biosynthesis pathways are depicted in bold and underlined.

The identification of pre-FDBRs in non-photosynthetic heterotrophic bacteria has shed more light on the origins of this enzyme family. The earliest FDBRs were active in bilin biosynthesis but only capable of $2e^-$-dependent reductions. It seems plausible that FDBRs initially emerged in these organisms as part of an O_2 detoxification pathway during the early stages of dawning photosynthesis. The biosynthesis of PCB eventually emerged in α-proteobacteria and was later acquired by cyanobacteria via HGT. In cyanobacteria, PcyA-produced PCB serves as chromophore for both PBPs and phytochromes, contributing to light harvesting and light sensing, respectively (Dagnino-Leone *et al.*, 2022; Hübschmann *et al.*, 2001; Lamparter *et al.*, 2001; Miyake *et al.*, 2020; Stadnichuk *et al.*, 2015). The emergence of the first photosynthetic eukaryotes following primary endosymbiosis led to a significant diversification of PCB biosynthetic pathways. Glaucophytes and the basal clades of Cyanidiophyceae, i.e.

the Cyanidioschyzonales and the Cyanidiales, retain PCYA-mediated PCB biosynthesis. In Glaucophytes, PCB continues to function as a chromophore for both light harvesting and light sensing (Rockwell *et al.*, 2014; Ueno & Akimoto, 2023; Watanabe *et al.*, 2012). The evolution of Rhodophytes coincided with the loss of phytochromes, therefore PCB serves solely for light harvesting (Duanmu *et al.*, 2014; Mathews, 2014; Rockwell & Lagarias, 2017b, 2020). Apart from these basal clades, Rhodophytes apparently evolved a more sophisticated PCB biosynthesis pathway, involving two FDBRs responsible for PEB production and, most likely, a chromophore isomerase to convert PEB to PCB (Beale & Cornejo, 1991a, 1991b, 1991c; Hartmann, 2018; Mudler, 2020). The emergence of Viridiplantae resulted in the loss of the PBS light harvesting machinery and partial reacquisition of phytochromes (Green, 2019; Koziol *et al.*, 2007; Kunugi *et al.*, 2016; Rockwell & Lagarias, 2020). Further divergence of Viridiplantae in Chlorophytes and Streptophytes is reflected in their FDBR pathways and light sensing-related strategies. Chlorophytes possess a PCYA, sister to cyanobacterial sequences, which is involved neither in light harvesting nor, in most cases, light sensing, but rather in retrograde signaling related to the detoxification of reactive oxygen species and iron acquisition (Duanmu *et al.*, 2013). Streptophytes encompass land plants and the clade within which they evolved, streptophyte algae (Becker & Marin, 2009; Bierenbroodspot *et al.*, 2024; Donoghue & Clark, 2024; Harris *et al.*, 2022; Wodniok *et al.*, 2011). Both clades are endowed with phytochromes and a phytochromobilin synthase (Rockwell & Lagarias, 2017a). The HY2 of streptophyte algae is, in contrast to phylogenetic classification, responsible for PCB biosynthesis. In these organisms, PCB represents the phytochrome chromophore. Divergence with land plants is here evident. Land plant HY2s eventually lost the second $2e^-$ reducing step catalyzed by their streptophyte algae counterpart, to yield the specific phytochrome chromophore PΦB (Frankenberg *et al.*, 2001; Hu *et al.*, 2021; Kohchi *et al.*, 2001; McDowell & Lagarias, 2001; Muramoto *et al.*, 2005; Rockwell *et al.*, 2017; Sawers *et al.*, 2004; Terry *et al.*, 1995; Tu *et al.*, 2008; Wu *et al.*, 1997).

The origin of plant phytochromes is, hitherto, the subject of controversy. Conflicting research perspectives suggest potential roots in either cyanobacterial phytochromes (Gabriel *et al.*, 2022; Kooß & Lamparter, 2017) or a, yet unknown, ancient eukaryotic phytochrome (Inoue *et al.*, 2017; Li *et al.*, 2015; Rockwell & Lagarias, 2017b, 2020). Nevertheless, it is widely acknowledged, and further confirmed by this study, that the corresponding FDBR sequences, responsible for chromophore production, have substantially diversified since primary endosymbiosis.

4.12 A first look into algal PUBS

Thus far, PUBS is the only FDBR whose activity has not been extensively investigated and structure not been solved. This reductase, responsible for the $4e^-$ reduction of BV to PUB via 15,16-DHBV, was discovered in the moss *Physcomitrium patens* around a decade ago (Chen *et al.*, 2012). Noteworthy, although possessing PUB in their light harvesting machinery, neither cyanobacteria nor Rhodophytes possess a PUBS. Instead, in these phyla, PUB is synthesized from PEB via isomerization (Blot *et al.*, 2009; Carrigee *et al.*, 2021, 2022; Mahmoud *et al.*, 2017; Sanfilippo *et al.*, 2019b; Shukla *et al.*, 2012). The emergence of newly sequenced genomes revealed both Viridiplantae lineages, Chlorophyta and Streptophyta, are endowed with PUBS but these sequences do not form a monophyletic clade (Carpenter *et al.*, 2019; Rockwell & Lagarias, 2017b). The presence of putative PUBS in streptophyte algae suggests that *Pp*PUBS, and consequently Embryophytes PUBSs, evolved from the algal sequences (Bowles *et al.*, 2023; Yang *et al.*, 2023). Among streptophyte algae, *K. nitens*, whose HY2 was extensively investigated in this study, was additionally selected for PUBS investigation in a heterologous approach. Recombinant putative *Kfla*PUBS was indeed confirmed to be a PUBS, exhibiting similar mechanism to *Pp*PUBS in catalyzing the $4e^-$-dependent reaction of BV to PUB. Specifically, BV D-ring C15=C16 double bond is firstly reduced to yield 15,16-DHBV. This initial step is followed by the reduction of 15,16-DHBV A-ring C4=C5 double bond to PUB.

As no crystal structure is hitherto available for PUBS, the AlphaFold model structure of *Kfla*PUBS was overlayed with the crystal structure of another $4e^-$ reducing FDBR metabolizing BV, PebS (Dammeyer *et al.*, 2008b; DeLano, 2020; Jumper *et al.*, 2021; Mirdita *et al.*, 2022) (Figure 4.9).

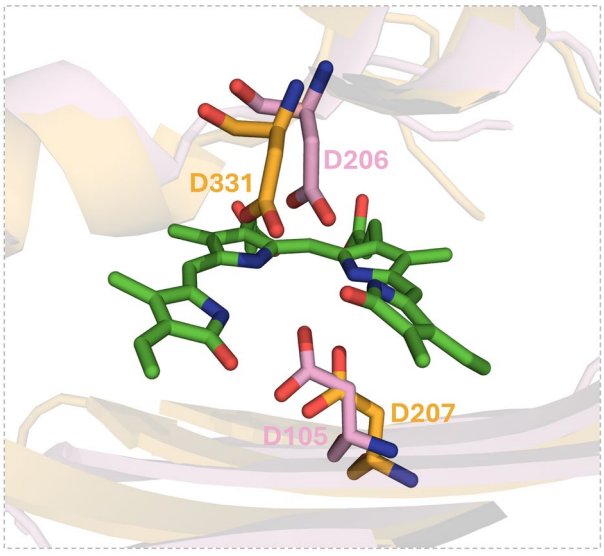

Figure 4.9 Structure alignments of *Kfla*PUBS and PebS
The model structure of *Kfla*PUBS (GenBank accession code: GAQ90251) was obtained using AlphaFold2 (https://colab.research.google.com/github/sokrypton/ColabFold/blob/main/AlphaFold2.ipynb) (Jumper *et al.*, 2021; Mirdita *et al.*, 2022). The alignment was generated using PyMOL (DeLano, 2020). The model structure of *Kfla*PUBS is displayed as transparent brightorange cartoon. The crystal structure of PebS (PDB accession code: 2VCK) is displayed as transparent pink cartoon. BV, in the conformation bound in the active site of PebS, is shown as green sticks. Amino acid residues of interest are shown as labeled sticks and colored as the belonging structure.

PUBS and PebS share the initial reaction step involving BV D-ring C15=C16 double bond reduction to 15,16-DHBV, solely diverging in the turnover of this intermediate. In PUBS, 15,16-DHBV C4=C5 double bond is reduced to yield PUB, whereas in PebS the object of reduction is the A-ring 2,3,3^1,3^2-diene system (Dammeyer *et al.*, 2008a; Busch *et al.*, 2011a). Previous studies on PebS have demonstrated that Asp^{105} and Asp^{206} serve as acid catalysts (Busch *et al.*, 2011a). Specifically, Asp^{105} is responsible for the initial D-ring reduction, whereas Asp^{206} is involved in the reduction of the A-ring of 15,16-DHBV. These residues are conserved in both *Kfla*PUBS and *Pp*PUBS and the structures overlay revealed a similar positioning to the active site of PebS. Based on this homology and suggesting a BV *ZZZ*-all-syn binding mode, as PUBS is also part of the PebA/PebS lineage, *Kfla*PUBS Asp^{207} (homologs to PebS Asp^{105} and *Pp*PUBS Asp^{187}; *Pp*PUBS numbering relative to the full protein sequence, including the transit peptide) might be involved in the reduction of BV to 15,16-DHBV, whereas *Kfla*PUBS Asp^{331} (homologs to PebS Asp^{206} and *Pp*PUBS Asp^{314}) could serve as acid catalysts for the reduction of 15,16-DHBV to PUB (Figure 4.10).

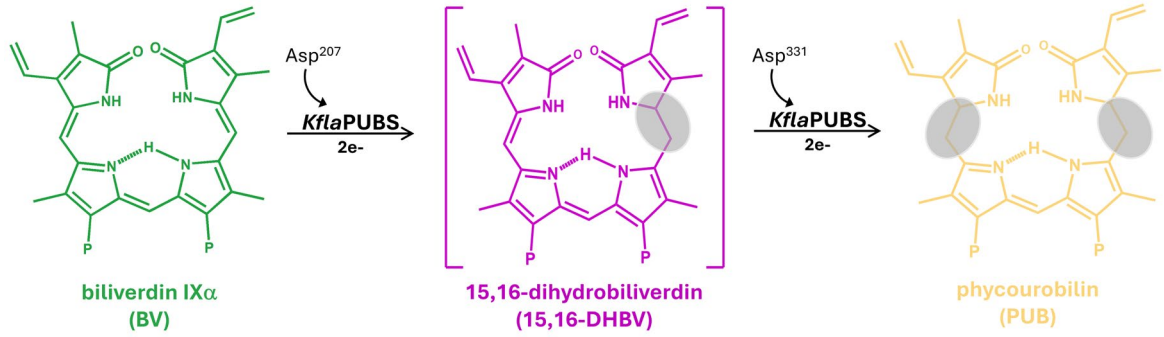

Figure 4.10 Overview of the proposed reaction mechanism of *Kfla*PUBS.
BV is the substrate of *Kfla*PUBS. "P" indicates the propionate side chains. *Kfla*PUBS catalyzes the 4e$^-$ reduction of BV to PUB via the intermediate 15,16-DHBV. BV reduction sites are highlighted in gray. Potential residues involved in each reaction step are highlighted on top of the reaction arrows.

4.13 Why is there a need for PUB in the Green lineage?

The presence of PUB in organisms that do not perform PBS-mediated light harvesting raises a question on its purpose. In theory, PUB cannot serve in light sensing as phytochrome chromophore since it lacks both the C3^1-ethylidine required for covalent binding and the C15=C16 double bond required for photoisomerization. *P. patens* phenotypical mutants provided insights into a possible physiological function of PUBS. The double knockout mutant

pubs hy2 exhibited chlorophyll deficiency, plausibly ascribable to feedback inhibition of tetrapyrrole biosynthesis due to heme accumulation (Chen *et al.*, 2012; Terry & Kendrick, 1999). However, the most striking feature of this mutant is the alteration of red-light sensing and related photomorphogenesis, thus implying a role of PUBS, alongside HY2, in phototropic responses. Therefore, a functionally redundant role in photomorphogenesis has been suggested for PUB and PΦB (Chen *et al.*, 2012). PUB could then serve one of two purposes. First, it could function as an alternative chromophore substitute for phytochrome action. Due to the absence of the $C3^1$-ethylidine, PUB can be bound non-covalently, and thus reversibly, to the apo-phytochrome and potentially induce signaling. Indeed, non-covalent binding of BV to apo-Cph1 was shown to still elicit photochemical activity (Lamparter & Michael, 2005). Moreover, the existence of PUBS homologs in Chlorophytes could reinforce this hypothesis. As mentioned in chapter 1.4, Chlorophytes possess a PCYA homolog. This enzyme is not responsible for PCB employment neither in light sensing nor light harvesting, since Chlorophyte lack PBPs completely and most of them lack phytochromes, but has rather been demonstrated to be involved in retrograde signaling (Duanmu *et al.*, 2013; Rockwell & Lagarias, 2010). Therefore, PUBS could serve a similar function. Secondly, PUB could function as precursor to a phytochrome chromophore, as light-dependent phenotypes were observed in *hy2* mutant, possessing PUB but not PΦB. In this context, PUB may be reduced and isomerized by an unknown protein or by the apo-phytochrome itself to form both the $C3^1$-ethylidene needed for covalent linkage and the C15=C16 double bond required for photoisomerization. This first scenario strongly reminds of the PEB to PCB isomerase activity reported in *G. sulphuraria* (Beale & Cornejo, 1991a, 1991b, 1991c; Hartmann, 2018; Mudler, 2020). The second is related to the ability of certain cyanobacteriochromes to autocatalytically isomerize PCB to PVB (Ishizuka *et al.*, 2007, 2011; Ma *et al.*, 2012; Rockwell *et al.*, 2012; Song *et al.*, 2011; Yoshihara *et al.*, 2004). Ultimately, one would suggest that PUBS might have emerged in streptophyte algae to serve similar light sensing-related purposes.

5 Summary

Photosynthesis stands as one of the most pivotal biological processes on our planet. To efficiently harvest light, photosynthetic organisms utilize chlorophyll antennae and carotenoids within their photosystems. However, the efficacy of light harvesting by chlorophyll and carotenoids is negligible in the green region of the light spectrum. To fully exploit light energy, several photosynthetic organisms employ specialized proteins named phycobiliproteins, which are able to harvest light in the green gap. Furthermore, most of these organisms are endowed with photoreceptors, enabling them to sense the quality and intensity of the harvested light and to modulate biological activities based on this information. Both light harvesting and light sensing functions are mediated by linear tetrapyrrole chromophores named bilins. The biosynthesis of bilins is catalyzed by enzymes known as ferredoxin-dependent bilin reductases (FDBRs). The origin of both biliproteins and this class of enzymes remain elusive. This work aimed to delineate the evolution of phycocyanobilin (PCB) biosynthesis, from emergence to primary endosymbiosis. The recent identification of FDBR-related sequences in heterotrophic, non-photosynthetic bacteria (pre-FDBRs) provided a foundation for investigating the emergence and original bioactivity of this enzyme class. Biochemical characterization of a representative from each pre-FDBR clade revealed FDBRs initially emerged as $2e^-$ reducing enzymes yielding phytochromobilin (PΦB) production, to evolve a $4e^-$ reducing capability in ultimately yielding phycoerythrobilin (PEB). The latter reaction represents the first described instance of PEB production occurring via PΦB as the intermediate. PCB biosynthesis catalyzed by phycocyanobilin-ferredoxin oxidoreductase (PcyA) finally evolved in α-proteobacteria and was ultimately acquired by cyanobacteria, potentially via horizontal gene transfer. The primary endosymbiosis event giving birth to the Archaeplastida supergroup resulted in a significant divergence of FDBRs, particularly related to PCB biosynthesis. While Glaucophytes retained typical cyanobacterial PCB biosynthesis catalyzed by a PCYA homolog, in Rhodophytes and Viridiplantae PCB biosynthesis underwent substantial divergence. In Rhodophytes, PCB biosynthesis is believed to rely on a chromophore isomerase rather than on specific PCB-producing FDBRs. Indeed, more than three decades ago, the biosynthesis of PCB in *Galdieria sulphuraria* was shown to occur first via PEB production by FDBRs and subsequent PEB to PCB isomerization. As technical problems hindered further confirmation of this scenario, the focus of this part of the project shifted to the full characterization of the activity of *G. sulphuraria* FDBRs to ultimately confirm only PEB production is catalyzed by these enzymes. The Viridiplantae lineage further diverged into Streptophytes and Chlorophytes. While Chlorophytes retained PCYA-mediated PCB biosynthesis, Streptophytes present an intricate situation. The Streptophyta lineage encompasses streptophyte algae and, their descendent, land plants. As land plants do not

possess PCB and use PΦB-phytochromes, streptophyte algae were instead indicated to use PCB-phytochromes. However, this clade is endowed with a plant type HY2-homolog, theoretically responsible for PΦB production. The biochemical investigation of several members of the streptophyta HY2 lineage revealed that HY2 was originally a $4e^-$ reducing FDBR, catalyzing PCB production for phytochrome incorporation in streptophyte algae, and evolved in Bryophytes to lose the second $2e^-$ reducing step and only yield PΦB. The characterization of this FDBR lineage further proved that the activity of FDBRs cannot be solely predicted from amino acid sequence and structure model, as conserved residues and a similar overall fold can still lead to different activities. Overall, this study provides an outline of PCB biosynthesis evolution, from its emergence to primary endosymbiosis-triggered diversification.

A final brief section of this work provides insights into the production of phycourobilin (PUB) in Streptophytes. The production of PUB, resulting from PEB isomerization in cyanobacteria and red algae, was solely thought to be required for light-harvesting purposes, as PUB is usually attached to PE in these organisms. However, about a decade ago, a new FDBR responsible for PUB production was discovered in *Physcomitrium patens*. This enzyme, named phycourobilin synthase (PUBS), catalyzes the $4e^-$ reduction of biliverdin to PUB via 15,16-dihydrobiliverdin as the intermediate. With the constant emergence of new sequenced genomes, *PUBS* homologs were also identified in several streptophyte algae. The characterization of the PUBS from *Klebsormidium nitens* revealed a similar catalytic activity to the one of *P. patens*. Hitherto, PUBS remains the only FDBR whose activity and structure have not been extensively characterized. Moreover, the significance of PUB in organisms which do not perform phycobiliprotein-mediated light harvesting is still an open question.

6 Zusammenfassung

Die Photosynthese ist einer der zentralsten biologischen Prozesse auf unserem Planeten. Um das Licht effizient zu nutzen, verwenden photosynthetische Organismen Chlorophyll-Antennen und Carotinoide in ihren Photosystemen. Allerdings ist die Effizienz der Lichtausbeute durch Chlorophyll und Carotinoide im grünen Bereich des Lichtspektrums vernachlässigbar. Um die Lichtenergie in vollem Umfang zu nutzen, verwenden mehrere photosynthetische Organismen spezialisierte Proteine, die so genannten Phycobiliproteine, die in der Lage sind, Licht im grünen Bereich zu absorbieren. Darüber hinaus sind die meisten dieser Organismen mit Photorezeptoren ausgestattet, die es ihnen ermöglichen, die Qualität und Intensität des wahrgenommenen Lichts zu erkennen und ihre biologischen Aktivitäten auf der Grundlage dieser Informationen zu modulieren. Sowohl die Lichtsammel- als auch die Lichtsensor-Funktionen werden von linearen Tetrapyrrol-Chromophoren, den Bilinen, vermittelt. Die Biosynthese von Bilinen wird von einer Enzymklasse katalysiert, welche als Ferredoxin-abhängige Bilin-Reduktasen (FDBRs) bekannt sind. Der Ursprung sowohl der Biliproteine als auch dieser Enzymklasse ist nach wie vor ungeklärt. Ziel dieser Arbeit war es, die Evolution der Phycocyanobilin (PCB)-Biosynthese von der Entstehung bis zur primären Endosymbiose zu beschreiben. Die kürzlich erfolgte Identifizierung von FDBR-verwandten Sequenzen in heterotrophen, nicht-photosynthetischen Bakterien (Prä-FDBRs) bot eine Grundlage für die Untersuchung der Entstehung und der ursprünglichen Bioaktivität dieser Enzymklasse. Die biochemische Charakterisierung eines Vertreters aus jeder Prä-FDBR-Gruppe ergab, dass FDBRs zunächst als $2e^-$ reduzierende Enzyme bei der Produktion von Phytochromobilin (PΦB) auftraten, um dann eine $4e^-$ reduzierende Fähigkeit zu entwickeln und schließlich Phycoerythrobilin (PEB) zu produzieren. Die letztgenannte Reaktion ist der erste beschriebene Fall der PEB-Produktion, die über PΦB als Zwischenprodukt erfolgt. Die PCB-Biosynthese, die durch die Phycocyanobilin-Feredoxin-Oxidoreduktase (PcyA) katalysiert wird, entwickelte sich schließlich in α-Proteobakterien und wurde schließlich von Cyanobakterien übernommen, möglicherweise durch horizontalen Gentransfer. Die primäre Endosymbiose, aus der die Supergruppe der Archaeplastida hervorging, führte zu einer erheblichen Divergenz der FDBR, insbesondere im Zusammenhang mit der PCB-Biosynthese. Während die Glaukophyten die typische cyanobakterielle PCB-Biosynthese beibehielten, die durch ein PCYA-Homolog katalysiert wird, kam es bei den Rhodophyten und Viridiplantae zu einer erheblichen Divergenz der PCB-Biosynthese. Es wird angenommen, dass die PCB-Biosynthese in Rhodophyten eher auf einer Chromophor-Isomerase als auf spezifischen PCB-produzierenden FDBRs beruht. In der Tat wurde vor mehr als drei Jahrzehnten gezeigt, dass die PCB-Biosynthese in *Galdieria sulphuraria* zunächst durch die Produktion von PEB durch FDBRs und die anschließende Isomerisierung

von PEB zu PCB erfolgt. Da technische Probleme eine weitere Bestätigung dieses Szenarios verhinderten, verlagerte sich der Schwerpunkt dieses Projektteils auf die vollständige Charakterisierung der Aktivität der FDBRs von *G. sulphuraria*, um letztlich zu bestätigen, dass nur die PEB-Produktion durch diese Enzyme katalysiert wird. Der Viridiplantae-Stamm teilte sich weiter in Streptophyten und Chlorophyten auf. Während die Chlorophyten die PCYA-vermittelte PCB-Biosynthese beibehalten haben, stellt sich die Situation bei den Streptophyten etwas komplizierter dar. Zu den Streptophyten gehören die Streptophyten-Algen und ihre Nachfahren, die Landpflanzen. Da Landpflanzen kein PCB besitzen und PΦB-Phytochrome verwenden, wurde angenommen, dass Streptophyten-Algen stattdessen PCB-Phytochrome verwenden. Diese Gruppe verfügt jedoch über ein HY2-Homolog des Pflanzentyps, das theoretisch für die PΦB-Produktion verantwortlich ist. Die biochemische Untersuchung mehrerer Mitglieder der Streptophyten-HY2-Linie ergab, dass HY2 ursprünglich ein $4e^-$ reduzierender FDBR war, der die PCB-Produktion für den Phytochrom-Einbau in Streptophyten-Algen katalysierte, und sich in Bryophyten so entwickelte, dass der zweite $2e^-$ reduzierende Schritt entfiel und nur noch PΦB gebildet wurde. Die Charakterisierung des FDBR-Stammbaums hat außerdem gezeigt, dass die Aktivität von FDBRs nicht allein aus der Aminosäuresequenz und dem Strukturmodell vorhergesagt werden kann, da konservierte Reste und eine ähnliche Gesamtfaltung immer noch zu unterschiedlichen Aktivitäten führen können. Insgesamt bietet diese Studie einen Überblick über die Evolution der PCB-Biosynthese, von ihrer Entstehung bis zur primären, durch Endosymbiose ausgelösten Diversifizierung.

Ein letzter kurzer Abschnitt dieser Arbeit bietet Einblicke in die Produktion von Phycourobilin (PUB) in Streptophyten. Es wurde angenommen, dass die Produktion von PUB, die aus der Isomerisierung von PEB in Cyanobakterien und Rotalgen resultiert, ausschließlich für die Lichtsammlung erforderlich ist, da PUB in diesen Organismen normalerweise an PE gebunden ist. Vor etwa einem Jahrzehnt wurde jedoch in *Physcomitrium patens* eine neue FDBR entdeckt, das für die PUB-Produktion verantwortlich ist. Dieses Enzym mit dem Namen Phycourobilin-Synthase (PUBS) katalysiert die $4e^-$ Reduktion von Biliverdin zu PUB über 15,16-Dihydrobiliverdin als Zwischenprodukt. Mit der ständigen Sequenzierung neuer Genome wurden PUBS-Homologe auch in mehreren Streptophytenalgen identifiziert. Die Charakterisierung der PUBS aus *Klebsormidium nitens* ergab eine ähnliche katalytische Aktivität wie die PUBS von *P. patens*. Bislang ist PUBS die einzige FDBR, deren Aktivität und Struktur noch nicht umfassend charakterisiert wurde. Darüber hinaus ist die Bedeutung von PUB in Organismen, die keine durch Phycobiliproteine vermittelte Lichtsammlung betreiben, immer noch eine offene Frage.

References

Aaij, C., & Borst, P. (1972). The gel electrophoresis of DNA. *BBA Section Nucleic Acids And Protein Synthesis*, 269(2), 192-200.

Adir, N., Dobrovetsky, Y., & Lerner, N. (2001). Structure of C-Phycocyanin from the thermophilic cyanobacterium *Synechococcus vulcanus* at 2.5 Å: Structural implications for thermal stability in phycobilisome assembly. *Journal of Molecular Biology*, 313(1), 71-81.

Adl, S. M., Simpson, A. G. B., Farmer, M. A., Andersen, R. A., Anderson, O. R., Barta, J. R., Bowser, S. S., Brugerolle, G., Fensome, R. A., Fredericq, S., James, T. Y., Karpov, S., Kugrens, P., Krug, J., Lane, C. E., Lewis, L. A., Lodge, J., Lynn, D. H., Mann, D. G., McCourt, R. M., Mendoza, L., Moestrup, O., Mozley-Standridge, S. E., Nerad, T. A., Shearer, C. A., Smirnov, A. V., Spiegel, F. W., & Taylor, M. F. J. R. (2005). The new higher level classification of eukaryotes with emphasis on the taxonomy of protists. *Journal of Eukaryotic Microbiology*, 52(5), 399-451.

Ago, H., Adachi, H., Umena, Y., Tashiro, T., Kawakami, K., Tian, N. K. L., Han, G., Kuang, T., Liu, Z., Wang, F., Zou, H., Enami, I., Miyano, M., & Shen, J. R. (2016). Novel features of eukaryotic photosystem II revealed by its crystal structure analysis from a red alga. *Journal of Biological Chemistry*, 291(11), 5676-5687.

Alboresi, A., Caffarri, S., Nogue, F., Bassi, R., & Morosinotto, T. (2008). *In silico* and biochemical analysis of *Physcomitrella patens* photosynthetic antenna: Identification of subunits which evolved upon land adaptation. *PLoS ONE*, 3(4), e2033.

Alvey, R. M., Biswas, A., Schluchter, W. M., & Bryant, D. A. (2011a). Attachment of noncognate chromophores to CpcA of *Synechocystis* sp. PCC 6803 and *Synechococcus* sp. PCC 7002 by heterologous expression in *Escherichia coli*. *Biochemistry*, 50(22), 4890-4902.

Alvey, R. M., Biswas, A., Schluchter, W. M., & Bryant, D. A. (2011b). Effects of modified phycobilin biosynthesis in the cyanobacterium *Synechococcus* sp. strain PCC 7002. *Journal of Bacteriology*, 193(7), 1663-1671.

Anders, K., & Essen, L. O. (2015). The family of phytochrome-like photoreceptors: Diverse, complex and multi-colored, but very useful. *Current Opinion in Structural Biology*, 35, 7-16.

Anders, K., Gutt, A., Gärtner, W., & Essen, L. O. (2014). Phototransformation of the red light sensor cyanobacterial phytochrome 2 from *Synechocystis* species depends on its tongue motifs. *Journal of Biological Chemistry*, 289(37), 25590-25600.

Apt, K. E., Collier, J. L., & Grossman, A. R. (1995). Evolution of the phycobiliproteins. *Journal of Molecular Biology*, 248(1), 79-96.

Aras, M. (2018). Metabolic channeling during phycoerythrobilin biosynthesis. *Technical University of Kaiserslautern: PhD Thesis*.

Aras, M., Hartmann, V., Hartmann, J., Nowaczyk, M. M., & Frankenberg-Dinkel, N. (2020). Proximity channeling during cyanobacterial phycoerythrobilin synthesis. *FEBS Journal*, 287(2), 284-294.

Archibald, J. M. (2009). The Puzzle of Plastid Evolution. *Current Biology*, 19(2), R81-R88.

Archibald, J. M., & Keeling, P. J. (2002). Recycled plastids: A “green movement” in eukaryotic evolution. *Trends in Genetics*, 18(11), 577-584.

Arciero, D. M., Bryant, D. A., & Glazer, A. N. (1988). *In vitro* attachment of bilins to apophycocyanin. I. Specific covalent adduct formation at cysteinyl residues involved in phycocyanobilin binding in C-phycocyanin. *The Journal of Biological Chemistry*, 263(34),18343-18349.

Auldridge, M. E., & Forest, K. T. (2011). Bacterial phytochromes: More than meets the light. *Critical Reviews in Biochemistry and Molecular Biology*, 46(1), 67-88.

Badshah, S. L., Mabkhot, Y., & Al-Showiman, S. S. (2017). Photosynthesis at the far-red region of the spectrum in *Acaryochloris marina*. *Biological Research*, 50(1), 16.

Bailey, R. W., & Staehelin, L. A. (1968). The Chemical composition of isolated cell walls of *Cyanidium caldarium*. *Journal of General Microbiology*, 54(2), 269-276.

Bar-Zvi, S., Lahav, A., Harris, D., Niedzwiedzki, D. M., Blankenship, R. E., & Adir, N. (2018). Structural heterogeneity leads to functional homogeneity in *A. marina* phycocyanin. *Biochimica et Biophysica Acta - Bioenergetics*, 1859(7), 544-553.

Barrera-Rojas, J., de la Vara, L. G., Ríos-Castro, E., Leyva-Castillo, L. E., & Gómez-Lojero, C. (2018). The distribution of divinyl chlorophylls *a* and *b* and the presence of ferredoxin-NADP+ reductase in *Prochlorococcus marinus* MIT9313 thylakoid membranes. *Heliyon*, 4(12), e01100.

Battersby, A. R. (1985). The Bakerian lecture, 1984. Biosynthesis of the pigments of life. *Proceedings of the Royal Society of London. Series B, Containing papers of a Biological character. Royal Society (Great Britain)*, 225(1238), 1-26.

Beale, S. I., & Cornejo, J. (1984a). Enzymatic heme oxygenase activity in soluble extracts of the unicellular red alga, *Cyanidium caldarium*. *Archives of Biochemistry and Biophysics*, 235(2), 371-384.

Beale, S. I., & Cornejo, J. (1984b). Enzymic transformation of biliverdin to phycocyanobilin by extracts of the unicellular red alga *Cyanidium caldarium*. *Plant Physiology*, 76(1), 7-15.

Beale, S. I., & Cornejo, J. (1991a). Biosynthesis of phycobilins: Ferredoxin-mediated reduction of biliverdin catalyzed by extracts of *Cyanidium caldarium*. *Journal of Biological Chemistry*, 266(33), 22328-22332.

Beale, S. I., & Cornejo, J. (1991b). Biosynthesis of phycobilins: 3(Z)-phycoerythrobilin and 3(Z)-phycocyanobilin are intermediates in the formation of 3(E)-phycocyanobilin from biliverdin IXα. *Journal of Biological Chemistry*, 266(33), 22333-22340.

Beale, S. I., & Cornejo, J. (1991c). Biosynthesis of phycobilins: 15,16-dihydrobiliverdin IXα is a partially reduced intermediate in the formation of phycobilins from biliverdin IXα. *Journal of Biological Chemistry*, 266(33), 22341-22345.

Beale, S. I. (1993). Biosynthesis of Phycobilins. *Chemical Reviews*, 93(2), 785-802.

Beale, S. I. (2008). Photosynthetic Pigments: Perplexing Persistent Prevalence of “Superfluous” Pigment Production. *Current Biology*, 18(8), R342-R343.

Becker, B., & Marin, B. (2009). Streptophyte algae and the origin of embryophytes. *Annals of Botany*, 103(7), 999-1004.

Benedikt, E., Gossauer, A., Köst, H. P., Miki, W., & Yamaguchi, K. (1988). Biliverdin IXδ and neobiliverdin IXδ, isolated from the ovaries of the marine snail, *Turbo cornutus*. *European Journal of Biochemistry*, 175(3), 643-648.

Bhattacharya, D., Yoon, H. S., & Hackett, J. D. (2004). Photosynthetic eukaryotes unite: Endosymbiosis connects the dots. *BioEssays*, 26, 50-60.

Bhoo, S. H., Davis, S. J., Walker, J., Karniol, B., & Vierstra, R. D. (2001). Bacteriophytochromes are photochromic histidine kinases using a biliverdin chromophore. *Nature*, 414(6865), 776-779.

Bibby, T. S., Mary, I., Nield, J., Partensky, F., & Barber, J. (2003). Low-light-adapted *Prochlorococcus* species possess specific antennae for each photosystem. *Nature*, 424(6952), 1051-1054.

Bibby, T. S., Nield, J., Chen, M., Larkum, A. W. D., & Barber, J. (2003). Structure of a photosystem II supercomplex isolated from *Prochloron didemni* retaining its chlorophyll *a*/*b* light-harvesting system. *Proceedings of the National Academy of Sciences of the United States of America*, 100(15), 9050-9054.

Bierenbroodspot, M. J., Darienko, T., de Vries, S., Fürst-Jansen, J. M. R., Buschmann, H., Pröschold, T., Irisarri, I., & de Vries, J. (2024). Phylogenomic insights into the first multicellular streptophyte. *Current Biology*, 34(3), 670-681.

Bishop, J. E., Nagy, J. O., O'Connell, J. F., & Rapoport, H. (1991). Diastereoselective Synthesis of Phycocyanobilin-Cysteine Adducts. *Journal of the American Chemical Society*, 113(21), 8024-8035.

Biswas, A., Vasquez, Y. M., Dragomani, T. M., Kronfel, M. L., Williams, S. R., Alvey, R. M., Bryant, D. A., & Schluchter, W. M. (2010). Biosynthesis of cyanobacterial phycobiliproteins in *Escherichia coli*: Chromophorylation efficiency and specificity of all bilin lyases from *Synechococcus* sp. strain PCC 7002. *Applied and Environmental Microbiology*, 76(9), 2729-2739.

Blankenship, R. E. (2008). *Molecular Mechanisms of Photosynthesis,* Wiley.

Blot, N., Wu, X. J., Thomas, J. C., Zhang, J., Garczarek, L., Böhm, S., Tu, J. M., Zhou, M., Plöscher, M., Eichacker, L., Partensky, F., Scheer, H., & Zhao, K. H. (2009). Phycourobilin in trichromatic phycocyanin from oceanic cyanobacteria is formed post-translationally by a phycoerythrobilin lyase-isomerase. *Journal of Biological Chemistry*, 284(14), 9290-9298.

Blumenstein, A., Vienken, K., Tasler, R., Purschwitz, J., Veith, D., Frankenberg-Dinkel, N., & Fischer, R. (2005). The *Aspergillus nidulans* phytochrome FphA represses sexual development in red light. *Current Biology*, 15(20), 1833-1838.

Boiadjiev, S. E., & Lightner, D. A. (2001). A water-soluble synthetic bilirubin with carboxyl groups replaced by sulfonyl moieties. *Monatshefte Fur Chemie*, 132(10), 1201-1212.

Boichenko, V. A., Pinevich, A. V., & Stadnichuk, I. N. (2007). Association of chlorophyll *a*/*b*-binding Pcb proteins with photosystems I and II in *Prochlorothrix hollandica*. *Biochimica et Biophysica Acta - Bioenergetics*, 1767(6), 801-806.

Bongards, C., & Gärtner, W. (2010). The role of the chromophore in the biological photoreceptor phytochrome: An approach using chemically synthesized tetrapyrroles. *Accounts of Chemical Research*, 43(4), 486-495.

Bonnett, R., & McDonagh, A. F. (1973). The meso-reactivity of porphyrins and related compounds. Part VI. Oxidative cleavage of the haem system. The four isomeric biliverdins of the IX series. *Journal of the Chemical Society, Perkin Transactions 1*, 881-888.

Borthwick, H. A., & Parker, M. W. (1938a). Influence of Photoperiods upon the Differentiation of Meristems and the Blossoming of Biloxi Soy Beans. *Botanical Gazette*, 99(4), 825-839.

Borthwick, H. A., & Parker, M. W. (1938b). Photoperiodic Perception in Biloxi Soy Beans. *Botanical Gazette*, 100(2), 374-387.

Borthwick, H. A., & Parker, M. W. (1939). Photoperiodic Responses of Several Varieties of Soybeans. *Botanical Gazette*, 101(2), 341-365.

Borthwick, H. A., Hendricks, S. B., Parker, M. W., Toole, E. H., & Toole, V. K. (1952). A Reversible Photoreaction Controlling Seed Germination. *Proceedings of the National Academy of Sciences*, 38(8), 662-666.

Borthwick, H. A., Hendricks, S. B., Toole, E. H., & Toole, V. K. (1954). Action of Light on Lettuce-Seed Germination. *Botanical Gazette*, 115(3), 205-225.

Bowles, A. M. C., Williamson, C. J., Williams, T. A., Lenton, T. M., & Donoghue, P. C. J. (2023). The origin and early evolution of plants. In *Trends in Plant Science*, 28(3), 312-329.

Brandt, S., Von Stetten, D., Günther, M., Hildebrandt, P., & Frankenberg-Dinkel, N. (2008). The fungal phytochrome FphA from *Aspergillus nidulans*. *Journal of Biological Chemistry*, 283(50), 34605-34614.

Braslavsky, S. E., Gärtner, W., & Schaffner, K. (1997). Phytochrome photoconversion. *Plant, Cell and Environment*, 20(6), 700-706.

Brejc, K., Ficner, R., Huber, R., & Steinbacher, S. (1995). Isolation, crystallization, crystal structure analysis and refinement of allophycocyanin from the cyanobacterium *Spirulina platensis* at 2.3 Å resolution. *Journal of Molecular Biology*, 249(2), 424-440.

Briggs, W. R., & Spudich, J. L. (2005). *Handbook of Photosensory Receptors*, Wiley.

Bryant, D. A. (1982). Phycoerythrocyanin and phycoerythrin: properties and occurrence in cyanobacteria. *Journal of General Microbiology*, 128, 835-844.

Bryant, D. A., Guglielmi, G., de Marsac, N. T., Castets, A. M., & Cohen-Bazire, G. (1979). The structure of cyanobacterial phycobilisomes: a model. *Archives of Microbiology*, 123(2), 113-127.

Bryant, D. A., Cohen-Bazire, G., & Glazer, A. N. (1981). Characterization of the biliproteins of *Gloeobacter violaceus* chromophore content of a cyanobacterial phycoerythrin carrying phycourobilin chromophore. *Archives of Microbiology*, 129, 190-198.

Bryant, D. A., & Canniffe, D. P. (2018). How nature designs light-harvesting antenna systems: Design principles and functional realization in chlorophototrophic prokaryotes. *Journal of Physics B: Atomic, Molecular and Optical Physics*, 51(3), 033001.

Brych, A., Haas, F. B., Parzefall, K., Panzer, S., Schermuly, J., Altmüller, J., Engelsdorf, T., Terpitz, U., Rensing, S. A., Kiontke, S., & Batschauer, A. (2021). Coregulation of

gene expression by White collar 1 and phytochrome in *Ustilago maydis*. *Fungal Genetics and Biology*, 152, 103570.

Burgie, E. S., Bussell, A. N., Walker, J. M., Dubiel, K., & Vierstra, R. D. (2014). Crystal structure of the photosensing module from a red/far-red light-absorbing plant phytochrome. *Proceedings of the National Academy of Sciences of the United States of America*, 111(28), 10179-10184.

Busch, A. W. U. (2011). Biosynthesis of Phycoerythrobilin and its Attachment to Phycobiliproteins. *Ruhr University Bochum: PhD Thesis.*

Busch, A. W. U., Reijerse, E. J., Lubitz, W., Hofmann, E., & Frankenberg-Dinkel, N. (2011a). Radical mechanism of cyanophage phycoerythrobilin synthase (PebS). *Biochemical Journal*, 433(3), 469-476.

Busch, A. W. U., Reijerse, E. J., Lubitz, W., Frankenberg-Dinkel, N., & Hofmann, E. (2011b). Structural and mechanistic insight into the ferredoxin-mediated two-electron reduction of bilins. *Biochemical Journal*, 439(2), 257-264.

Butler, W. L., Norris, K. H., Siegelman, H. W., & Hendricks, S. B. (1959). Detection, assay, and preliminary purification of the pigment controlling photoresponsive development of Plants. *Proceedings of the National Academy of Sciences*, 45(12), 1703-1708.

Caffarri, S., Kouřil, R., Kereïche, S., Boekema, E. J., & Croce, R. (2009). Functional architecture of higher plant photosystem II supercomplexes. *EMBO Journal*, 28(19), 3052-3063.

Caignan, G. A., Deshmukh, R., Wilks, A., Zeng, Y., Huang, H. wei, Moënne-Loccoz, P., Bunce, R. A., Eastman, M. A., & Rivera, M. (2002). Oxidation of heme to β- and δ-biliverdin by *Pseudomonas aeruginosa* heme oxygenase as a consequence of an unusual seating of the heme. *Journal of the American Chemical Society*, 124(50), 14897-14892.

Camara-Artigas, A., Bacarizo, J., Andujar-Sanchez, M., Ortiz-Salmeron, E., Mesa-Valle, C., Cuadri, C., Martin-Garcia, J. M., Martinez-Rodriguez, S., Mazzuca-Sobczuk, T., Ibañez, M. J., & Allen, J. P. (2012). pH-dependent structural conformations of B-phycoerythrin from *Porphyridium cruentum*. *FEBS Journal*, 279(19), 3680-3691.

Carpenter, E. J., Matasci, N., Ayyampalayam, S., Wu, S., Sun, J., Yu, J., Jimenez Vieira, F. R., Bowler, C., Dorrell, R. G., Gitzendanner, M. A., Li, L., Du, W., Ullrich, K., Wickett, N. J., Barkmann, T. J., Barker, M. S., Leebens-Mack, J. H., & Wong, G. K. S. (2019). Access to RNA-sequencing data from 1,173 plant species: The 1000 Plant transcriptomes initiative (1KP). *GigaScience*, 8(10), 1-7.

Carrigee, L. A., Frick, J. P., Karty, J. A., Garczarek, L., Partensky, F., & Schluchter, W. M. (2021). MpeV is a lyase isomerase that ligates a doubly linked phycourobilin on the β-subunit of phycoerythrin I and II in marine *Synechococcus*. *Journal of Biological Chemistry*, 296, 1000031.

Carrigee, L. A., Frick, J. P., Liu, X., Karty, J. A., Trinidad, J. C., Tom, I. P., Yang, X., Dufour, L., Partensky, F., & Schluchter, W. M. (2022). The phycoerythrobilin isomerization activity of MpeV in *Synechococcus* sp. WH8020 is prevented by the presence of a histidine at position 141 within its phycoerythrin-I β-subunit substrate. *Frontiers in Microbiology*, 13, 1011189.

Casal, J. J., & Sánchez, R. A. (1998). Phytochromes and seed germination. *Seed Science Research*, 8(3), 317-329.

Cashmore, A. R. (1998). Higher-plant phytochrome: "I used to date histidine, but now I prefer serine." *Proceedings of the National Academy of Sciences of the United States of America*, 95(23), 13358-13360.

Caspy, I., Neumann, E., Fadeeva, M., Liveanu, V., Savitsky, A., Frank, A., Kalisman, Y. L., Shkolnisky, Y., Murik, O., Treves, H., Hartmann, V., Nowaczyk, M. M., Schuhmann, W., Rögner, M., Willner, I., Kaplan, A., Schuster, G., Nelson, N., Lubitz, W., & Nechushtai, R. (2021). Cryo-EM photosystem I structure reveals adaptation mechanisms to extreme high light in *Chlorella ohadii*. *Nature Plants*, 7(9), 1314-1322.

Chapman, D. J., Cole, W. J., & Siegelman, H. W. (1967). The Structure of Phycoerythrobilin. *Journal of the American Chemical Society*, 89(23), 5976-5977.

Chen, M., Quinnell, R. G., & Larkum, A. W. D. (2002). The major light-harvesting pigment protein of *Acaryochloris marina*. *FEBS Letters*, 514(2-3), 149-152.

Chen, M., Chory, J., & Fankhauser, C. (2004). Light signal transduction in higher plants. *Annual Review of Genetics*, 38, 87-117.

Chen, M., & Bibby, T. S. (2005). Photosynthetic apparatus of antenna-reaction centres supercomplexes in oxyphotobacteria: Insight through significance of Pcb/IsiA proteins. *Photosynthesis Research*, 86(1-2), 165-173.

Chen, M., & Blankenship, R. E. (2011). Expanding the solar spectrum used by photosynthesis. *Trends in Plant Science*, 16(8), 427-431.

Chen, M., & Chory, J. (2011). Phytochrome signaling mechanisms and the control of plant development. *Trends in Cell Biology*, 21(11), 664-671.

Chen, Y. R., Su, Y. S., & Tu, S. L. (2012). Distinct phytochrome actions in nonvascular plants revealed by targeted inactivation of phytobilin biosynthesis. *Proceedings of the National Academy of Sciences of the United States of America*, 109(21), 8310-8315.

Chernov, K. G., Redchuk, T. A., Omelina, E. S., & Verkhusha, V. V. (2017). Near-Infrared Fluorescent Proteins, Biosensors, and Optogenetic Tools Engineered from Phytochromes. *Chemical Reviews*, 117(9), 6423-6446.

Chiu, F. Y., Chen, Y. R., & Tu, S. L. (2010). Electrostatic interaction of phytochromobilin synthase and ferredoxin for biosynthesis of phytochrome chromophore. *Journal of Biological Chemistry*, 285(7), 5056-5065.

Contreras-Martel, C., Martinez-Oyanedel, J., Bunster, M., Legrand, P., Piras, C., Vernede, X., & Fontecilla-Camps, J. C. (2001). Crystallization and 2.2 Å resolution structure of R-phycoerythrin from *Gracilaria chilensis*: A case of perfect hemihedral twinning. *Acta Crystallographica Section D: Biological Crystallography*, 57(1), 52-60.

Cornejo, J. (1992). Phytochrome assembly the structure and biological activity of 2(R),3(E)-phytochromobilin derived from phycobiliproteins. *Journal of Biological Chemistry*, 267(21), 14790-14796.

Cortazzo, P., Cerveñansky, C., Martín, M., Reiss, C., Ehrlich, R., & Deana, A. (2002). Silent mutations affect *in vivo* protein folding in *Escherichia coli*. *Biochemical and Biophysical Research Communications*, 293(1), 537-541.

Croce, R., & Van Amerongen, H. (2014). Natural strategies for photosynthetic light harvesting. *Nature Chemical Biology*, 10(7), 492-501.

Cunningham, O., Gore, M. G., & Mantle, T. J. (2000). Initial-rate kinetics of the flavin reductase reaction catalysed by human biliverdin-IXβ reductase (BVR-B). *Biochemical Journal*, 345, 393-399.

Cunningham, B. R., Greenwold, M. J., Lachenmyer, E. M., Heidenreich, K. M., Davis, A. C., Dudycha, J. L., & Richardson, T. L. (2019). Light capture and pigment diversity in marine and freshwater cryptophytes. *Journal of Phycology*, 55(3), 552-564.

Curtis, B. A., Tanifuji, G., Maruyama, S., Gile, G. H., Hopkins, J. F., Eveleigh, R. J. M., Nakayama, T., Malik, S. B., Onodera, N. T., Slamovits, C. H., Spencer, D. F., Lane, C. E., Gray, M. W., Archibald, J. M., Burki, F., Hirakawa, Y., Reyes-Prieto, A., Keeling, P. J., Fast, N. M., … Mc Fadden, G. I. (2012). Algal genomes reveal evolutionary mosaicism and the fate of nucleomorphs. *Nature*, 492, 59-65.

Dagnino-Leone, J., Figueroa, M., Mella, C., Vorphal, M. A., Kerff, F., Vásquez, A. J., Bunster, M., & Martínez-Oyanedel, J. (2017). Structural models of the different trimers present in the core of phycobilisomes from *Gracilaria chilensis* based on crystal structures and sequences. *PLoS ONE*, 12(5), e0177540.

Dagnino-Leone, J., Figueroa, C. P., Castañeda, M. L., Youlton, A. D., Vallejos-Almirall, A., Agurto-Muñoz, A., Pavón Pérez, J., & Agurto-Muñoz, C. (2022). Phycobiliproteins: Structural aspects, functional characteristics, and biotechnological perspectives. *Computational and Structural Biotechnology Journal*, 20, 1506-1527.

Dammeyer, T., & Frankenberg-Dinkel, N. (2006). Insights into phycoerythrobilin biosynthesis point toward metabolic channeling. *Journal of Biological Chemistry*, 281(37), 27081-27089.

Dammeyer, T., & Frankenberg-Dinkel, N. (2008). Function and distribution of bilin biosynthesis enzymes in photosynthetic organisms. *Photochemical and Photobiological Sciences*, 7, 1121-1130.

Dammeyer, T., Michaelsen, K., & Frankenberg-Dinkel, N. (2007). Biosynthesis of open-chain tetrapyrroles in *Prochlorococcus marinus*. *FEMS Microbiology Letters*, 271(2), 251-257.

Dammeyer, T., Bagby, S. C., Sullivan, M. B., Chisholm, S. W., & Frankenberg-Dinkel, N. (2008a). Efficient Phage-Mediated Pigment Biosynthesis in Oceanic Cyanobacteria. *Current Biology*, 18(6), 442-448.

Dammeyer, T., Hofmann, E., & Frankenberg-Dinkel, N. (2008b). Phycoerythrobilin synthase (PebS) of a marine virus: Crystal structures of the biliverdin complex and the substrate-free form. *Journal of Biological Chemistry*, 283(41), 27547-27554.

de Vries, J., & Archibald, J. M. (2018). Plant evolution: landmarks on the path to terrestrial life. *New Phytologist*, 217(4), 1428-1434.

DeBlasio, S. L., Mullen, J. L., Luesse, D. R., & Hangarter, R. P. (2003). Phytochrome Modulation of Blue Light-Induced Chloroplast Movements in *Arabidopsis*. *Plant Physiology*, 133(4), 1471-1479.

DeLange, R. J., Williams, L. C., & Glazer, A. N. (1981). The amino acid sequence of the beta subunit of allophycocyanin. *The Journal of Biological Chemistry*, 256(18), 9558-9566.

DeLano, W. L. (2020). The PyMOL Molecular Graphics System, Version 2.3. Schrödinger LLC.

Dodson, E. J., Ma, J., Suissa Szlejf, M., Maroudas-Sklare, N., Paltiel, Y., Adir, N., Sun, S., Sui, S. F., & Keren, N. (2023). The structural basis for light acclimation in phycobilisome light harvesting systems systems in *Porphyridium purpureum*. *Communications Biology*, 6(1), 1210.

Domínguez-Martín, M. A., Sauer, P. V., Kirst, H., Sutter, M., Bína, D., Greber, B. J., Nogales, E., Polívka, T., & Kerfeld, C. A. (2022). Structures of a phycobilisome in light-harvesting and photoprotected states. *Nature*, 609(7928), 835-845.

Donoghue, P. C. J., & Clark, J. W. (2024). Plant evolution: Streptophyte multicellularity, ecology, and the acclimatisation of plants to life on land. *Current Biology*, 34(3), R86-R89.

Douglas, S. E. (1992). Eukaryote-eukaryote endosymbioses: insights from studies of a cryptomonad alga. *BioSystems*, 28(1-3), 57-68.

Downs, R. J., & Borthwick, H. A. (1956). Effects of Photoperiod on Growth of Trees. *Botanical Gazette*, 117(4), 310-326.

Downs, R. J., Hendricks, S. B., & Borthwick, H. A. (1957). Photoreversible Control of Elongation of Pinto Beans and Other Plants under Normal Conditions of Growth. *Botanical Gazette*, 118(4), 199-208.

Duanmu, D., Casero, D., Dent, R. M., Gallaher, S., Yang, W., Rockwell, N. C., Martin, S. S., Pellegrini, M., Niyogi, K. K., Merchant, S. S., Grossman, A. R., & Lagarias, J. C. (2013). Retrograde bilin signaling enables *Chlamydomonas* greening and phototrophic survival. *Proceedings of the National Academy of Sciences of the United States of America*, 110(9), 3621-3626.

Duanmu, D., Bachy, C., Sudek, S., Wong, C. H., Jiménez, V., Rockwell, N. C., Martin, S. S., Ngan, C. Y., Reistetter, E. N., Van Baren, M. J., Price, D. C., Wei, C. L., Reyes-Prieto, A., Lagarias, J. C., & Worden, A. Z. (2014). Marine algae and land plants share conserved phytochrome signaling systems. *Proceedings of the National Academy of Sciences of the United States of America*, 111(44), 15827-15832.

Duanmu, D., Rockwell, N. C., & Lagarias, J. C. (2017). Algal light sensing and photoacclimation in aquatic environments. *Plant Cell and Environment*, 40(11), 2558-2570.

Duerring, M., Schmidt, G. B., & Huber, R. (1991). Isolation, crystallization, crystal structure analysis and refinement of constitutive C-phycocyanin from the chromatically adapting cyanobacterium *Fremyella diplosiphon* at 1.66 Å resolution. *Journal of Molecular Biology*, 217(3), 577-592.

Eichler, E. (2016). Characterization of two ferredoxin-dependent bilin reductases in *Galdieria sulphuraria. Technical University of Kaiserslautern: Bachelor's Thesis.*

Eisele, L. E., Bakhru, S. H., Liu, X., MacColl, R., & Edwards, M. R. (2000). Studies on C-phycocyanin from *Cyanidium caldarium*, a eukaryote at the extremes of habitat. *Biochimica et Biophysica Acta-Bioenergetics*, 1456(2-3), 99-107.

Elich, T. D., & Chory, J. (1997). Phytochrome: If it looks and smells like a histidine kinase, is it a histidine kinase? *Cell*, 91(6), 713-716.

Essen, L. O., Mailliet, J., & Hughes, J. (2008). The structure of a complete phytochrome sensory module in the Pr ground state. *Proceedings of the National Academy of Sciences of the United States of America*, 105(38), 14709-14714.

Fairchild, C. D., Zhao, J., Zhou, J., Colson, S. E., Bryant, D. A., & Glazer, A. N. (1992). Phycocyanin α-subunit phycocyanobilin lyase. *Proceedings of the National Academy of Sciences of the United States of America*, 89(15), 7017-7021.

Falk, H. (1989). *The Chemistry of Linear Oligopyrroles and Bile Pigments*, Springer-Verlag.

Ferraro, G., Imbimbo, P., Marseglia, A., Lucignano, R., Monti, D. M., & Merlino, A. (2020). X-ray structure of C-phycocyanin from *Galdieria phlegrea*: Determinants of thermostability and comparison with a C-phycocyanin in the entire phycobilisome. *Biochimica et Biophysica Acta - Bioenergetics*, 1861(9), 148236.

Fiege, K., & Frankenberg-Dinkel, N. (2020). Construction of a new T7 promoter compatible *Escherichia coli* Nissle 1917 strain for recombinant production of heme-dependent proteins. *Microbial Cell Factories*, 19, 190.

Fischer, H. (1937). Chlorophyll. *Chemical Reviews*, 20(1), 41-68.

Fischer, H., & Röse, H. (1914). Zur Kenntnis der Gallenfarbstoffe. V. Mitteilung. *Hoppe-Seyler's Zeitschrift Für Physiologische Chemie*, 89(4), 255-271.

Fischer, H., & Reindel, F. (1923). Über Hämatoidin. *Hoppe-Seyler's Zeitschrift Fur Physiologische Chemie*, 127(4-6), 299-316.

Fischer, H., & Plieninger, H. (1942). Synthese des Biliverdins (Uteroverdins) und Bilirubins. *Die Naturwissenschaften*, 30(25-26), 382-387.

Fischer, A. J., Rockwell, N. C., Jang, A. Y., Ernst, L. A., Waggoner, A. S., Duan, Y., Lei, H., & Lagarias, J. C. (2005). Multiple roles of a conserved GAF domain tyrosine residue in cyanobacterial and plant phytochromes. *Biochemistry*, 44(46), 15203-15215.

Fischer, T., Xu, Q., Zhao, K. H., Gärtner, W., Slavov, C., & Wachtveitl, J. (2020). Effect of the PHY Domain on the Photoisomerization Step of the Forward Pr→Pfr Conversion of a Knotless Phytochrome. *Chemistry - A European Journal*, 26(71), 17261-17266.

Fodor, S. P. A., Lagarias, J. C., & Mathies, R. A. (1988). Resonance Raman Spectra of the Pr-form of Phytochrome. *Photochemistry and Photobiology*, 48(2), 129-136.

Frank, G., Sidler, W., Widmer, H., & Zuber, H. (1978). The Complete Amino Acid Sequence of Both Subunits of C-Phycocyanin from the Cyanobacterium *Mastigocladus laminosus*. *Hoppe-Seyler's Zeitschrift Für Physiologische Chemie*, 359(2), 1491-1507.

Frankenberg, N., Mukougawa, K., Kohchi, T., & Lagarias, J. C. (2001). Functional genomic analysis of the HY2 family of ferredoxin-dependent bilin reductases from oxygenic photosynthetic organisms. *Plant Cell*, 13(4), 965-978.

Frankenberg, N., & Lagarias, J. C. (2003a). Biosynthesis and Biological Functions of Bilins. In *The Porphyrin Handbook: Chlorophylls and Bilins: Biosynthesis, Synthesis and Degradation*, 211-235, Academic Press.

Frankenberg, N., & Lagarias, J. C. (2003b). Phycocyanobilin:ferredoxin oxidoreductase of *Anabaena* sp. PCC 7120: Biochemical and spectroscopic characterization. *Journal of Biological Chemistry*, 278(11), 9219-9226.

Frankenberg-Dinkel, N. (2004). Bacterial heme oxygenases. *Antioxidants and Redox Signaling*, 6(5), 825-834.

Franklin, K. A. (2008). Shade avoidance. *New Phytologist*, 179, 930-944.

Frascogna, F., Ledermann, B., Hartmann, J., Patallo, E. P., Zeqiri, F., Hofmann, E., & Frankenberg-Dinkel, N. (2023). On the evolution of the plant phytochrome chromophore biosynthesis. *Plant Physiology*, 193(1), 246-258.

Froehlich, A. C., Noh, B., Vierstra, R. D., Loros, J., & Dunlap, J. C. (2005). Genetic and molecular analysis of phytochromes from the filamentous fungus *Neurospora crassa*. *Eukaryotic Cell*, 4(12), 2140-2152.

Fu, E., Friedman, L., & Siegelman, H. W. (1979). Mass-spectral identification and purification of phycoerythrobilin and phycocyanobilin. *The Biochemical Journal*, 179(1), 1-6.

Furuya, M., & Schäfer, E. (1996). Photoperception and signalling of induction reactions by different phytochromes. *Trends in Plant Science*, 1(9), 301-307.

Gabriel, E., Krauß, N., & Lamparter, T. (2022). Evidence for evolutionary relationship between archaeplastidal and cyanobacterial phytochromes based on their chromophore pockets. *Photochemical and Photobiological Sciences*, 21(11), 1961-1974.

Gantt, E., & Conti, S. F. (1966). Phycobiliprotein localization in algae. *Brookhaven Symposia in Biology*, 19, 393-405.

Garner, W. W., & Allard, H. A. (1920). Effect of the Relative Length of Day and Night and other factors of the Environment on Growth and Reproduction in Plants. *Monthly Weather Review*, 48(7), 415.

Gasteiger, E., Hoogland, C., Gattiker, A., Duvaud, S., Wilkins, M. R., Appel, R. D., & Bairoch, A. (2005). Protein Identification and Analysis Tools on the ExPASy Server. In *The Proteomics Protocols Handbook*, 571-607, Humana Press.

Gibson, D. G., Young, L., Chuang, R. Y., Venter, J. C., Hutchison, C. A., & Smith, H. O. (2009). Enzymatic assembly of DNA molecules up to several hundred kilobases. *Nature Methods*, 6(5), 343-345.

Gisk, B., Wiethaus, J., Aras, M., & Frankenberg-Dinkel, N. (2012). Variable composition of heme oxygenases with different regiospecificities in *Pseudomonas species*. *Archives of Microbiology*, 194, 597-606.

Glazer, A. N. (1977). Structure and molecular organization of the photosynthetic accessory pigments of cyanobacteria and red algae. *Molecular and Cellular Biochemistry*, 18(2-3), 125-140.

Glazer, A. N. (1994a). Adaptive Variations in Phycobilisome Structure. *Advances in Molecular and Cell Biology*, 10, 119-149.

Glazer, A. N. (1994b). Phycobiliproteins - a family of valuable, widely used fluorophores. *Journal of Applied Phycology*, 6, 105-112.

Glazer, A. N., & Wedemayer, G. J. (1995). Cryptomonad biliproteins - an evolutionary perspective. *Photosynthesis Research*, 46, 93-105.

Gossauer, A., & Klahr, E. (1979). Synthesen von Gallenfarbstoffen, VIII. Totalsynthese des racem. Phycoerythrobilin-dimethylesters. *Chemische Berichte*, 112(6), 2243-2255.

Green, B. R. (2019). What happened to the phycobilisome? *Biomolecules*, 9(11), 748.

Green, B. R., & Parson, W. W. (2003). Light-harvesting antennas in photosynthesis. In *Advances in photosynthesis and respiration,* Vol. 13, Springer-Science+Business Media, B.V.

Greenwold, M. J., Cunningham, B. R., Lachenmyer, E. M., Pullman, J. M., Richardson, T. L., & Dudycha, J. L. (2019). Diversification of light capture ability was accompanied by the evolution of phycobiliproteins in cryptophyte algae. *Proceedings of the Royal Society B: Biological Sciences*, 286(1902), 20190655.

Grombein, S., Rüdiger, W., & Zimmermann, H. (1975). The structures of the phytochrome chromophore in both photoreversible forms. *Hoppe-Seyler's Zeitschrift Fur Physiologische Chemie*, 356(2), 1709-1714.

Grossman, A. R., Schaefer, M. R., Chiang, G. G., & Collier, J. L. (1993). The phycobilisome, a light-harvesting complex responsive to environmental conditions. *Microbiological Reviews*, 57(3), 725-749.

Guglielmi, G., Cohen-Bazire, G., & Bryant, D. A. (1981). The structure of *Gloeobacter violaceus* and its phycobilisomes. *Archives of Microbiology*, 129(3), 181-189.

Guindon, S., Dufayard, J. F., Lefort, V., Anisimova, M., Hordijk, W., & Gascuel, O. (2010). New algorithms and methods to estimate maximum-likelihood phylogenies: Assessing the performance of PhyML 3.0. *Systematic Biology*, 59(3), 307-321.

Hagiwara, Y., Sugishima, M., Takahashi, Y., & Fukuyama, K. (2006a). Crystal structure of phycocyanobilin:ferredoxin oxidoreductase in complex with biliverdin IXα, a key enzyme in the biosynthesis of phycocyanobilin. *Proceedings of the National Academy of Sciences of the United States of America*, 103(1), 27-32.

Hagiwara, Y., Sugishima, M., Takahashi, Y., & Fukuyama, K. (2006b). Induced-fitting and electrostatic potential change of PcyA upon substrate binding demonstrated by the crystal structure of the substrate-free form. *FEBS Letters*, 580(16), 3823-3828.

Hagiwara, Y., Sugishima, M., Khawn, H., Kinoshita, H., Inomata, K., Shang, L., Lagarias, J. C., Takahashi, Y., & Fukuyama, K. (2010). Structural insights into vinyl reduction regiospecificity of phycocyanobilin:ferredoxin oxidoreductase (PcyA). *Journal of Biological Chemistry*, 285(2), 1000-1007.

Hagiwara, Y., Wada, K., Irikawa, T., Sato, H., Unno, M., Yamamoto, K., Fukuyama, K., & Sugishima, M. (2016). Atomic-resolution structure of the phycocyanobilin:ferredoxin oxidoreductase I86D mutant in complex with fully protonated biliverdin. *FEBS Letters*, 590(19), 3425-3434.

Hahn, J., Strauss, H. M., Landgraf, F. T., Gimenèz, H. F., Lochnit, G., Schmieder, P., & Hughes, J. (2006). Probing protein-chromophore interactions in Cph1 phytochrome by mutagenesis. *FEBS Journal*, 273(7), 1415-1429.

Hamchand, R., Hanley, D., Prum, R. O., & Brückner, C. (2020). Expanding the eggshell colour gamut: uroerythrin and bilirubin from tinamou (*Tinamidae*) eggshells. *Scientific Reports*, 10(1), 11264.

Han, X., Chang, X., Zhang, Z., Chen, H., He, H., Zhong, B., & Deng, X. W. (2019). Origin and Evolution of Core Components Responsible for Monitoring Light Environment Changes during Plant Terrestrialization. *Molecular Plant*, 12(6), 847-862.

Hanahan, D. (1983). Studies on transformation of *Escherichia coli* with plasmids. *Journal of Molecular Biology*, 166(4), 557-580.

Hanzawa, H., Shinomura, T., Inomata, K., Kakiuchi, T., Kinoshita, H., Wada, K., & Furuya, M. (2002). Structural requirement of bilin chromophore for the photosensory specificity of phytochromes A and B. *Proceedings of the National Academy of Sciences of the United States of America*, 99(7), 4725-4729.

Harholt, J., Moestrup, Ø., & Ulvskov, P. (2016). Why Plants Were Terrestrial from the Beginning. *Trends in Plant Science*, 21(2), 96-101.

Harris, B. J., Clark, J. W., Schrempf, D., Szöllősi, G. J., Donoghue, P. C. J., Hetherington, A. M., & Williams, T. A. (2022). Divergent evolutionary trajectories of bryophytes and tracheophytes from a complex common ancestor of land plants. *Nature Ecology and Evolution*, 6(11), 1634-1643.

Hartmann, J. (2018). Untersuchungen zur Biosynthese von Phycocyanobilin in der Rotalge *Galdieria sulphuraria*. *Technical University of Kaiserslautern: Master's Thesis*.

Haupt, W. (1982). Light-Mediated Movement of Chloroplasts. *Annual Review of Plant Physiology*, 33(1), 205-233.

Hegemann, P. (2008). Algal sensory photoreceptors. *Annual Review of Plant Biology*, 59, 668-676.

Heidenreich, K. M., & Richardson, T. L. (2020). Photopigment, Absorption, and Growth Responses of Marine Cryptophytes to Varying Spectral Irradiance. *Journal of Phycology*, 56(2), 507-520.

Heintzen, C. (2012). Plant and fungal photopigments. *Wiley Interdisciplinary Reviews: Membrane Transport and Signaling*, 1(4), 411-432.

Heirwegh, K. P. M., Blanckaert, N., & Van Hees, G. (1991). Synthesis, chromatographic purification, and analysis of isomers of biliverdin IX and bilirubin IX. *Analytical Biochemistry*, 195(2), 273-278.

Hendricks, S. B., Borthwick, H. A., & Downs, R. J. (1956). Pigment conversion in the formative responses of Plants to radiation. *Proceedings of the National Academy of Sciences*, 42(1), 19-26.

Hérivaux, A., So, Y. S., Gastebois, A., Latgé, J. P., Bouchara, J. P., Bahn, Y. S., & Papon, N. (2016). Major Sensing Proteins in Pathogenic Fungi: The Hybrid Histidine Kinase Family. *PLoS Pathogens*, 12(7), e1005683.

Hess, W. R., Partensky, F., Van Der Staay, G. W. M., Garcia-Fernandez, J. M., Börner, T., & Vaulot, D. (1996). Coexistence of phycoerythrin and a chlorophyll *a*/*b* antenna in a marine prokaryote. *Proceedings of the National Academy of Sciences of the United States of America*, 93(20), 1126-1130.

Hess, W. R., Steglich, C., Lichtlé, C., & Partensky, F. (1999). Phycoerythrins of the oxyphotobacterium *Prochlorococcus marinus* are associated to the thylakoid membrane and are encoded by a single large gene cluster. *Plant Molecular Biology*, 40(3), 1126-1130.

Hill, D. R. A., & Rowan, K. S. (1989). The biliproteins of the Cryptophyceae. *Phycologia*, 28(4), 455-463.

Hiller, R. G., & Larkum, A. W. D. (1985). The chlorophyll-protein complexes of *Prochloron* sp. (Prochlorophyta). *BBA - Bioenergetics*, 806(1), 107-115.

Hirooka, S., Itabashi, T., Ichinose, T. M., Onuma, R., Fujiwara, T., Yamashita, S., Jong, L. W., Tomita, R., Iwane, A. H., & Miyagishima, S. Y. (2022). Life cycle and functional genomics of the unicellular red alga *Galdieria* for elucidating algal and plant evolution and industrial use. *Proceedings of the National Academy of Sciences of the United States of America*, 119(41), e2210665119.

Hirose, Y., Chihong, S., Watanabe, M., Yonekawa, C., Murata, K., Ikeuchi, M., & Eki, T. (2019). Diverse Chromatic Acclimation Processes Regulating Phycoerythrocyanin and Rod-Shaped Phycobilisome in Cyanobacteria. *Molecular Plant*, 12(5), 715-725.

Hoef-Emden, K., & Archibald, J. M. (2017). Cryptophyta (cryptomonads). In *Handbook of the Protists: Second Edition*, Springer.

Hoffman, G. E., Puerta, M. V. S., & Delwiche, C. F. (2011). Evolution of light-harvesting complex proteins from Chl *c*-containing algae. *BMC Evolutionary Biology*, 11, 101.

Hori, K., Maruyama, F., Fujisawa, T., Togashi, T., Yamamoto, N., Seo, M., Sato, S., Yamada, T., Mori, H., Tajima, N., Moriyama, T., Ikeuchi, M., Watanabe, M., Wada, H., Kobayashi, K., Saito, M., Masuda, T., Sasaki-Sekimoto, Y., Mashiguchi, K., … Ohta, H. (2014). *Klebsormidium flaccidum* genome reveals primary factors for plant terrestrial adaptation. *Nature Communications*, 5, 3978.

Hu, J. H., Chang, J. W., Xu, T., Wang, J., Wang, X., Lin, R., Duanmu, D., & Liu, L. (2021). Structural basis of bilin binding by the chlorophyll biosynthesis regulator GUN4. *Protein Science*, 30(10), 2083-2091.

Hu, L., Liu, P., Jin, Z., Sun, J., Weng, Y., Chen, P., Du, S., Wei, A., & Li, Y. (2021). A mutation in *CsHY2* encoding a phytochromobilin (PΦB) synthase leads to an *elongated hypocotyl 1* (*elh1*) phenotype in cucumber (*Cucumis sativus* L.). *Theoretical and Applied Genetics*, 134, 2639-2652.

Huber, C., Strack, M., Schultheiß, I., Pielage, J., Mechler, X., Hornbogen, J., Diller, R., & Frankenberg-Dinkel, N. (2024). Darkness inhibits autokinase activity of bacterial bathy phytochromes. *Journal of Biological Chemistry*, 300(4), 107148.

Hübschmann, T., Börner, T., Hartmann, E., & Lamparter, T. (2001). Characterization of the Cph1 holo-phytochrome from *Synechocystis* sp. PCC 6803. *European Journal of Biochemistry*, 268(7), 2055-2063.

Hughes, J. (2010). Phytochrome three-dimensional structures and functions. *Biochemical Society Transactions*, 38(2), 710-716.

Hughes, J., & Lamparter, T. (1999). Prokaryotes and phytochrome. The connection to chromophores and signaling. *Plant Physiology*, 121(4), 1059-1068.

Huq, E., Al-Sady, B., & Quail, P. H. (2003). Nuclear translocation of the photoreceptor phytochrome B is necessary for its biological function in seedling photomorphogenesis. *Plant Journal*, 35(5), 660-664.

Idnurm, A., & Heitman, J. (2005). Photosensing fungi: Phytochrome in the spotlight. *Current Biology*, 15(20), R829-R832.

Inoue, K., Nishihama, R., & Kohchi, T. (2017). Evolutionary origin of phytochrome responses and signaling in land plants. *Plant Cell and Environment*, 40(11), 2502-2508.

Inoue, K., Nishihama, R., Araki, T., & Kohchi, T. (2019). Reproductive induction is a far-red high irradiance response that is mediated by phytochrome and phytochrome interacting factor in *Marchantia polymorpha*. *Plant and Cell Physiology*, 60(5), 1136-1145.

Ishizuka, T., Narikawa, R., Kohchi, T., Katayama, M., & Ikeuchi, M. (2007). Cyanobacteriochrome TePixJ of *Thermosynechococcus elongatus* harbors phycoviolobilin as a chromophore. *Plant and Cell Physiology*, 48(9), 1385-1390.

Ishizuka, T., Kamiya, A., Suzuki, H., Narikawa, R., Noguchi, T., Kohchi, T., Inomata, K., & Ikeuchi, M. (2011). The cyanobacteriochrome, TePixJ, isomerizes its own chromophore by converting phycocyanobilin to phycoviolobilin. *Biochemistry*, 50(6), 953-961.

Itoh, S., Mino, H., Itoh, K., Shigenaga, T., Uzumaki, T., & Iwaki, M. (2007). Function of chlorophyll *d* in reaction centers of photosystems I and II of the oxygenic photosynthesis of *Acaryochloris marina*. *Biochemistry*, 46(43), 12473-12481.

Iwai, M., Patel-Tupper, D., & Niyogi, K. K. (2024). Structural Diversity in Eukaryotic Photosynthetic Light Harvesting. *Annual Review of Plant Biology*, 75(9), 1-34.

Jackson, C., Clayden, S., & Reyes-Prieto, A. (2015). The Glaucophyta: The blue-green plants in a nutshell. *Acta Societatis Botanicorum Poloniae*, 84(2), 149-165.

Jaubert, M., Lavergne, J., Fardoux, J., Hannibal, L., Vuillet, L., Adriano, J. M., Bouyer, P., Pignol, D., Giraud, E., & Verméglio, A. (2007). A singular bacteriophytochrome acquired by lateral gene transfer. *Journal of Biological Chemistry*, 282(10), 7320-7328.

Jiang, H. W., Wu, H. Y., Wang, C. H., Yang, C. H., Ko, J. T., Ho, H. C., Tsai, M. D., Bryant, D. A., Li, F. W., Ho, M. C., & Ho, M. Y. (2023). A structure of the relict phycobilisome from a thylakoid-free cyanobacterium. *Nature Communications*, 14(1), 8009.

Jiao, Y., Lau, O. S., & Deng, X. W. (2007). Light-regulated transcriptional networks in higher plants. *Nature Reviews Genetics*, 8(3), 217-230.

Joutsuka, T., Nanasawa, R., Igarashi, K., Horie, K., Sugishima, M., Hagiwara, Y., Wada, K., Fukuyama, K., Yano, N., Mori, S., Ostermann, A., Kusaka, K., & Unno, M. (2023). Neutron crystallography and quantum chemical analysis of bilin reductase PcyA mutants reveal substrate and catalytic residue protonation states. *Journal of Biological Chemistry*, 299(1), 102763.

Jumper, J., Evans, R., Pritzel, A., Green, T., Figurnov, M., Ronneberger, O., Tunyasuvunakool, K., Bates, R., Žídek, A., Potapenko, A., Bridgland, A., Meyer, C., Kohl, S. A. A., Ballard, A. J., Cowie, A., Romera-Paredes, B., Nikolov, S., Jain, R., Adler, J., Back, T., Petersen, S., Reiman, D., Clancy, E., Zielinski, M., Steinegger, M., Pacholska, M., Berghammer, T., Bodenstein, S., Silver, D., Vinyals, O., Senior,

A. W., Kavukcuoglu, K., Kohli, P., & Hassabis, D. (2021). Highly accurate protein structure prediction with AlphaFold. *Nature*, 596(7873), 583-589.

Kabasakal, B. V., Gae, D. D., Li, J., Lagarias, J. C., Koehl, P., & Fisher, A. J. (2013). His74 conservation in the bilin reductase PcyA family reflects an important role in protein-substrate structure and dynamics. *Archives of Biochemistry and Biophysics*, 537(2), 233-242.

Kadish, K. M., Smith, K. M., & Guilard, R. (2012). *The Porphyrin Handbook*, Vol. 11, Academic Press.

Kadota, A., Sato, Y., & Wada, M. (2000). Intracellular chloroplast photorelocation in the moss *Physcomitrella patens* is mediated by phytochrome as well as by a blue-light receptor. *Planta*, 210(6), 932-937.

Kami, C., Mukougawa, K., Muramoto, T., Yokota, A., Shinomura, T., Lagarias, J. C., & Kohchi, T. (2004). Complementation of phytochrome chromophore-deficient *Arabidopsis* by expression of phycocyanobilin:ferredoxin oxidoreductase. *Proceedings of the National Academy of Sciences of the United States of America*, 101(4), 1099-1104.

Kamo, T., Eki, T., & Hirose, Y. (2021). Pressurized Liquid Extraction of a Phycocyanobilin Chromophore and Its Reconstitution with a Cyanobacteriochrome Photosensor for Efficient Isotopic Labeling. *Plant and Cell Physiology*, 62(2), 334-347.

Kane, J. F. (1995). Effects of rare codon clusters on high-level expression of heterologous proteins in *Escherichia coli*. *Current Opinion in Biotechnology*, 6(5), 494-500.

Kaneko, T., Sato, S., Kotani, H., Tanaka, A., Asamizu, E., Nakamura, Y., Miyajima, N., Hirosawa, M., Sugiura, M., Sasamoto, S., Kimura, T., Hosouchi, T., Matsuno, A., Muraki, A., Nakazaki, N., Naruo, K., Okumura, S., Shimpo, S., Takeuchi, C., Wada, T., Watanabe, A., Yamada, M, Yasuda, M., & Tabata, S. (1996). Sequence analysis of the genome of the unicellular cyanobacterium *Synechocystis* sp. strain PCC6803. II. Sequence determination of the entire genome and assignment of potential protein-coding regions. *DNA Research*, 3(3), 109-136.

Karniol, B., Wagner, J. R., Walker, J. M., & Vierstra, R. D. (2005). Phylogenetic analysis of the phytochrome superfamily reveals distinct microbial subfamilies of photoreceptors. *Biochemical Journal*, 392(1), 103-116.

Kawakami, K., Hamaguchi, T., Hirose, Y., Kosumi, D., Miyata, M., Kamiya, N., & Yonekura, K. (2022). Core and rod structures of a thermophilic cyanobacterial light-harvesting phycobilisome. *Nature Communications*, 13(1), 3389.

Keeling, P. J. (2004). Diversity and evolutionary history of plastids and their hosts. *American Journal of Botany*, 91(10), 1481-1493.

Keeling, P. J. (2010). The endosymbiotic origin, diversification and fate of plastids. *Philosophical Transactions of the Royal Society B: Biological Sciences*, 365(1541), 729-748.

Kehoe, D. M., & Gutu, A. (2006). Responding to color: The Regulation of Complementary Chromatic Adaptation. *Annual Review of Plant Biology*, 57, 127-150.

Kevei, E., Schafer, E., & Nagy, F. (2007). Light-regulated nucleo-cytoplasmic partitioning of phytochromes. *Journal of Experimental Botany*, 58(12), 3113-3124.

Kikuchi, G., Yoshida, T., & Noguchi, M. (2005). Heme oxygenase and heme degradation. *Biochemical and Biophysical Research Communications*, 338(1), 558-567.

Kircher, S., Gil, P., Kozma-Bognár, L., Fejes, E., Speth, V., Husselstein-Muller, T., Bauer, D., Ádám, É., Schäfer, E., & Nagy, F. (2002). Nucleocytoplasmic partitioning of the plant photoreceptors phytochrome A, B, C, D, and E is regulated differentially by light and exhibits a diurnal rhythm. *Plant Cell*, 14(7), 1541-1555.

Klose, C., Nagy, F., & Schäfer, E. (2020). Thermal Reversion of Plant Phytochromes. *Molecular Plant*, 13(3), 386-397.

Klose, C., Viczián, A., Kircher, S., Schäfer, E., & Nagy, F. (2015). Molecular mechanisms for mediating light-dependent nucleo/cytoplasmic partitioning of phytochrome photoreceptors. *New Phytologist*, 206(3), 965-971.

Kneip, C., Hildebrandt, P., Schlamann, W., Braslavsky, S. E., Mark, F., & Schaffner, K. (1999). Protonation state and structural changes of the tetrapyrrole chromophore during the P(r) → P(fr) phototransformation of phytochrome: A resonance Raman Spectroscopic study. *Biochemistry*, 38(46), 15185-15192.

Koglin, M., & Behrends, S. (2002). Biliverdin IX is an endogenous inhibitor of soluble guanylyl cyclase. *Biochemical Pharmacology*, 64(1), 109-116.

Kohchi, T., Mukougawa, K., Frankenberg, N., Masuda, M., Yokota, A., & Lagarias, J. C. (2001). The *Arabidopsis HY2* gene encodes phytochromobilin synthase, a ferredoxin-dependent biliverdin reductase. *Plant Cell*, 13(2), 425-436.

Komar, A. A., Lesnik, T., & Reiss, C. (1999). Synonymous codon substitutions affect ribosome traffic and protein folding during in vitro translation. *FEBS Letters*, 462(3), 387-391.

Kooß, S., & Lamparter, T. (2017). Cyanobacterial origin of plant phytochromes. *Protoplasma*, 254(1), 603-607.

Koziol, A. G., Borza, T., Ishida, K. I., Keeling, P., Lee, R. W., & Durnford, D. G. (2007). Tracing the evolution of the light-harvesting antennae in chlorophyll *a*/*b*-containing organisms. *Plant Physiology*, 143(4), 1802-1816.

Krogmann, D. W., Pérez-Gómez, B., Gutiérrez-Cirlos, E. B., Chagolla-López, A., González De La Vara, L., & Gómez-Lojero, C. (2007). The presence of multidomain linkers determines the bundle-shape structure of the phycobilisome of the cyanobacterium *Gloeobacter violaceus* PCC 7421. *Photosynthesis Research*, 93(1-3), 27-43.

Kunugi, M., Satoh, S., Ihara, K., Shibata, K., Yamagishi, Y., Kogame, K., Obokata, J., Takabayashi, A., & Tanaka, A. (2016). Evolution of Green Plants Accompanied Changes in Light-Harvesting Systems. *Plant and Cell Physiology*, 57(6), 1231-1243.

Kurland, C., & Gallant, J. (1996). Errors of heterologous protein expression. *Current Opinion in Biotechnology*, 7(5), 483-493.

Laemmli, U. K. (1970). Cleavage of structural proteins during the assembly of the head of bacteriophage T4. *Nature*, 227, 680-685.

Lagarias, J. C., & Rapoport, H. (1980). Chromopeptides from Phytochrome. The Structure and Linkage of the PR Form of the Phytochrome Chromophore. *Journal of the American Chemical Society*, 102(14), 4821-4828.

Lagarias, J. C., & Lagarias, D. M. (1989). Self-assembly of synthetic phytochrome holoprotein in vitro. *Proceedings of the National Academy of Sciences*, 86(15), 5778-5780.

Lamparter, T., & Michael, N. (2005). *Agrobacterium* phytochrome as an enzyme for the production of *ZZE* bilins. *Biochemistry*, 44(23), 8461-8469.

Lamparter, T., Podlowski, S., Mittmann, F., Schneider-Poetsch, H., Hartmann, E., & Hughes, J. (1995). Phytochrome from Protonemal Tissue of the Moss *Ceratodon purpureus*. *Journal of Plant Physiology*, 147(3-4).

Lamparter, T., Esteban, B., & Hughes, J. (2001). Phytochrome Cph1 from the cyanobacterium *Synechocystis* PCC6803. Purification, assembly, and quaternary structure. *European Journal of Biochemistry*, 268(17), 4720-4730.

Lamparter, T., Michael, N., Mittmann, F., & Esteban, B. (2002). Phytochrome from *Agrobacterium tumefaciens* has unusual spectral properties and reveals an N-terminal chromophore attachment site. *Proceedings of the National Academy of Sciences of the United States of America*, 99(18), 11628-11633.

Lamparter, T., Carrascal, M., Michael, N., Martinez, E., Rottwinkel, G., & Abian, J. (2004). The Biliverdin Chromophore Binds Covalently to a Conserved Cysteine Residue in the N-Terminus of *Agrobacterium* Phytochrome Agp1. *Biochemistry*, 43(12), 3659-3669.

Ledermann, B., Béjà, O., & Frankenberg-Dinkel, N. (2016). New biosynthetic pathway for pink pigments from uncultured oceanic viruses. *Environmental Microbiology*, 18(12), 4337-4347.

Ledermann, B., Aras, M., & Frankenberg-Dinkel, N. (2017). Biosynthesis of cyanobacterial light-harvesting pigments and their assembly into phycobiliproteins. In *Modern Topics in the Phototrophic Prokaryotes: Metabolism, Bioenergetics, and Omics*, 305-340, Springer.

Ledermann, B., Schwan, M., Sommerkamp, J. A., Hofmann, E., Béjà, O., & Frankenberg-Dinkel, N. (2018). Evolution and molecular mechanism of four-electron reducing ferredoxin-dependent bilin reductases from oceanic phages. *FEBS Journal*, 285(2), 339-356.

Lemoine, F., Domelevo Entfellner, J. B., Wilkinson, E., Correia, D., Dávila Felipe, M., De Oliveira, T., & Gascuel, O. (2018). Renewing Felsenstein's phylogenetic bootstrap in the era of big data. *Nature*, 556(7702), 452-456.

Letunic, I., & Bork, P. (2021). Interactive tree of life (iTOL) v5: An online tool for phylogenetic tree display and annotation. *Nucleic Acids Research*, 49(W1), W283-W296.

Li, C., Wu, H., Xiang, W., Wu, H., Wang, N., Wu, J., & Li, T. (2022). Comparison of Production and Fluorescence Characteristics of Phycoerythrin from Three Strains of *Porphyridium*. *Foods*, 11(14), 2069.

Li, F. W., Melkonian, M., Rothfels, C. J., Villarreal, J. C., Stevenson, D. W., Graham, S. W., Wong, G. K. S., Pryer, K. M., & Mathews, S. (2015). Phytochrome diversity in green plants and the origin of canonical plant phytochromes. *Nature Communications*, 6, 7852.

Li, J., Li, G., Wang, H., & Wang Deng, X. (2011). Phytochrome Signaling Mechanisms. *The Arabidopsis Book*, 9, e0148.

Li, L., & Lagarias, J. C. (1992). Phytochrome assembly. Defining chromophore structural requirements for covalent attachment and photoreversibility. *Journal of Biological Chemistry*, 267(27), 19204-19210.

Li, L., Murphy, J. T., & Lagarias, J. C. (1995). Continuous Fluorescence Assay of Phytochrome Assembly in Vitro. *Biochemistry*, 34(24), 7923-7930.

Li, W., Su, H. N., Pu, Y., Chen, J., Liu, L. N., Liu, Q., & Qin, S. (2019). Phycobiliproteins: Molecular structure, production, applications, and prospects. *Biotechnology Advances*, 37(2), 340-353.

Liberti, D., Imbimbo, P., Giustino, E., D'Elia, L., Ferraro, G., Casillo, A., Illiano, A., Pinto, G., Di Meo, M. C., Alvarez-Rivera, G., Corsaro, M. M., Amoresano, A., Zarrelli, A., Ibáñez, E., Merlino, A., & Monti, D. M. (2023). Inside out *Porphyridium cruentum*: Beyond the Conventional Biorefinery Concept. *ACS Sustainable Chemistry and Engineering*, 11(1), 381-389.

Lin, S., Offner, G. D., & Troxler, R. F. (1990). Studies on *Cyanidium caldarium* phycobiliprotein pigment mutants. *Plant Physiology*, 93(2), 381-389.

Lokstein, H., Steglich, C., & Hess, W. R. (1999). Light-harvesting antenna function of phycoerythrin in *Prochlorococcus marinus*. *Biochimica et Biophysica Acta - Bioenergetics*, 1410(1), 97-98.

Lu, L., Zhao, B. Q., Miao, D., Ding, W. L., Zhou, M., Scheer, H., & Zhao, K. H. (2017). A Simple Preparation Method for Phytochromobilin. *Photochemistry and Photobiology*, 93(3), 675-680.

Ma, J., You, X., Sun, S., Wang, X., Qin, S., & Sui, S. F. (2020). Structural basis of energy transfer in *Porphyridium purpureum* phycobilisome. *Nature*, 579, 146-151.

Ma, Q., Hua, H. H., Chen, Y., Liu, B. Bin, Krämer, A. L., Scheer, H., Zhao, K. H., & Zhou, M. (2012). A rising tide of blue-absorbing biliprotein photoreceptors - Characterization of seven such bilin-binding GAF domains in *Nostoc* sp. PCC7120. *FEBS Journal*, 279(21), 4095-4108.

MacColl, R. (1991). Fluorescence studies on R-phycoerythrin and C-phycoerythrin. *Journal of Fluorescence*, 1, 135-140.

MacColl, R. (1998). Cyanobacterial phycobilisomes. *Journal of Structural Biology*, 124(2-3), 311-334.

MacColl, R., & Guard-Friar, D. (2018). *Phycobiliproteins*, CRC Press.

Madeira, F., Pearce, M., Tivey, A. R. N., Basutkar, P., Lee, J., Edbali, O., Madhusoodanan, N., Kolesnikov, A., & Lopez, R. (2022). Search and sequence analysis tools services from EMBL-EBI in 2022. *Nucleic Acids Research*, 50(W1), W276–W279.

Mahmoud, R. M., Sanfilippo, J. E., Nguyen, A. A., Strnat, J. A., Partensky, F., Garczarek, L., El Kassem, N. A., Kehoe, D. M., & Schluchter, W. M. (2017). Adaptation to blue light in marine *Synechococcus* requires MpeU, an enzyme with similarity to phycoerythrobilin lyase isomerases. *Frontiers in Microbiology*, 8, 243.

Mathews, S. (2014). Algae hold clues to eukaryotic origins of plant phytochromes. *Proceedings of the National Academy of Sciences of the United States of America*, 111(44), 15608-15609.

Matsushita, T., Mochizuki, N., & Nagatani, A. (2003). Dimers of the N-terminal domain of phytochrome B are functional in the nucleus. *Nature*, 424(6948), 571-574.

Matysik, J., Hildebrandt, P., Schlamann, W., Braslavsky, S. E., & Schaffner, K. (1995). Fourier-Transform Resonance Raman Spectroscopy of Intermediates of the Phytochrome Photocycle. *Biochemistry*, 34(33), 10497-10507.

McDowell, M. T., & Lagarias, J. C. (2001). Purification and biochemical properties of phytochromobilin synthase from etiolated oat seedlings. *Plant Physiology*, 126(4), 1546-1554.

Medzihradszky, M., Bindics, J., Ádám, É., Viczián, A., Klement, É., Lorrain, S., Gyula, P., Mérai, Z., Fankhauser, C., Medzihradszky, K. F., Kunkel, T., Schäfer, E., & Nagy, F. (2013). Phosphorylation of phytochrome B inhibits light-induced signaling via accelerated dark reversion in *Arabidopsis*. *Plant Cell*, 25(2), 534-544.

Mendoza-Hernández, G., Pérez-Gómez, B., Krogmann, D. W., Gutiérrez-Cirlos, E. B., & Gómez-Lojero, C. (2010). Interactions of linker proteins with the phycobiliproteins in the phycobilisome substructures of *Gloeobacter violaceus*. *Photosynthesis Research*, 106(3), 247-261.

Mercer, F. V., Bogorad, L., & Mullens, R. (1962). Studies with *Cyanidium Caldarium*. *The Journal of Cell Biology*, 13(3), 393-403.

Merritt, K. A., & Richardson, T. L. (2024). Variability in spectral absorption within cryptophyte phycobiliprotein types. *Journal of Phycology*, 60(2), 528-540.

Michie, K. A., Harrop, S. J., Rathbone, H. W., Wilk, K. E., Teng, C. Y., Hoef-Emden, K., Hiller, R. G., Green, B. R., & Curmi, P. M. G. (2023). Molecular structures reveal the origin of spectral variation in cryptophyte light harvesting antenna proteins. *Protein Science*, 32(3), e4586.

Minami, Y., Yamada, F., Hase, T., Matsubara, H., Murakami, A., Fujita, Y., Takao, T., & Shimonishi, Y. (1985). Amino acid sequences of allophycocyanin α- and β-subunits isolated from *Anabaena cylindrica*. Presence of an unknown derivative of aspartic acid in the β-subunit. *FEBS Letters*, 191(2), 216-220.

Mirdita, M., Schütze, K., Moriwaki, Y., Heo, L., Ovchinnikov, S., & Steinegger, M. (2022). ColabFold: making protein folding accessible to all. *Nature Methods*, 19(6), 679-982.

Mirkovic, T., Wilk, K. E., Curmi, P. M. G., & Scholes, G. D. (2009). Phycobiliprotein diffusion in chloroplasts of cryptophyte *Rhodomonas* CS24. *Photosynthesis Research*, 100, 7-17.

Miyabe, Y., Furuta, T., Takeda, T., Kanno, G., Shimizu, T., Tanaka, Y., Gai, Z., Yasui, H., & Kishimura, H. (2017). Structural Properties of Phycoerythrin from Dulse *Palmaria palmata*. *Journal of Food Biochemistry*, 41(1), e12301.

Miyake, K. (2022). Light-utilizing strategy of cyanobacterium *Acaryochloris marina* MBIC 11017 based on the bilin chromophore. *Shizuoka University: PhD Thesis*.

Miyake, K., Fushimi, K., Kashimoto, T., Maeda, K., Ni-Ni-Win, Kimura, H., Sugishima, M., Ikeuchi, M., & Narikawa, R. (2020). Functional diversification of two bilin reductases for light perception and harvesting in unique cyanobacterium *Acaryochloris marina* MBIC 11017. *FEBS Journal*, 287(18), 4016-4031.

Miyake, K., Kimura, H., & Narikawa, R. (2022). Identification of significant residues for intermediate accumulation in phycocyanobilin synthesis. *Photochemical and Photobiological Sciences*, 21, 437-446.

Möglich, A., Yang, X., Ayers, R. A., & Moffat, K. (2010). Structure and function of plant photoreceptors. *Annual Review of Plant Biology*, 61, 21-47.

Montgomery, B. L., & Lagarias, J. C. (2002). Phytochrome ancestry: Sensors of bilins and light. *Trends in Plant Science*, 7(8), 357-366.

Montorzi, M., Dziedzic, T. S., & Falchuk, K. H. (2002). Biliverdin during *Xenopus laevis* oogenesis and early embryogenesis. *Biochemistry*, 41(31), 10115-10122.

Moon, Y. J., Kim, S. Y., Jung, K. H., Choi, J. S., Park, Y. M., & Chung, Y. H. (2011). Cyanobacterial phytochrome Cph2 is a negative regulator in phototaxis toward UV-A. *FEBS Letters*, 585(2), 335-340.

Moore, J. C. (1964). Gel permeation chromatography. I. A new method for molecular weight distribution of high polymers. *Journal of Polymer Science Part A: General Papers*, 2(2), 835-843.

Mudler, J. M. (2020). Biosynthesis of the open chain tetrapyrrole phycocyanobilin in *Galdieria sulphuraria*. *Technical University of Kaiserslautern: Master's Thesis*.

Mukougawa, K., Kanamoto, H., Kobayashi, T., Yokota, A., & Kohchi, T. (2006). Metabolic engineering to produce phytochromes with phytochromobilin, phycocyanobilin, or phycoerythrobilin chromophore in *Escherichia coli*. *FEBS Letters*, 580(5), 1333-1338.

Mullis, K., Faloona, F., Scharf, S., Saiki, R., Horn, G., & Erlich, H. (1986). Specific enzymatic amplification of DNA in vitro: The polymerase chain reaction. *Cold Spring Harbor Symposia on Quantitative Biology*, 51(1), 263-273.

Muñoz-Dorado, J., & Arias, J. M. (1995). The social behavior of myxobacteria. *Microbiología (Madrid, Spain)*, 11(4), 429-438.

Muramoto, T., Kohchi, T., Yokota, A., Hwang, I., & Goodman, H. M. (1999). The *Arabidopsis* photomorphogenic mutant *HY1* is deficient in phytochrome chromophore biosynthesis as a result of a mutation in a plastid heme oxygenase. *Plant Cell*, 11(3), 335-347.

Muramoto, T., Tsurui, N., Terry, M. J., Yokota, A., & Kohchi, T. (2002). Expression and biochemical properties of a ferredoxin-dependent heme oxygenase required for phytochrome chromophore synthesis. *Plant Physiology*, 130(4), 1958-1966.

Muramoto, T., Kami, C., Kataoka, H., Iwata, N., Linley, P. J., Mukougawa, K., Yokota, A., & Kohchi, T. (2005). The Tomato photomorphogenetic mutant, *aurea*, is deficient in phytochromobilin synthase for phytochrome chromophore biosynthesis. *Plant and Cell Physiology*, 46(4), 661-665.

Murphy, J. T., & Lagarias, J. C. (1997). The phytofluors: A new class of fluorescent protein probes. *Current Biology*, 7(11), 870-876.

Murray, J. W., Maghlaoui, K., & Barber, J. (2007). The structure of allophycocyanin from *Thermosynechococcus elongatus* at 3.5 Å resolution. *Acta Crystallographica Section F: Structural Biology and Crystallization Communications*, 63(12), 998-1002.

Nagano, S. (2016). From photon to signal in phytochromes: similarities and differences between prokaryotic and plant phytochromes. *Journal of Plant Research*, 129(2), 123-135.

Nagatani, A. (2010). Phytochrome: structural basis for its functions. *Current Opinion in Plant Biology*, 13(5), 565-570.

Nagy, F., & Schäfer, E. (2002). Phytochromes control photomorphogenesis by differentially regulated, interacting signaling pathways in higher plants. *Annual Review of Plant Biology*, 53, 329-335.

Neilson, J. A. D., & Durnford, D. G. (2010). Structural and functional diversification of the light-harvesting complexes in photosynthetic eukaryotes. *Photosynthesis Research*, 106(1-2), 57-71.

Niedzwiedzki, D. M., Bar-Zvi, S., Blankenship, R. E., & Adir, N. (2019). Mapping the excitation energy migration pathways in phycobilisomes from the cyanobacterium *Acaryochloris marina*. *Biochimica et Biophysica Acta - Bioenergetics*, 1860(4), 286-296.

Nozaki, H., Takano, H., Misumi, O., Terasawa, K., Matsuzaki, M., Maruyama, S., Nishida, K., Yagisawa, F., Yoshida, Y., Fujiwara, T., Takio, S., Tamura, K., Chung, S. J., Nakamura, S., Kuroiwa, H., Tanaka, K., Sato, N., & Kuroiwa, T. (2007). A 100%-complete sequence reveals unusually simple genomic features in the hot-spring red alga *Cyanidioschyzon merolae*. *BMC Biology*, 5, 28.

Ó Carra, P., & Colleran, E. (1969). Haem catabolism and coupled oxidation of haemproteins. *FEBS Letters*, 5(4), 295-298.

Oesterhelt, C., Vogelbein, S., Shrestha, R. P., Stanke, M., & Weber, A. P. M. (2008). The genome of the thermoacidophilic red microalga *Galdieria sulphuraria* encodes a small family of secreted class III peroxidases that might be involved in cell wall modification. *Planta*, 227(2), 353-362.

Offner, G. D., & Troxler, R. F. (1983). Primary structure of allophycocyanin from the unicellular rhodophyte, *Cyanidium caldarium*. The complete amino acid sequences of the alpha and beta subunits. *Journal of Biological Chemistry*, 258(16), 9931-9940.

Ohashi, S., Miyashita, H., Okada, N., Iemura, T., Watanabe, T., & Kobayashi, M. (2008). Unique photosystems in *Acaryochloris marina*. *Photosynthesis Research*, 98(1-3), 141-149.

Ohta, N., Matsuzaki, M., Misumi, O., Miyagishima, S. ya, Nozaki, H., Tanaka, K., Shin-i, T., Kohara, Y., & Kuroiwa, T. (2003). Complete sequence and analysis of the plastid genome of the unicellular red alga *Cyanidioschyzon merolae*. *DNA Research*, 10(2), 67-77.

Ong, L. J., & Glazer, A. N. (1991). Phycoerythrins of marine unicellular cyanobacteria: I. Bilin types and locations and energy transfer pathways in *Synechococcus* spp. phycoerythrins. *Journal of Biological Chemistry*, 266(15), 9515-9527.

Orešič, M., & Shalloway, D. (1998). Specific correlations between relative synonymous codon usage and protein secondary structure. *Journal of Molecular Biology*, 281(1), 31-48.

Ortiz De Montellano, P. R. (2000). The mechanism of heme oxygenase. *Current Opinion in Chemical Biology*, 4(2), 221-227.

Overkamp, K. E., Gasper, R., Kock, K., Herrmann, C., Hofmann, E., & Frankenberg-Dinkel, N. (2014). Insights into the biosynthesis and assembly of cryptophycean phycobiliproteins. *Journal of Biological Chemistry*, 289(39), 26691-26707.

Overkamp, K. E., Langklotz, S., Aras, M., Helling, S., Marcus, K., Bandow, J. E., Hoef-Emden, K., & Frankenberg-Dinkel, N. (2014). Chromophore composition of the phycobiliprotein Cr-PC577 from the cryptophyte *Hemiselmis pacifica*. *Photosynthesis Research*, 122, 293-304.

Oxford, G. S., & Gillespie, R. G. (1998). Evolution and ecology of spider coloration. *Annual Review of Entomology*, 43, 619-643.

Padyana, A. K., Bhat, V. B., Madyastha, K. M., Rajashankar, K. R., & Ramakumar, S. (2001). Crystal structure of a light-harvesting protein C-phycocyanin from *Spirulina platensis*. *Biochemical and Biophysical Research Communications*, 282(4), 893-898.

Pagels, F., Guedes, A. C., Amaro, H. M., Kijjoa, A., & Vasconcelos, V. (2019). Phycobiliproteins from cyanobacteria: Chemistry and biotechnological applications. In *Biotechnology Advances*, 37(3), 422-443.

Paiva-Silva, G. O., Cruz-Oliveira, C., Nakayasu, E. S., Maya-Monteiro, C. M., Dunkov, B. C., Masuda, H., Almeida, I. C., & Oliveira, P. L. (2006). A heme-degradation pathway in a blood-sucking insect. *Proceedings of the National Academy of Sciences of the United States of America*, 103(21), 8030-8035.

Park, S. I., Cho, C. H., Ciniglia, C., Huang, T. Y., Liu, S. L., Bustamante, D. E., Calderon, M. S., Mansilla, A., McDermott, T., Andersen, R. A., & Yoon, H. S. (2023). Revised classification of the Cyanidiophyceae based on plastid genome data with descriptions of the Cavernulicolales ord. nov. and Galdieriales ord. nov. (Rhodophyta). *Journal of Phycology*, 59(3), 444-466.

Parker, M. W., Hendricks, S. B., Borthwick, H. A., & Jenner, C. E. (1952). Photoperiodic responses of plants and animals. *Nature*, 169(4293), 242-243.

Partensky, F., Six, C., Ratin, M., Garczarek, L., Vaulot, D., Probert, I., Calteau, A., Gourvil, P., Marie, D., Grébert, T., Bouchier, C., Le Panse, S., Gachenot, M., Rodríguez, F., & Garrido, J. L. (2018). A novel species of the marine cyanobacterium *Acaryochloris* with a unique pigment content and lifestyle. *Scientific Reports*, 8(1), 9142.

Parys, E., Krupnik, T., Kułak, I., Kania, K., & Romanowska, E. (2021). Photosynthesis of the *Cyanidioschyzon merolae* cells in blue, red, and white light. *Photosynthesis Research*, 147(1), 61-73.

Pendrak, M. L., Chao, M. P., Yan, S. S., & Roberts, D. D. (2004). Heme Oxygenase in *Candida albicans* is Regulated by Hemoglobin and is Necessary for Metabolism of Exogenous Heme and Hemoglobin to α-Biliverdin. *Journal of Biological Chemistry*, 279(5), 3426-3433.

Penno, S., Campbell, L., & Hess, W. R. (2000). Presence of phycoerythrin in two strains of *Prochlorococcus* (Cyanobacteria) isolated from the subtropical north Pacific Ocean. *Journal of Phycology*, 36(4), 723-729.

Pereira, L. O. R., Oliveira, P. L., Almeida, I. C., & Paiva-Silva, G. O. (2007). Biglutaminyl-biliverdin IX alpha as a heme degradation product in the dengue fever insect-vector *Aedes aegypti*. *Biochemistry*, 46(23), 6822-6829.

Perevedentseva, E., Melnik, N., Muronets, E., Averyushkin, A., Karmenyan, A., & Elanskaya, I. (2024). Raman spectroscopy with near IR excitation for study of structural components of cyanobacterial phycobilisomes. *Journal of Luminescence*, 265, 120224.

Perez Saura, P., Chabi, M., Corato, A., Cardol, P., & Remacle, C. (2022). Cell adaptation of the extremophilic red microalga *Galdieria sulphuraria* to the availability of carbon sources. *Frontiers in Plant Science*, 13, e978246.

Perez-Santangelo, S., Napier, N., Robson, F., Weller, J. L., Bond, D. M., & Macknight, R. C. (2022). A Point Mutation in Phytochromobilin synthase Alters the Circadian Clock and Photoperiodic Flowering of *Medicago truncatula*. *Plants*, 11(3), e239.

Pierik, R., & De Wit, M. (2014). Shade avoidance: Phytochrome signalling and other aboveground neighbour detection cues. *Journal of Experimental Botany*, 65(11), 2815-2824.

Polívka, T., & Frank, H. A. (2010). Molecular factors controlling photosynthetic light harvesting by carotenoids. *Accounts of Chemical Research*, 43(8), 1125-1134.

Price, D. C., Chan, C. X., Yoon, H. S., Yang, E. C., Qiu, H., Weber, A. P. M., Schwacke, R., Gross, J., Blouin, N. A., Lane, C., Reyes-Prieto, A., Durnford, D. G., Neilson, J. A. D., Lang, B. F., Burger, G., Steiner, J. M., Löffelhardt, W., Meuser, J. E., Posewitz, M. C., Ball, S., Arias, M. C., Hernissat, B., Coutinho, P. M., Rensing, S. A., Symeonidi, A., Doddapaneni, H., Green, B. R., Rajah, V. D., Boore, J., & Bhattacharya, D. (2012). *Cyanophora paradoxa* genome elucidates origin of photosynthesis in algae and plants. *Science*, 335(6070), 843-847.

Price, D. C., Steiner, J. M., Yoon, H. S., Bhattacharya, D., & Löffelhardt, W. (2017). Glaucophyta. In *Handbook of the Protists: Second Edition*, 23-87, Springer.

Psakis, G., Mailliet, J., Lang, C., Teufel, L., Essen, L. O., & Hughes, J. (2011). Signaling kinetics of cyanobacterial phytochrome Cph1, a light regulated histidine kinase. *Biochemistry*, 50(28), 6178-6188.

Purschwitz, J., Müller, S., Kastner, C., Schöser, M., Haas, H., Espeso, E. A., Atoui, A., Calvo, A. M., & Fischer, R. (2008). Functional and Physical Interaction of Blue- and Red-Light Sensors in *Aspergillus nidulans*. *Current Biology*, 18(4), 255-259.

Quail, P. H. (2010). Phytochromes. *Current Biology*, 20(12), R504-R507.

Quest, B., Hübschmann, T., Sharda, S., Tandeau De Marsac, N., & Gärtner, W. (2007). Homologous expression of a bacterial phytochrome: The cyanobacterium *Fremyella diplosiphon* incorporates biliverdin as a genuine, functional chromophore. *FEBS Journal*, 274(8), 2088-2098.

Rathbone, H. W., Michie, K. A., Landsberg, M. J., Green, B. R., & Curmi, P. M. G. (2021). Scaffolding proteins guide the evolution of algal light harvesting antennas. *Nature Communications*, 12, 1890.

Rathbone, H. W., Laos, A. J., Michie, K. A., Iranmanesh, H., Biazik, J., Goodchild, S. C., Thordarson, P., Green, B. R., & Curmi, P. M. G. (2023). Molecular dissection of the soluble photosynthetic antenna from the cryptophyte alga *Hemiselmis andersenii*. *Communications Biology*, 6(1), 1158.

Ratliff, M., Zhu, W., Deshmukh, R., Wilks, A., & Stojiljkovic, I. (2001). Homologues of Neisserial heme oxygenase in gram-negative bacteria: Degradation of heme by the

product of the *pigA* gene of *Pseudomonas aeruginosa*. *Journal of Bacteriology*, 183(21), 6394-6403.

Rhie, G. E., & Beale, S. I. (1992). Biosynthesis of phycobilins: Ferredoxin-supported NADPH-independent heme oxygenase and phycobilin-forming activities from *Cyanidium caldarium*. *Journal of Biological Chemistry*, 267(23), 16088-16093.

Richardson, T. L., & Campbell, L. (2022). The colorful world of cryptophyte phycobiliproteins. *Journal of Plankton Research*, 44(6), 806-818.

Rindi, F., Guiry, M. D., & López-Bautista, J. M. (2008). Distribution, morphology, and phylogeny of *Klebsormidium* (Klebsormidiales, Charophyceae) in urban environments in Europe. *Journal of Phycology*, 44(6), 1529-1540.

Rippka, R., Waterbury, J., & Cohen-Bazire, G. (1974). A cyanobacterium which lacks thylakoids. *Archives of Microbiology*, 100(1), 419-436.

Ritter, S., Hiller, R. G., Wrench, P. M., Welte, W., & Diederichs, K. (1999). Crystal structure of a phycourobilin-containing phycoerythrin at 1.90-Å resolution. *Journal of Structural Biology*, 126(2), 86-97.

Rockwell, N. C., & Lagarias, J. C. (2006). The structure of phytochrome: A picture is worth a thousand spectra. *Plant Cell*, 18(1), 4-14.

Rockwell, N. C., & Lagarias, J. C. (2010). A brief history of phytochromes. In *ChemPhysChem*, 11(6), 1172-1180.

Rockwell, N. C., & Lagarias, J. C. (2017a). Ferredoxin-dependent bilin reductases in eukaryotic algae: Ubiquity and diversity. *Journal of Plant Physiology*, 217, 57-67.

Rockwell, N. C., & Lagarias, J. C. (2017b). Phytochrome diversification in cyanobacteria and eukaryotic algae. *Current Opinion in Plant Biology*, 37, 87-93.

Rockwell, N. C., & Lagarias, J. C. (2020). Phytochrome evolution in 3D: deletion, duplication, and diversification. *New Phytologist*, 225(6), 2283-2300.

Rockwell, N. C., & Lagarias, J. C. (2023). GUN4 appeared early in cyanobacterial evolution. *PNAS Nexus*, 2(5), 1-16.

Rockwell, N. C., Su, Y. S., & Lagarias, J. C. (2006). Phytochrome structure and signaling mechanisms. *Annual Review of Plant Biology*, 57, 837-858.

Rockwell, N. C., Martin, S. S., Gulevich, A. G., & Lagarias, J. C. (2012). Phycoviolobilin formation and spectral tuning in the DXCF cyanobacteriochrome subfamily. *Biochemistry*, 51(7), 1449–1463.

Rockwell, N. C., Duanmu, D., Martin, S. S., Bachy, C., Price, D. C., Bhattacharya, D., Worden, A. Z., & Lagarias, J. C. (2014). Eukaryotic algal phytochromes span the visible spectrum. *Proceedings of the National Academy of Sciences of the United States of America*, 111(10), 3871-3876.

Rockwell, N. C., Martin, S. S., Li, F. W., Mathews, S., & Lagarias, J. C. (2017). The phycocyanobilin chromophore of streptophyte algal phytochromes is synthesized by HY2. *New Phytologist*, 214(3), 1145-1157.

Rockwell, N. C., Martin, S. S., & Lagarias, J. C. (2023). Elucidating the origins of phycocyanobilin biosynthesis and phycobiliproteins. *Proceedings of the National Academy of Sciences of the United States of America*, 120(17), e2300770120.

Roda-Serrat, M. C., Christensen, K. V., El-Houri, R. B., Fretté, X., & Christensen, L. P. (2018). Fast cleavage of phycocyanobilin from phycocyanin for use in food colouring. *Food Chemistry*, 240, 655-661.

Rodriguez, A., Wright, G., Emrich, S., & Clark, P. L. (2018). %MinMax: A versatile tool for calculating and comparing synonymous codon usage and its impact on protein folding. *Protein Science*, 27(1), 356-362.

Rodríguez-Ezpeleta, N., Brinkmann, H., Burey, S. C., Roure, B., Burger, G., Löffelhardt, W., Bohnert, H. J., Philippe, H., & Lang, B. F. (2005). Monophyly of primary photosynthetic eukaryotes: Green plants, red algae, and glaucophytes. *Current Biology*, 15(14), 1325-1330.

Rottwinkel, G., Oberpichler, I., & Lamparter, T. (2010). Bathy phytochromes in rhizobial soil bacteria. *Journal of Bacteriology*, 192(19), 5124-5133.

Rüdiger, W., & Thümmler, F. (1994). The phytochrome chromophore. In *Photomorphogenesis in Plants*, 51-69, Springer-Science+Business Media, B. V.

Sage, L. C. (1992). *Pigment of the Imagination: A History of Phytochrome Research*, Academic Press.

Sahdev, S., Khattar, S. K., & Saini, K. S. (2008). Production of active eukaryotic proteins through bacterial expression systems: A review of the existing biotechnology strategies. *Molecular and Cellular Biochemistry*, 307, 249-264.

Samsonoff, W. A., & MacColl, R. (2001). Biliproteins and phycobilisomes from cyanobacteria and red algae at the extremes of habitat. *Archives of Microbiology*, 176(6), 400-405.

Sanfilippo, J. E., Garczarek, L., Partensky, F., & Kehoe, D. M. (2019a). Chromatic acclimation in cyanobacteria: A diverse and widespread process for optimizing photosynthesis. *Annual Review of Microbiology*, 73, 407-433.

Sanfilippo, J. E., Nguyen, A. A., Garczarek, L., Karty, J. A., Pokhrel, S., Strnat, J. A., Partensky, F., Schluchter, W. M., & Kehoe, D. M. (2019b). Interplay between differentially expressed enzymes contributes to light color acclimation in marine *Synechococcus*. *Proceedings of the National Academy of Sciences of the United States of America*, 116(13), 6457-6462.

Sanger, F., Nicklen, S., & Coulson, A. R. (1977). DNA sequencing with chain-terminating inhibitors. *Proceedings of the National Academy of Sciences of the United States of America*, 74(12), 5463-5467.

Sawers, R. J. H., Linley, P. J., Gutierrez-Marcos, J. F., Delli-Bovi, T., Farmer, P. R., Kohchi, T., Terry, M. J., & Brutnell, T. P. (2004). The *Elm1* (*ZmHy2*) gene of maize encodes a phytochromobilin synthase. *Plant Physiology*, 136(1), 2771-2781.

Schacter, B. A., Marver, H. S., & Meyer, U. A. (1973). Hemoprotein catabolism during stimulation of microsomal lipid peroxidation. *BBA - General Subjects*, 1(1), 286-292.

Schäfer, E., & Nagy, F. (2006). *Photomorphogenesis in Plants and Bacteria: Function and Signal Transduction Mechanisms*, Springer.

Scheer, H., & Zhao, K. H. (2008). Biliprotein maturation: The chromophore attachment. *Molecular Microbiology*, 68(2), 263-276.

Schirmer, T., Bode, W., Huber, R., Sidler, W., & Zuber, H. (1985). X-ray crystallographic structure of the light-harvesting biliprotein C-phycocyanin from the thermophilic cyanobacterium *Mastigocladus laminosus* and its resemblance to globin structures. *Journal of Molecular Biology*, 184(2), 257-277.

Schirmer, T., Huber, R., Schneider, M., Bode, W., Miller, M., & Hackert, M. L. (1986). Crystal Structure Analysis and Refinement at 2.5 A of Hexameric C-phycocyanin from the cyanobacterium *Agmenellum quadruplicatum*. The Molecular Model and its Implications for Light-harvesting. *Journal of Molecular Biology*, 188(4), 651-676.

Schirmer, T., Bode, W., & Huber, R. (1987). Refined three-dimensional structures of two cyanobacterial C-phycocyanins at 2.1 and 2.5 Å resolution. A common principle of phycobilin-protein interaction. *Journal of Molecular Biology*, 196(3), 677-695.

Schluchter, W. M., Shen, G., Alvey, R. M., Biswas, A., Saunée, N. A., Williams, S. R., Mille, C. A., & Bryant, D. A. (2010). Phycobiliprotein biosynthesis in cyanobacteria: structure and function of enzymes involved in post-translational modification. *Recent Advances in Phototrophic Prokaryotes*, 675, 211-228.

Schmidt, G., Siebzehnrübl, S., Fischer, R., Rüdiger, W., Scheer, H., Schirmer, T., Bode, W., & Huber, R. (1987). *ZZE*-configuration of chromophore ß-153* in C-Phycocyanin from *Mastigocladus laminosus*. *Zeitschrift Fur Naturforschung - Section C Journal of Biosciences*, 42(7-8), 845-848.

Schneider, T., Tan, Y., Li, H., Fisher, J. S., & Zhang, D. (2022). Photoglobin, a distinct family of non-heme binding globins, defines a potential photosensor in prokaryotic signal transduction systems. *Computational and Structural Biotechnology Journal*, 20, 261-273.

Schönknecht, G., Chen, W. H., Ternes, C. M., Barbier, G. G., Shrestha, R. P., Stanke, M., Bräutigam, A., Baker, B. J., Banfield, J. F., Garavito, R. M., Carr, K., Wilkerson, C., Rensing, S. A., Gagneul, D., Dickenson, N. E., Oesterhelt, C., Lercher, M. J., & Weber, A. P. M. (2013). Gene transfer from bacteria and archaea facilitated evolution of an extremophilic eukaryote. *Science*, 339(6124), 1207-1210.

Seckbach, J. (1995). The first eukaryotic cells? Acid hot-spring algae. *Journal of Biological Physics*, 20(1-4), 335-345.

Seckbach, J. (2010). Overview on Cyanidian Biology. In *Red Algae in the Genomic Age*, 345-356, Springer.

Sekar, S., & Chandramohan, M. (2008). Phycobiliproteins as a commodity: Trends in applied research, patents and commercialization. *Journal of Applied Phycology*, 20(2), 113-136.

Sepúlveda-Ugarte, J., Brunet, J. E., Matamala, A. R., Martínez-Oyanedel, J., & Bunster, M. (2011). Spectroscopic parameters of phycoerythrobilin and phycourobilin on phycoerythrin from *Gracilaria chilensis*. *Journal of Photochemistry and Photobiology A: Chemistry*, 219(2-3), 211-216.

Sharrock, R. A. (2008). The phytochrome red/far-red photoreceptor superfamily. *Genome Biology*, 9(8), 230.

Shen, L., Gao, Y., Tang, K., Qi, R., Fu, L., Chen, J. H., Wang, W., Ma, X., Li, P., Chen, M., Kuang, T., Zhang, X., Shen, J. R., Wang, P., & Han, G. (2024). Structure of a unique

PSII-Pcb tetrameric megacomplex in a chlorophyll *d*-containing cyanobacterium. *Science Advances*, 10(8), eadk7140.

Shimkets, L. J. (1990). Social and developmental biology of the myxobacteria. *Microbiological Reviews*, 54(4), 473-501.

Shinomura, T., Nagatani, A., Hanzawa, H., Kubota, M., Watanabe, M., & Furuya, M. (1996). Action spectra for phytochrome A- and B-specific photoinduction of seed germination in *Arabidopsis thaliana*. *Proceedings of the National Academy of Sciences of the United States of America*, 93(15), 8129-8133.

Shukla, A., Biswas, A., Blot, N., Partensky, F., Karty, J. A., Hammad, L. A., Garczarek, L., Gutu, A., Schluchter, W. M., & Kehoe, D. M. (2012). Phycoerythrin-specific bilin lyase-isomerase controls blue-green chromatic acclimation in marine *Synechococcus*. *Proceedings of the National Academy of Sciences of the United States of America*, 109(49), 20136-20141.

Sibbald, S. J., & Archibald, J. M. (2020). Genomic insights into plastid evolution. *Genome Biology and Evolution*, 12(7), 978-990.

Sidler, W. A. (1994). Phycobilisome and Phycobiliprotein Structures. In *The Molecular Biology of Cyanobacteria*, 139-216, Springer-Science+Business Media, B. V.

Sidler, W., Gysi, J., Isker, E., & Zuber, H. (1981). The complete amino acid sequence of both subunits of allophycocyanin, a light harvesting protein-pigment complex from the cyanobacterium *Mastigocladus laminosus*. *Hoppe-Seyler's Zeitschrift Fur Physiologische Chemie*, 362(6), 611-627.

Siedel, W., & Fischer, H. (1933). Über die Konstitution des Bilirubins, Synthesen der Neo- und der Iso-neoxanthobilirubinsäure. *Hoppe-Seyler's Zeitschrift Fur Physiologische Chemie*, 214(3-4), 145-172.

Siegelman, H. W., Turner, B. C., & Hendricks, S. B. (1966). The Chromophore of Phytochrome. *Plant Physiology*, 41, 1289-1292.

Six, C., Thomas, J. C., Garczarek, L., Ostrowski, M., Dufresne, A., Blot, N., Scanlan, D. J., & Partensky, F. (2007). Diversity and evolution of phycobilisomes in marine *Synechococcus* spp.: A comparative genomics study. *Genome Biology*, 8, R259.

Smith, H., & Whitelam, G. C. (1997). The shade avoidance syndrome: multiple responses mediated by multiple phytochromes. *Plant, Cell and Environment*, 20(6), 840-844.

Sommerkamp, J. A., Frankenberg-Dinkel, N., & Hofmann, E. (2019). Crystal structure of the first eukaryotic bilin reductase GtPEBB reveals a flipped binding mode of dihydrobiliverdin. *Journal of Biological Chemistry*, 294(38), 13889-13901.

Sonani, R. R., Gupta, G. D., Madamwar, D., & Kumar, V. (2015). Crystal structure of allophycocyanin from marine cyanobacterium *Phormidium* sp. A09DM. *PLoS ONE*, 10(4), e0124580.

Song, J. Y., Cho, H. S., Cho, J. Il, Jeon, J. S., Lagarias, J. C., & Park, Y. Il. (2011). Near-UV cyanobacteriochrome signaling system elicits negative phototaxis in the cyanobacterium *Synechocystis* sp. PCC 6803. *Proceedings of the National Academy of Sciences of the United States of America*, 108(26), 10780-10785.

Spangler, L. C., Yu, M., Jeffrey, P. D., & Scholes, G. D. (2022). Controllable Phycobilin Modification: An Alternative Photoacclimation Response in Cryptophyte Algae. *ACS Central Science*, 8(3), 340-350.

Spear-Bernstein, L., & Miller, K. R. (1989). Unique location of the Phycobiliprotein Light-Harvesting pigment in the Cryptophyceae. *Journal of Phycology*, 25(3), 412-419.

Stadnichuk, I. N., Krasilnikov, P. M., & Zlenko, D. V. (2015). Cyanobacterial phycobilisomes and phycobiliproteins. *Microbiology (Russian Federation)*, 84(2), 101-111.

Stadnichuk, I. N., & Kusnetsov, V. V. (2023). Phycobilisomes and Phycobiliproteins in the Pigment Apparatus of Oxygenic Photosynthetics: From Cyanobacteria to Tertiary Endosymbiosis. *International Journal of Molecular Sciences*, 24(3), 2290.

Stavenga, D. G. (2023). Butterfly blues and greens caused by subtractive colour mixing of carotenoids and bile pigments. *Journal of Comparative Physiology A: Neuroethology, Sensory, Neural, and Behavioral Physiology*, online ahead of print.

Stec, B., Troxler, R. F., & Teeter, M. M. (1999). Crystal structure of C-phycocyanin from *Cyanidium caldarium* provides a new perspective on phycobilisome assembly. *Biophysical Journal*, 76(6), 2912-2921.

Steglich, C., Mullineaux, C. W., Teuchner, K., Hess, W. R., & Lokstein, H. (2003). Photophysical properties of *Prochlorococcus marinus* SS120 divinyl chlorophylls and phycoerythrin *in vitro* and *in vivo*. *FEBS Letters*, 553(1-2), 79-84.

Steglich, C., Frankenberg-Dinkel, N., Penno, S., & Hess, W. R. (2005). A green light-absorbing phycoerythrin is present in the high-light-adapted marine cyanobacterium *Prochlorococcus* sp. MED4. *Environmental Microbiology*, 7(10), 1611-1618.

Steiner, J. M., & Löffelhardt, W. (2011). The Photosynthetic Apparatus of the Living Fossil, *Cyanophora paradoxa*. In *Bioenergetic Processes of Cyanobacteria*, 71-87.

Studier, F. W., & Moffatt, B. A. (1986). Use of bacteriophage T7 RNA polymerase to direct selective high-level expression of cloned genes. *Journal of Molecular Biology*, 189(1), 113-130.

Sugishima, M., Wada, K., Fukuyama, K., & Yamamoto, K. (2020). Crystal structure of phytochromobilin synthase in complex with biliverdin IXα, a key enzyme in the biosynthesis of phytochrome. *Journal of Biological Chemistry*, 295(3), 771-782.

Sun, H., Wang, Y., He, Y., Liu, B., Mou, H., Chen, F., & Yang, S. (2023). Microalgae-Derived Pigments for the Food Industry. *Marine Drugs*, 21(2),82.

Swanson, R. V., Ong, L. J., Wilbanks, S. M., & Glazer, A. N. (1991). Phycoerythrins of marine unicellular cyanobacteria: II. Characterization of phycobiliproteins with unusually high phycourobilin content. *Journal of Biological Chemistry*, 266(15), 9528-9534.

Taniguchi, M., & Lindsey, J. S. (2023). Absorption and fluorescence spectra of open-chain tetrapyrrole pigments-bilirubins, biliverdins, phycobilins, and synthetic analogues. *Journal of Photochemistry and Photobiology C: Photochemistry Reviews*, 55, 100585.

Tasler, R., Moises, T., & Frankenberg-Dinkel, N. (2005). Biochemical and spectroscopic characterization of the bacterial phytochrome of *Pseudomonas aeruginosa*. *FEBS Journal*, 272(8), 1927-1936.

Taylor, A. O. (1968). *In Vitro* Phytochrome Dark Reversion Process. *Plant Physiology*, 43(5), 767-774.

Tenhunen, R., Marver, H. S., & Schmid, R. (1968). The enzymatic conversion of heme to bilirubin by microsomal heme oxygenase. *Proceedings of the National Academy of Sciences of the United States of America*, 61(2), 197-201.

Tenhunen, R., Marver, H. S., & Schmid, R. (1969). Microsomal heme oxygenase. Characterization of the enzyme. *Journal of Biological Chemistry*, 244(23), 6388-6394.

Terry, M. J., & Kendrick, R. E. (1999). Feedback inhibition of chlorophyll synthesis in the phytochrome chromophore-deficient *aurea* and *yellow-green-2* mutants of tomato. *Plant Physiology*, 119(1), 143-152.

Terry, M. J., Maines, M. D., & Lagarias, J. C. (1993). Inactivation of phytochrome- and phycobiliprotein-chromophore precursors by rat liver biliverdin reductase. *Journal of Biological Chemistry*, 268(35), 26099-26106.

Terry, M. J., McDowell, M. T., & Lagarias, J. C. (1995). (3Z)- and (3E)-phytochromobilin are intermediates in the biosynthesis of the phytochrome chromophore. *Journal of Biological Chemistry*, 270(19), 11111-11118.

Theiss, C., Schmitt, F. J., Pieper, J., Nganou, C., Grehn, M., Vitali, M., Olliges, R., Eichler, H. J., & Eckert, H. J. (2011). Excitation energy transfer in intact cells and in the phycobiliprotein antennae of the chlorophyll *d* containing cyanobacterium *Acaryochloris marina. Journal of Plant Physiology*, 168(12), 1473-1487.

Timme, R. E., Bachvaroff, T. R., & Delwiche, C. F. (2012). Broad phylogenomic sampling and the sister lineage of land plants. *PLoS ONE*, 7(1), e29696.

Ting, C. S., Rocap, G., King, J., & Chisholm, S. W. (2001). Phycobiliprotein genes of the marine photosynthetic prokaryote *Prochlorococcus*: Evidence for rapid evolution of genetic heterogeneity. *Microbiology*, 147(11), 3171-3182.

Tomitani, A., Okada, K., Miyashita, H., Matthijs, H. C. P., Ohno, T., & Tanaka, A. (1999). Chlorophyll *b* and phycobilins in the common ancestor of cyanobacteria and chloroplasts. *Nature*, 400(6740), 159-162.

Tu, S. L., & Lagarias, J. C. (2005). The Phytochromes. In *Handbook of Photosensory Receptors*, 121-149, Wiley.

Tu, S. L., Gunn, A., Toney, M. D., Britt, R. D., & Lagarias, J. C. (2004). Biliverdin reduction by cyanobacterial phycocyanobilin:ferredoxin oxidoreductase (PcyA) proceeds via linear tetrapyrrole radical intermediates. *Journal of the American Chemical Society*, 126(28), 8682-8693.

Tu, S. L., Rockwell, N. C., Lagarias, J. C., & Fisher, A. J. (2007). Insight into the radical mechanism of phycocyanobilin-ferredoxin oxidoreductase (PcyA) revealed by X-ray crystallography and biochemical measurements. *Biochemistry*, 46(6), 1484-1494.

Tu, S. L., Chen, H. C., & Ku, L. W. (2008). Mechanistic studies of the phytochromobilin synthase HY2 from *Arabidopsis*. *Journal of Biological Chemistry*, 283(41), 27555-27564.

Ueno, Y., Aikawa, S., Kondo, A., & Akimoto, S. (2015). Light adaptation of the unicellular red alga, *Cyanidioschyzon merolae*, probed by time-resolved fluorescence spectroscopy. *Photosynthesis Research*, 125(1-2), 211-218.

Ueno, Y., & Akimoto, S. (2023). Long-term light adaptation of light-harvesting and energy-transfer processes in the glaucophyte *Cyanophora paradoxa* under different light conditions. *Photosynthesis Research*, 159(2-3), 165-175.

Unno, M., Ishikawa-Suto, K., Kusaka, K., Tamada, T., Hagiwara, Y., Sugishima, M., Wada, K., Yamada, T., Tomoyori, K., Hosoya, T., Tanaka, I., Niimura, N., Kuroki, R., Inaka, K., Ishihara, M., & Fukuyama, K. (2015). Insights into the proton transfer mechanism of a bilin reductase PcyA following neutron crystallography. *Journal of the American Chemical Society*, 137(16), 5452-5460.

Van Etten, J. (2020). Red Algal Extremophiles: Novel Genes and Paradigms. *Microscopy Today*, 28(6), 28-35.

Vásquez-Suárez, A., Lobos-González, F., Cronshaw, A., Sepúlveda-Ugarte, J., Figueroa, M., Dagnino-Leone, J., Bunster, M., & Martínez-Oyanedel, J. (2018). The γ33 subunit of R-phycoerythrin from *Gracilaria chilensis* has a typical double linked phycourobilin similar to γ subunit. *PLoS ONE*, 13(4), e0195656.

Wada, K., Hagiwara, Y., Yutani, Y., & Fukuyama, K. (2010). One residue substitution in PcyA leads to unexpected changes in tetrapyrrole substrate binding. *Biochemical and Biophysical Research Communications*, 402(2), 373-377.

Wagner, J. R., Brunzelle, J. S., Forest, K. T., & Vierstra, R. D. (2005). A light-sensing knot revealed by the structure of the chromophore-binding domain of phytochrome. *Nature*, 438(7066), 325-331.

Wahlgren, W. Y., Claesson, E., Tuure, I., Trillo-Muyo, S., Bódizs, S., Ihalainen, J. A., Takala, H., & Westenhoff, S. (2022). Structural mechanism of signal transduction in a phytochrome histidine kinase. *Nature Communications*, 13(1), 7673.

Walsh, I. M., Bowman, M. A., Soto Santarriaga, I. F., Rodriguez, A., & Clark, P. L. (2020). Synonymous codon substitutions perturb cotranslational protein folding *in vivo* and impair cell fitness. *Proceedings of the National Academy of Sciences of the United States of America*, 117(7), 3528-354.

Wang, A., Zeng, Y., Han, H., Weeratunga, S., Morgan, B. N., Moënne-Loccoz, P., Schönbrunn, E., & Rivera, M. (2007). Biochemical and structural characterization of *Pseudomonas aeruginosa* Bfd and FPR: Ferredoxin NADP+ reductase and not ferredoxin is the redox partner of heme oxygenase under iron-starvation conditions. *Biochemistry*, 46(43), 12198-12211.

Wang, F., & Chen, M. (2022). Chromatic Acclimation Processes and Their Relationships with Phycobiliprotein Complexes. *Microorganisms*, 10(8), 1562.

Wang, J., & Ortiz de Montellano, P. R. (2003). The binding sites on human heme oxygenase-1 for cytochrome P450 reductase and biliverdin reductase. *Journal of Biological Chemistry*, 278(22), 20069-20076.

Wang, S., Li, L., Li, H., Sahu, S. K., Wang, H., Xu, Y., Xian, W., Song, B., Liang, H., Cheng, S., Chang, Y., Song, Y., Çebi, Z., Wittek, S., Reder, T., Peterson, M., Yang, H., Wang, J., Melkonian, B., Van de Peer, Y., Xu, X., Wong, K. S., Melkonian, M., Liu, H., & Liu, X. (2020). Genomes of early-diverging streptophyte algae shed light on plant terrestrialization. *Nature Plants*, 6(2), 95-106.

Watanabe, M., & Ikeuchi, M. (2013). Phycobilisome: Architecture of a light-harvesting supercomplex. *Photosynthesis Research*, 116(2-3), 265-276.

Watanabe, M., Sato, M., Kondo, K., Narikawa, R., & Ikeuchi, M. (2012). Phycobilisome model with novel skeleton-like structures in a glaucocystophyte *Cyanophora paradoxa*. *Biochimica et Biophysica Acta - Bioenergetics*, 1817(8), 1428-1435.

Waterhouse, A. M., Procter, J. B., Martin, D. M. A., Clamp, M., & Barton, G. J. (2009). Jalview Version 2-A multiple sequence alignment editor and analysis workbench. *Bioinformatics*, 25(9), 1189-1191.

Wedemayer, G. J., Kidd, D. G., Wemmer, D. E., & Glazer, A. N. (1992). Phycobilins of cryptophycean algae: Occurrence of dihydrobiliverdin and mesobiliverdin in cryptomonad biliproteins. *Journal of Biological Chemistry*, 267(11), 7315-7331.

Wedemayer, G. J., Kidd, D. G., & Glazer, A. N. (1996). Cryptomonad biliproteins: Bilin types and locations. *Photosynthesis Research*, 48, 163-170.

Wehrmeyer, W. (1983). Phycobiliproteins and Phycobiliprotein Organization in the Photosynthetic Apparatus of Cyanobacteria, Red Algae, and Cryptophytes. In *Proteins and Nucleic Acids in Plant Systematics*, 143-167, Springer-Verlag.

Weller, J. L., Terry, M. J., Rameau, C., Reid, J. B., & Kendrick, R. E. (1996). The phytochrome-deficient *pcd1* mutant of pea is unable to convert heme to biliverdin IXα. *Plant Cell*, 8(1), 55-67.

Weller, J. P, & Gossauer, A. (1980). Synthesen von Gallenfarbstoffen, X. Synthese und Photoisomerisierung des racem. Phytochromobilin-dimethylesters. *Chemische Berichte*, 113(4), 1603-1611.

Whitelam, G. C., & Devlin, P. F. (1997). Roles of different phytochromes in *Arabidopsis* photomorphogenesis. *Plant, Cell and Environment*, 20(6), 752-758.

Wiethaus, J., Busch, A. W. U., Dammeyer, T., & Frankenberg-Dinkel, N. (2010). Phycobiliproteins in *Prochlorococcus marinus*: Biosynthesis of pigments and their assembly into proteins. *European Journal of Cell Biology*, 89(12), 1005-1110.

Wilbanks, S. M., & Glazer, A. N. (1993). Rod Structure of a Phycoerythrin II-containing Phycobilisome. *The Journal of Biological Chemistry*, 286(2), 1226-1241.

Wilde, A., Fiedler, B., & Börner, T. (2002). The cyanobacterial phytochrome Cph2 inhibits phototaxis towards blue light. *Molecular Microbiology*, 44(4), 981-988.

Wilkinson, I. V. L., Castro-Falcón, G., Roda-Serrat, M. C., Purdy, T. N., Straetener, J., Brauny, M. M., Maier, L., Brötz-Oesterhelt, H., Christensen, L. P., Sieber, S. A., & Hughes, C. C. (2023). The Cyanobacterial "Nutraceutical" Phycocyanobilin Inhibits Cysteine Protease Legumain. *ChemBioChem*, 24(5), e202200455.

Wilks, A. (2002). Heme oxygenase: Evolution, structure, and mechanism. *Antioxidants and Redox Signaling,* 4(4), 603-614.

Wilks, A., & Schmitt, M. P. (1998). Expression and characterization of a heme oxygenase (HmuO) from *Corynebacterium diphtheriae*: Iron acquisition requires oxidative cleavage of the heme macrocycle. *Journal of Biological Chemistry*, 273(2), 837-841.

Wiltbank, L. B., & Kehoe, D. M. (2019). Diverse light responses of cyanobacteria mediated by phytochrome superfamily photoreceptors. *Nature Reviews Microbiology*, 17(1), 37-50.

Wodniok, S., Brinkmann, H., Glöckner, G., Heidel, A. J., Philippe, H., Melkonian, M., & Becker, B. (2011). Origin of land plants: Do conjugating green algae hold the key? *BMC Evolutionary Biology*, 11(1), 104.

Wollman, F. A. (1979). Ultrastructural Comparison of *Cyanidium caldarium* Wild Type and III-C Mutant Lacking Phycobilisomes. *Plant Physiology*, 63(2), 375-381.

Wright, G., Rodriguez, A., Li, J., Milenkovic, T., Emrich, S. J., & Clark, P. L. (2022). CHARMING: Harmonizing synonymous codon usage to replicate a desired codon usage pattern. *Protein Science*, 31(1), 221-231.

Wu, S. H., McDowell, M. T., & Lagarias, J. C. (1997). Phycocyanobilin is the natural precursor of the phytochrome chromophore in the green alga *Mesotaenium caldariorum*. *Journal of Biological Chemistry*, 272(41), 25700-25705.

Xie, M., Li, W., Lin, H., Wang, X., Dong, J., Qin, S., & Zhao, F. (2021). Difference in light use strategy in red alga between *Griffithsia pacifica* and *Porphyridium purpureum*. *Scientific Reports*, 11(1), 14367.

Xu, C., Zhu, Q., Chen, J. H., Shen, L., Yi, X., Huang, Z., Wang, W., Chen, M., Kuang, T., Shen, J. R., Zhang, X., & Han, G. (2021). A unique photosystem I reaction center from a chlorophyll *d*-containing cyanobacterium *Acaryochloris marina*. *Journal of Integrative Plant Biology*, 63(10), 1740-1752.

Xu, Q. Z., Bielytskyi, P., Otis, J., Lang, C., Hughes, J., Zhao, K. H., Losi, A., Gärtner, W., & Song, C. (2019). MAS NMR on a red/far-red photochromic cyanobacteriochrome All2699 from *Nostoc*. *International Journal of Molecular Sciences*, 20(15), 3656.

Yang, X., Kuk, J., & Moffat, K. (2008). Crystal structure of *Pseudomonas aeruginosa* bacteriophytochrome: Photoconversion and signal transduction. *Proceedings of the National Academy of Sciences of the United States of America*, 105(38), 14175-14720.

Yang, Z., Ma, X., Wang, Q., Tian, X., Sun, J., Zhang, Z., Xiao, S., De Clerck, O., Leliaert, F., & Zhong, B. (2023). Phylotranscriptomics unveil a Paleoproterozoic-Mesoproterozoic origin and deep relationships of the Viridiplantae. *Nature Communications*, 14(1), m5542.

Yeh, K. C., & Lagarias, J. C. (1998). Eukaryotic phytochromes: Light-regulated serine/threonine protein kinases with histidine kinase ancestry. *Proceedings of the National Academy of Sciences of the United States of America*, 95(23), 13976-13981.

Yeh, K. C., Wu, S. H., Murphy, J. T., & Lagarias, J. C. (1997). A cyanobacterial phytochrome two-component light sensory system. *Science*, 277(5331), 1505-1508.

Yokono, M., Akimoto, S., Koyama, K., Tsuchiya, T., & Mimuro, M. (2008). Energy transfer processes in *Gloeobacter violaceus* PCC 7421 that possesses phycobilisomes with a unique morphology. *Biochimica et Biophysica Acta - Bioenergetics*, 1777(1), 55-65.

Yoshida, T., & Migita, C. T. (2000). Mechanism of heme degradation by heme oxygenase. *Journal of Inorganic Biochemistry*, 82(1-4), 33-41.

Yoshihara, S., Katayama, M., Geng, X., & Ikeuchi, M. (2004). Cyanobacterial phytochrome-like PixJ1 holoprotein shows novel reversible photoconversion between blue- and green-absorbing forms. *Plant and Cell Physiology*, 45(12), 1729-1737.

Yu, M. H., Glazer, A. N., Spencer, K. G., & West, J. A. (1981). Phycoerythrins of the Red Alga *Callithamnion*: VARIATION IN PHYCOERYTHROBILIN AND PHYCOUROBILIN CONTENT. *Plant Physiology*, 68(2), 482-488.

Yu, Z., Ali, A., Igbalajobi, O. A., Streng, C., Leister, K., Krauß, N., Lamparter, T., & Fischer, R. (2019). Two hybrid histidine kinases, TcsB and the phytochrome FphA, are involved in temperature sensing in *Aspergillus nidulans*. *Molecular Microbiology*, 112(6), 1814-1830.

Zhang, J., Ma, J., Liu, D., Qin, S., Sun, S., Zhao, J., & Sui, S. F. (2017). Structure of phycobilisome from the red alga *Griffithsia pacifica*. *Nature*, 551, 57-63.

Zhang, W., Willows, R. D., Deng, R., Li, Z., Li, M., Wang, Y., Guo, Y., Shi, W., Fan, Q., Martin, S. S., Rockwell, N. C., Lagarias, J. C., & Duanmu, D. (2021). Bilin-dependent regulation of chlorophyll biosynthesis by GUN4. *Proceedings of the National Academy of Sciences of the United States of America*, 118(20), e2104443118.

Zhao, C., Höppner, A., Xu, Q. Z., Gärtner, W., Scheer, H., Zhou, M., & Zhao, K. H. (2017). Structures and enzymatic mechanisms of phycobiliprotein lyases CpcE/F and PecE/F. *Proceedings of the National Academy of Sciences of the United States of America*, 114(50), 13170-13175.

Zhao, K. H., Su, P., Tu, J. M., Wang, X., Liu, H., Plöscher, M., Eichacker, L., Yang, B., Zhou, M., & Scheer, H. (2007). Phycobilin:cystein-84 biliprotein lyase, a near-universal lyase for cysteine-84-binding sites in cyanobacterial phycobiliproteins. *Proceedings of the National Academy of Sciences of the United States of America*, 104(36), 14300-14305.

Zhao, K. H., Wu, D., Zhang, L., Zhou, M., Böhm, S., Bubenzer, C., & Scheer, H. (2006). Chromophore attachment in phycocyanin: Functional amino acids of phycocyanobilin – α-phycocyanin lyase and evidence for chromophore binding. *FEBS Journal*, 273(6), 1262-1274.

Zhao, K. H., Wu, D., Zhou, M., Zhang, L., Böhm, S., Bubenzer, C., & Scheer, H. (2005). Amino acid residues associated with enzymatic activities of the isomerizing phycoviolobilin-lyase PecE/F. *Biochemistry*, 44(22), 8126-8137.

Zheng, L., Zheng, Z., Li, X., Wang, G., Zhang, K., Wei, P., Zhao, J., & Gao, N. (2021). Structural insight into the mechanism of energy transfer in cyanobacterial phycobilisomes. *Nature Communications*, 12(1), 5497.

Zhou, L. J., Höppner, A., Wang, Y. Q., Hou, J. Y., Scheer, H., & Zhao, K. H. (2024). Crystallographic and biochemical analyses of a far-red allophycocyanin to address the mechanism of the super-red-shift. *Photosynthesis Research*, online ahead of print.

Appendix

Synthetic genes

>MCC5789364
AAGACATCAATAGAAAAACCACCCTTACTACTTGGCAACCTGTGGCAGGACATGTTTCA
GATTCACACCGCGAACTTGACCCCGCAACCGCTGCCGGATCCGTTCCAAACGACTGA
GAAACGTGGTGAGATTGAACTTAAGACCCAGCTGTACAGCCTGTTCAACCAGTGGGAG
ATCCGCCTCGCGCGTGTAACCAGCCCGAAAATCGACATCCTGAATCTCTACGCCTTCC
CATTCGAGAAGAAGGACCTGCCGGTGGTGGTCATGGAAATGGTTCGTTTTGGCCCAAA
ACCGTTGGTTGCGGTCGCCGATCTGATTGGTTTTGGTGAGCAGAGCCGCCTGGCTGC
ACGCAAAGTGCTGCGTCTGGTGCATAGCGCATATCCGTCCCTGAAGAACTCTCAGGAC
CCGCCTGTTTGGTTTCAAGAGTGCCGTAGCGGTGAAGATTTTTTCATCCGTCCGCAAA
ATTTGCTGGAATGGCAAACGTGCTGTTTTGCGTTTCGTCAACTGTGGAAAAAGGCGTT
CTTCCCGTTACCGGGTGTTGATCCGTCCCCGGAAGCGCATCAGGCTCTGGGCCAGTA
CAAACAGCACCACCTGGTTAATTCGCCGTCTAGACCTTTCTTGCAGAAAACCTTCGGC
GCAAGCTGGACCGAAGACTATCTGCATAAGGTGTTGCTGCAA

>CAP_1520
ATTGACGCTTCCTCGCTTAAGGCGCTGGTGCGTCGTGCCGAGGGTGGCTTGGTGGAA
GCGTTGGGCTTACGTCCGCTGCAACTGGACCCGGAAGCTACCCATGCAGTTGGCACG
TACCGCGGTCGTGCAGTTACCTTGGAGACAAGAGCGTACCGTGGCCAGCCGCTGCAT
TACGCACGCTTTGTCGAAATCACCGGTGAAGGTTTGGCAATTGGCAACATGTTATGCA
CGCCGTGTGTTGACCACCCGCTGCCGATCCTGGGGGTGGATTTGGTGATGCTGGGTG
ATACCTTGATGCTCGTCGCCGATCTTAGCCCGACCCTGCCGCCGGGTAAAGAGCGTG
AAGCGCAGCTGGCACCGCTGGACGCCGCGTGCGCAGCTAGAAGCTCCACTCTGCCG
CCAGGCGGTGCGCTGCCGGCGTGGTGTACGGCTTGGTTCAGCCCGTTTGCACTGTAT
ACCCGCGTGGCGGGTGCGGACCTGGCACGTGCGGCGAGCGCCTGCGATGATCTTGT
GCGTGTTCATGTTAGCCTGTGCACCGCAAGCGCGCCAGCCCCGCAACACCGCCTAGG
CACCGCGCGTGCTGTTGAGGGCTATGCGGCAGCGCACCGTGAGCACGACAAAGGTCT
GCGCATGCTGGCGAAACTGTTCGGTGAGGGATGGGCTGCTCGCTATATCGCCGAAAC
CCTGTTCCCGGCGTTGCTGACGATGGGTGAGGCGCCCGAGGTGCCGGTAGCGCCGG
AAGCCCCTACTTCTGCTCCGGCTAGCTCTGCGCCGGACCCGGCGACCCCGCTGTTGA
AGTCCCCGCCACAAAGCTCCCCTAATATTGCTCGTCTCCTGGGCAGCCCG

>MBL9008304
ACCAACCCGGATTGTGCAACCTATCTGGCGCTGTGCCAGGCTTGGCTGGATGTTCTGT
TCATCCAGCGTCTGGGCCTGCACGAGGTGACCATCCCGCAGGATCTAGCGCTCGCGC
ACGGCTTGCTGAGAGGTACACCGGTTAGCCTCCGCACGCGTCGTTTCGTGGGCCCAG
GTTTCTCTCCGCTTAGCATCGCCCGTATTCAGACTGAACAAGGTCAGGTGTGCAGCCT
GACCGTCGTGGGTTTACCGCCTACCGGTGGCGGTCTGCCGATTCTGGGTATGGATCT
GATTGCCCTGTCGGGCGCGTTGTCCCTGGTCGCAGTTGACCTAGCTCCGACCGACGC
GCGTACCTGGCAGGCGGACTGTGAACCGGTGCTTCTGCGCTTGGCGCAGCAAACGGA
GAGCTGCCTGGTTCCGCGTAAGAGACCGCAATTCACCGTGGACACCTTTTCCCCGCG
TGCTGTGATCGCCGGTGCGCGTAGCGGCAGCGAGTGGTCAGTTTTCTGCGCTCTGGT
GGAGTTCCTGCAACAAGCTAGCGACCTGTGGTTGCGTTCTGTTCTTCGTGAACCACTG
TGCGGTCAAGCCGCGCATGCAGCCGAAGCATGTGTTTTACGCTGGCTGGCGGCGGAG
CAACAAAACCGCAAAGAGCACAATGCACTGGCTGGTATTTTTGGTGCGGCGTTTGCAG
AACGTTACTTGAATCAGTTTTTGTTTAGCACCAACCGCGCGGGTGAACAGTCTGGCAC
GACGCATGCGACCAATCGCAACGAGTGCGGCTTCACCAGCGGCGGCGGTCCG

>*GsPEBA*_harmo
GATTCGAACAGCTTAGTTAGTTCGCTGAACCGCAAGCTGTGGAAAACTTCGGTGGCCG
GTAGTGATATTCCGATGATTTATAGCCCGTTTTTGGAAGATATGCAGAACACGCTGTTT
GCGAGTTTTGAAACAGTGGAAGACTATCCGCTGTCAGAGTTCCTGGCCAGTGCGCAGT
CTTCTAAGAAGCCGGCGCGTATCGAAAGCTGGTGTTATCAATGCCCGAAGTTTCGGAA
AATTCGTTTGACCTATCTGGATGCCGGTGTGGCGGCGCAGGTTTTTAACGCCGTGTGG
TATCCAATCTCAAGTTTGGAATTACCGATCCTCGGAGTTGACTTTCTTTCATTTGGAGG
GAAAAACGTACTGTGTGTTATGGACTTTCAGCCGCTGATGAACGATCAATATTATTTAG
ATAAATATATTCAACCATTACATCCTATTCGTGAACGCTATGCCGATCTGGCCGGTCGC
ATGTCAAGTCGTTTTTATGATGAAAACAGGTTTTTTAGTAAAGAGCTGCTGTTCGGTCG
CTTTGATTCGACAAAACCGATATACGAACGCCTCTTTCCGGCATTTCGGGAATATTTAG
ATCTGTATATAACGTTAGCGAAACAGACGGTGGAAGATGATAAGAGCCGGTCCATCAT
TTGGCAGTTGCAGTGCGAATATGATCGCTATTCCGCCGAGAAGGATCCGGCGATGTCT
CTGTTTCGGAGCTACTTTGGTAGTACCTGGGCGCATCGTTTTGTGTATGAATTTTTATTT
GAAAATAGTCGTTATGAGTCTAGTCTTGATAACAAGACC

>*GsPEBA*_revtrans
GATTCTAACTCACTAGTAAGCAGTTTAAATCGCAAGCTGTGGAAAACCAGCGTGGCAG
GTAGCGACATCCCGATGATTTACAGTCCGTTTTTAGAGGATATGCAGAATACCCTGTTC
GCCAGCTTTGAAACTGTAGAGGACTATCCGCTCTCGGAATTCCTGGCGAGCGCACAAA
GCTCCAAGAAGCCAGCTCGTATTGAAAGCTGGTGCTATCAGTGCCCGAAATTTCGTAA
GATTCGTTTGACCTATTTGGACGCTGGCGTTGCGGCCCAAGTGTTTAACGCCGTTTGG
TATCCGATCAGCTCACTAGAGTTGCCGATCCTGGGTGTGGATTTCTTGTCGTTCGGCG
GTAAAAATGTTCTTTGCGTGATGGATTTCCAGCCTCTGATGAATGATCAGTACTACCTG
GACAAGTACATCCAACCGCTGCATCCGATCCGTGAACGCTACGCAGATTTGGCGGGT
CGTATGTCCAGCAGATTCTACGACGAAAACCGTTTCTTTAGCAAAGAGCTGCTGTTTGG
CCGTTTCGACAGCACGAAGCCGATCTACGAGCGTTTATTTCCGGCGTTTCGCGAGTAC
CTGGACCTGTATATCACCCTGGCGAAACAAACCGTTGAGGACGATAAGTCCCGCTCTA
TTATTTGGCAGCTGCAGTGTGAATATGATCGTTACAGCGCGGAAAAAGATCCGGCTAT
GTCCCTGTTCCGCAGCTATTTTGGCTCTACGTGGGCGCACCGCTTCGTCTATGAGTTC
CTGTTTGAGAACTCCCGTTACGAATCGTCCCTGGACAACAAAACC

>*Kfla*PUBS
GACAGGTTTCCCGATGATAGACTACAAAAAGTCGCGCATCCGAGCGCGACCCCGCTG
TTGTTCCTGGAGCATATCCAATATCAGTGGAAAACCCTGCAAGAACGTGTTCCGGACTT
GGCGGACCTGCCGCTTCCGCCTGAAATTGCTCTGCAAACCAGCGCTAAGGGTAAGTG
CGGCGCACGTGTGGAAAATTGGGCATTTCAGTCCGATACGATGAGACGTGTACGCAT
GACCTATTTTTACAGCGGTGATGGTGGTCAGGCTTACAACTGCCTGGTGTACCCGGAC
ACGCGTTTTGATGTGCCGTTGCTGGGTGTTGATCTTATCTGTCTGGGCAAAGATCGTAT
TCTGTATGTTATTGATTTTCAACCGCTCCAGATGTCCGATGATTATCTCGAGAAATACAC
CGCCATCTTAGCGCCAGTGCACGAGCAGTACCTGGACTTGATTGGCTCTATGTCCGCG
AAGCACTTTGACGAGGCCCAATTTTTCAGCAAACGTATGCTGTTTGTGCGTACCGCAG
ATACTGACCTGTTCAAGGCACCACATGGTCGTCTGTTCCACGCGCTGATGGAATATCT
GGCGGCGTACCACGCCGTTCTGGAGCGCGCAGTTCCGGACGGCTCGGCGGACGCGC
GTCAGGCCGTCCAGGCGGCGCAGGATGCGTACGACGTTTACAGCGAACAACGCGATC
CGGCGATCGGCTTGTTTCGCAGCTATTTCGGCCATGAGTGGGCAGAATCGTTCACCAA
AGACTTCTTGTTCCCGGGTTCTCGTCGCACCGACGCTAAGGACGAGCACTTCGACGTG
AGC

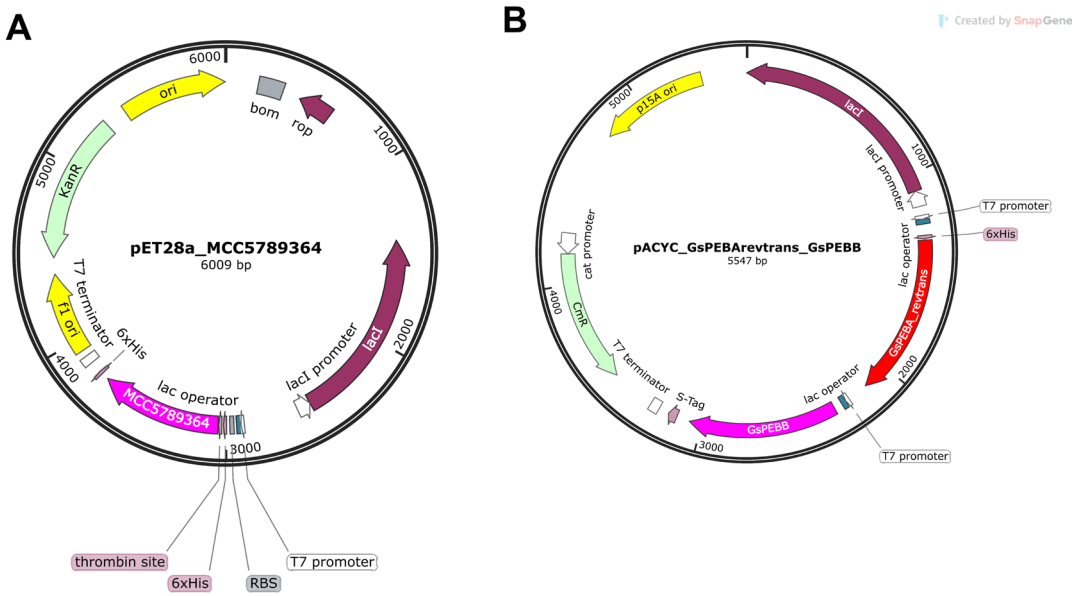

Figure S1 Expression constructs.
(A) pET28a(+) vector backbone. Gene cloned in *Nde*I restriction site downstream the His-tag via Gibson Assembly®. An identical cloning procedure was performed for all the expression constructs based on this vector backbone.
(B) pACYCDuet-1 vector backbone. *GsPEBA*revtrans cloned in MCS1 using *Bam*HI downstream the His-tag. *GsPEBB* cloned in MCS2 using *Nde*I.

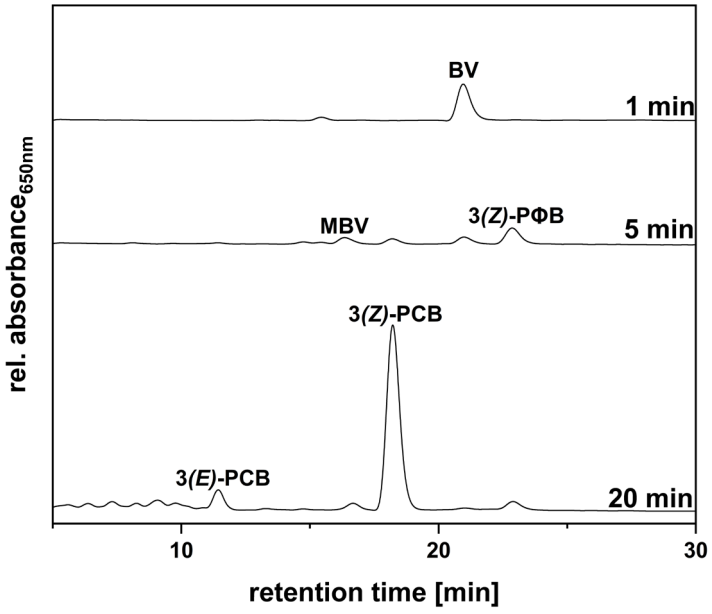

Figure S2 Characterization of *Kfla*HY2_N105D products.
HPLC analyses of the reaction products of a *Kfla*HY2_N105D time course assay with BV as substrate. The products were analyzed using a reversed-phase 5 µm C18 Luna column (Phenomenex) as stationary phase. The mobile phase consisted of 50%$_{v/v}$ acetone and 50%$_{v/v}$ 20 mM formic acid flowing at 0.6 mL/min. Absorbance was continuously recorded at 650 nm. MBV, 18^1,18^2-dihydrobiliverdin; 3(*Z*)-PΦB, 3(*Z*)-phytochromobilin; 3(*E*)-PCB, 3(*E*)-phycocyanobilin; 3(*Z*)-PCB, 3(*Z*)-phycocyanobilin.

Figure S3 Sequence alignment of PcyAs and HY2s.
The alignment was constructed using Clustal Omega (Madeira *et al.*, 2022) (https://www.ebi.ac.uk/jdispatcher/msa/clustalo) and modified using Jalview (Waterhouse *et al.*, 2009). The amino acid residues essential for catalysis are highlighted in different colors and labeled according to *Syn*PcyA sequence numbering. Accession codes of the employed sequences are listed in Table S1. *Syn*PcyA: PcyA from *Synechocystis* sp. PCC 6803; *Nos*PcyA: PcyA from *Nostoc* sp. PCC 7120; *Syc*PcyA: PcyA from *Synechococcus* sp. PC 7002; *Pro*PcyA: PcyA from *Prochlorococcus marinus* CCMP 1375; *Cm*PCYA: PCYA from *Cyanidioschyzon merolae* 10D; *Ca*HY2: HY2 from *Chlorokybus atmophyticus*; *Kfla*HY2: HY2 from *Klebsormidium nitens*; *Mc*HY2: HY2 from *Mesotaenium caldariorum*; *Nedi*HY2: HY2 from *Netrium digitus*; *Cepu*HY2: HY2 from *Ceratodon purpureus*; *Sl*HY2: HY2 from *Solanum lycopersicum*; *At*HY2: HY2 from *Arabidopsis thaliana*.

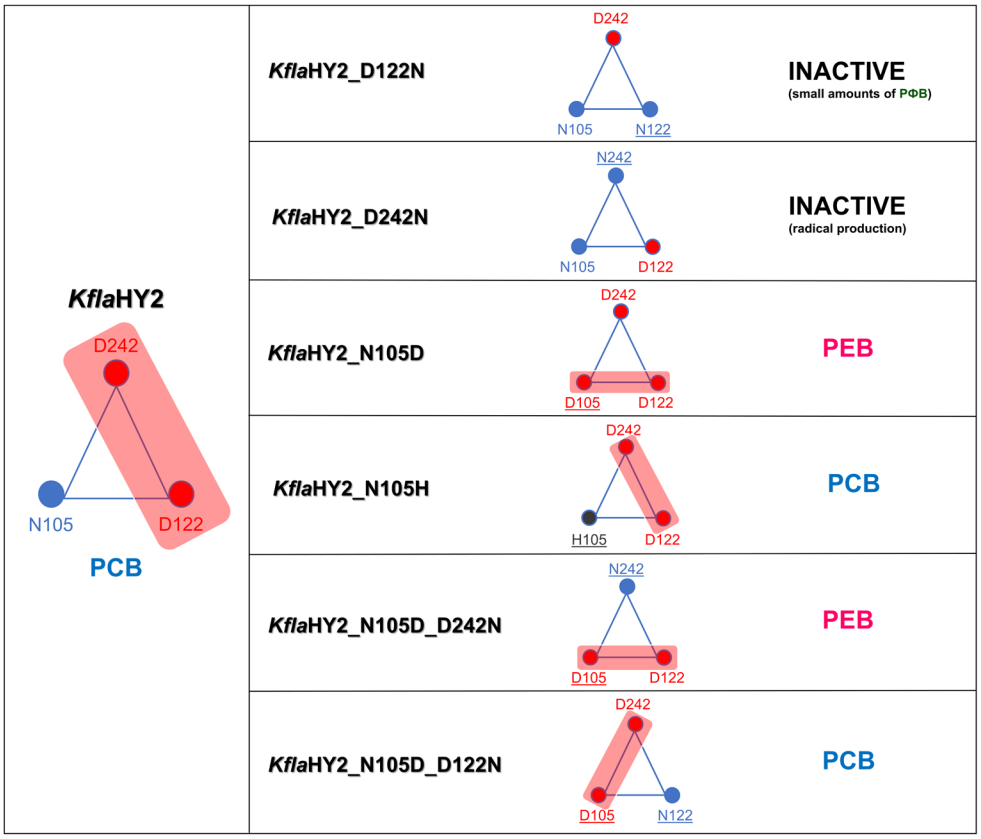

Figure S4 Schematical representation of the active sites and products of *Kfla*HY2 and its variants.
The red box highlights the position of the two aspartate residues. Exchanged residues are underlined. The production of either phycocyanobilin (PCB) or phycoerythrobilin (PEB) is determined by the position of aspartate couple in the active site. Variants in which the aspartate residues are opposite to each other are catalyzing BV reduction to PCB. Variants in which the aspartates are laying on the same side show reductases-isomerase activity, first catalyzing BV reduction to PCB and then isomerizing it to PEB.

Table S1 Sequences employed for the generation of alignments and the construction of full FDBRs phylogenetic tree (Figure 3.28)

Protein|Organism	Database	Accession number
PcyA|*Nostoc* sp. PCC 7120	JGI/IMG	alr3707
PcyA|*Nostoc punctiforme* PCC 73102	JGI/IMG	Npun_R5577
PcyA|*Trichodesmium erythraeum* IMS 101	JGI/IMG	Tery_4156
PcyA|*Synechococcus elongatus* PCC 7942	JGI/IMG	Synpcc7942_1225
PcyA|*Synechocystis sp.* PCC 6803	PDB	2D1E
PcyA|*Tolypothrix* sp. PCC 7601	JGI/IMG	fdiDRAFT29270
PcyA|*Phormidium* sp. OSCR	JGI/IMG	HLUCCO16_03155
PcyA|*Nodosilinea nodulosa* PCC 7104	JGI/IMG	Lepto7104DRAFT_5008
PcyA|*Crocosphaera watsonii* WH 8501	JGI/IMG	CwatDRAFT_2748
PcyA|*Synechococcus* sp. PCC 7002	JGI/IMG	SYNPCC7002_A2228
PcyA|*Gloeobacter violaceus* PCC 7421	JGI/IMG	gvip359
PcyA|*Thermosynechococcus elongatus* BP-1	JGI/IMG	tll2308
PcyA|*Synechococcus* sp. RCC307	JGI/IMG	SynRCC307_1284
PcyA|*Prochlorococcus* sp. WH8102	JGI/IMG	SYNW1084
PcyA|*Prochlorococcus* sp. CC9605	JGI/IMG	Syncc9605_1216
PcyA|*Prochlorococcus* sp. CC9902	JGI/IMG	Syncc9902_1252
PcyA|*Prochlorococcus marinus* CCMP 1375	JGI/IMG	Pro0819
PcyA|*Prochlorococcus marinus* MIT 9313	JGI/IMG	PMT0590
PCYA|*Cyanidioschyzon merolae* 10D	GenBank	CYME_CMG100C
PCYA|*Cyanoptyche gloeocystis*	MMETSP1086	36603_1
PCYA|*Gloeochaete wittrockiana*	MMETSP	177546_1
PCYA|*Cyanophora paradoxa*	Rockwell et al, 2017, New Phytologist	
PCYA|*Nephroselmis pyriformis*	MMETSP0034	35417_1
PCYA|*Pycnococcus* sp.	MMETSP1085	7414_1
PCYA|*Mantoniella antarctica*	MMETSP1106	20204_1
PCYA|*Ostreococcus mediterraneus*	MMETSP0932	4952_1
PCYA|*Picochlorum oklahomensis*	MMETSP1161	3223_1
PCYA|*Dunaliella tertiolecta*	MMETSP	38532_1
PCYA|*Chlamydomonas euryale*	MMETSP0063	48966_1
PCYA|*Chlamydomonas reinhardtii*	GenBank	XP_001693622
PebA|*Gloeobacter violaceus* PCC 7421	JGI/IMG	gvip179
PebA|*Tolypothrix* sp. PCC 7601	JGI/IMG	fdiDRAFT24420

PebA_1|*Crocosphaera watsonii* WH 8501	JGI/IMG	CwatDRAFT_2853
PebA_2|*Crocosphaera watsonii* WH 8501	JGI/IMG	CwatDRAFT_0676
PebA|*Nostoc punctiforme* PCC 73102	JGI/IMG	Npun_R0730
PebA|*Trichodesmium erythraeum* IMS101	JGI/IMG	Tery_5051
PebA|*Prochlorococcus marinus* CCMP 1375	JGI/IMG	Pro1749
PebA|*Prochlorococcus marinus* MIT 9313	JGI/IMG	PMT1686
PebA|*Synechococcus* sp. WH 8020	JGI/IMG	Ga0078671_111491
PebA|*Prochlorococcus* sp. WH 8102	JGI/IMG	SYNW2020
PebA|*Prochlorococcus* sp. CC 9605	JGI/IMG	Syncc9605_0423
PebA|*Prochlorococcus* sp. CC 9902	JGI/IMG	Syncc9902_1906
PEBA|*Galdieria sulphuraria*	GenBank	Gasu_55890
PEBA|*Rhodosorus marinus*	MMETSP0011	7168_1
PEBA|unclassified sp.	MMETSP1475	17257_1
PEBA|*Porphyridium aerugineum*	MMETSP0313	1488_1
PEBA|*Rhodella maculata*	MMETSP	6728_1
PEBA|*Erythrolobus australicus*	MMETSP1353	532_1
PEBA|*Madagascaria erythrocladiodes*	MMETSP1450	49920_1
PUBS|*Ostreococcus mediterraneus*	MMETSP0932	4217_1
PUBS|*Ostreococcus lucimarinus*	MMETSP0939	5045_1
PUBS|*Prasinococcus capsulatus*	MMETSP0941	2435_1
PUBS|*Mantoniella antarctica*	MMETSP1106	8279_1
PUBS|*Physcomitrella patens*	GenBank	AFK50337
PUBS|*Mougeotia* sp.	OneKP	ZRMT-2001364
HY2|*Cosmarium ochtodes*	OneKP	STKJ-2007533
PUBS|*Penium margaritaceum*	GenBank	HO601495
PUBS|*Klebsormidium nitens*	GenBank	GAQ90251
PEBB|*Galdieria sulphuraria*	GenBank	Gasu_58250
PEBB|*Rhodella maculata*	MMETSP	23469_1
PEBB|*Porphyridium aerugineum*	MMETSP0313	2204_1
PEBB|*Erythrolobus australicus*	MMETSP1353	9977_1
PEBB|*Rhodosorus marinus*	MMETSP0011	7399_1
PEBB|*Madagascaria erythrocladiodes*	MMETSP1450	12871_1
PEBB|unclassified sp.	MMETSP1475	3608_1
PebB|*Gloeobacter violaceus* PCC 7421	JGI/IMG	gvip180
PebB|*Tolypothrix* sp. PCC 7601	JGI/IMG	fdiDRAFT24430
PebB|*Crocosphaera watsonii* WH 8501	JGI/IMG	CwatDRAFT_5247
PebB|*Nostoc punctiforme* PCC 73102	JGI/IMG	Npun_R0729
PebB|*Trichodesmium erythraeum* IMS 101	JGI/IMG	Tery_5050
PebB|*Synechococcus* sp. WH 8020	JGI/IMG	Ga0078671_111492
PebB|*Prochlorococcus* sp. WH 8102	JGI/IMG	SYNW2021
PebB|*Prochlorococcus* sp. CC 9605	JGI/IMG	Syncc9605_0422

PebB|*Prochlorococcus* sp. CC 9902	JGI/IMG	Syncc9902_1907
PebB|*Prochlorococcus marinus* MIT 9313	JGI/IMG	PMT1687
PebB|*Prochlorococcus marinus* CCMP 1375	JGI/IMG	Pro1748
HY2|*Arabidopsis thaliana*	UniProt	Q9SR43
HY2|*Oryza sativa*	GenBank	BAD87875.1
HY2|*Zea mays*	GenBank	NP_001105256.1
HY2|*Solanum lycopersicum*	UniProt	Q588D6
HY2|*Adiantum capillus-veneris*	GenBank	BAF02518.1
HY2|*Physcomitrium patens*	GenBank	BAF02520.1
HY2|*Chaetosphaeridium globosum*	OneKP	DRGY-2006866
HY2|*Klebsormidium nitens*	GenBank	GAQ84116.1
HY2|*Chlorokybus atmophyticus*	OneKP	AZZW-2019954
HY2|*Marchantia polymorpha*	OneKP	JPYU-2037290
HY2|*Nothoceros vicentianus*	OneKP	TCBC-2082726
HY2|*Ceratodon purpureus*	OneKP	FFPD-2057880
HY2|*Cycas micholitzii*	OneKP	XZUY-2012311
HY2|*Posidonia australis*	OneKP	BYQM-2011005
HY2|*Netrium digitus*	OneKP	FFGR-2000050
HY2|*Mesotaenium endlicherianum*	OneKP	WDCW-2047152
HY2|*Entransia fimbriata*	OneKP	BFIK-2028189
HY2|*Klebsormidium subtile*	OneKP	FQLP-2031011
HY2|*Mesotaenium caldariorum*	OneKP	HKZW-2005125
RCCR|*Batis maritima*	OneKP	DZTK-2041775
RCCR|*Akania lucens*	OneKP	HYZL-2141617
RCCR|*Arabidopsis thaliana*	GenBank	NP_195417

Curriculum vitae

Personal data

Name	Federica
Surname	Frascogna

Education

10/2020 – now	**PhD Candidate** Rheinland-Pfälzische Technische Universität Kaiserslautern-Landau (RPTU, Kaiserslautern, Germany) Department of Microbiology
01/2018 – 03/2020	**MSc in Molecular & Industrial Biotechnology** University of Naples Federico II (Naples, Italy) Thesis in Protein Biochemistry
09/2014 – 12/2017	**BSc in Biomolecular & Industrial Biotechnology** University of Naples Federico II (Naples, Italy) Thesis in Protein Biochemistry
09/2009 – 07/2014	**High School Scientific Diploma** Liceo Scientifico Statale "A.M. De Carlo" (Giugliano in Campania, Italy)

Publication

Federica Frascogna, Benjamin Ledermann, Jana Hartmann, Eugenio Pérez Patallo, Fjoralba Zeqiri, Eckhard Hofmann, Nicole Frankenberg-Dinkel, On the evolution of the plant phytochrome chromophore biosynthesis, Plant Physiology, Volume 193, Issue 1, September 2023, Pages 246 - 258, https://doi.org/10.1093/plphys/kiad327

Conference contributions

Talks

21/09/2023: "On the evolution of the plant phytochrome chromophore biosynthesis"
15th International Conference on Tetrapyrrole Photoreceptors in Photosynthetic Organisms (ICTPPO)
Shizuoka, Japan

27/04/2023: “On the evolution of the plant phytochrome chromophore biosynthesis”
Tetrapyrrole Discussion Group Meeting (TPDG)
Canterbury, United Kingdom

07/06/2022: “Phycocyanobilin biosynthesis in algae”
Biology Department Seminar of RPTU Kaiserslautern
Thallichtenberg, Germany

Posters

12/12/2023 – 15/12/2023: “Unravelling the biosynthesis of phycocyanobilin in streptophyte algae”
AlgaEurope 2023
Prague, Czech Republic

18/09/2023 – 22/09/2023: “On the evolution of the plant phytochrome chromophore biosynthesis”
15th International Conference on Tetrapyrrole Photoreceptors in Photosynthetic Organisms (ICTPPO)
Shizuoka, Japan

21/02/2022 – 23/02/2022: “Phycocyanobilin biosynthesis in an early diverging streptophyta”
VAAM 2022
Online conference

Erklärung

Erklärungen lt. § 6 (4) der Promotionsordnung des Fachbereichs Biologie vom 27.11.2018:

Ich erkläre wahrheitsgemäß, dass ich die eingereichte Dissertation selbst angefertigt und alle für die Arbeit benutzten Hilfsmittel und Hilfestellungen in der Arbeit angegeben habe.
Die Dissertation oder Teile hiervon habe ich bisher nicht als Prüfungsarbeit für eine staatliche oder andere wissenschaftliche Prüfung eingereicht.
Ebenso habe ich die gleiche oder eine andere Abhandlung nicht bei einem anderen Fachbereich oder einer anderen Universität als Dissertation eingereicht.

Kaiserslautern, 16.05.2024

Federica Frascogna

Darlegung des Eigenanteils

Name: Federica Frascogna

Titel: Tracing the evolution of bilin biosynthesis: from emergence to primary endosymbionts

Die Konzeption, die Planung, das Versuchsdesign und die Methodenentwicklung der vorliegenden Arbeit wurde in Teilen von Prof. Nicole Frankenberg-Dinkel und, teilweise, von Dr. Eugenio Pérez Patallo unterstützt.

Die Literaturrecherche, die Datenerhebung, die Datenanalyse, die Interpretation und Diskussion der Ergebnisse wurden, sofern im Folgenden nicht anders dargelegt, nicht von Dritten unterstützt.

Bakterienstämme sowie Plasmide, die von dritter Seite generiert wurden, sind, in Tabelle 2.3 und Tabelle 2.4, mit der entsprechenden Quelle, aufgeführt.

Die Datenerhebung für Abbildungen 3.21, 3.22, 3.23 wurde von Benjamin Ledermann (ehemaliger Doktorand, RPTU, Mikrobiologie) unterstützt. Die Datenanalyse und -auswertung für diese Abbildung wurde nicht von Dritten unterstützt. Diese Ergebnisse sind, in unterschiedlichen Darstellungen, Teil der Dissertationsarbeit von Dr. Ledermann.

Die folgenden Abschnitte dieser Arbeit enthalten Daten, Beschreibungen und Auswertungen, die, in unterschiedlicher Form, im Rahmen von Frascogna *et al.*, 2023 bereits veröffentlicht wurden:

2 Materials and Methods: 2.5.14, 2.5.15, 2.5.16, 2.5.17, 2.5.18

3 Results: 3.9, 3.10, 3.11, 3.12, 3.13

4 Discussion: 4.7, 4.8, 4.10

Kaiserslautern, 16.05.2024

Prof. Dr. Nicole Frankenberg-Dinkel Federica Frascogna

Darlegung aller benutzen Hilfestellungen und Hilfsmittel

Name: Federica Frascogna

Titel: Tracing the evolution of bilin biosynthesis: from emergence to primary endosymbionts

Die Analyse der Daten erfolgte mit Hilfe von Origin 2022 und 2024. Weitere verwendete Programme und Webseiten waren Microsoft Word sowie PowerPoint, Mendeley Reference Manager, ChemDraw 23.0.1, PyMOL, BLAST® (https://blast.ncbi.nlm.nih.gov/Blast.cgi) sowie BLAST+, SnapGene, NEBuilder®, NEB Tm calculator (https://tmcalculator.neb.com/), NEBioCalculator® (https://nebiocalculator.neb.com), ProtParam (https://web.expasy.org/protparam/), Clustal Omega (https://ebi.ac.uk/jdispatcher/msa/clustalo), PyMOL, AlphaFold2 (https://colab.research.google.com/github/sokrypton/ColabFold/blob/main/AlphaFold2.ipynb), PhyML 3.0 (http://www.atgc-montpellier.fr/phyml/), BOOSTER (https://booster.pasteur.fr/) und iTOL (https://itol.embl.de/).

Handelt es sich nicht um frei nutzbare Programme oder Webseiten wurden sie von der RPTU oder der Abteilung Mikrobiologie zur Verfügung gestellt.

Die Übersetzungsseite DeepL wurde genutzt, um diesen und andere Abschnitte (Zusammenfassung, Darlegung des Eigenanteils) ins Deutsche zu übersetzen.

Kaiserslautern, 16.05.2024

Federica Frascogna

Acknowledgements

This section cannot start any differently than with expressing my deepest gratitude to Prof. Dr. Nicole Frankenberg-Dinkel. Thanks for the support, the guidance, for always making time when I needed a quick chat and allowing me to bring this thesis to somewhere it was not planned to. Although the *Galdieria* project, which initially brought me here, has not yielded the hoped results, I can honestly say I still made the right decision to move here and work under your supervision.

I extend my gratitude to Prof. Dr. Michael Schroda and Prof. Dr. Stefanie Müller-Schüssele for agreeing to be part of my thesis committee.

I am profoundly grateful to Prof. Dr. J. Clark Lagarias and Dr. Nathan Rockwell (UC Davis, USA) for the enlightening discussions on FDBRs and phytochromes and precious gift of plasmids.

I also wish to acknowledge Prof. Dr. Eckhard Hofmann and Fjoralba Zeqiri (Ruhr University Bochum) for the fruitful collaboration in the *Kfla*HY2 project.

Un mónton de gracias a Dr. Eugenio Pérez Patallo. You have been there when I was a lost, foreign, PhD Student, dealing with all sorts of new techniques and helped me A LOT. I am greatly thankful for your supporting words and life-related discussions too. I wish you the best, I know your new students will greatly benefit from your knowledge.

A special shout-out to the MiBis, especially Nora, Bin, Thomas, Jacqueline, Christina and Anna, as well as the Latin Gang, Giuseppe, Miguel and Nicola. Thanks for fun times out of the lab and not-so-fun times in the lab every time a device broke down or something did not work. Being on the same boat definitely helped in surviving lab life. I would particularly like to thank Nora, who has been there for me since the beginning and helped me through it all (in sickness and in health…). Life as an expat has been much easier thanks to your infinite willingness to help.

Special thanks to Prof. Dr. Daria Maria Monti and Dr. Paola Imbimbo (University of Naples Federico II). My hands-on scientific journey started in that Monte Sant'Angelo lab many years ago now, where you helped shape my scientific mindset. I immensely appreciate your support, even from afar, and the warm welcome I receive every time I come to visit.

Moving to the Italian family, heartfelt gratitude goes to Carlo, Gabriella, Marika, Massimiliano and Mattia. You have always been there, listening to extra-long voice messages, recurring complaints and nervous breakdowns. I was not alone in this challenging part of my life as you've been there, aware of it ALL, at any time.

I would like to thank my family. My aunts and uncles for constantly supporting every small result and always calling me “Dottoressa”, although the title was still not there… now you can finally say it!

Lastly, infinite gratitude to my parents. For supporting my education throughout the years and accepting the difficult decision to leave home to pursue my objectives abroad. I know it hasn’t been easy, especially after the big grieving we had to endure in 2020. Everything I have accomplished is as much a reflection of your sacrifices as it is of my own efforts. You will always be the overbearing and OVERCARING presence in my life: chi ten ‘E GENITOR è ricc e nun ‘o sap.

This work was financially supported by a grant from the Deutsche Forschungsgemeinschaft.

Corrigendum

Die Abbildungen 1.2 und 4.6 wurden nach der Annahme der Arbeit im Dekanat des Fachbereichs Biologie geringfügig geändert, um übersehene Fehler zu korrigieren. Siehe unten die vorherige Version.

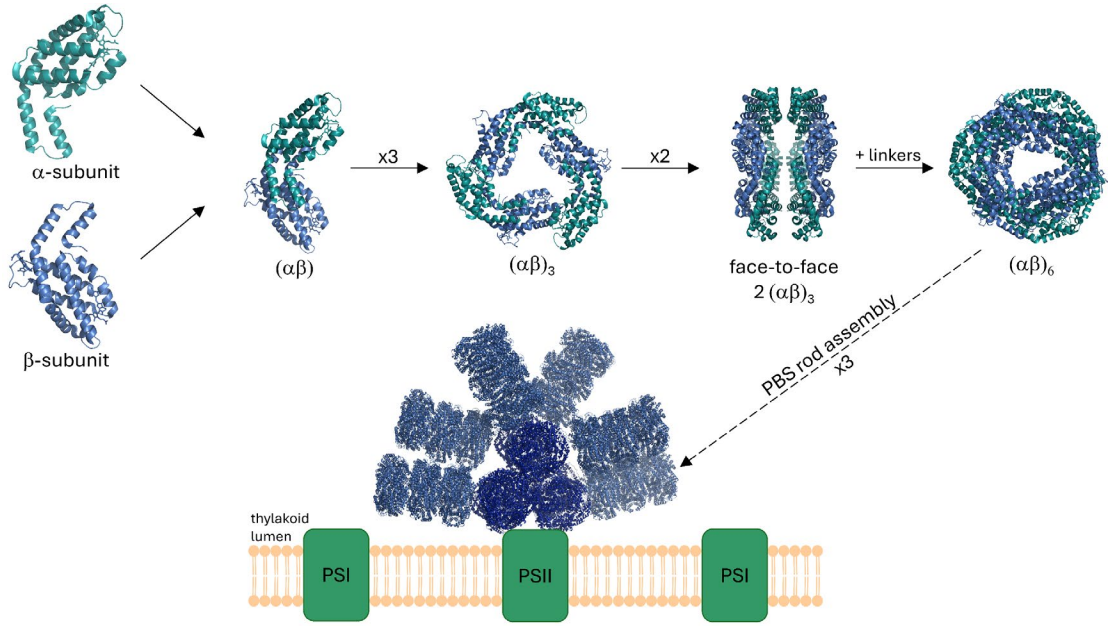

Figure 1.2 Phycobiliprotein oligomerization process and assembly in the phycobilisome.
Incorrect placement of the thylakoid lumen.

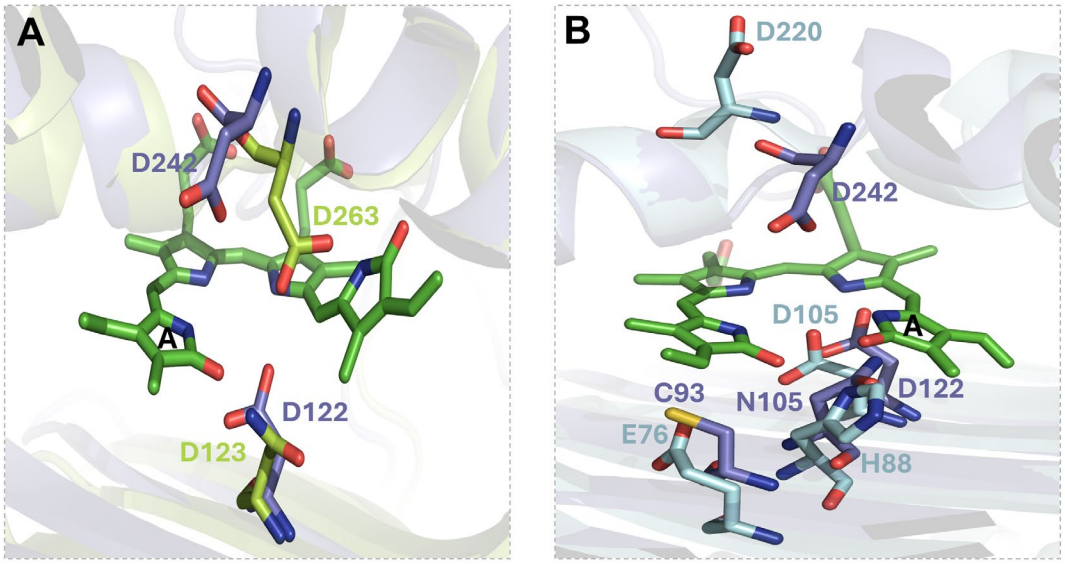

Figure 4.6 Structure alignments of *Kfla*HY2 with *Sl*HY2 and *Syn*PcyA.
Incorrect labeling in A.